**University of Alberta**

# Geochemical, radiogenic tracer isotopic, and U-Pb geochronological studies of Yukon Tanana terrane rocks from the Money klippe, southeastern Yukon, Canada.

by

Steven Lloyd Grant ©

A thesis submitted to the Faculty of Graduate Studies and Research in partial fulfillment

of the requirements for the degree of Master of Science

Department of Earth and Atmospheric Sciences

Edmonton, Alberta

Fall, 1997

National Library
of Canada

Acquisitions and
Bibliographic Services

395 Wellington Street
Ottawa ON K1A 0N4
Canada

Bibliothèque nationale
du Canada

Acquisitions et
services bibliographiques

395, rue Wellington
Ottawa ON K1A 0N4
Canada

Your file Votre référence

Our file Notre référence

The author has granted a non-exclusive licence allowing the National Library of Canada to reproduce, loan, distribute or sell copies of this thesis in microform, paper or electronic formats.

The author retains ownership of the copyright in this thesis. Neither the thesis nor substantial extracts from it may be printed or otherwise reproduced without the author's permission.

L'auteur a accordé une licence non exclusive permettant à la Bibliothèque nationale du Canada de reproduire, prêter, distribuer ou vendre des copies de cette thèse sous la forme de microfiche/film, de reproduction sur papier ou sur format électronique.

L'auteur conserve la propriété du droit d'auteur qui protège cette thèse. Ni la thèse ni des extraits substantiels de celle-ci ne doivent être imprimés ou autrement reproduits sans son autorisation.

0-612-22600-X

Canada

## University of Alberta

## Library Release Form

**Name of Author:** Steven Lloyd Grant

**Title of Thesis:** Geochemical, radiogenic tracer isotopic, and U-Pb geochronological studies of Yukon Tanana terrane rocks from the Money klippe, southeastern Yukon, Canada.

**Degree:** Master of Science

**Year this Degree Granted:** 1997

Permission is hereby granted to the University of Alberta Library to reproduce single copies of this thesis and to lend such copies for private, scholarly, or scientific research purposes only.

The author reserves all other publication and other rights in association with the copyright in the thesis, and except as hereinbefore provided, neither the thesis nor any substantial portion thereof may be printed or otherwise reproduced in any material form whatever without the author's prior written permission.

Steven Grant

Steven Grant
5 MacRae Avenue
Dartmouth, Nova Scotia, Canada
B2Y 1Z3

Date: June 12, 1997

University of Alberta

Faculty of Graduate Studies and Research

The undersigned certify that they have read, and recommend to the Faculty of Graduate Studies and Research for acceptance, a thesis entitled Geochemical, Radiogenic Tracer Isotopic, and U-Pb Geochronological Studies of Yukon Tanana Terrane Rocks from the Money Klippe, Southeastern Yukon, Canada submitted by Steven Lloyd Grant in partial fulfillment of the requirements for the degree of Master of Science.

Dr. R.A. Creaser (co-supervisor)

Philippe Erdmer

Dr. P. Erdmer (co-supervisor)

Dr. R.W. Luth

Dr. M.E. Evans

Date 28/5/97

# ABSTRACT

This study presents geochemical and isotopic analyses of supracrustal and igneous rock from the Money klippe in southeastern Yukon in order to constrain the tectonic evolution of the pericratonic Yukon Tanana terrane. Samples from the supracrustal Nisutlin assemblage have $\varepsilon Nd_0$ ranges of -20.4 to +4.9, indicating that while some Nisutlin assemblage rocks are similar to the North American miogeocline, juvenile material (uncommon in the miogeocline) also contributed to the Nisutlin provenance. These data support models indicating that the Nisutlin assemblage formed as a distal portion of the miogeocline. Some of the samples from the mafic Anvil assemblage have geochemical characteristics of calc-alkalic basalt, which does not support the correlation of the Anvil assemblage to the ocean floor-dominated Slide Mountain terrane. Geochemistry indicates that the Simpson Range plutonic suite (SRPS) is the product of calc-alkalic continental arc magmatism. U-Pb dating of zircons shows that all SRPS rocks were formed between 344 and 360 Ma. Inherited zircon of broadly Proterozoic age, Nd model ages ( $T_{DM}$ = 1.67 to 2.10 Ga), initial Sr ratios ($^{87}Sr/^{86}Sr$ = 0.7074 to 0.7099), and $^{207}Pb/^{204}Pb$, $^{206}Pb/^{204}Pb$ and $^{208}Pb/^{204}Pb$ ratios in excess of those of the uniform reservoir all show that older crust has contributed significantly to the petrogenesis of the SRPS, although to varying amounts, perhaps depending on the thickness of the intruded crust. These studies are compatible with a model which suggests that the Yukon Tanana terrane consists in part of a Devonian-Mississippian fringing arc built on the distal portion of the North American miogeocline.

# ACKNOWLEDGMENTS

I would like to thank my advisors Dr. Robert Creaser and Dr. Philippe Erdmer for their support and guidance. Rob Creaser provided expert training in his top-notch geochemistry and mass-spectrometer labs, and laboured through various drafts of this thesis with great speed and patience. Despite his hectic schedule, Rob never failed to find time to give advice when needed. Philippe Erdmer outfitted me and introduced me to a great field area, and also gave valuable comments on many chapters. This work was made possible by a generous Northern Scientific Training grant I received in 1995 from the Canadian Circumpolar Institute. Financial support provided by Dr. Robert Creaser is also greatly appreciated.

I would also like to thank Dr. Larry Heaman for allowing me to use his lab and equipment, and especially for sharing with me his philosophy on zircon-picking and on running U-Pb on the mass-spectrometer. Taro Yamashita gave generously of his time and knowledge in the chemistry and mass-spectrometry labs, and I enjoyed the many late-night chat sessions we often had. Thanks are also due to Paul Wagner, for crushing and bulk separation of my geochron samples; to James McDonnell, who provided able assistance in the field; and to Ray Roberts, who powdered many of my samples.

I will fondly remember good times with fellow graduate students, especially Mark (Tea-Towel) Hearn, Joanne Jensen, the house gang (Matt (Master of the Cusholith) Perks, Karen Fallas, Dayve Hills), Dave Selby, Jen Vézina, Suman De, Jochen Mezger; but also many others.

I owe so much to Erinn Horrigan, whose never-failing belief in me helped me preserve my faith in myself.

Finally, I would like to thank my parents for their love and encouragement, not to mention the substantial financial assistance, without which I could not have finished this thesis.

## TABLE OF CONTENTS

**CHAPTER 1. INTRODUCTION ........ 1**

**CHAPTER 2. BACKGROUND AND GEOLOGY ........ 6**

2.1 TECTONIC FRAMEWORK OF THE NORTHERN CORDILLERA TERRANES ........ 6
- *Cordilleran overview* ........ 6
- *Relation of the YT terrane to North America and pericratonic terranes* ........ 7
- *Relations between the YT terrane and terranes of the Intermontane Belt* ........ 11

2.2 REGIONAL GEOLOGY OF THE YT TERRANE ........ 16
- *Previous work* ........ 16
- *Terminology* ........ 18

2.2 GEOLOGY IN THE VICINITY OF THE MONEY KLIPPE ........ 20
- *Location* ........ 20
- *Previous work* ........ 20
- *Relations* ........ 22

2.4 LITHOLOGICAL DESCRIPTIONS ........ 24
- *Nisutlin assemblage* ........ 24
- *Anvil assemblage* ........ 28
- *Simpson Range Plutonic Suite* ........ 29

**CHAPTER 3. STRUCTURE ........ 43**

3.1 INTRODUCTION ........ 43

3.2 PENETRATIVE PLANAR FABRIC ........ 44
- *Map-scale observations* ........ 44
- *Meso- and micro-scale observations* ........ 45
- *Evidence for volume loss* ........ 45
- *Structural analysis* ........ 46
- *Shear-sense analysis* ........ 47

3.4 THRUST RELATIONS ........ 50

3.5 DISCUSSION ........................................................................................................50

**CHAPTER 4. PROVENANCE OF NISUTLIN AND ANVIL ASSEMBLAGES ............................................................ 63**

4.1 INTRODUCTION ....................................................................................................63

4.2 PROVENANCE OF THE NISUTLIN ASSEMBLAGE ............................................................66
- *Major elements* ..........................................................................................66
- *Rare-earth elements*......................................................................................67
- *Provenance-sensitive trace elements* ....................................................................69
- *Sm-Nd isotope sytematics* ..............................................................................73
- *Summary* ...................................................................................................76

4.3 ANVIL ASSEMBLAGE ................................................................................................77
- *Summary* ...................................................................................................80

4.4 DISCUSSION ..........................................................................................................82
- *Nisutlin assemblage*......................................................................................82
- *Anvil assemblage* .........................................................................................84
- *Comparison to the miogeocline and Alberta basement*..................................................86

**CHAPTER 5. GEOCHEMISTRY AND ISOTOPE SYSTEMATICS OF THE SIMPSON RANGE PLUTONIC SUITE ...... 102**

5.1 INTRODUCTION ....................................................................................................102

5.2 GEOCHEMISTRY....................................................................................................103
- *Major elements* ..........................................................................................103
- *Rare-earth elements*......................................................................................105
- *Trace-element discrimination diagrams*..................................................................106
- *Summary of geochemical evidence*..........................................................................109

5.3 PRECISE U-Pb GEOCHRONOLOGY ..................................................................................110
- *Biotite-monzogranite (SG94-2)* ..........................................................................110
- *Hornblende-granodiorite (SG94-14)*.......................................................................111
- *Sheared-granodiorite (SG94-55)*..........................................................................111
- *Quartz-porphyry volcanic (SG94-11)*.......................................................................112
- *Gabbro (SG94-1)* ..........................................................................................112

*Summary of U-Pb data* ........ 113

5.4 RADIOGENIC TRACER ISOTOPES ........ 114
*Rb-Sr* ........ 114
*Sm-Nd* ........ 115
*Pb-Pb* ........ 116

5.5 DISCUSSION ........ 117

**CHAPTER 6. DISCUSSION AND CONCLUSIONS ........ 139**

*Relations from the Money klippe field area* ........ 139
*Nisutlin and Anvil assemblage provenance* ........ 140
*Devonian-Mississippian magmatism* ........ 142
*Tectonic setting* ........ 144

CONCLUSIONS ........ 146

**LITERATURE CITED ........ 150**

**APPENDIX 1. LOCATION OF FIELD STATIONS ........ 162**

**APPENDIX 2. HANDSAMPLE DESCRIPTION OF NISUTLIN ASSEMBLAGE SAMPLES ........ 163**

**APPENDIX 3. THIN-SECTION DESCRIPTIONS OF NISUTLIN ASSMBLAGE SAMPLES ........ 164**

**APPENDIX 4. STRUCTURAL MEASUREMENTS ........ 168**

**APPENDIX 5. SHEAR-SENSE INDICATOR DATA ........ 169**

APPENDIX 6. SAMPLE CLEANING, CRUSHING, AND POWDERING .......... 170

APPENDIX 7. Sm- Nd CHEMICAL SEPARATION AND ISOTOPE ANALYSIS TECHNIQUES .......... 171

APPENDIX 8. ZIRCON EXTRACTION, CLEANING, AND DISSOLUTION; U-Pb SEPARATION CHEMISTRY AND ISOTOPIC ANALYSIS .......... 172

APPENDIX 9. Rb-Sr CHEMICAL SEPARATION AND ISOTOPE ANALYSIS TECHNIQUES .......... 174

APPENDIX 10. K-FELDSPAR SEPARATION TECHNIQUES AND Pb-Pb ANALYSIS .......... 175

APPENDIX 11. ANALYTICAL ERROR FOR XRF AND ICP MS GEOCHEMICAL DATA .......... 177

# LIST OF TABLES

TABLE 4.1. GEOCHEMISTRY OF NISUTLIN AND ANVIL SAMPLES....91
TABLE 4.2. Sm-Nd ISOTOPE SYSTEMATICS OF THE NISUTLIN AND ANVIL ASSEMBLAGES....92
TABLE 5.1. GEOCHEMISTRY OF SRPS ROCKS....121
TABLE 5.2. U-Pb ZIRCON ANALYSES OF SRPS ROCKS....122
TABLE 5.3. Rb-Sr ANALYSES OF SRPS ROCKS....123
TABLE 5.4. Sm-Nd ANALYSES OF SRPS ROCKS....124
TABLE 5.5. Pb-Pb ANALYSES OF SRPS ROCKS....125

# LIST OF FIGURES

FIGURE 1.1. SIMPLIFIED MAP OF THE CANADIAN CORDILLERA ........................................5

FIGURE 2.1. SIMPLIFIED TERRANE MAP OF THE CANADIAN CORDILLERA ........................33
FIGURE 2.2. TERRANES OF THE NORTHERN CORDILLERA ........................................34
FIGURE 2.3. LOCATION MAPS FOR THE FIELD AREA ........................................35
FIGURE 2.4. GEOLOGY OF THE FIELD AREA ........................................36
FIGURE 2.5. MQS SAMPLE SG94-24 PHOTOGRAPH ........................................37
FIGURE 2.6. QP SAMPLE SG94-35 PHOTOGRAPH ........................................37
FIGURE 2.7. GRAPHITE-BEARING QP SAMPLE SG94-90D PHOTOGRAPH ........................38
FIGURE 2.8. MS SAMPLE SG94-82 PHOTOGRAPH ........................................38
FIGURE 2.9. ANVIL ASSEMBLAGE SAMPLE SG94-52 PHOTOGRAPH ........................39
FIGURE 2.10. HbGd SAMPLE SG94-90B PHOTOGRAPH ........................................39
FIGURE 2.11. BtMg SAMPLE SG94-78 PHOTOGRAPH ........................................40
FIGURE 2.12. GABBRO SAMPLE SG94-44 PHOTOGRAPH ........................................40
FIGURE 2.13. FVP SAMPLE SG94-11A PHOTOGRAPH ........................................41
FIGURE 2.14. MVP SAMPLE SG94-10B PHOTOGRAPH ........................................41
FIGURE 2.15. Sh-Gd SAMPLE SG94-57 PHOTOGRAPH ........................................42

FIGURE 3.1. GEOLOGY AND LOCATION OF STRUCTURAL MEASUREMENTS ........................54
FIGURE 3.2. PHOTOGRAPH OF NISUTLIN ASSEMBLAGE OUTCROP ........................................55
FIGURE 3.3. PHOTOGRAPH OF SMALL FOLDS IN A MQS SAMPLE ........................................55
FIGURE 3.4. PHOTOGRAPH OF PORPHYROCLAST ROTATION IN Sh-Gd SAMPLE ................56
FIGURE 3.5. PHOTOGRAPH OF QP SAMPLE SG94-90B ........................................56
FIGURE 3.6. PHOTOGRAPH SHOWING VOLUME LOSS IN MQS SAMPLE SG94-53..............57
FIGURE 3.7. FOLIATION MEASUREMENTS FROM THE MONEY KLIPPE AREA........................58
FIGURE 3.8. LINEATION MEASUREMENTS FROM THE MONEY KLIPPE AREA ........................59
FIGURE 3.9. PHOTOGRAPH OF F-TYPE AESB ........................................60
FIGURE 3.10. PHOTOGRAPH OF D-TYPE AESB ........................................60

FIGURE 3.11. MAP OF SHEAR SENSE INDICATORS IN THE MONEY KLIPPE AREA ................61
FIGURE 3.12. PHOTOGRAPH OF CONTACT BETWEEN GABBRO AND BtMg ..........................62
FIGURE 3.13. PHOTOGRAPH OF CONTACT BETWEEN HbGd AND BtMg.............................62

FIGURE 4.1. LOCATION OF ANALYZED NISUTLIN AND ANVIL SAMPLES ...........................93
FIGURE 4.2. MAJOR ELEMENT PLOTS OF NISUTLIN AND ANVIL DATA..............................94
FIGURE 4.3. REE PLOTS OF NISUTLIN AND ANVIL ASSEMBLAGE DATA ..........................95
FIGURE 4.4. TRACE ELEMENT PLOTS OF NISUTLIN AND ANVIL DATA...............................96
FIGURE 4.5. TRACE ELEMENT DISCRIMINATION DIAGRAMS ..............................................97
FIGURE 4.6. Nd ISOTOPE PLOTS OF NISUTLIN AND ANVIL DATA ......................................98
FIGURE 4.7. TECTONIC DISCRIMINATION OF ANVIL AND MS SAMPLES ...........................99
FIGURE 4.8. COMPARISON PLOTS OF MONEY KLIPPE AND TTZ NISUTLIN DATA ...........100
FIGURE 4.9. HISTOGRAMS OF YT TERRANE AND MIOGEOCLINE Nd DATA .....................101

FIGURE 5.1. LOCATION MAP OF ANALYZED SRPS SAMPLES...........................................126
FIGURE 5.2. MAJOR ELEMENT PLOTS OF SRPS DATA .....................................................127
FIGURE 5.3. VARIOUS DISCRIMINATION DIAGRAMS OF SRPS DATA ..............................128
FIGURE 5.4. CLASSIFICATION OF SRPS ROCKS ...........................................................129
FIGURE 5.5. REE PLOTS FOR THE SRPS ROCKS ............................................................130
FIGURE 5.6. TRACE ELEMENTS VERSES $SiO_2$ FOR SRPS ROCKS ....................................131
FIGURE 5.7. TECTONIC DISCRIMINATION DIAGRAMS FOR FELSIC SRPS SAMPLES..........132
FIGURE 5.8. TECTONIC DISCRIMINATION DIAGRAMS FOR MAFIC SRPS SAMPLES ..........133
FIGURE 5.9. U-Pb CONCORDIA DIAGRAM FOR SRPS ZIRCON ANALYSES .......................134
FIGURE 5.10. Rb-Sr GROWTH CURVES AND $^{87}Sr/^{86}Sr$ VERSES $^{87}Rb/^{86}Sr$ PLOT.................135
FIGURE 5.11. εNd VERSES TIME DIAGRAM ......................................................................136
FIGURE 5.12. $^{207}Pb/^{204}Pb$ AND $^{208}Pb/^{204}Pb$ VERSES $^{206}Pb/^{204}Pb$ PLOTS ...........................137
FIGURE 5.13. εNd VERSES $SiO_2$ AND $FeO^*/MgO$ PLOTS.................................................138

# CHAPTER 1. INTRODUCTION

The Cordillera of North America is composed of an eastern belt of deformed and displaced North American miogeoclinal rocks and a western belt of accreted lithostratigraphic terranes (Fig. 1.1); widespread plutonic and volcanic rocks are also widespread throughout the Cordillera. Occupying the boundary between accreted terranes and ancestral North America in Alaska and Yukon territory, the metamorphic-plutonic Yukon-Tanana (YT) terrane possesses properties that ally it to both (Mortensen 1992b). The fact that strong deformation and Late Paleozoic magmatism affected the YT terrane but not the North American miogeocline (Mortensen and Jilson 1985, Coney 1989, Mortensen 1992b) indicates that the YT terrane possesses a distinct history from the craton (Mortensen and Jilson 1985). However, the strongly continental character of geochemical and isotopic data of many YT terrane rocks (Aleinikoff et al. 1981, Mortensen 1983, Bennett and Hansen 1988), coupled with the fact that the YT terrane is the most inboard of suspect terranes, suggests ties to the craton. Poor exposure and a high degree of deformation have hampered investigations of the YT terrane, and although the last two decades have seen a marked increase of study, much about its origin and mode of accretion remains unresolved (Mortensen 1992b). The goal of this thesis is to provide better constraints to these problems.

A field area encompassing the Money klippe (Fig. 2.3; described below) in southeast Yukon was chosen for study because of the wide variety of YT terrane rock types and deformational structures contained within it. Field work at this locality and analyses of collected samples forms the basis of this thesis, which explores three main avenues of research: (1) structural analysis of penetrative and brittle deformational features, (2) provenance characterization of the Nisutlin metasedimentary-metavolcanic assemblage using geochemical and tracer isotopic methods, and (3) geochemical, tracer isotopic and U-Pb geochronological examination of a suite of YT terrane plutonic rocks.

The remainder of this chapter will provide a brief review of the rationale and methods involved in the formation of this thesis.

Chapter 2 will provide the background information necessary to put the present investigation in a regional context. Lithological descriptions and field observations will also be presented in Chapter 2.

Chapter 3 contains a study of structures associated with the penetrative deformation affecting the Nisutlin assemblage schist, with special attention given to shear-sense indicators. Thrust faults found in the upper portions of the Money klippe are also examined. These investigations were undertaken in part to determine whether small scale kinematics are able to help constrain the mechanics of large scale transport during accretion of the YT terrane to North America.

Chapter 4 presents an analysis of the provenance of the supracrustal Nisutlin assemblage, incorporating geochemical, and Nd-isotopic analysis of Nisutlin assemblage schist cropping out in and around the Money klippe. Investigations of these units are hampered by the fact that in almost all locations, original depositional structures and relations between units are destroyed by strong deformation. Metamorphism of the Nisutlin assemblage, mostly greenschist facies but ranging to lower amphibolite facies in some localities (Mortensen 1983), has changed the original mineralogy. However, trace element geochemistry and tracer isotope applications are useful tools for examining the bulk characteristics of these rocks, because some trace elements (including Sm and Nd) are relatively immobile and insensitive to metamorphic and weathering processes (Taylor and McLennan 1985, Bhatia and Crook 1986). Thus, the trace element and Nd isotopic signature of the Nisutlin assemblage should reflect that of its sources. Creaser et al. (1997a) have recently used trace elements and Nd isotopes to show that both evolved crustal material and juvenile arc-derived material supplied detritus to the Nisutlin assemblage sedimentary protolith in the Teslin tectonic zone. More broadly, Nd isotopes can be used to compare and differentiate between terranes, as Samson et al. (1991) have done by linking several metamorphic assemblages of the Alexander-Wrangellia-Peninsular composite terrane in the Coast Belt with the inboard YT terrane based on similarity in Nd systematics. The only studies that have directly examined the Sm-Nd systematics of YT terrane metasedimentary rock are those of Creaser et al. (1997a), Samson et al. (1991), and McCulloch and Wasserburg (1978), so the work done for this study will further constrain the geochemical and isotopic identity of the Nisutlin assemblage. Identifying the crustal affinity of the source of sediment will help establish the tectonic regime of the YT terrane in general.

The nature of the mafic rock of the Anvil assemblage is also discussed in Chapter 4. Mafic rock bodies are common throughout the YT terrane, where they are structurally interleaved with the more felsic supracrustal rocks of the Nisutlin assemblage. Many of these mafic rocks were originally mapped as the Anvil assemblage, but later were correlated to the Slide Mountain (SM) terrane (Monger 1984, Wheeler et al. 1991, Mortensen 1992a,b), which has the geochemical characteristics of mid-ocean ridge basalt MORB (Roback et al. 1994). Plint and Gordon (1997) suggest that the correlation of YT terrane mafic rock to the SM terrane is justified because the mafic rock from near the YT terrane - North America contact in the Campbell Range have geochemical characteristics of MORB. Not all mafic rock in the YT terrane are similar to the SM terrane, however. Creaser et al. (1997a) determined that mafic rock from the Teslin Tectonic Zone in the YT terrane are compatible with derivation from calc-alkalic magmatism in a continental arc, and thus do not directly correlate to the SM terrane. In order to provide new constraints to the origins of mafic rocks in the YT terrane, Chapter 4 of this thesis presents geochemistry and Nd isotopic analyses of the mafic Anvil assemblage rocks from the Money klippe.

Late-Devonian to Middle-Mississippian magmatism, responsible for the largest volume of plutonic rocks in the YT terrane, has produced two distinct igneous suites (Mortensen 1992b). The most widespread and studied suite, generally called the ‘peraluminous orthogneiss’ (e.g. Mortensen 1992b, Hansen 1989, Hansen et al. 1989, 1991), are deformed S-type granitoids that have isotopic characteristics of magma derived largely from Precambrian continental crust (Mortensen 1983, Bennett and Hansen 1988, Aleinikoff et al. 1981). The second, less-widespread and less-studied suite is named the

Simpson Range plutonic suite (SRPS) after its best-preserved location in the Simpson Range of southeast Yukon (Mortensen 1983), although a few other locations are documented in western Yukon and eastern Alaska (Tempelman-Kluit and Wanless 1980, Mortensen 1986). Mortensen (1983, 1986) found that unlike the 'peraluminous orthogneiss' suite, SRPS rocks have zircons with very minor inherited components, suggesting that either continental material did not constitute a large component of the SRPS magmas (Mortensen 1983, 1986, 1992a) or that zircon was almost completely assimilated by the SRPS magmas. These results could be better constrained by geochemical and tracer isotopic analysis, which up to this point, have been performed on SRPS rocks in a very limited fashion. Thus, one of the goals of this thesis is to study the trace element geochemistry as well as the Sm-Nd, Rb-Sr, Pb-Pb, and U-Pb systematics of SRPS rocks in order to get a more complete picture of SRPS magmatism, and also help to fit it into the regional picture of YT terrane magmatism at ~350 Ma. These analyses, presented in Chapter 5, have been performed on SRPS rocks found in and around the Money klippe.

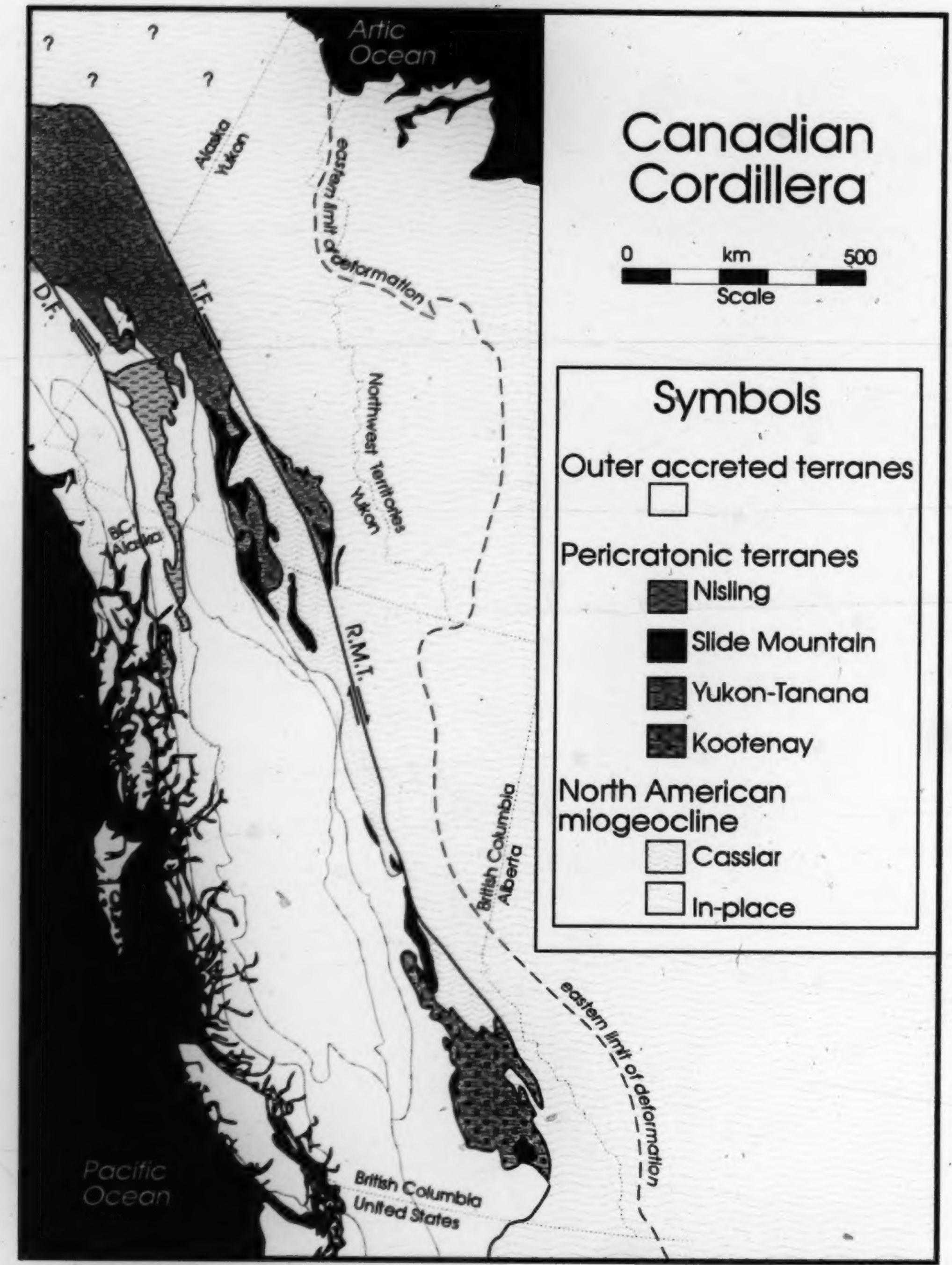

Figure 1.1 Simplified map of the Canadian Cordillera. The YT terrane and the Kootenay terrane (shaded), occupy the position between true North American miogeocline (wavy lines), including the displaced Cassiar terrane, and accreted terranes with more exotic origins. T.F. = Tintina Fault, R.M.T. = Rocky Mountain Trench, D.F. = Denali Fault. Modified from Wheeler and McFreely (1991), Coney (1989), Monger (1984, 1992), Monger et al. (1982) and Mortensen (1992).

# CHAPTER 2. BACKGROUND AND GEOLOGY

## 2.1 TECTONIC FRAMEWORK OF THE NORTHERN CORDILLERA TERRANES

### *Cordilleran overview*

The Canadian Cordillera is composed of five morphogeological belts (Fig. 2.1); two of these, the Omineca and Coast Belts, contain metamorphic and plutonic rock that contrast strongly with the Foreland, Intermontane, and Insular Belts, which are low grade to unmetamorphosed. Whereas the Foreland Belt is composed exclusively of deformed North American craton and passive margin sequences, the remaining four belts contain fault-bound lithostratigraphic assemblages difficult to correlate to each other (Coney et al. 1980, Coney 1989, Monger et al. 1982, Monger 1984) and sometimes to the craton (Fig. 2.1). These fault-bound assemblages, or 'terranes', are referred to as 'suspect terranes', because the paleogeographic origins of terranes are often uncertain; or 'accreted terranes' because they have been tectonically added to the margin of the craton (Coney 1989). Terranes preserve widely different types of crust (Fig. 2.1). Some preserve crust that has close affinity with ocean floor and related sediments (Slide Mountain, Cache Creek), whereas others record plutonism, volcanism, and sedimentation suggesting formation in an arc setting (Quesnellia, Stikinia, Alexander, Wrangellia, YT) (Coney et al. 1980, Monger 1984). However, not all fault-bound terranes have strata foreign to North America; for example, the Cassiar terrane of Yukon Territory and British Columbia contains North American miogeoclinal rocks (Monger 1984, Coney 1989) that have been displaced parallel to the edge of North America by 450 km of dextral movement on the Tintina Fault (Tempelman-Kluit et al. 1976). Other terranes, such as the YT and Kootenay terranes, are compositionally and isotopically similar to passive margin sequences. However, unlike the miogeocline, they also experienced Paleozoic and Mesozoic plutonism and metamorphism, which suggests that they evolved as distal portions of the craton, and are therefore called 'pericratonic' terranes (Monger 1992). Because some part of the history of the YT and Kootenay terranes diverges from that of the craton, they still may in some sense be considered 'suspect' terranes.

Generally, eastern terranes are considered to have “docked” first, whereas western terranes docked later. However, it is not necessarily the case that terranes docked one by one against North America. There is evidence that terranes may have first assembled into larger composite terranes, or ‘superterranes’, before finally colliding with the western margin of North America. For instance, many workers adhere to the idea proposed by Monger et al. (1982) and Monger (1984) that terranes of the Intermontane Belt (Stikinia, Cache Creek, Quesnellia, Slide Mountain, YT) assembled into a coherent crustal block (the ‘Intermontane Superterrane’) before colliding with North America during the Jurassic. The ‘Insular Superterrane’, constructed from terranes now found in the Insular Belt (Alexander, Wrangellia), collided in the Cretaceous with the eastern edge of the Intermontane Superterrane, which by that time had already docked with North America. The metamorphic-plutonic Omineca and Coast belts may represent ‘tectonic welts’ that sutured the Intermontane Superterrane to the Foreland Belt of the craton, and the Insular Superterrane to the Intermontane Belt, respectively (Monger et al. 1982; Monger 1984). Other models, some of which are examined below, suggest different relationships between terranes (eg. Wernicke and Klepacki 1988, Nelson and Mihalynuk 1993, Rubin et al. 1991). The YT terrane, one of the easternmost terranes in the Cordillera, is of particular interest because it marks the transition from passive margin to active magmatism and tectonism. The following two sub-sections will examine the relationship of the YT terrane to North America and to nearby terranes of the Omineca and Intermontane Belts and parts of the Coast belt; more outboard terranes contained in the Insular Belt and the majority of the Coast Belt will not be discussed in detail.

### *Relation of the YT terrane to North America and pericratonic terranes*

In eastern Alaska, the YT terrane underlies much of the Yukon-Tanana uplands (Fig. 2.1), for which the terrane was named (Coney et al. 1980). The width of the terrane decreases as it extends southeastward into the Yukon, until it reaches a highly deformed, north-south trending, steeply dipping shear zone in its narrowest portion located roughly 60 km northeast of Whitehorse, called the Teslin tectonic zone (TTZ) (Stevens 1994). Between the TTZ and Northern British Columbia, the YT terrane occurs as discontinuous bodies, closely associated with mafic bodies correlated to the Slide Mountain terrane (Wheeler et al. 1991). North of the Tintina fault in southeast Yukon, a narrow ~350 km long portion of the YT terrane has been separated from the YT main body by 450 km of dextral displacement (Tempelman-Kluit et al. 1976). Everywhere else, the YT terrane occurs south of the Tintina Fault. The YT terrane may have correlatives further to the south as well. The pericratonic Kootenay terrane in southeastern British Columbia shares similarities with the YT terrane, prompting Wheeler et al. (1991) to redesignate the YT terrane as the 'Nisutlin subterrane' of the Kootenay terrane (Fig. 2.1).

The Nisling terrane, straddling the boundary between the Omineca and Coast Belts (Fig. 2.1), consists of the lower Nisling assemblage and the upper Nasina assemblage (Wheeler and McFreely 1991, Mortensen 1992b). The Nisling assemblage contains mica-schist, phyllite, micaceous quartzite, minor chloritic schist, gabbro, and marble. The Nasina assemblage is composed of carbonaceous quartzite, quartz muscovite schist, mafic metavolcanic rock, metagabbro, marble, and rare stretched pebble conglomerate (Wheeler and McFreely 1991, Mortensen 1992b). The 'main body' of the deformed and metamorphosed Nisling terrane, formerly called the Tracy Arm terrane (Coney et al. 1980), generally rests outboard of the Stikinia terrane in northwestern British Columbia and southwest Yukon (Fig. 2.2). The exact nature of the YT-Nisling boundary is obscure (Coney 1989) and there is disagreement over which rocks belong in the YT terrane and which belong in the Nisling terrane. Wheeler and McFreely (1991) propose that the Nisling terrane contains not only those 'main body' Nisling terrane rocks outboard of the Stikinia terrane, but also a wide swath of rock in west-central Yukon normally assigned to the YT terrane (Fig. 2.2). Alternatively, some publications (Fig. 1 of Samson et al. 1991) allocate most Nisling terrane rocks into the YT terrane or combine the two into the 'Yukon Tanana and Nisling terranes' (Nokleberg et al. 1994, Boghossian et al. 1996). This discrepancy reflects the similarity between the YT and Nisling terranes with respect to lithology, metamorphism and state of deformation, which may point to their equivalence (Mortensen 1992b). The Nisling and Nasina assemblages of the Nisling terrane may correlate with the 'Lower Unit' and 'Middle Unit' (respectively) of the YT

'Layered Metamorphic Sequence' (Mortensen 1992b; see below). The convention followed in this thesis will be to apply the term 'Nisling terrane' to the 'main body' of the Nisling terrane outboard of the Stikinia terrane (Fig. 2.2), while recognizing that the exact nature of the relationship between the YT and Nisling terranes is unresolved. Regardless of whether the Nisling terrane is or is not correlatable with the YT terrane, the existence of a terrane with strong continental affinity outboard of oceanic arc and ocean-floor terranes remains a problem.

Mafic rock bodies, often correlated to the Slide Mountain (SM) terrane (Monger 1984, Wheeler et al. 1991, Mortensen 1992a,b), share a close association with the YT terrane, occurring as fault-bound panels that are structurally interleaved with (or resting as klippen upon) YT terrane rocks (Fig. 2.2). Whereas some of these mafic rocks correlate well to the oceanic floor assemblages comprising the SM terrane or Anvil assemblage (Plint and Gordon 1997), not all do (Creaser et al. 1997a); however, the SM designation will be used for the remainder of Section 2.1 for simplicity (see Section 2.2 for discussion of the 'Slide Mountain' and 'Anvil assemblage' terminology). The SM terrane, as defined by Monger (1984), contains intermediate to ultramafic plutonic and volcanic rocks with associated sedimentary rocks. Fossil and isotopic ages range from latest Devonian to Early Permian (Mortensen 1992a).

Although Middle-Cretaceous to Early-Tertiary strike-slip motion on the Tintina fault has modified the original accretionary fault between the YT terrane and North America (Tempelman-Kluit et al. 1976), the Teslin tectonic zone (TTZ) in south central Yukon and the Finlayson Lake fault zone (FLFZ) in southeast Yukon (Fig. 2.2) are believed to preserve contact relationships between the two crustal blocks (eg. Tempelman-Kluit 1979; Erdmer 1985; Hansen 1988, 1989; Mortensen 1983, 1992b; Mortensen and Jilson (1985). The TTZ, a name proposed by Stevens (1994) and Stevens et al. (1996) to replace the previous, more genetic, 'Teslin suture zone' (eg.: Tempelman-Kluit 1979, Erdmer 1985, Hansen 1988, Mortensen 1992b), is a zone of steeply dipping fault-bound lenses of highly strained YT and SM terrane rocks. Rocks within the TTZ are directly juxtaposed by steep faults against the Cassiar terrane, a displaced fragment of the

North American miogeocline (Wheeler et al. 1991). Cassiar terrane rocks show minor amounts of deformation, in contrast to the highly strained and metamorphosed YT and SM terrane rocks. Eclogite crops out at several localities along the northeastern edge of the combined YT and SM terranes in the TTZ and the FLFZ (eg. Erdmer and Helmstaedt 1983, Erdmer 1987, 1992). That the apparent hanging wall block should contain assemblages of high-pressure metamorphic origin implies that this is a major crustal break (Mortensen 1983).

Foliations in cataclasite of the SM and YT terranes progressively shallow as the TTZ widens to the north (Tempelman-Kluit 1979). Throughout much of the YT and SM terranes, fabrics are shallowly dipping. In places, flat-lying klippen of allochthonous SM terrane rocks rest directly on autochthonous North America (Tempelman-Kluit 1979, Mortensen 1983, Hansen 1988). These observations led Tempelman-Kluit (1979) to suggest that the TTZ is the steeply dipping root zone from which thin allochthonous sheets were thrust in a northeastward direction over North America during collision of North America with an arc assemblage (Stikinia). Hansen (1988, 1989, 1990, 1991) and Hansen et al. (1989, 1991), noting that TTZ lineations record both dip-slip and strike-slip motion, modified the collision model of Tempelman-Kluit (1979) by proposing that the TTZ is a dextrally transpressive margin caused by oblique convergence of the YT terrane and North America. Mortensen (1992b) argues that if the YT terrane were a thin tectonic flap, then windows through the YT terrane to North America rocks below should be more abundant than actually observed.

Before the structures along the northeastern edge of the YT terrane northeast of the Tintina Fault were called the FLFZ by Mortensen (1983) (Fig. 2.2), Tempelman-Kluit (1979) believed that they represented the leading edge of the YT and SM terranes (the Yukon Cataclastic Complex) being thrust from the root zone (TTZ) to the northeast, and calculated that 175 km of craton-ward overlap occurred between Finlayson Lake rocks and the obscured northwest extension of the TTZ. However, Mortensen (1983) and Plint and Gordon (1995, 1996) proposed that the TTZ and FLFZ formed a single continuous fault zone before being dextrally offset by the Tintina fault. Mortensen (1983, 1992b) suggested that steep faults between the YT terrane and North America underlie klippen of SM in the FLFZ, although Plint and Gordon (1995, 1996) found no evidence for steep faults. Instead, the faults beneath the greenstone were found to be shallow to moderately dipping thrust faults with southeast and northwest displacements of hangingwall rocks (Plint and Gordon 1995, 1996).

### *Relations between the YT terrane and terranes of the Intermontane Belt*

Intermontane Belt terranes crop out on the southwest margin of the YT terrane (Fig. 2.1; Fig. 2.2). In Yukon and British Columbia, the prominent terranes are from east to west, the Quesnellia, Cache Creek, Stikinia, and Nisling terranes. The Quesnellia terrane, lying directly outboard of the Kootenay and Cassiar terranes in British Columbia and Yukon (Fig. 2.1), is composed of a Late Paleozoic - Early Mesozoic arc assemblage that contains Permian McCloud-type fossils (Wernicke and Klepacki 1988, Coney 1989). The Quesnellia arc terrane was probably built on oceanic substrate (Coney 1989, Mortimer 1986, 1987); however, there is evidence to suggest that the Quesnellia terrane was part of a fringing volcanic arc adjacent to western North America in Mesozoic time (Coney 1989, Wernicke and Klepacki). For instance, clasts interpreted to be from the pericratonic Kootenay terrane of southern British Columbia are locally contained within the Carboniferous Quesnellia terrane strata (Wernicke and Klepacki 1988).

The boundary of the Cache Creek terrane with the Quesnellia terrane is a large dextral strike-slip fault, along which several hundred kilometres of movement occurred from Jurassic to Cretaceous times (Coney 1989). The Cache Creek terrane (Fig. 2.1) contains sedimentary and volcanic ocean floor and plateau assemblages (Nelson and Mihalynuk 1993) whose rock types include: argillite, radiolarian chert, pillow basalt, reefoid limestones, and Alpine-type ultramafics (Monger 1977, Miller 1987, Coney 1989). Fossil assemblages of the Cache Creek terrane are dominantly Late Paleozoic to Early Mesozoic Tethyan fauna (Monger and Ross 1971), implying a large degree of transport (Jackson et al. 1991) between the place of deposition and its place of docking.

Outboard of the Cache Creek terrane lies the Stikinia terrane, which is the largest suspect terrane in the Canadian Cordillera (Fig. 2.1). These two terranes may be depositionally tied by Middle Jurassic time; subsequently, the Stikinia terrane was thrust to the southwest over the Cache Creek terrane (Coney 1989). The Stikinia terrane is composed of Triassic to Jurassic arc assemblages built on older Paleozoic arcs (Monger 1977, Coney 1989). Permian limestones from the sequence contain McCloud-type faunas (Stevens and Rycerski 1989). Generally, the substrate of the Stikinia terrane is believed to have been oceanic (Samson et al. 1989). However, evidence from some localities indicates that the Stikinia terrane may share links with the more crustally influenced Nisling and YT terranes to the north and west. For instance, Johnston and Erdmer (1995) suggest that the lower Jurassic Aishihik batholith, long known to intrude the Stikinia terrane, intrudes the Nisling terrane as well. Also, clasts from upper Triassic units within the Stikinia terrane share lithologic and Nd-isotopic similarities to rocks of the Nisling terrane (Jackson et al. 1991). These ties suggest that the Stikinia and Nisling terranes were 'joined' by latest Jurassic time.

The Stikinia terrane shares many similarities with the Quesnellia terrane. Both contain Mesozoic arcs built on Paleozoic arc assemblages. The types of volcanic rock in each are very similar in composition, and both contain McCloud-type fauna. The Quesnellia and Stikinia volcanic arc terranes are separated by the ocean-floor sequences of the Cache Creek terrane. In contrast to the YT and Nisling terranes, which in part also contain arc assemblages (e.g. Coney 1989, Mortensen 1992b), the Stikinia and Quesnellia terrane rocks typically have isotopic characteristics indicating that they are primarily mantle-derived. For instance, the majority of the Stikinia terrane has positive εNd values (Samson et. al. 1989) and the Quesnellia terrane has low initial $^{87}Sr/^{86}Sr$ (0.7025 to 0.7046) (Preto et al. 1979). Some studies, however have revealed inherited zircon component in Jurassic plutons of the Stikinia terrane (Bevier and Anderson 1991; Thorkelson et al. 1995), suggesting that it may in part be built on continental crust. Both the Quesnellia and Stikinia terranes also have ties that link them to the YT, Kootenay and Nisling terranes.

Two contrasting Permian fossil assemblages are contained in the Intermontane Belt terranes. The first fossil assemblage is defined by Tethyan fusilinids, corals, and conodonts and is contained in the Cache Creek terrane and several other related terranes in the western United States (Miller 1987, Coney 1989). This fauna was apparently widespread in the paleo-Pacific Tethys ocean and is well represented in Permian rocks of Japan, China, and Indonesia (Monger and Ross 1971, Monger 1977). The presence of Tethyan fauna in the Cache Creek terrane has led many workers to suggest that it is exotic with respect to North America.

The second major faunal assemblage in the Cordillera is the McCloud fauna, which is contained within Late Paleozoic arc assemblages of the Quesnellia, Stikinia, and other terranes in the western United States (Miller 1987, Wernicke and Klepacki 1988, and Nelson and Mihalynuk 1993). Most of these terranes, with the exception of the Stikinia terrane, have evidence linking them, at least in-part, to North America (Rubin et al. 1991). The McCloud fauna is not well constrained with respect to paleolatitude; however, paleomagnetic data for these terranes do not conflict with those of North America at the time of their formation (Miller 1987). Collectively, these Paleozoic and Mesozoic arc terranes containing McCloud fauna assemblages are known as the 'McCloud Belt' (Miller 1987, Mortensen 1992b) and are interpreted to have been a fringing arc proximal to the western margin of North America (Miller 1987, Wernicke and Klepacki 1988, Rubin 1991, Mortensen 1992b). Increasingly, the YT and Kootenay terranes are considered to form part of the McCloud Belt despite the lack of McCloud fossils, because of the similarity of stratigraphy and timing of magmatism (Rubin et al. 1991, Mortensen 1992b). The role of the Stikinia terrane in such a fringing arc system is a matter of contention, because of its position outboard of the oceanic Cache Creek terrane (Miller 1987, Wernicke and Klepacki 1988, Nelson and Mihalynuk 1993), despite the similarity to the Quesnellia terrane in terms of timing of magmatism, lithology, and fossil assemblages.

Any model that attempts to explain the present distribution of 'inner' terranes must contend with the following evidence, summarized from above: (1) The YT and Nisling terranes, interpreted to be passive margin sequences, contain evidence of Paleozoic-Mesozoic magmatism, metamorphism and deformation, which is lacking or only weakly represented in the North American miogeocline; (2) the Nisling terrane, possibly correlatable to the YT terrane, is outboard of the geochemically primitive Quesnellia, Cache Creek, and Stikinia terranes; (3) the Quesnellia terrane, and possibly the Kootenay and YT terranes, are similar in stratigraphy and timing of magmatism to McCloud Belt arcs in the western United States; (4) the southern part of the Quesnellia terrane may have ties to the miogeocline; (5) the Stikinia terrane, similar in lithology, faunal assemblages, overall stratigraphy, and timing of magmatism to the Quesnellia terrane, is outboard of the Cache Creek terrane; and (6) the Stikinia terrane may have ties to the Nisling terrane. This may be condensed into two main problems. Firstly, the strongly continentally-influenced Nisling and/or YT terrane is outboard of accreted terranes that are largely mantle-derived. Secondly, the Stikinia terrane shares many similarities to the Quesnellia terrane and the McCloud belt, but is separated from them by the Cache Creek terrane.

Models that deal with the first problem may assume that the portion of the Nisling/YT terrane outboard of the Stikinia terrane is either in-situ or transported. If it is in-place passive margin, then it remains to be explained why the Nisling and YT terranes, unlike the "true" miogeocline, are intruded and metamorphosed; and some mechanism must be suggested for placing the Stikinia, Cache Creek and Quesnellia terranes in-board of the Nisling terrane. This latter point has been addressed by the suggestion that the Stikinia and possibly the Cache Creek terranes were thrust eastward over the Nisling terrane (Coney 1989, Samson et al. 1991). Timing constraints make this scenario unlikely, however (Nelson and Mihalynuk 1993). Another possibility is that the Nisling terrane is a rifted passive-margin fragment from elsewhere in North America (or alternatively, from a foreign craton), transported and accreted to its present position outboard of the Stikinia terrane by Late-Triassic time (Samson et al. 1991). This model suggests that the Nisling terrane has a different pre-Triassic tectonic history than North America, which would allow for the Nisling terrane to have acquired the extensive magmatic and deformational features not present in North America. The model does not explain, however, how the YT terrane, which is in-board of the Intermontane Belt, acquired similar magmatic and deformational features.

The second main problem, which concerns the relationship between the Stikinia terrane and the McCloud belt remains to be discussed. It is possible that the age and lithologic similarities of the Stikinia terrane to the McCloud Belt rocks are coincidental, and that the Stikinia terrane is not related to them. This view is expressed by Coney (1989), who suggests that the Quesnellia terrane had close ties to the craton whereas the Stikinia and Cache Creek terranes were thrust over the in-place Nisling terrane to their present location. If, however, the Stikinia terrane represents a displaced portion of the McCloud belt, then its displacement must be explained. It has been suggested that the Stikinia terrane formed part of a once-continuous fringing arc off the western margin of North America, but has subsequently been displaced northward by dextral transcurrent faulting, or by extrusion northward following an oblique collision of Wrangelia with the arc (Wernicke and Klepacki 1988).

Another model suggests that the Stikinia and Quesnellia terranes, west and east flanking segments of a south-facing arc proximal to the western margin of North America during Early- to Middle- Mesozoic time, folded oroclinally and enclosed the Cache Creek terrane (Nelson and Mihalynuk 1993). In this model, the central portion of the arc was built over (rifted?) passive margin sequences, represented by the basement of the YT and Nisling terranes, whereas the flanking arms (Stikinia and Quesnellia terranes) were built on oceanic floor. As the Cache Creek oceanic floor subducted to the northeast under this arc, oceanic plateaus collided with and deformed and indented the central portion of the arc, causing the flanking segments of the arc to rotate inwards, eventually enclosing the Cache Creek oceanic terrane. The amalgamated assemblage accreted to the edge of North America by the Middle Jurassic (Nelson and Mihalynuk 1993). This model explains the problematical position of the Nisling terrane outboard of the Stikinia terrane and the placement of the Stikinia terrane outboard of the Cache Creek terrane. The model also explains the plutonism and deformation of the YT and Nisling terranes, which otherwise shares many similarities to the North American miogeocline, and apparent links that the broadly juvenile Stikinia and Quesnellia terranes share with the Nisling and YT (and Kootenay) terranes. While this model is somewhat speculative, it indicates that a Paleozoic arc system was adjacent to the North American margin, which is generally similar to the McCloud belt 'fringing' arc model (eg. Rubin et al. 1991).

## 2.2 REGIONAL GEOLOGY OF THE YT TERRANE

### *Previous work*

The bulk of the YT terrane contains two main components: a metamorphosed and deformed sedimentary - volcanic assemblage and numerous plutonic and volcanic bodies Fig. 2.2). Various subdivision schemes have been suggested for the YT terrane. Tempelman-Kluit et al. (1975, 1976) and Tempelman-Kluit (1976, 1977a,b) mapped a large area of the YT terrane (then the Yukon Crystalline Terrane) and described a structural sequence containing three allochthons, which together comprise the Yukon Cataclastic Complex (Tempelman-Kluit 1979), a term that has been superseded by "Yukon Tanana terrane" (Coney et al. 1980). The sequence includes, from bottom to top, the Nisutlin Allochthon, composed of metasedimentary and metavolcanic schist; the Anvil Allochthon, represented by mafic igneous and related sedimentary ocean floor assemblages; and the Simpson Allochthon, composed of intermediate to felsic Devonian-Mississippian plutons and related (sub-) volcanic rock (Tempelman-Kluit 1979). The Nisutlin Allochthon incorporates the 'schist-gneiss' unit (Tempelman-Kluit 1976), believed to contain both metasedimentary and meta-igneous rocks; and the Klondike Schist (McConnell 1905), which is predominantly meta-igneous (Tempelman-Kluit 1976). In southeast Yukon, Tempelman-Kluit (1977a) divided the Klondike Schist into five main groups (see Section 2.3)

Subsequent mapping by Mortensen (1983) and Mortensen and Jilson (1985) suggested that the structural sequence is more complicated than the three-allochthon model of Tempelman-Kluit (1979) and recognized six packages of rock. Three of these packages: the 'Layered Metamorphic Sequence', 'Mafic and Ultramafic Rocks', and

'Paleozoic Metaplutonic Rocks' make up the bulk of the YT terrane and are roughly correlatable to the Nisutlin, Anvil, and Simpson Allochthons, respectively, of Tempelman-Kluit (1979). The Layered Metamorphic Sequence, interpreted to be transposed stratigraphy, is divided into the Lower Unit, Middle Unit, and Upper Unit (see Section 2.3) The 'Paleozoic Metaplutonic Rocks' unit contains the Simpson Range plutonic suite (synonymous with the Simpson Allochthon) as well as the previously unrecognized 'augen orthogneiss' and 'monzonitic orthogneiss' units, collectively called the 'peraluminous orthogneiss' for the remainder of the thesis (Fig. 2.2). Following the practice of Monger (1984), Mortensen (1992a,b) grouped the 'Mafic and Ultramafic Rocks' unit (Mortensen and Jilson 1985) with the Slide Mountain terrane (Fig. 2.2). Mortensen (1992b) further characterized magmatic events in the YT terrane by identifying three distinct plutonic episodes, represented by the Devonian-Mississippian SRPS and peraluminous orthogneiss, the Permian Sulphur Creek orthogneiss, and various Late Triassic to Middle Jurassic plutons.

Hansen (1990) and Hansen et al. (1991), primarily working in the Teslin tectonic zone (TTZ) take subdivision a step further and suggest that the YT terrane is a composite terrane containing upper and lower crustal blocks recording significantly different metamorphic and deformational histories. The lower block, called the 'orthogneiss assemblage' is composed of peraluminous orthogneiss and host metasedimentary rocks. The 'orthogneiss assemblage', correlatable to the peraluminous orthogneiss described by Mortensen (1983, 1992b) and Mortensen and Jilson (1985) represents parautochthonous North American strata that are interpreted to have been exhumed slowly during the Late Jurassic and Middle Cretaceous based on $^{40}$Ar/$^{39}$Ar thermochronology. The upper block, containing the remaining portion of the YT terrane (and the Slide Mountain terrane), represents material thrust over the western margin of North America and records fast cooling during the Early Jurassic. The YT terrane portion of the upper block is divided into Nisutlin and Teslin-Taylor Mountain terranes (Hansen et al. 1991). Quartz-rich schist makes up the bulk of the Nisutlin terrane, which Hansen et al. (1991) correlate to the Nisutlin allochthon of Tempelman-Kluit (1979). The Teslin-Taylor Mountain terrane, composed of mafic to ultramafic igneous rock and related sediments, is equivalent to the Slide Mountain terrane. Hansen (1990) and Hansen et al. (1991) also suggest that the Teslin-Taylor Mountain terrane hosts the Simpson Range plutonic suite.

Stevens et al. (1996) subdivided the YT terrane in another manner, based on studies in the Teslin tectonic zone. Two broad packages are suggested: the Nisutlin assemblage and the Anvil assemblage. The Nisutlin assemblage is further subdivided into siliceous schist/quartzite and graphitic phyllite units, both of which Stevens et al. (1996) correlate with the Middle Unit of the Layered Metamorphic Sequence of Mortensen and Jilson (1985) and Mortensen (1992b). The Anvil assemblage contains dioritic to gabbroic rocks and mafic schist (Stevens et al. 1996), and perhaps is correlative to the 'Middle Unit' of the Layered Metamorphic Sequence of Mortensen and Jilson (1985). Depositional and intrusive relationships indicate that the Nisutlin assemblage formed a coherent crustal block by Early Mississippian time (Stevens et al. 1996).

Metamorphism of the YT terrane north of the Tintina Fault is mostly greenschist to lower amphibolite facies, although locally some assemblages record sillimanite grade metamorphism (Mortensen and Jilson 1985). Similarly, quartz microstructures in the allochthonous assemblages imply a minimum of 350°C and 15 km depth (Erdmer 1985).

### *Terminology*

For rocks occurring in the field area, the terms 'Nisutlin assemblage', 'Anvil assemblage', and 'Simpson Range plutonic suite' (SRPS) will refer to the micaceous quartzofeldspathic schist, the mafic metavolcanic rock, and the felsic plutonic rocks (excepting the peraluminous orthogneiss) respectively, throughout the remainder of this text. The terms 'Nisutlin assemblage' and 'Anvil assemblage' have been advocated by Stevens (1994) and Stevens et al. (1996) and closely follow the usage of Tempelman-Kluit (1979). While 'Slide Mountain' is widely used in literature, 'Anvil assemblage' is preferred for the Money Klippe area for reasons discussed below. The designation 'Simpson Range plutonic suite' has found wide use in the literature (eg. Mortensen 1983, 1992b, Coney 1989, Stevens et al. 1996).

The 'Slide Mountain' and 'Anvil' terms can be confusing. Mafic and ultramafic rocks of the YT terrane have been referred to as the 'Anvil allochthon' by Tempelman-Kluit (1979). This usage was retained by Erdmer (1985), but Mortensen (1983) and Mortensen and Jilson (1985) grouped the majority of these rocks into the 'Mafic and Ultramafic Rocks' unit. Monger (1984) correlated these rocks with the Slide Mountain terrane of British Columbia, a convention that most subsequent authors have followed (eg. Mortensen 1992a,b, Wheeler et al. 1991, Rubin et al. 1991, Nokleberg et al. 1994). Hansen et al. (1991) grouped mafic igneous rocks of the YT terrane near the Teslin tectonic zone into the 'Teslin Taylor Mountain terrane', but suggested that these were correlatable with Slide Mountain terrane rocks found outside of the YT terrane. Stevens (1994) and Stevens et al. (1996), however, designate mafic Teslin Tectonic zone rocks as the 'Anvil assemblage' and correlate them with volcanic interbeds of the Middle Unit of the Layered Metamorphic Sequence of Mortensen and Jilson (1985) and suggest that there is little evidence to support grouping these rocks into other terranes. Furthermore, Mortensen (1992b) also makes the suggestion that not all rocks grouped as Slide Mountain terrane are in fact related. He suggests that those rocks that lie as klippen near or on the contact between YT terrane and the autochthon are correlatable to the Slide Mountain as defined in southern British Columbia, but that mafic bodies imbricated elsewhere within the YT terrane may be unrelated to the SM terrane. Preliminary evidence, summarized below, may support this argument. Plint and Gordon (1997) show that mafic bodies associated with the YT terrane - North America boundary in the Campbell Range have MORB-like geochemical characteristics, whereas Creaser et al. (1997a) demonstrate that Anvil assemblage tectonites from the TTZ have rare-earth element (REE) and incompatible element patterns characteristic of calc-alkalic volcanic arc basalt. This suggests that Anvil assemblage rocks from the TTZ may not be correlatable to the SM terrane rocks from southeastern British Columbia (Creaser et al. 1997a) (see discussion in Section 4.3).

## 2.3 GEOLOGY IN THE VICINITY OF THE MONEY KLIPPE

### *Location*

The field area covers a portion of the YT terrane rocks between the Tintina Fault and the Robert Campbell Highway (Highway 4), roughly equidistant between Watson Lake and Ross River in east-southeast Yukon (Fig. 2.3a). It is located in an upland area south of the Money Creek headwaters, northeast of Fire Lake, and (mostly) north-northwest of Waters Creek. (Fig. 2.3b). The southwest corner of the Wolverine Lake NTS 1:50000 map sheet and the northwest corner of the Waters Creek NTS 1:50000 map sheet almost completely cover the entire field area, although a small spur crosses into the northeast corner of the Fire Lake NTS 1:50000 map sheet (Fig. 2.3b). Because the nearest road, the Robert Campbell Highway, is 45 km distant at its closest approach northeast of the area, a helicopter was used to transport supplies to the base camp. Except for three stations visited on the last day by helicopter, all stations were accessed by one- to four-day hiking traverses (see Appendix 1 for field station locations). The majority of sampling and mapping was accomplished between the tree-line (~1500 m above sea-level) and the maximum elevation of roughly 2100 m above sea-level, where bare outcrop was relatively common.

### *Previous work*

The geology in the field area (Fig. 2.4) was first mapped by Wheeler et al. (1960) as two assemblages of igneous rock, together forming a roughly oval-shaped area occupying ~100 km$^2$, surrounded by micaceous quartz-rich schist. The first of the two igneous packages, occupying the southern half of the 'oval', includes granodiorite and quartz monzonite interpreted to be Middle to Late Mesozoic in age. The second package, occupying the northern side of the area, contains mafic metavolcanic rock interpreted to be Mississippian in age (Wheeler et al. 1960).

Tempelman-Kluit (1977a) mapped numerous thrust faults in southeast Yukon and indicated that the two igneous units mapped by Wheeler et al. (1960) were preserved in the field area as distinctive thrust sheets within a structure he called the Money klippe, named for its location south of the headwaters of Money Creek (Tempelman-Kluit 1979). The felsic plutonic rocks and the mafic metavolcanic rocks (the former structurally above the latter) in the field were named the 'Simpson Allochthon' and 'Anvil Allochthon', respectively. The Simpson Allochthon was assigned a Mesozoic age and the Anvil Allocthon was assigned a Late Paleozoic age, based on indirect evidence (Tempelman-Kluit 1979). The quartzofeldspathic schist, interpreted to underlie the Anvil Allochthonous Assemblage, was correlated to the Klondike Schist unit (Tempelman-Kluit 1977a) and incorporated into the Nisutlin Allochthon, the third and lowermost panel of the three- allochthon model of Tempelman-Kluit (1979). The map of Tempelman-Kluit (1977a, 1979) also included an apparently fresh composite volcanic plug, a feature not differentiated on the map of Wheeler et al. (1960). Based on similarity to other dated extrusives in the area, Tempelman-Kluit (1979) assigned a Cretaceous age to the composite plug, which he interpreted as intruding all three allochthons in the northern portion of the Money klippe.

Erdmer (1985) largely retained the terminology of Tempelman-Kluit (1979) with respect to the Money klippe area and refined the mapping of contacts and distribution of units within the klippe. An earlier publication by Erdmer (1981) indicated that the composite plug intruded the Anvil and Simpson Allochthons during the Cretaceous; further field work (summarized below) and age dates prompted Erdmer (1985) to include the composite plug with the Simpson Allochthon as a transported assemblage. Erdmer (1981) also noted that a gabbro unit, considered to be a subunit of the Anvil Assemblage, was in places thrust on top of felsic Simpson Allochthon rocks, somewhat contrary to the three-allochthon model of Tempelman-Kluit (1979). Erdmer (1981) suggests the possibility that the gabbro is a part of the Simpson Allochthon, but largely discounts the idea because serpentinite and sheared basalt are associated with the gabbro.

Mortensen (1983) obtained several igneous samples from the Money klippe for geochronology work. The composite plug unit is again given a new treatment. Mortensen suggests that the composite plug is a component of the Anvil assemblage. He suggests that the plug intruded the Anvil assemblage and was transported with it during thrusting, based on the observation that it is truncated at its base by a shallowly-dipping fault that separates it from the Nisutlin assemblage. Also, Middle-Paleozoic U-Pb zircon ages obtained for this unit show that it is a not a young post-deformational volcanic plug intruding the Money klippe as Tempelman-Kluit (1979) suggested (Mortensen 1983, 1992a). Mortensen (1983) also hints that the gabbro unit of the Anvil assemblage has a close association with the Simpson Range plutonic suite (formally the Simpson Allochthon) rocks, based on a similar U-Pb zircon ages and several intrusive relationships.

### *Relations*

In the present study, the composite plug and gabbro units are considered to belong to the SRPS (Fig. 2.4). Whereas Erdmer (1985) also includes the composite plug in the SRPS, Mortensen (1983, 1992a) considered this unit to be a part of the Anvil assemblage. Based on observations that the sheared base of the composite plug rests directly on the Nisutlin assemblage, Mortensen (1992a) suggests that the plug intruded the Anvil assemblage before thrusting and was subsequently transported with the Anvil assemblage. Erdmer (1985), however, mapped thrust faults not only between the base of the plug and underlying Nisutlin assemblage, but between the composite plug and the Anvil assemblage and the hornblende-granodiorite unit (HbGd) of the SRPS as well, putting it at a structural position more similar to the SRPS rocks. Zircon U-Pb ages of approximately 350 Ma (Mortensen 1992a; Chapter 5 of this study) and geochemistry (Chapter 5) also supports the inclusion of the composite plug with the SRPS.

The gabbro unit, formerly included with the Anvil assemblage (Erdmer 1985, Mortensen 1983), is here also included with the SRPS, based in part on observations made by Erdmer (1981) and Mortensen (1983) as outlined above, and on evidence found in the present study. For instance, at a locality near SG94-1 (Fig. 2.4), a ~10 m sill of the biotite-monzogranite unit (BtMg) of the SRPS intrudes the gabbro. At another location (SG94-8) small (<1m) dykes of BtMg intrude the gabbro. The gabbro, unlike the sheared metavolcanic unit, is largely undeformed and has similar geochemical and isotopic trends to the SRPS (see Chapter 5). In addition, the ~350 Ma age indicated by a nearly concordant U-Pb zircon analysis (Chapter 5) overlaps the age of other SRPS members (see Chapter 5).

Contacts between the igneous units within the Money klippe, where not obscured by talus or fluvial fill, are largely shallowly dipping sheared contacts. Units within the klippe are sheared and chloritized within 1 to 2 m of a contact, but are only mildly deformed (brittle cracking of grains) further away from the contact. These sheared contacts are interpreted to be thrust faults (Tempelman-Kluit 1977a, 1979, Erdmer 1981, 1985). A brief analysis of the thrust faults will be presented in Section 3.4.

Previous mappings by Erdmer (1985) and Tempelman-Kluit (1979) feature a normal fault between the sheared SRPS granodiorite south of the Money klippe and the Nisutlin assemblage on a ridge near samples SG94-34 through SG94-40 (Fig. 2.4). Mineralization in the area of the contact supports the presence of a late normal fault; however, the units repeat in the structural sequence and foliations within each of the units are parallel to each other and to their contact at this locality, which implies more complex relations between the units than simple normal faulting. The repetition of units may be the result of thrust faulting subparallel to the regional foliation. Another possible explanation for the repetition of units is by dyking of the SRPS unit into the Nisutlin assemblage before non-coaxial shear deformed the intrusive contact into parallelism with the foliation. If this is a sheared dyke of SRPS rocks (and it is not firmly established that it is) , then the age of the supracrustal Nisutlin assemblage would have a minimum age of ~350 Ma, the approximate age of the SRPS rocks as determined by U-Pb zircon geochronology. This finding echoes the better substantiated interpretation by Stevens et al. 1996 that similarly aged plutons (~350Ma) cut the fabric of the Nisutlin assemblage in the TTZ, establishing a minimum age of deposition.

A NNW-SSE normal fault cuts the planar fabric of the Nisutlin assemblage rocks to the west of the Money klippe (Tempelman-Kluit 1979, Erdmer 1985). This fault serves to separate two distinct subunits of the Nisutlin assemblage, as outlined in Section 2.4. Foliations of the schist are rotated and disturbed in the locality of the fault, and mineralization has been documented nearby (Morin 1981).

## 2.4 LITHOLOGICAL DESCRIPTIONS

### *Nisutlin assemblage*

Highly schistose Nisutlin assemblage rocks surround the Money klippe. Nisutlin assemblage rocks in the field area (Fig. 2.4), were divided into three lithological types, based on characteristics noted in the field: the mica-quartz schist (MQS), the quartz-rich phyllites (QP), and the mafic schists (MS). Handsample and thin-section descriptions are presented in Appendices 2 and 3, respectively. The MQS, the most widespread Nisutlin assemblage rock type in the area studied, crops out predominantly on the northwestern side of the Money klippe, but occurs on the south and west sides as well. Where MQS is the dominant rock type in an area, minor amphibole- and chlorite- bearing schists are frequently interbedded. The MQS rock type (Fig. 2.5) typically has 60 to 80 percent quartz, 5 to 15 percent potassium feldspar (usually both as groundmass and as fractured porphyroclasts) and 10 to 20 percent mica; amphibole, chlorite and/or plagioclase constitute a significant portion in a few samples. The groundmass is dominated by small (0.1 to 0.5 mm) interlocking quartz (and some potassium feldspar) grains that often display undulatory extinction and subgraining. Several samples also contain calcite as interstitial material. Potassium feldspar, constituting the most common porphyroclast mineral, often forms small augen, either as single crystals or as tiled aggregate masses of fractured porphyroclasts. Where present, plagioclase is usually chemically altered to sericite. Amphibole usually occurs as large masses of partially or completely disaggregated fragments. In some samples, significant chemical alteration has destroyed all but the interiors of amphibole crystals. Garnet was found in only one sample, SG94-18B, which occupies a relatively low position in the structural section. Trace minerals, such as zircon, allanite, and monazite, are present in most samples to varying degrees. Compositional bands, typically layered on the scale of 1-2 mm, and aligned mica fish or other platy minerals define the foliation. Many of the samples may be described as mylonites or phyllonites and a few samples, such as SG94-5, are blastomylonites.

The quartz-rich phyllite (QP) rock type is located on the west and southwest sides of the Money klippe (Fig. 2.4). The QP rocks are composed of 85 to 95 % quartz (small amounts of K-feldspar were also detected) (Fig. 2.6). Mica and graphite, although present in small quantities (5-15 % total), impart a slight sheen to the surfaces of these rocks. Samples that are dark as a result of high graphite content form a subset: the graphitic quartz-rich phyllite (QP-g) (Fig. 2.7). Anastomozing stylolitic fractures are a pervasive feature of these rocks (Fig.2.6 and 2.7). In areas of low stress, they are kinked and discontinuous; in areas of greater stress they form gentle shears that offset previous foliation. Graphite and mica tend to occupy these fractures. The interpretation is that quartz volume loss, caused by dissolution, once occurred at these zones and concentrated relatively insoluble minerals such as graphite and mica. Quartz grain sizes are highly variable, ranging from 0.1 to 2 mm; stylolitic fractures often serve as the boundary between areas of different quartz grain sizes. The foliation in the QP rock type is defined by the anastomozing fractures, sometimes making them less planar than foliation in the MQS samples. In the graphitic QP samples, the fractures seem to cut and transpose an earlier compositional foliation (Fig. 2.7), described near the end of this section. See also Appendices 2 and 3.

The third Nisutlin rock type sampled in the field area, the mafic schists (MS), occurs west of a NNW-trending steep normal fault on the west side of the Money klippe (Fig. 2.4). MS samples have the lowest quartz contents of the three Nisutlin rock types (10-50 %) and higher concentrations of amphibole, chlorite, and biotite (40 to 80%) (Fig. 2.8). Dark graphite-bearing phyllites were also present in this area. Foliation in the MS rocks is defined by compositional layering and alignment of chlorite, biotite and amphibole. Also see Appendices 2 and 3.

The three rock types form spatial as well as lithological groups. Figure 2.4 shows that each rock type occupies a relatively extensive, continuous area. Other rock types are sometimes interlayered with the main rock type in an area - for instance, minor amphibole-chlorite bearing schist is interlayered with the quartzofeldspathic MQS rocks-types. Within the areas sampled, however, either the MQS, QP, or MS rock type dominates. The total area from which Nisutlin assemblage rocks were sampled is small, however, so the three rock types defined in this study will be compared with more regional units defined in Tempelman-Kluit (1977a) and Mortensen and Jilson (1985). A brief review of the terminology and mapping of these studies is warranted in order to allow the samples to be put in a regional context.

Much of the area later to become the Nisutlin Allochthon was mapped as the Klondike Schist (Tempelman-Kluit 1977a, 1979). The Precambrian-Cambrian 'ꝐꞒSC' biotite-garnet-muscovite schist is possibly the autochthonous basement to the Klondike Schist (Tempelman-Kluit 1977a). The Klondike schist in southeast Yukon was divided into five subunits, prefixed with the 'Ꝑℙ' designation to indicate that they range from Precambrian to Paleozoic age. The ꝐℙK4 is predominantly a mica-rich quartzofeldspathic gneiss. This unit grades into the ꝐℙK2 and ꝐℙK3 units ; the former includes interlayered black siliceous phyllite and chlorite-amphibole phyllite; the later contains muscovite-chlorite phyllite, and amphibole chlorite phyllite (Tempelman-Kluit 1977a). The three units listed above comprise the majority of Klondike Schist exposure in SE Yukon. The remaining ꝐℙK1 and ꝐℙK5 units, occupying relatively less area, contain muscovite-quartz blastomylonite and metaquartzite, respectively.

Mortensen (1983) and Mortensen and Jilson (1985) mapped the Nisutlin assemblage rocks as the Layered Metamorphic Sequence, and divided it into three units: the Lower Unit, Middle Unit, and Upper Unit (Mortensen and Jilson 1985). The Lower Unit is composed of quartz-mica schist and micaceous feldspathic quartzite. The Middle Unit is composed of interlayered metasedimentary and metavolcanic components, each comprising roughly half of the volume of the unit. The metasedimentary component is dominated by carbonaceous siliceous phyllite and quartzite. The remaining volume of the Middle Unit contains mostly mafic metavolcanics with minor amounts of felsic metavolcanic rock. The Upper Unit, containing carbonate and quartzite, is not as areally extensive as the Lower Unit and Middle Unit (Mortensen and Jilson 1985)

The maps of Tempelman-Kluit (1977a) and Mortensen and Jilson (1985) package rock in different manners, complicating the present attempt to correlate work done in this thesis with regional observations. On the scale of the southeast Yukon, the Lower Unit of Mortensen and Jilson (1985) and the ꝐꞒSC and ꝐℙK4 units of Tempelman-Kluit (1977a) probably describe the same package of metasedimentary mica-feldspar-quartz (sporadically garnetiferous) schists. Likewise, the Middle Unit of Mortensen and Jilson (1985) and the P̲ℙK2 and P̲ℙK3 units of Tempelman-Kluit (1977a) both broadly describe the same sequence of interlayered carbonaceous siliceous phyllite (metasedimentary) and chlorite-amphibole phyllite (metavolcanic). In the field area around the Money klippe, however, the distribution of units as mapped by Tempelman-Kluit (1979) does not correspond well to that of that of Mortensen and Jilson (1985).

According to the map of Tempelman-Kluit (1977a), the P̲ℙK1 unit encompasses both MQS and QP rock types as defined in the current study, whereas the P̲ℙK2 unit coincides with the location of the MS samples. Thus, this map emphasizes the contrast between quartzofeldspathic (MQS and PS) rocks and mafic (MS) rocks. The map of Mortensen and Jilson (1985) does make the distinction between the MQS and QP rock types, mapping these as Lower Unit and Middle Unit, respectively. The presence of 1mm garnets in one MQS sample helps justify its inclusion into the Lower Unit. The map of Mortensen and Jilson (1985) does not distinguish between the dissimilar MS and the QP rock types, but instead groups them into the Middle Unit. The description of the Middle Unit, however, suggests that it comprises interlayered carbonaceous siliceous rocks and mafic volcanic rocks. Thus, MS and QP rock types may simply be contrasting interlayers (on a relatively large scale, judging by the continuity of unit in the field) of the same unit. This fact is also suggested by an outcrop of dark siliceous phyllites (SG94-84) found in the area dominated by the MS samples.

In light of the relationships outlined above, the work of Mortensen and Jilson (1985) is favoured for purposes of correlation because of better and more explicitly stated stratigraphic control for the Layered Metamorphic Sequence (Nisutlin assemblage). Also, whereas Mortensen and Jilson (1985) explicitly state that the three units of the Layered Metamorphic Sequence comprise a transposed stratigraphy, no such assurance is given for the five units of the Klondike Schist by Tempelman-Kluit (1977a). The MQS sample is tentatively correlated with the Lower Unit and the QP and MS units are correlated with the metasedimentary and metavolcanic (respectively) layers of the Middle Unit.

The high degree of mylonitization in Nisutlin assemblage rocks cropping out around the Money klippe all but precludes the observation of primary sedimentary structures, but some field evidence does suggest sedimentary origins. For instance, Tempelman-Kluit (1979) notes that muscovite-quartz schist can be traced into sandstone with interbedded slate southeast of Wolverine Lake (Fig. 2.3a). This and other similar observations have prompted Tempelman-Kluit (1979) to suggest that quartzo-feldspathic clastic rock is the protolith for the siliceous mylonite. In the Teslin Tectonic Zone, Stevens et al. (1996) describe large scale compositional layering within the Nisutlin Assemblage that can be traced for 7km, which is interpreted as a transposed sedimentary sequence. Quartz diorite intruded the sedimentary sequence at ~350 Ma ago (Stevens et al. 1996), which provides the minimum age for deposition of metasediments in the Nisutlin assemblage. Also, Mortensen and Jilson (1985) interpret the Layered Metamorphic Sequence as being a transposed stratigraphy.

A faint compositional banding, different in nature and orientation to the mylonitic foliation, was found in sample SG94-90 (Fig. 2.7). This foliation is observed in a relatively strain -free portion of the rock, where it is undissected by anastomozing, stylolitic fractures (discussed above). The foliation occurs in a quartz-rich portion of the rock and is defined by wispy, unsheared bands of graphite inclusion trails. The quartz grains have recrystallized over the bands, and are relatively equant, unstrained grains. The bands occur at a roughly 45° angle to the phyllonitic foliation of the rock, except where they can be seen to be intersected by the anastomozing fractures and bent into parallelism with the fracture. In such a fracture, the graphite is concentrated as quartz dissolves, as seen in figure 2.7. It is possible that these wispy graphitic bands represent the original bedding.

### *Anvil assemblage*

The Anvil assemblage hosts a wide variety of rock types, but because of time constraints, was one of the least sampled units in the area. The majority of Anvil rocks collected were dark green, relatively fine-grained metavolcanic rocks. These rocks were composed of chlorite, amphibole, plagioclase and quartz, for the most part. Many had large aligned amphibole phenocrysts (Fig. 2.9). These rocks generally had a weak foliation, which was more strongly developed in areas directly above the Nisutlin assemblage rocks. Serpentinites were noted in some localities (eg. SG94-74); these were generally highly fractured and contained typical serpentinite microscopic textures.

### ***Simpson Range plutonic suite***

Four main SRPS units crop out within the klippe and one unit crops out on the south side of the klippe. From structural top to bottom the units within the klippe include a composite volcanic plug, hornblende-granodiorite, biotite-monzogranite, and gabbro. SRPS rocks were also studied from the northern tip (within 2-4 km of the Money klippe) of a large block of SRPS (roughly 25 x 50 km) that extends southeastward from the Money klippe (Fig. 2.3a). The SRPS rocks from this large southeast block are more strongly deformed than those in the Money klippe and typically have granodioritic composition, although more felsic compositions have been noted as well. This unit will be termed the 'sheared-granodiorite' (Sh-Gd) for simplicity. The remainder of this section will present brief lithological descriptions of the five units found in the field area.

The hornblende granodiorite (HbGd) unit occupies the central portion of the Money klippe (Fig. 2.4). It is typically medium grained (2 to 5mm), has a moderate colour index (CI = 20 to 35), and the quartzofeldspathic component typically weathers pale yellow to pale pink, although several samples have a deep red weathering. They are composed of quartz (25 to 35 %), plagioclase (30 to 40 %), potassium feldspar (15 to 25 %), and ferromagnesian minerals (20 to 30 % - chiefly hornblende (sometimes highly chloritized) and minor biotite). Figure 2.10 shows a typical thin-section view of a HbGd sample. Much of the plagioclase, and some of the potassium feldspar, has been altered to sericite. HbGd rocks are virtually undeformed except near their contact with the biotite monzogranite, where shears and cracks are associated with increased alteration. Dark (CI = 80), ferromagnesian-rich, crystalline enclaves with slightly smaller grain size (0.5 to 1 mm) are common in the HbGd, and have relatively distinct margins; a few fine-grained, dark green, enclaves were present as well.

The biotite-monzogranite (BtMg) generally crops out around the HbGd unit within the Money klippe (Fig. 2.4). It is a relatively coarse-grained (5 to 10 mm), light coloured (CI = 5 to 15) rock. Large (5 to 20 mm) smoky-grey quartz grains, porcelain-white plagioclase (1-2 mm) phenocrysts and distinctive, peach-pink potassium feldspars (0.5 to 1 mm) are apparent in weathered surfaces. Its mineralogy primarily consists of quartz (30 - 40 %), potassium feldspar (25 to 30 %), plagioclase (25 to 30 %), and biotite ( 5 to 10 %). Figure 2.11 shows a typical thin-section view of a BtMg sample. Two samples contain large (20 mm) euhedral potassium feldspar phenocrysts. Plagioclase, and potassium feldspar to a lesser degree, have been partially altered to sericite; biotite has been altered to chlorite. Enclaves are present in some samples; most are dark, fine-grained crystalline enclaves with relatively indefinite boundaries. One sample, however, contains an enclave of what appears to be fine-grained (~1 mm) BtMg. Except near contacts with other units, deformation in the BtMg unit is limited to slight cracking and undulatory extinction in quartz grains.

The gabbro unit crops out in close association with the BtMg unit in the southern portion of the Money klippe (Fig. 2.4). The appearance of this unit is variable, because of differences in grain size and degree and type of weathering. Grain size ranges from <1 mm to 10 mm. Samples that are plagioclase-rich have a porcelain-white appearance in hand-sample. The mafic component typically weathers black or brown-green in hand-sample. The finer grained samples typically have a 'salt and pepper' appearance and an intergranular texture. The mineralogy has been strongly altered, such that little remains of the primary mineralogy, although it is evident that plagioclase once made up a large volume of this rock (Fig. 2.12). Plagioclase has in most cases been altered, but faint ghost images of the polysynthetic twinning are visible. The samples contain amphiboles, which contain dark opaque material in their cleavage planes. Common alteration products are chlorite, epidote, clinozoisite, and opaque iron rich minerals. Quartz (< 5%) was present in a few samples, and zircon was separated from a coarse-grained, plagioclase- rich, quartz-normative sample (SG94-1).

Although only a small portion of the composite plug unit (Fig. 2.4) was visited during the present study, a wide variety of rocks was encountered. Felsic members of the volcanic plug (hereafter referred to as 'FVP') include fine grained rhyolite, sometimes flow-banded, and quartz-potassium feldspar porphyry (rhyolitic composition). Phenocrysts (2 to 5 mm) in the quartz feldspar porphyry were dominantly euhedral quartz and potassium feldspar grains, which were surrounded by largely quartzofeldspathic groundmass (Fig. 2.13). Feldspars were mostly altered to sericite. This unit was used for geochemical and isotopic studies because the porphyry was one of the most voluminous rock types encountered. Mafic rocks of the composite plug (hereafter referred to as 'MVP') included fine grained black-green rocks, sometimes with small (1mm) thin altered plagioclase laths or large (2 to 5 mm) twinned augite crystals (partially altered to amphibole and chlorite) Fig. 2.14). Samples of other rocks in the composite plug have intrusive textures. For instance, at one location fine grained dark purple material injected into fine grained-light green rock, breaking it into 2 x 5 cm brick-like blocks. The plug rocks are not deformed and have a 'fresh' appearance.

The last unit to be discussed is the sheared granodiorite (Sh-Gd) unit south of the Money klippe. Deformation in this unit ranges from a weak foliation defined by incomplete parallel alignment of platy minerals to well-developed schistosity (see Chapter 3). The unit is broadly composed of quartz (30 to 40 %), plagioclase (30 to 40 %), potassium feldspar (5 to 20 %), white mica (10 to 20%), chlorite (10%), amphibole and biotite (Fig. 2.15). As in the BtMg and HbGd samples, the plagioclase is heavily sericitized. Also, chlorite likely replaced much of the original amphibole and biotite. The majority of the unit has a granodioritic composition (hence its field name) although some samples seem to have compositions more similar to the BtMg. For instance, one sample selected for geochemical and isotopic analysis (SG94-88) has 1 x 2 cm potassium feldspar porphyroclasts, a feature not found in other Sh-Gd or HbGd samples, but occasionally present in the BtMg unit.

Enclaves of various types of rock are common within the BtMg and the HbGd. Most are small ( < 5 cm), but in two locations the Bt-monzogranite contains relatively large (metre scale) enclaves of sheared metavolcanic rock. If these xenoliths represent Anvil assemblage rocks, this indicates that the SRPS suite intruded a predeformed Anvil assemblage. Some of the smaller enclaves seem to be of this type as well, but the rest appear to be cognate enclaves that are finer grained and more mafic than their host rocks. These could represent earlier crystallized portion of the same magma that produced the felsic plutonic rocks.

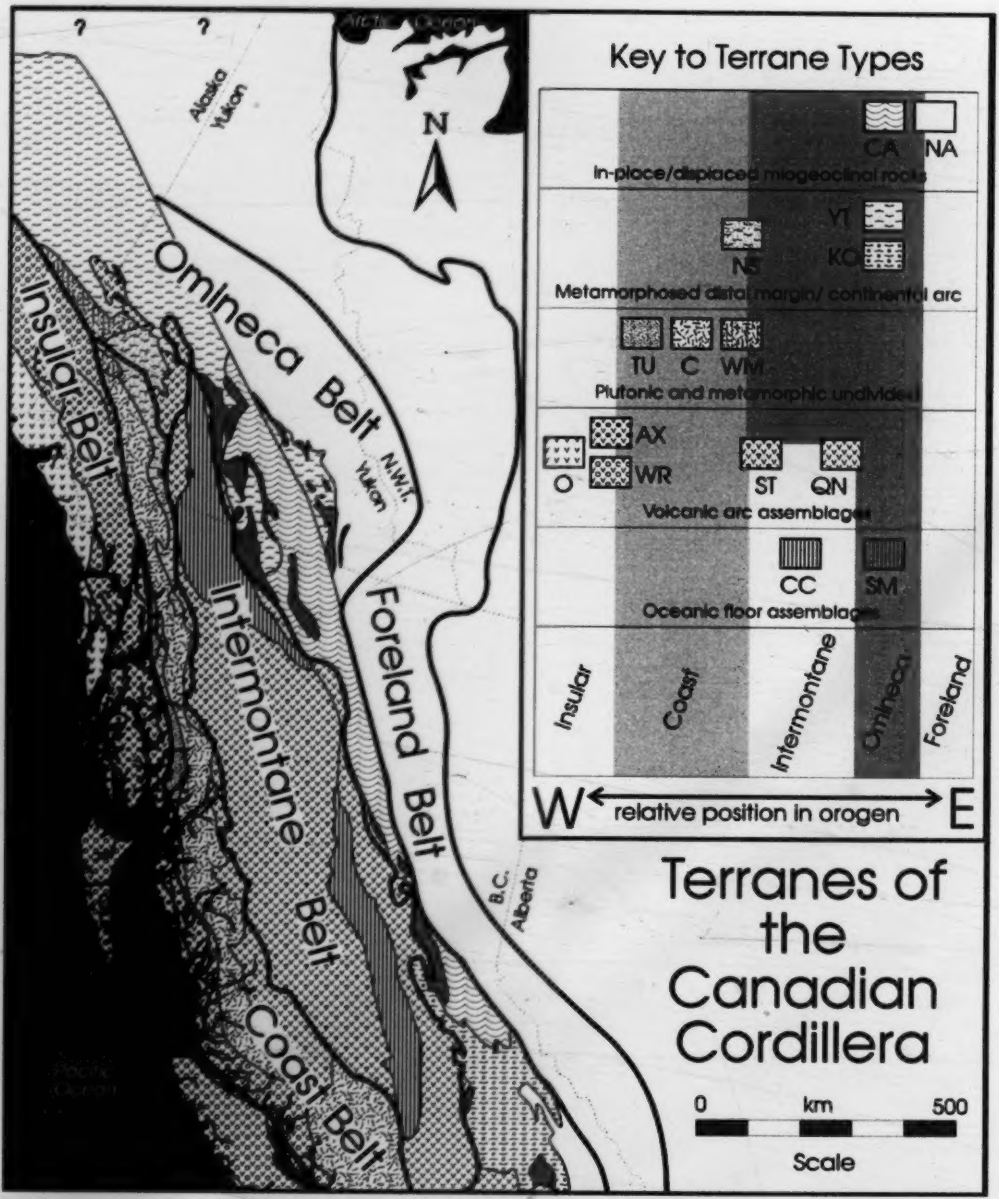

Figure 2.1. Simplified terrane map of the Canadian Cordillera. Heavy lines on the map show the borders of the five major physiogeological belts, labelled on the map. Major terranes in the Canadian segment of the Cordillera are shown on the map and indentified in the key (box in upper right) by their abbreviation (listed below). The key groups terranes according to their lithologic/tectonic affinity (horizontal rows) and according to the belts in which they belong (vertical boxes). The two shaded belts in the key represent more highly deformed and metamorphosed belts. Terranes shown include Alexander (AX), undivided metamorphic and plutonic terranes of the Coast Belt (C), Cassiar (CA), Cache Creek (CC), Kootenay (KO), Nisling (NS), undivided outer terranes of the Insular belt (O), Quesnellia (Q), Slide Mountain (SM), Stikinia (ST), Taku (TU), Wrangell (WR), Windy-McKinley (WM), and Yukon-Tanana (YT). Also shown is non-displaced ancestral North America (NA). Modified from Wheeler et al. (1991), Wheeler and McFreely (1991), Coney (1989), Monger (1984, 1992), Monger et al. (1982) and Mortensen (1992).

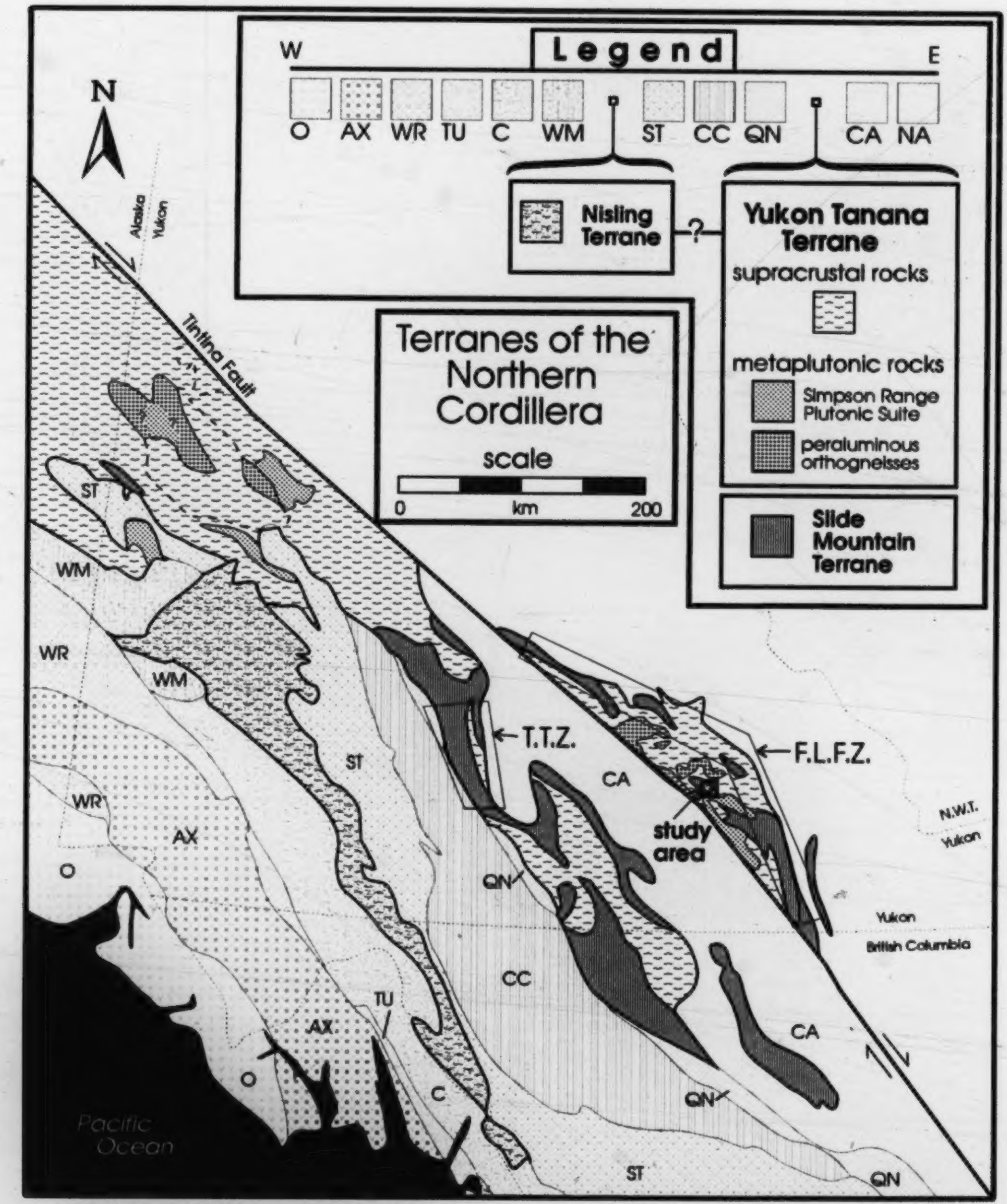

Figure 2.2. Terranes of the northern Cordillera. Boxed areas show the locations of the Teslin tectonic zone (T.T.Z.), the Finlayson Lake fault zone (F.L.F.Z.), and the study area examined during the present thesis. For simplicity, mafic bodies associated with the YT terrane are labelled on the map as SM terrane; however some of these bodies may belong to another assemblage entirely (see text). The two most voluminous componants of the YT terrane are illustrated on the map, including Devonian -Mississippian metaplutonic rocks and the deformed supracrustal assemblage. The area shown as Nisling on the map is referred to as the 'main body' of the Nisling in the text; the dashed line shows the area (here shown as YT terrane) that Wheeler et al. (1991) correlate to the Nisling terrane. The legend box (top right) shows the terranes (see Fig. 2.1 for abbreviations) arranged according to their east-west position in the orogen. The line connecting the Nisling and YT terrane boxes indicates their possible relationship. Modified from Wheeler et al. (1991), Wheeler and McFreely (1991), Coney (1989), and Mortensen (1992).

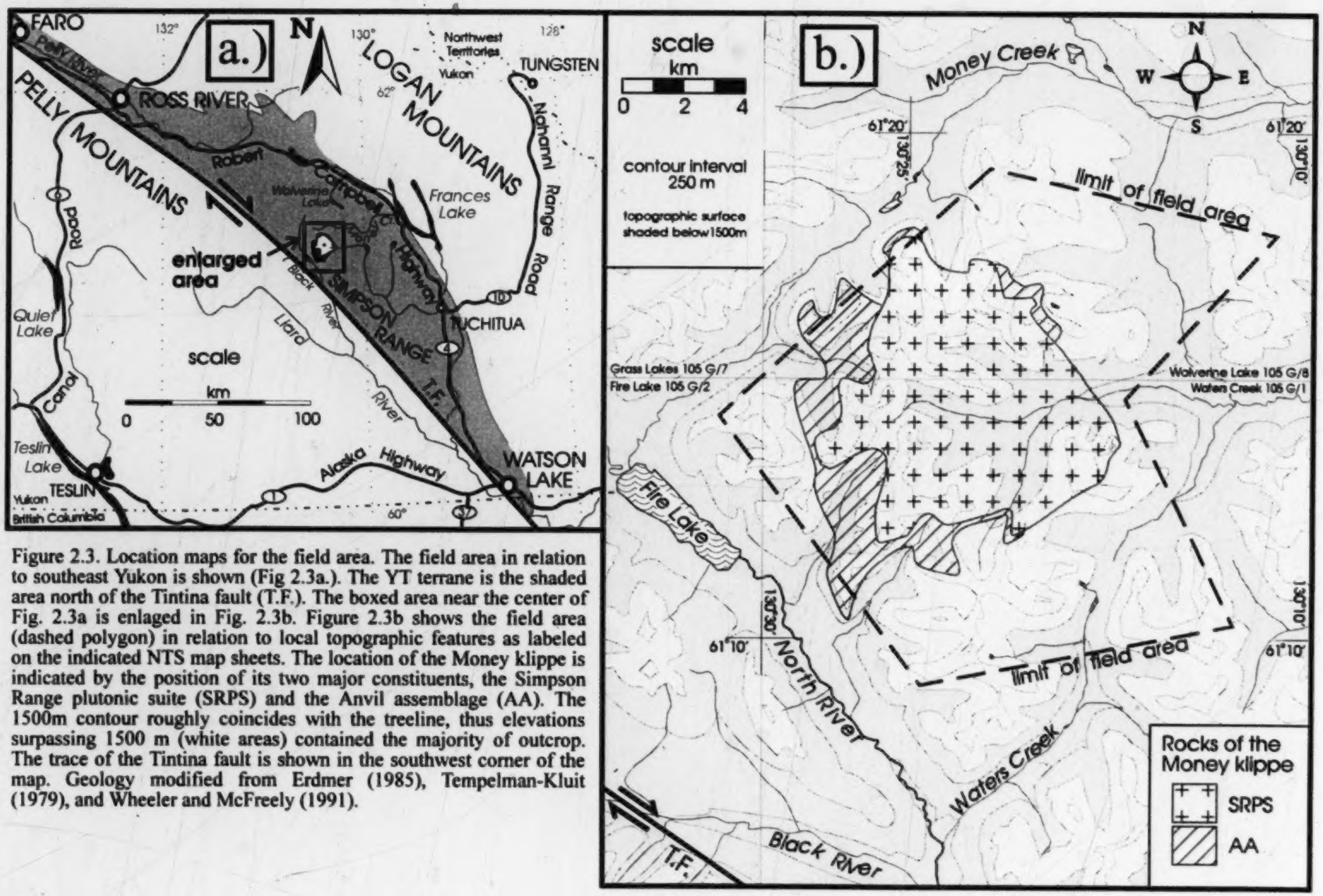

Figure 2.3. Location maps for the field area. The field area in relation to southeast Yukon is shown (Fig 2.3a.). The YT terrane is the shaded area north of the Tintina fault (T.F.). The boxed area near the center of Fig. 2.3a is enlaged in Fig. 2.3b. Figure 2.3b shows the field area (dashed polygon) in relation to local topographic features as labeled on the indicated NTS map sheets. The location of the Money klippe is indicated by the position of its two major constituents, the Simpson Range plutonic suite (SRPS) and the Anvil assemblage (AA). The 1500m contour roughly coincides with the treeline, thus elevations surpassing 1500 m (white areas) contained the majority of outcrop. The trace of the Tintina fault is shown in the southwest corner of the map. Geology modified from Erdmer (1985), Tempelman-Kluit (1979), and Wheeler and McFreely (1991).

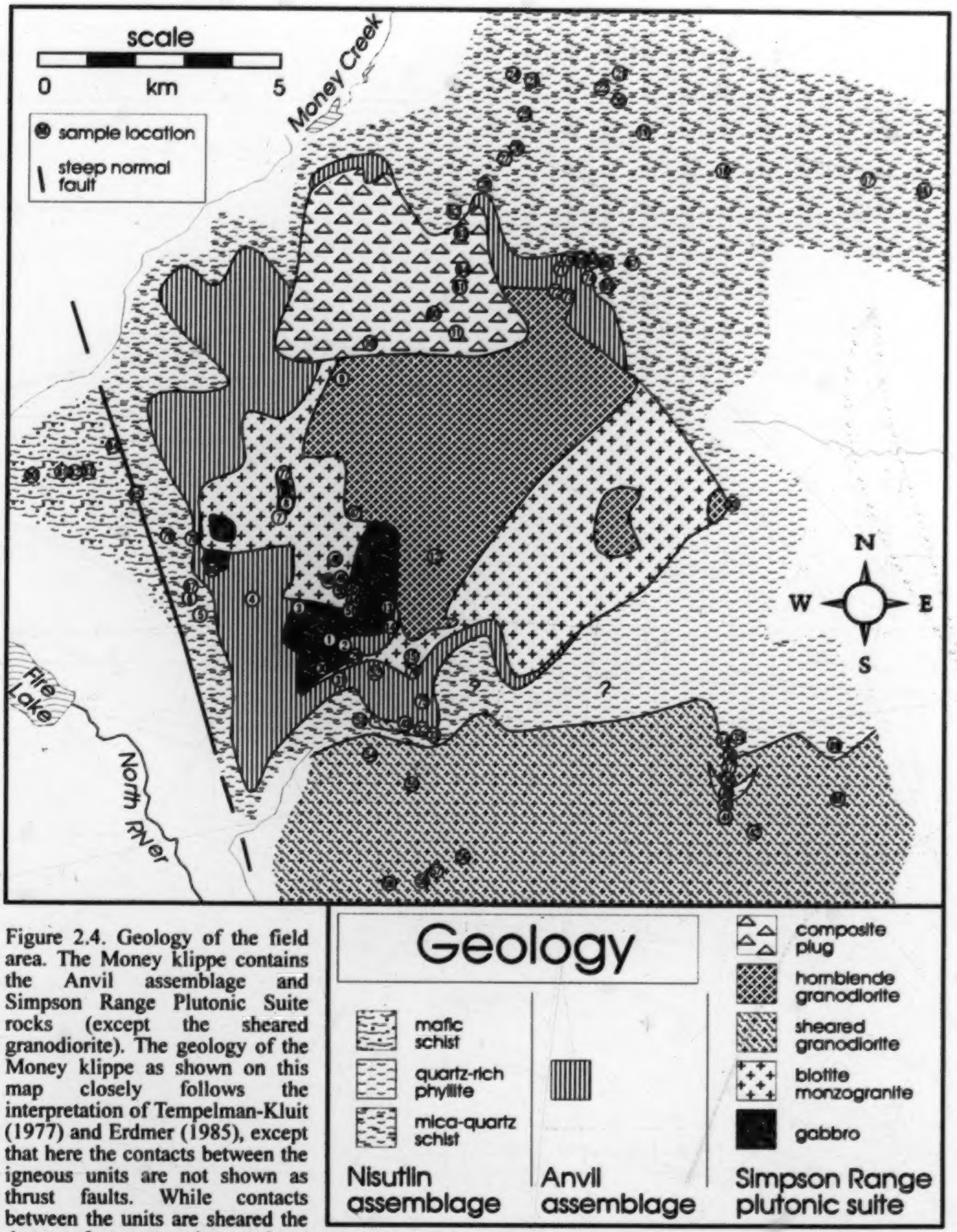

Figure 2.4. Geology of the field area. The Money klippe contains the Anvil assemblage and Simpson Range Plutonic Suite rocks (except the sheared granodiorite). The geology of the Money klippe as shown on this map closely follows the interpretation of Tempelman-Kluit (1977) and Erdmer (1985), except that here the contacts between the igneous units are not shown as thrust faults. While contacts between the units are sheared the degree of movement has not been proven to be large. The contact between the sheared granodiorite unit to the south of the Money klippe and the Nisutlin assemblage is shown to be a sheared contact rather than a steep normal fault as previously thought (Tempelman-Kluit 1977; Erdmer 1985). Contacts between the quartz-rich phyllite (QP) and the mica-quartz schist (MQS) are uncertain.

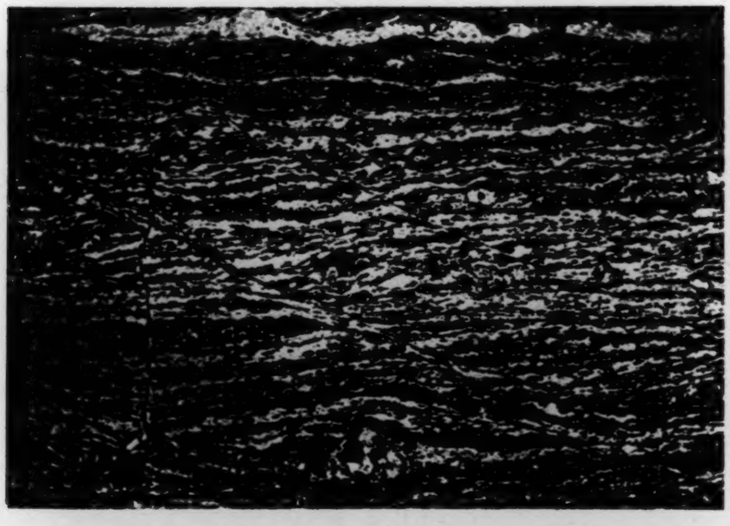

Figure 2.5. Typical MQS sample (SG94-24) taken under plane-polarized light (PPL). Light coloured bands are predominantly composed of quartz and feldspar. Darker bands are mica and chlorite. Brittle-type AESB (f-type) cut the foliation (parallel to the bottom edge of photograph), which represents the flow plane (compare with Fig 3.10); the implied shear-sense is dextral. Magnification : 10X (10 mm x 7 mm view).

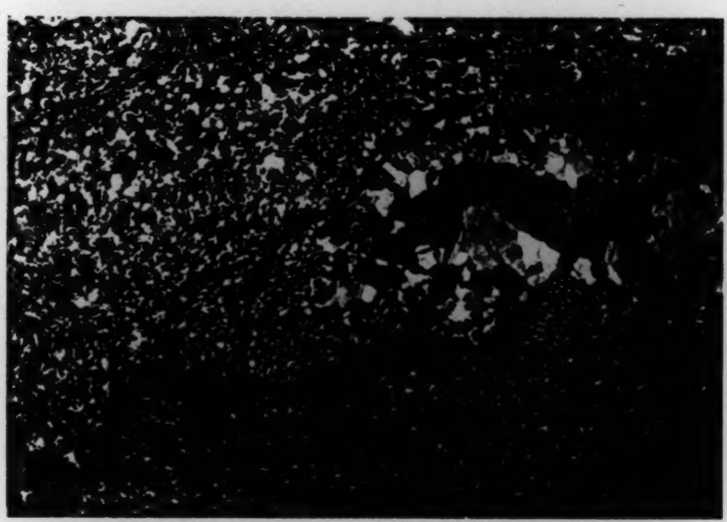

Figure 2.6. QP sample (SG94-35) taken under crossed polars (XNL). Subgrained quartz fills the majority of the field of view although some muscovite occurs in small kinked bands near the top of the field of view and in a large mica-book at the right. Note the contrasting grain sizes of quartz on either side of dark anstomozing fractures. Magnification: 10X (10 mm x 7 mm view).

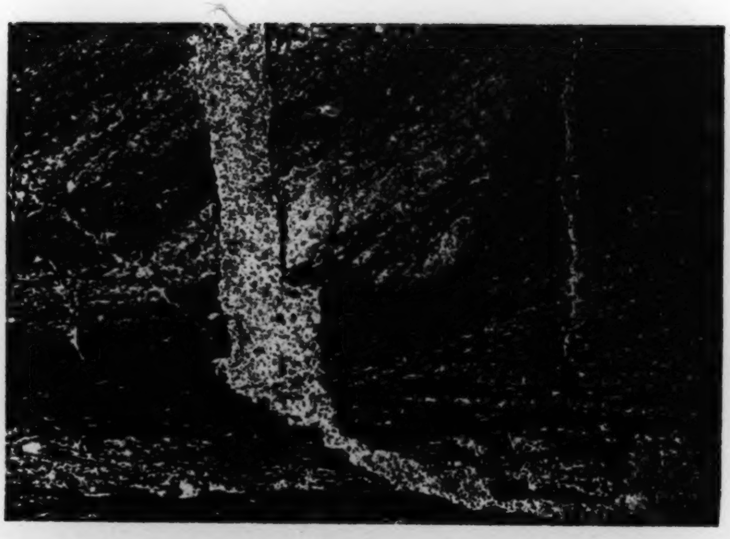

Figure 2.7. Graphite-bearing QP (QP-g) sample SG94-90D taken under PPL. The upper half of the photograph shows foliation defined by alternating carbonaceous and noncarbonaceous bands. In the bottom half of the photograph, dark shears in which carbonaceous material has been concentrated (parallel to the bottom of the photograph) deflect the compositional bands, giving a dextral shear-sense. Magnification: 40X (2.5 mm x 1.75 mm view).

Figure 2.8. MS sample (SG94-82) taken under XNL. Amphiboles (1° to 2° pink and blue minerals) and chlorite (small grains in groundmass) comprise the dominant mineralogy of ths sample. Quartz and feldspar are present in the groundmass and in dispersed, thin layers (not shown). The shear plane is parallel to the bottom of the photograph. Magnification: 40X (2.5 mm x 1.75 mm view).

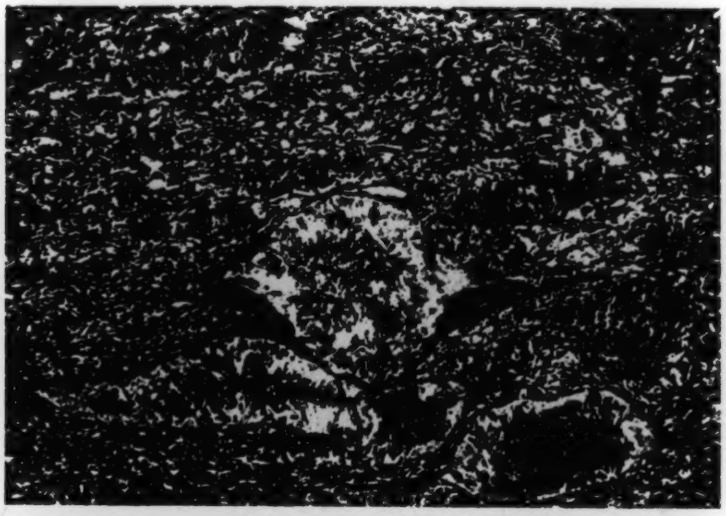

Figure 2.9. Anvil assemblage sample SG94-52 taken under PPL. Large green augen contain cores of amphibole (yellow-brown) and mantles of chlorite. Opaque material (ferromagnesian oxide?) is present in the augen as well. The shear plane is parallel to the bottom of the photograph. Magnification: 10X (10 mm x 7 mm view).

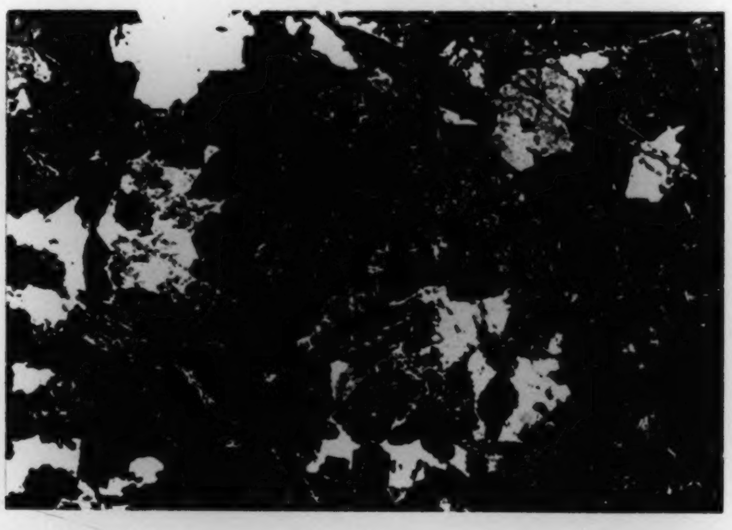

Figure 2.10. Hornblende granodiorite (HbGd) sample SG94-90B taken unde XNL. Laths of 2° blue and green are amphibole. Large 1° white to grey minerals are quartz and potassium feldspars. Plagioclase (now mostly altered to sericite) appears as mottled grey masses with euhedral to subhedral outlines. Magnification: 10X (10 mm x 7 mm view).

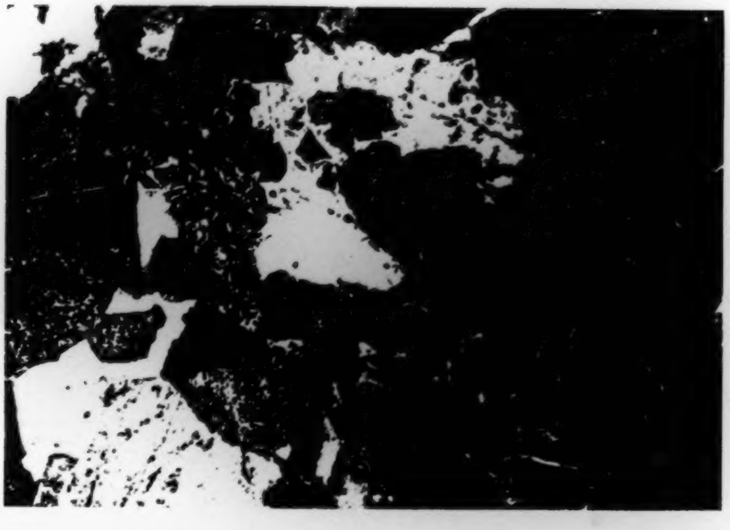

Figure 2.11. Biotite-monzogranite (BtMg) sample SG94-78 photographed under XNL. Large (2 to 4 mm) quartz grains show undulose exinction. Subhedral to anhedral potassium feldspar have a slightly mottled appearance due to alteration. A mass of chlorite showing typical blue anomalous extinction is situated near the upper left corner of the photograph  Magnification: 10X (10 mm x 7 mm view).

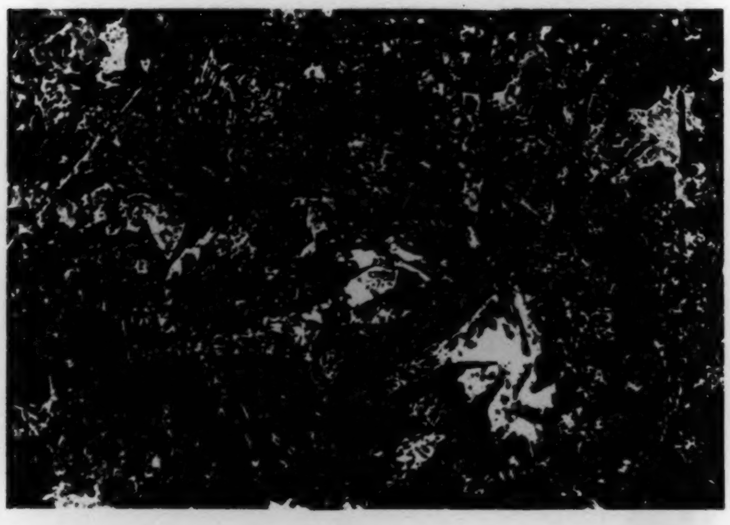

Figure 2.12. Gabbro sample SG94-44 photographed under XNL. Dark mottled grey laths are former plagioclase crystals which have largely altered to sericite. Yellow to blue (1° to 2° birenfringence) minerals are amphiboles. Magnification: 10X (10 mm x 7 mm view).

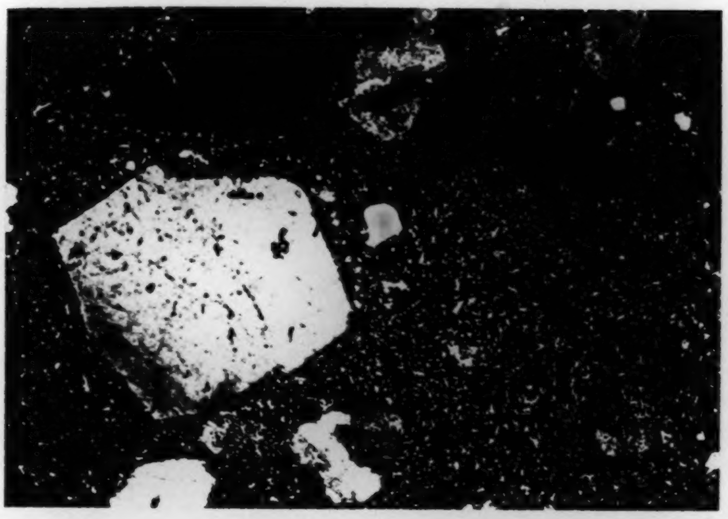

Figure 2.13. Felsic volcanic plug sample SG94-11A photographed under XNL. Large euhedral to subhedral crystals include quartz (untwinned, unaltered 1° grey crystals) and potassium feldspar (simply-twinned, slightly altered 1° grey crystal). A small amount of polysynthetic twinned plagioclase feldspar is also apparent (bottom centre of photograph) Magnification: 10X (10 mm x 7 mm view).

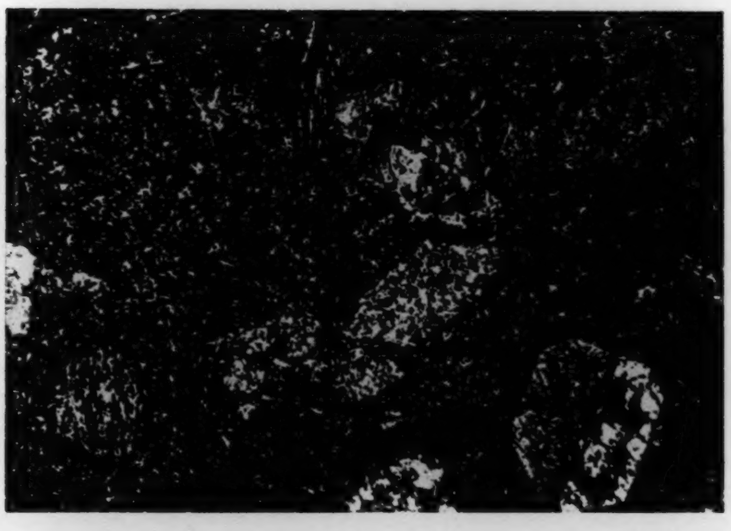

Figure 2.14. Mafic volcanic plug sample SG94-10B photographed under XNL. Large twinned euhedral 3° pink to blue crystals are clinopyroxenes. Mottled grey masses represent highly altered plagioclase crystals Magnification: 10X (10 mm x 7 mm view).

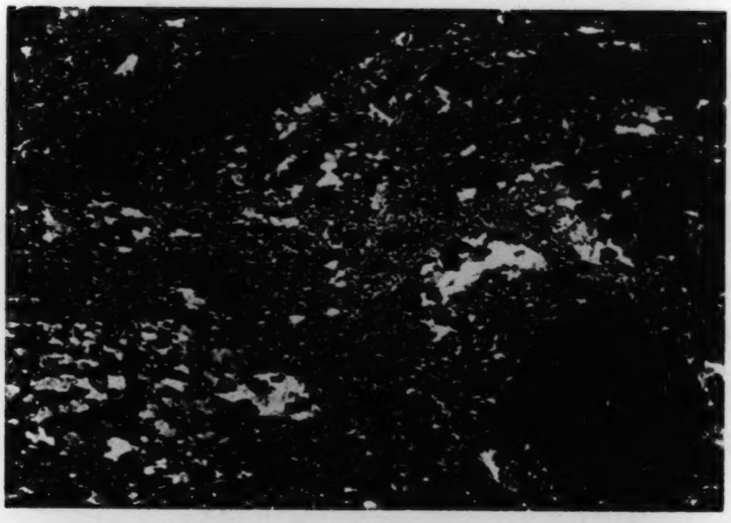

Figure 2.15. Sheared granodiorite (Sh-Gd) sample SG94-57 photographed under XNL. Quartz masses show undulatory extinction and subgraining. Altered amphiboles (large equant brown mass at the bottom right and long narrow mineral at the top left) are highly fractured and disaggregated due to shear. The groundmass, predominantly composed of fine-grained quartz and feldspar, also contains abundant muscovite in areas, as evidenced by a pinkish hue (3° pink). The shear plane is parallel to the bottom of the photograph. Magnification: 10X (10 mm x 7 mm view).

# CHAPTER 3. STRUCTURE

## 3.1 INTRODUCTION

Structures within the YT terrane are normally attributed to the collision of the YT terrane with North America; this interpretation, however, is dependent on the nature of the collision between them. If the bulk of the YT terrane represents a thin allochthonous sheet thrust from its root zone (the TTZ) to the northeast over North America (Tempelman-Kluit 1979), then it may be expected that the subhorizontal fabrics common throughout much of the YT terrane should record this movement. If however, the boundary between the YT terrane and North America is a steep fault, as Mortensen (1983, 1992b) suggest, then the subhorizontal fabrics contained within much of the YT terrane may have no bearing on the emplacement of the YT terrane against North America. Instead they may be the result of pre-collisional deformation or the result of gravitational spreading of over-thickened crust (Mortensen 1983). Kinematic studies may help establish the origin of this fabric.

Several in-depth kinematic investigations have been performed in the highly strained, steeply dipping TTZ in south central Yukon (e.g. Hansen 1989, Stevens 1994), but fewer kinematic studies have been performed on more shallowly dipping fabrics contained in the YT terrane rocks northeast of the Tintina Fault in southeastern Yukon. Mortensen (1983) mapped foliation and lineation in the YT terrane northeast of the Tintina Fault, and Erdmer (1985) performed larger scale mapping and microscopic fabric analysis of rocks in and around the Money klippe, but shear-sense results proved inconclusive. In order to test further whether meaningful shear-sense results may be obtained from the Money klippe area, the field area was reexamined and new oriented hand samples were collected (Fig. 3.1). The remainder of this chapter presents the results obtained.

Four stages of deformation are recognized in the field. The first, D1, produced penetrative planar fabric (S1), which generally contains mineral stretching lineations

(L1). A second deformational stage, D2, is represented by a weak crenulation of the penetrative planar fabric of the Nisutlin schists (S2). These S2 crenulations were only observed in a few locations on one ridge near the large north-south trending normal fault on the west side of the Money klippe (Fig. 3.1), although Mortensen (1983) documents crenulation cleavage throughout much of the YT terrane in the region. The third deformational episode is represented by thrust faulting, which in the field area occurs between the three major rock assemblages and also within the upper SRPS assemblage between individual igneous units. The fourth deformational feature, late-stage normal faulting, is exemplified by the large north-south trending normal fault on the west side of the Money klippe (see Chapter 2). The penetrative planar fabric, S1, and thrust faulting will be discussed in some detail in Section 3.2.

Thrust faults were only directly observed between igneous units in the Money klippe, thus, direct relationships between thrust faults and S1 in the Nisutlin assemblage were not determined in this study. However, Mortensen (1983) documents thrust faults cutting S1 foliation within the Nisutlin assemblage in nearby areas, establishing thrust faulting as the later event, Mortensen (1983) also suggests that the S2 crenulation may be related to the thrust faulting.

## 3.2 PENETRATIVE PLANAR FABRIC

### *Map-scale observations*

The highly planar schistose fabric of the Nisutlin assemblage, typically shallowly dipping in much of the region (Fig. 3.2), surrounds and locally dips toward the Money klippe. Within the klippe, some Anvil assemblage rocks possess S1 fabrics similar in style to those in the underlying Nisutlin assemblage; other Anvil rocks in the klippe are affected only by brittle fracturing. The SRPS rocks resting above the Anvil assemblage in the upper portion of the Money klippe are not obviously affected by D1. However, the Sh-Gd south of the Money klippe has suffered D1 deformation. S1 has a variable expression in the Sh-Gd, ranging from coarse schistosity to a weak foliation defined by parallel alignment of grains. Lineations are generally poorly developed and difficult to discern in the Sh-Gd.

### *Meso- and micro-scale observations*

Nisutlin assemblage schist offers the best and most widespread exposure of S1 and L1 fabrics in the study area, thus observations documented throughout the remainder of this section are principally from the Nisutlin assemblage. Nisutlin assemblage rocks are termed 'schists' for simplicity, although texturally they include schist, phyllite, quartzite, mylonite, and phyllonite. (Appendix 2) Generally, they are mica-rich quartzofeldspathic schists with prominent flaggy foliation (Fig. 3.2), although chlorite-amphibole schist is common as minor layers in the Nisutlin assemblage as well. Mineral stretching lineations are relatively common on foliation surfaces, especially in schist located northeast of the Money klippe. Segregation into compositional bands parallel to schistosity on the millimetre scale is common in most of the schist, but in some localities banding is absent and the foliation is defined by dispersed mica or amphibole. Rare rootless isoclinal folds, whose axial surfaces are parallel to the schistosity, have been passively transported, stretched and refolded along with small perturbation folds in the foliation (Fig. 3.3).

Minerals have undergone comminution during development of the planar fabric, apparent from quartz grains with undulose extinction in the process of being divided into subgrains (Fig. 3.4). This process has resulted in very small grain size in some samples (< .05 mm). Some samples from the Nisutlin assemblage and the Sh-Gd have porphyroclasts, usually feldspars, which are rotated and cracked by the deformation (Fig. 3.4) (see below).

### *Evidence for volume loss*

Several quartz-rich samples located in the southeastern part of the field area (SG94-35, SG94-89, and SG94-90) have small anastomozing fractures that are roughly sub-parallel to the mylonitic foliation (Fig. 3.5; Fig. 2.6, 2.7). The anastomozing fractures appear to be stylolitic, so that material such as graphite or mica became concentrated in the fracture after silica had gone into solution. Juxtaposition of domains with contrasting grain sizes is common along such fractures (Fig. 2.6). Volume loss is also documented in one sample lacking anastomozing fractures. A small quartz veinlet cuts the mylonitic foliation in sample SG94-53, but is offset with opposing senses of displacement along several planar micaceous bands parallel to mylonitic foliation (Fig. 3.6). It is interpreted that compression applied orthogonally to foliation caused volume-loss and concentration of insoluble micas along planes parallel to foliation in this sample. Imperfect juxtaposition of the undissolved portions of the rock slightly misaligned the segments of the vein along each dissolution plane. Because of the flat, planar nature of these bands, as contrasted with the more obvious anastomozing stylolites documented above, they blend with schistosity. The danger is that veins at an acute angle to the foliation would be juxtaposed with an apparently consistent offset, possibly prompting an observer to interpret the dissolution planes as discrete shears caused by a consistent sense of shear.

Quartz-filled fractures at sample locality SG94-23 are regularly spaced on well-exposed foliation surfaces, where they are perpendicular to the lineation and foliation. At another locality (SG94-65), quartz-filled fractures cut foliation at a ~30°, in a regular north-dipping manner.

### *Structural analysis*

Foliation and lineation measurements were collected from the perimeter of the Money klippe, principally from Nisutlin assemblage schists, but also from the Anvil assemblage and the Sh-Gd. Data are divided into three geographical groupings based on the side of the klippe on which they were collected: the 'north group', the 'south group', and the 'west group' (Fig. 3.7 - also see Appendix 4). Although plotted on separate stereonets, which were generated using Spheristat 2.0 software: (Pangaea Scientific 1995), the poles-to-foliation of the north, south and west groups appear to overlap in a loose cluster near the center of the stereonets, indicating that broadly, foliation is only moderately to shallowly dipping. The center of the cluster of poles to planes are slightly different for each group, however, reflecting the general observation that foliation dips toward the klippe (Fig. 3.7). Otherwise, no other map-scale features are apparent in the stereonet plots of poles to foliation planes.

Mineral stretching lineations on foliation surfaces are presented in Figure 3.8 (Also see Appendix 4). Lineation in north group schists are very pronounced on flaggy foliation surfaces. North group lineations are consistently oriented north-south, as evidenced by the tight cluster of data near the north and south poles of the stereonet, which was generated using Spheristat 2.0 software (Pangaea Scientific 1995). Schists of the west and south groups are more varied in foliation character, and lineations are less frequent and more variable in orientation. Fewer lineations were obtained for the south and west group schists, but taken together, they do suggest a rough east-west trend (see stereonet; map Fig.3.8).

### *Shear-sense analysis*

Few reliable shear-sense indicators were observed in the field, thus oriented samples were collected for slab and thin-section analysis. In a strongly deformed rock such as a mylonite, the foliation plane is subparallel to the bulk shear plane (Hanmer and Passchier 1991). Mineral stretching lineations result from elongate minerals preferentially aligning their long axes parallel to the shear plane. It is not necessarily the case that the shear plane results from simple shear alone; a more reasonable assumption is that of general non-coaxial shear (Hanmer and Passchier 1991), which includes a componant of pure shear (applied orthogonally to the shear plane) in addition to simple shear. Strain markers are best observed on planes cut parallel to lineation and perpendicular to foliation. Thus, oriented samples were slabbed in this manner, and thin-sections made from the slabs.

The most widely found shear-sense indicators were asymmetrical extensional shear bands (AESB), using the terminology of Hanmer and Passchier (1991); other names for these features include *C′ planes* ( Berthé et al. 1979a) or *extensional crenulation cleavages* (Platt and Vissers. 1980). AESB are common features of mylonites where the C-S fabric has developed to the point that S-planes have progressively rotated into parallelism with C-planes (Berthé et al. 1979b, Hanmer and Passchier 1991). AESB normally occur as discrete shears at a 15 to 45° angle to mylonitic foliation and have a sympathetic sense of displacement to shear on the flow plane (Platt and Vissers 1980, White et al. 1980; Hanmer and Passchier 1991) (Fig. 3.9). The development of conjugate sets of AESB, the first set sympathetic as described above and the second set antithetic (and often, but not necessarily, at a larger angle to foliation), complicates the interpretation of shear-sense. Generally, however, only a single sympathetic set of AESB's form (White et al. 1980, Norrell et al. 1989). In most circumstances, a single sympathetic set of AESB's will provide a unique and consistent shear-sense, at least at a local level (White et al. 1980, Norrell et al. 1989, Hanmer and Passchier 1991), although several problems with these features are discussed in Section 3.4. The AESB's studied in this study are listed in Appendix 5; following the usage of Norrell et al. (1989) they have been divided into 'd-type' and 'f-type' AESB. A compositional band cut by a ductile 'd-type' AESB ('d' for 'ductile') has the appearance of an asymmetrically folded layer, with the compositional band thicker on unsheared limbs and thinner on sheared limbs (Fig. 3.10). Brittle 'f-type' AESB ('f' for fracture) have the appearance of small brittle faults that offset S1 foliation (Norrell et al. 1989) (Fig. 3.9, Fig. 2.5).

Large AESB were visible in outcrop and handsample at some localities; for instance, at locality SG94-16, 10 cm long shear bands displaced foliations by 2-3 cm (Fig. 3.9). Typically, however, AESB were much smaller, and best observed at microscopic scales (Fig. 3.10). In most of the field area, AESB were the only shear-sense indicators (see below). The spacing of the AESB is also variable; in some samples, they are relatively widely spaced, discrete shears, whereas in other samples they are spaced with greater frequency. Further discussions on the use of these features as shear-sense indicators is presented in Section 3.4.

Porphyroclasts with reliable sense of shear are relatively rare in schist from the field area. Where present, porphyroclasts and their appendages usually do not display asymmetry. However, they proved useful for shear-sense determination in a few samples (Fig. 3.4). Porphyroclasts were observed on planes cut perpendicular to their implied axes of rotation (Fig. 3.4). In some samples, abundant porphyroclasts pile up against one another, in a feature known as *tiling*. The asymmetry of tiled porphyroclasts gives the impression that these structures would aid in determining shear-sense; however, more than one stress field can result in the same feature, making tiled porphyroclasts unsuitable for shear-sense analysis (Hanmer and Passchier 1990). In thin-sections where tiling was observed, single porphyroclasts in less cluttered layers were sought.

Ten sites in the north group gave unambiguous shear-sense results. Seven sites in the north group record top-to-the-south shear parallel to the north-south trending mineral stretching lineations, (Fig. 3.11, Appendix 5) based on microscopic scale AESB. Roughly half of the AESB are f-type and half are d-type. One sample (SG94-20) had both AESB and reliable porphyroclast wings that both gave the same sense of shear. Three of the ten north-group rocks give a top-to-the-north shear-sense (Fig. 3.11, Appendix 5). At one of these locations, SG94-71, the top-to-the-north d-type AESB resemble the top-to-the-south AESB at other locations, except that SG94-71 is a mylonite of the Anvil assemblage. Another locality with a top-to-the-north shear-sense, SG94-90, contains d-type AESB, but also has likely suffered volume loss through quartz dissolution (as described above), which reduces the reliability of this indicator. Perhaps coincidentally, the three stations that have top-to-the-north shear are the closest north group stations to plutonic rock contained within the Money klippe.

Eight oriented rocks from the 'south group' and 'west group' were analyzed for shear-sense indicators. Of these, only two west group samples yielded reliable shear-sense indicators. One sample, SG94-5A, had reliable δ type porphyroclasts, and the other sample, SG94-6A had reliable d-type AESB (Fig. 3.11, Appendix 5). Both samples indicate top-to-the-east-by-southeast shear-sense. Other south group rocks either had no reliable indicators because of very chaotic anastomozing crinkly fractures, volume loss by dissolution, or tiled porphyroclasts. The broadly top-to-the-east shear-sense indicated by the two west group samples must be viewed with skepticism because of the small number of data.

### 3.4 THRUST RELATIONS

Deformation in the SRPS rocks of the Money klippe is concentrated near contacts, where anastomozing shears and chloritization occurs within 1 to 2 metre-wide bands (Fig. 3.12 and 3.13). Samples of BtMg and HbGd from the center of the Money klippe generally retain their primary igneous textures but in thin-section most large quartz grains show undulose extinction (Figures 2.10 and 2.11) and brittle cracking of quartz grains is apparent, suggesting that these rocks have suffered at least a small degree of internal strain. The individual plutonic bodies occur as panels between subhorizontal sheared contacts. These contacts are interpreted as thrusts (Tempelman-Kluit 1979, Erdmer 1985). Several intrusive relationships are also present however, such as a large sill of BtMg that intrudes the gabbro, which establishes igneous links between these units (see below and Section 2.3 for discussion)

Examination of the contact between the HbGd and the BtMg units near the center of the klippe was undertaken in order to find kinematic structures. Anastomozing shears with a small degree of tectonic intermixing and chloritization occur within the 1-2m fault zone (Fig. 3.13). The overall orientation of the fault, incorporating both direct measurements, and more distant observations, is that it is dipping 30-40° to the northeast, although there is a considerable degree of scatter as a result of the anastomozing nature of the contact. Few shear surfaces yielded slickenlines for measurement; the few slickenlines were broadly oriented east-west.

### 3.5 DISCUSSION

Before attempting to make interpretations about shear-sense, it is instructive to review the validity of AESB as shear-sense indicators. AESB may sometimes be unreliable as shear-sense indicators in shear zones because of the development of conjugate sets of shear bands that imply an opposite sense of shear. (Behrman 1987) Also, Behrman (1987) suggests that some AESB develop after the primary phase of mylonitization occurred, thus their implied sense of shear may not be that of the mylonitic shear zone. Norrell et al. (1989), however, suggest that d-type AESB are likely to have formed during ductile deformation. Another pitfall of AESB interpretation is that volume loss in shear bands may cause foliation offsets that imply erroneous senses of shear (Platt and Vissers 1980). Finally, it is generally suggested that more than one type of the shear-sense indicator be used, because different shear-sense indicators have different responses to the strain regime. For instance, where conditions of simple shear can be demonstrated, as in a near vertical shear zone between two rigid crustal blocks, the AESB give results consistent with other indicators (Behrman 1987). In cases where the sheared rocks are subhorizontal and the boundary conditions of the presumed shear zone are unknown, however, the AESB may give senses of shear conflicting with other indicators (Behrman 1987). In the latter case, AESB may be the result of local mechanical effects rather than regional scale transport (Behrman 1987).

In light of the constraints outlined above, a critical examination of the AESB noted in the field area is warranted. Several lines of evidence suggest that AESB may yield reliable senses of shear. For instance, no conjugate sets were observed, and f-type AESB indicated the same sense of shear as more reliable d-type AESB located nearby. Also, despite the fact that volume loss has been demonstrated in several samples, samples for which the shear-sense is reported (except SG94-90) have little evidence for volume loss. Doubt is cast over the validity of the implied shear-sense of the AESB, however, by the fact that the subhorizontal S1 foliation has little in the way of boundary constraints. In these circumstances AESB may form as a result of local mechanical effects and have no bearing on the kinematics of the allochthon in general (Behrman 1987). The potential for misinterpretation is compounded, moreover, by the almost complete dependence on one type of shear-sense indicator (AESB) in the field area.

Field area constraints present further difficulty in interpreting shear-sense. Even if, despite cautions noted above, it is interpreted that the north group schists do form a coherent set of top-to-the-south shear-sense indicators, it must be placed in a regional context. Here problems arise because it is difficult to reconcile the shear-sense of the north group with the west group lineations, which, though sparse, are roughly at 90° to the lineation of the north group. Furthermore, interpreting the overall movement of a large allochthonous terrane is best based on a broad-scale structural mapping study, in order to outweigh any local deviations with a large amount of measurements over a wide area. Clearly, the small area covered by this study does not meet that requirement. Mortensen (1983) mapped much of the YT terrane northeast of the Tintina Fault and produced a map of foliations and lineations. Looking at this larger picture reveals complex lineation trends. Because shear-sense indicators give movement direction parallel to lineation trends, it is difficult to imagine that a single transport direction could be obtained by determining shear-sense on the variably oriented lineations. However, more detailed study of structure and shear-sense indicators in the surrounding region is needed.

Because the Nisutlin assemblage rocks in the study area have few constraints on boundary conditions, it is likely that even the nearly consistent sense of shear of the north group is a result of local effects present at that scale. Comparing the north group structures to those in the south and west groups of this study area, as well as to the variable regional lineation trends as mapped by Mortensen (1983), it becomes apparent that they could not reflect the overall sense of transport for the allochthonous rocks. Erdmer (1985), working in the area around the Money klippe, similarly suggested that kinematic structures do not reflect the tectonic transport direction, although Erdmer (1985) used different shear-sense criteria.

Relatively brittle shear occurred between panels of Anvil assemblage and SRPS rock and also between individual panels of plutonic rock contained within the Money klippe. Slickenlines on one contact indicate movement along an east west-axis. Erdmer (1985) notes that steps on the slip surfaces face northeast, indicating transport in that direction. Mortensen (1983) documents many thrust faults throughout much of the region, noting that they truncate the penetrative planar fabric of the Nisutlin assemblage rocks. This indicates that thrusting postdated the earlier ductile mylonitic foliation (Mortensen 1983). Mortensen (1983) goes on to say that the thrusts may have rotated the panels of

Nisutlin assemblage rock. It is possible that this later stage of deformation may have contributed to the inconstant lineation trends throughout much of the YT terrane; however, the effect of local inhomogeneities in the D1 penetrative deformation may be the principal cause of inconstant lineation trends.

Another important question is whether or not the sheared contacts between the various members of the SRPS rocks indicate a large degree of transport. There is evidence to suggest that the SRPS units share a close igneous relationship. All of the SRPS units were dated (see Chapter 5) and have similar ages. They also share some geochemical trends that are compatible with the units being comagmatic. Finally, several intrusive contacts are present (see Chapter 5); diabasic dykes intrude the gabbro, HbGd and BtMg. More significantly, the Bt-monzogranite intrudes the gabbro. These age and intrusive relationships at least argue for an initially close association spatially as well as genetically, so the shear zones between SRPS units may represent only a small degree of movement.

The shear-sense and structural findings presented above cannot help resolve the differing tectonic models for the YT terrane presented at the beginning of the chapter. As noted, a more regional study of kinematic structures may be more suited to addressing the problem of accretion of the YT terrane. Other structural studies that could help constrain the accretionary history of the YT terrane may include direct dating of deformational fabrics, perhaps by Rb-Sr dating of mica grown during shear.

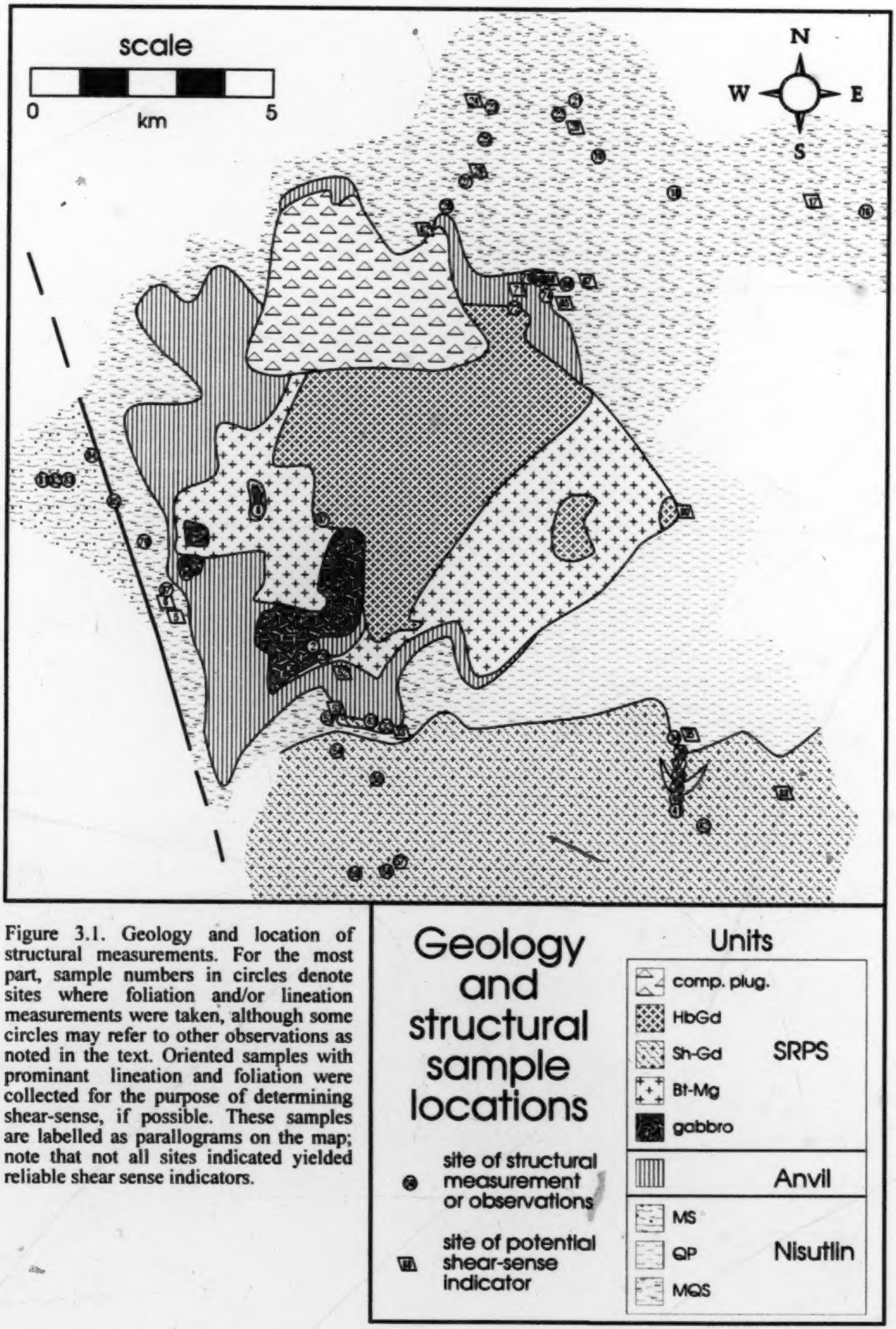
scale
0
km
5
N
W
E
S
Geology and structural sample locations
site of structural measurement or observations
site of potential shear-sense indicator
Units
comp. plug.
HbGd
Sh-Gd
SRPS
Bt-Mg
gabbro
Anvil
MS
QP
Nisutlin
MQS

Figure 3.1. Geology and location of structural measurements. For the most part, sample numbers in circles denote sites where foliation and/or lineation measurements were taken, although some circles may refer to other observations as noted in the text. Oriented samples with prominant lineation and foliation were collected for the purpose of determining shear-sense, if possible. These samples are labelled as parallograms on the map; note that not all sites indicated yielded reliable shear sense indicators.

Figure 3.2. Cliff exposing Nisutlin assemblage in the field area. Figure in the photo is ~1.7 m.

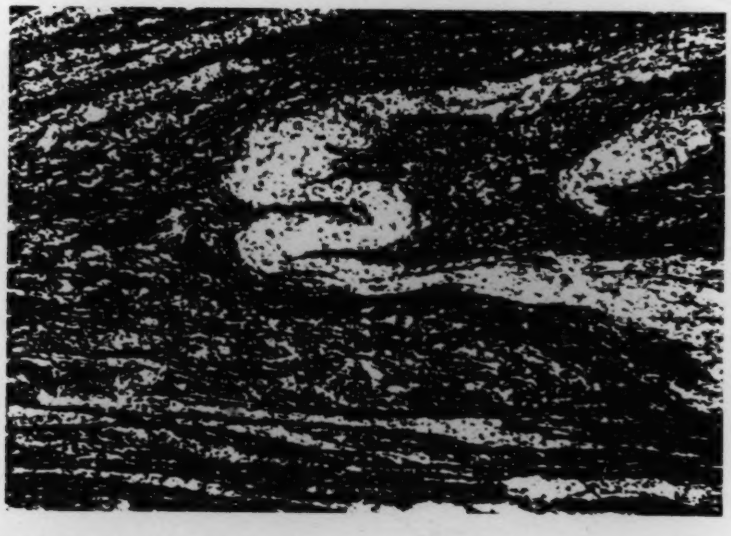

Figure 3.3. MQS sample SG94-62 displaying small rootless folds photographed under XNL. Light-grey layer in the fold is predominatly composed of quartz. The medium grey groundmass is composed of micaceous quartzofeldspathic material. The shear plane is parallel to the bottom of the photograph. Magnification: 10X (10 mm x 7 mm view).

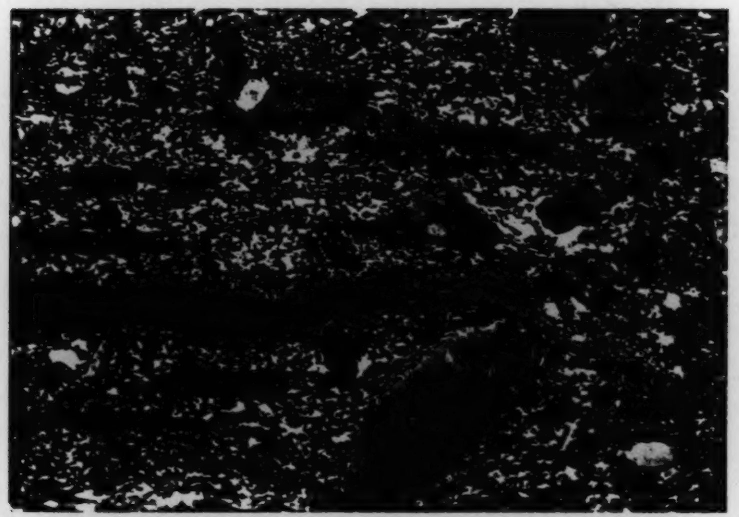

Figure 3.4. Rotation of porphyroclasts in Sh-Gd sample SG94-88, photographed under XNL. Quartz grains (smoky grey) show undulose extinction. Potassium feldspars (blue-grey with simple twins) have rough abraded edges and are rotated. The large twinned potassium feldspar near the bottom right shows dextral rotation. Large books of muscovite (3° pink) are aligned parallel to the flow (the shear plane is parallel to the bottom of the photograph). Magnification: 10X (10 mm x 7 mm view).

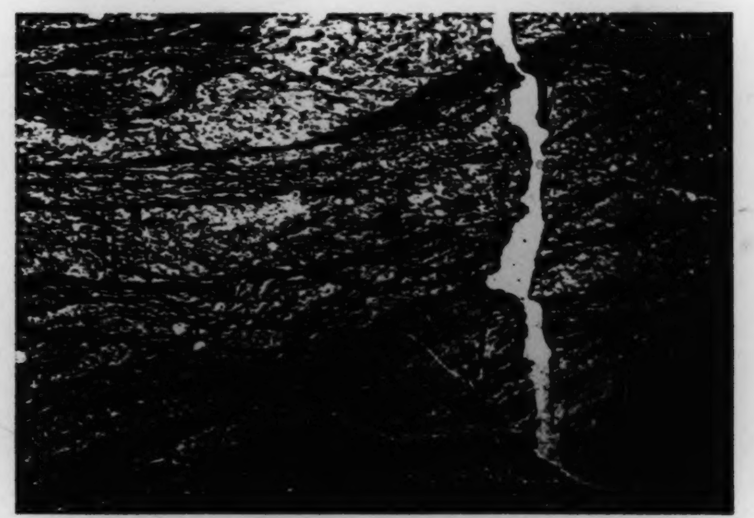

Figure 3.5. QP sample SG94-90B, taken under PPL, showing anastomozing shears, highlighted by high graphite concentrations. In regions which are undissected by the shears, the graphite is dispersed in the quartz-rich matrix, and help define a previous foliation (Fig. 2.7 is an enlargement of the bottom right of this photograph). The shear plane is parallel to the bottom of the photograph; the implied sense of shear is dextral. Magnification: 10X (10 mm x 7 mm view).

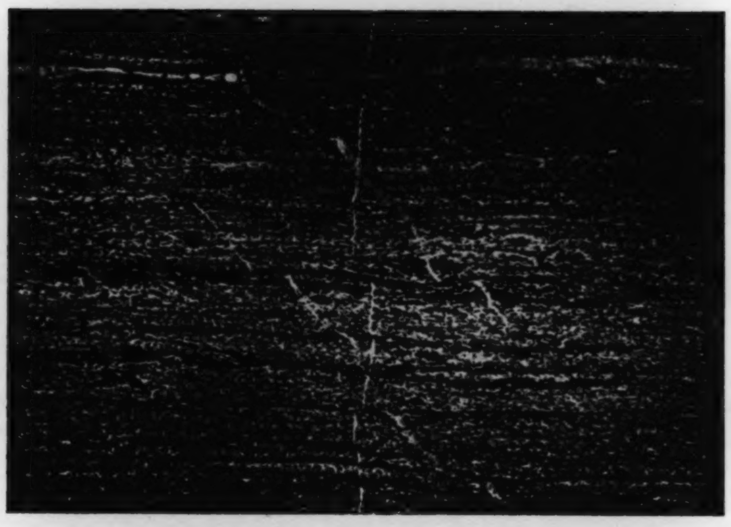

Figure 3.6. MQS sample SG94-53 photographed under PPL, showing dissolution along foliation planes, which are parallel to the bottom of the photograph. A veinlet oriented normal to foliation (centre of photograph) is offset at several places by foliation planes, but not with a consistant sense. See text. Magnification: 10X (10 mm x 7 mm view).

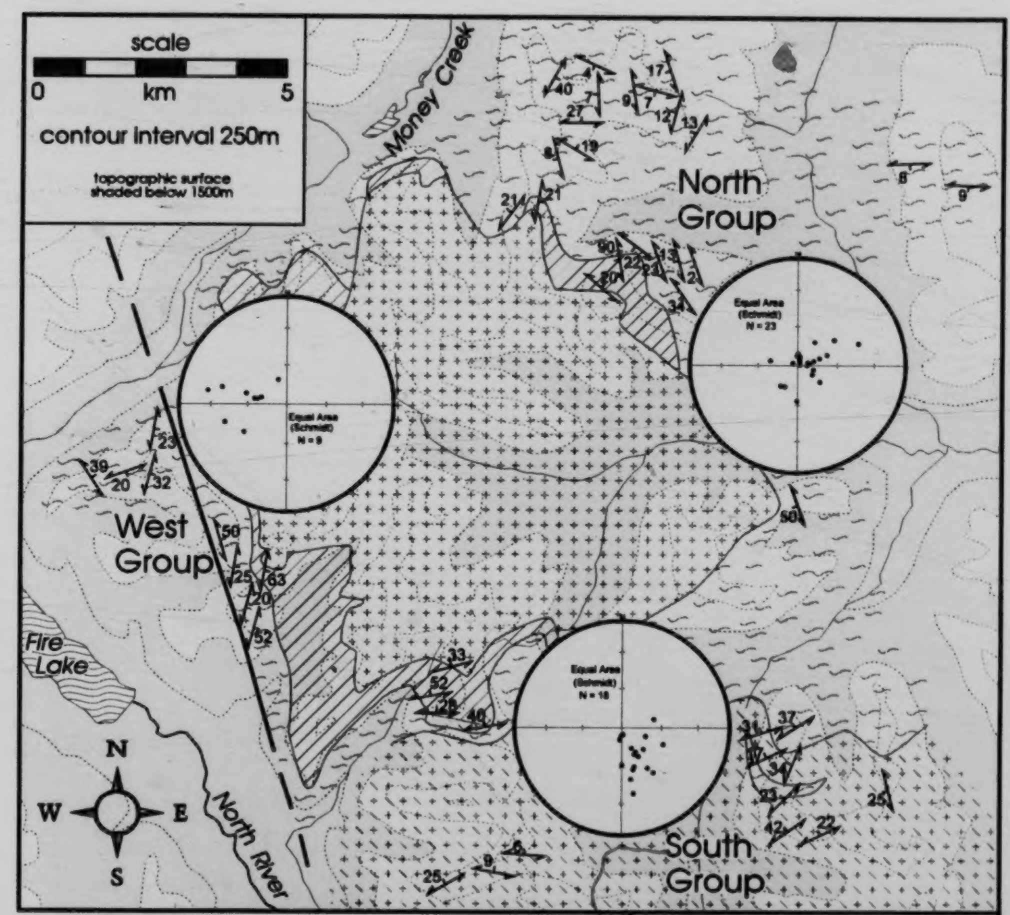

Figure 3.7. Foliation measurements from around the perimeter of the Money klippe. Data are divided into three groupings based on geographic location and plotted on equal-area stereonets. The stereonets were plotted using the Spheristat 2.0 software package (Pangaea Scientific 1995).

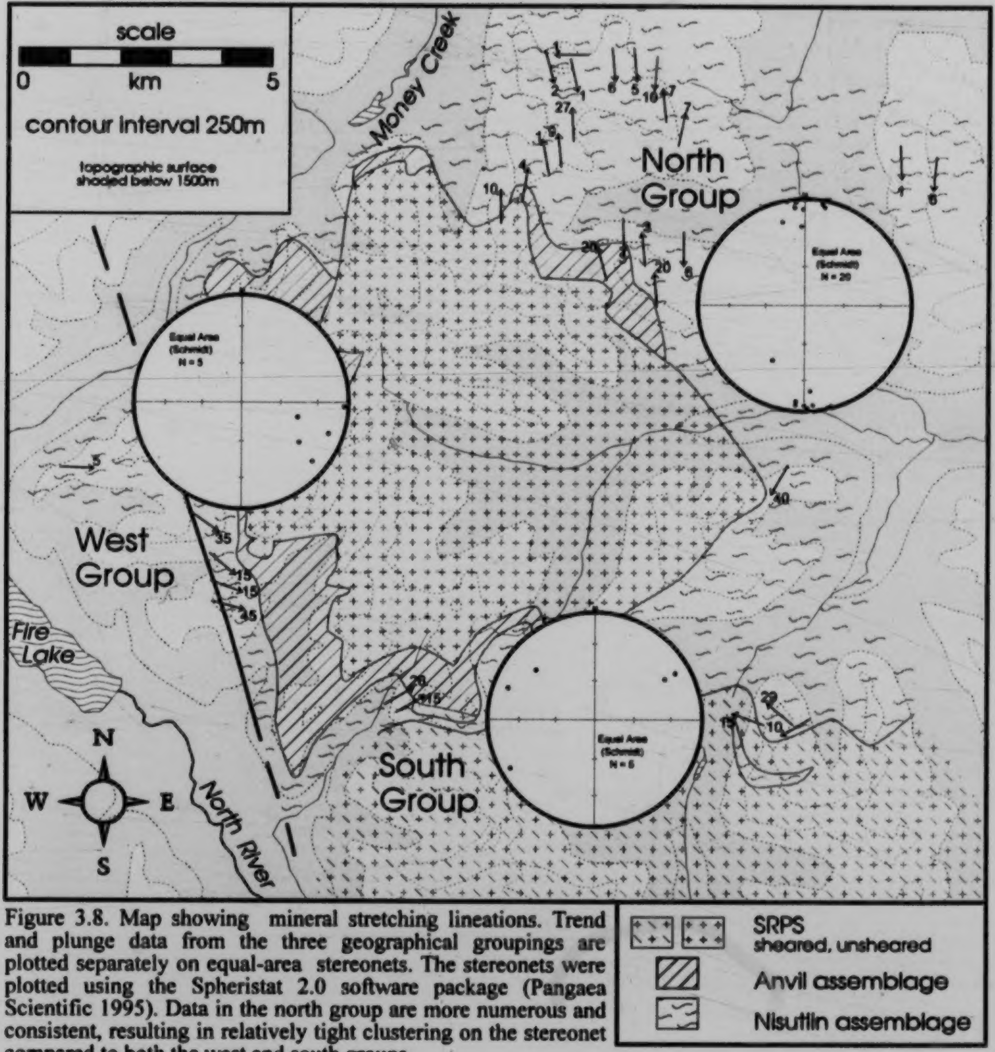

Figure 3.8. Map showing mineral stretching lineations. Trend and plunge data from the three geographical groupings are plotted separately on equal-area stereonets. The stereonets were plotted using the Spheristat 2.0 software package (Pangaea Scientific 1995). Data in the north group are more numerous and consistent, resulting in relatively tight clustering on the stereonet compared to both the west and south groups.

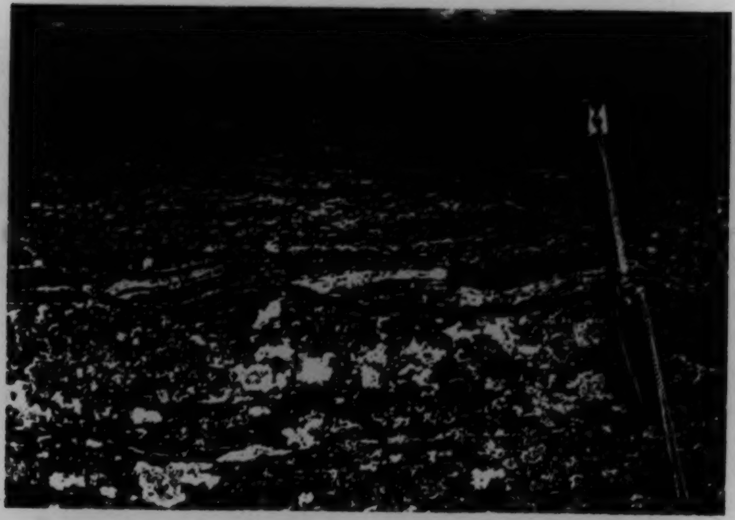

Figure 3.9. Large f-type AESB (dipping at a shallow angle to the right) offsetting the foliation (oriented parallel to the bottom of the photograph) of a MQS sample (near SG94-17) photographed in the field. The pocketknife is approximately 100 mm long.

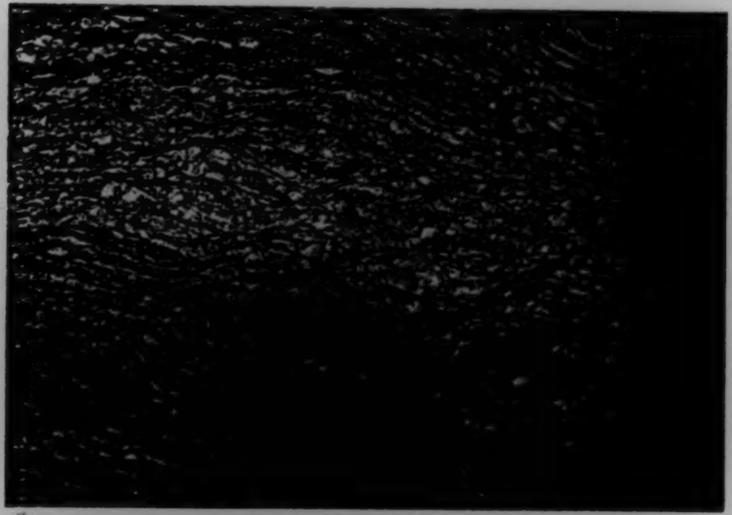

Figure 3.10. Ductile AESB (d-type AESB) in MQS sample SG94-6A, taken under PPL. Compare with figure 2.5 and figure 3.9. The shear plane is parallel to the bottom of the photograph; the shear-sense is sinistral. Magnification: 10X (10 mm x 7 mm view).

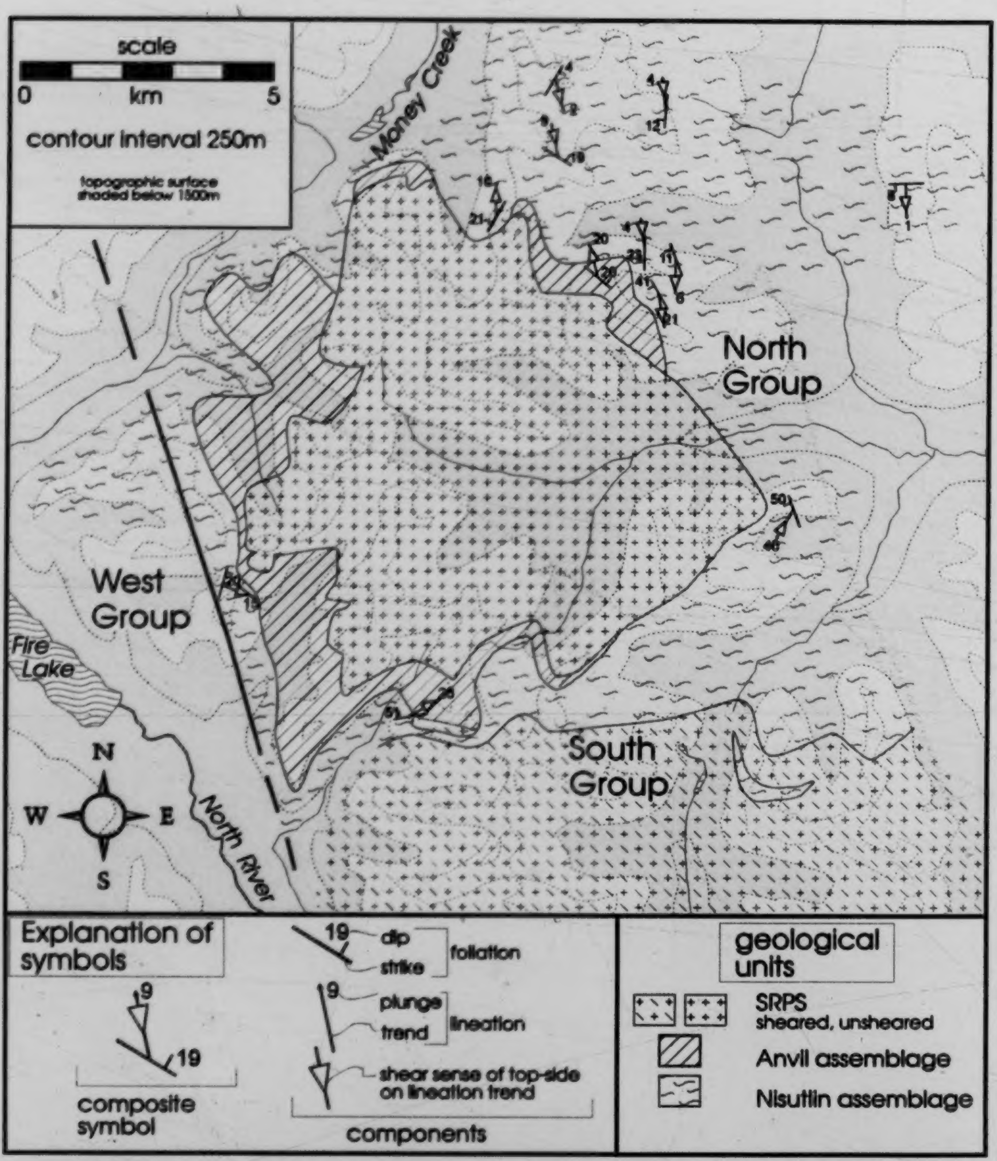

Figure 3.11. Shear-sense indicators. The large open triangles on lineation trends points in the direction that the hangingwall portion moved. South and west groups combined have only two reliable indicators, which broadly suggest top-to-the-east. Seven out of ten shear-sense indicators from the north group indicate top-to-the-south movement; the remainder of north group shear- sense indicators indicate top-to-the-north.

Figure 3.12. Sheared contact (parallel to the bottom of the photograph) between the gabbro (top) and BtMg (bottom) near sample SG94-29. The 5 cm zone between the two units is composed of quartz and chlorite. The hammer-head is approximately 18 cm long.

Figure 3.13. Contact between the HbGd (top) and BtMg (bottom) near sample site SG94-47. The contact (difficult to discern due to shadows) runs from the top left to the botton right of the photograph. Green-brown material occupies the contact zone. Lineations, though somewhat variable, dominantly trend east west in this zone which dips 30-40° to the northeast. View is to the north. The width of the field of view is roughly 1 m.

# CHAPTER 4. PROVENANCE OF THE NISUTLIN AND ANVIL SUPRACRUSTAL ASSEMBLAGES

## 4.1 INTRODUCTION

Much of the YT terrane is underlain by deformed and metamorphosed supracrustal rocks, composed of the largely quartzofeldspathic Nisutlin assemblage and associated mafic bodies of the Anvil assemblage (also called the Slide Mountain terrane). The Nisutlin assemblage of the YT terrane is a metamorphosed supracrustal sequence (Mortensen and Jilson 1985, Mortensen 1992b, Stevens 1994) interpreted to have been a distal portion of the western North American miogeocline in the Early Phanerozoic (Mortensen and Jilson 1985, Mortensen 1983, 1992b, Coney, 1989, Rubin et al. 1991, Nokleberg et al. 1994, Creaser et al. 1997a). Arguments supporting this interpretation are based largely on lithological comparison of the deformed and metamorphosed YT terrane with the relatively intact miogeoclinal sequence to the east. Geochemical and isotopic analyses of the YT terrane plutonic rock show that the contribution of the Nisutlin assemblage host rock (and its basement) is generally crustal in character (Mortensen 1983, 1992b, Bennett and Hansen 1988, Stevens et al. 1996, Aleinikoff et al. 1981, 1986, 1987). However, only a handful of studies have directly examined the geochemistry and isotopic composition of the Nisutlin assemblage and its correlatives. These studies include Sm-Nd characterization of the Birch Creek schist from central Alaska (McCulloch and Wasserburg 1978) and the Nisling terrane schist from the Coast Range in the Alaskan panhandle and adjacent British Columbia (Samson et al. 1991) and combined Sm-Nd and trace element studies of Nisutlin assemblage schist from the TTZ in the Yukon (Creaser et al. 1997a). The Sm-Nd signature of these schists is compatible with derivation in-part from ancient cratonal sources, but juvenile material is a significant component as well (Creaser et al. 1997a). These studies provide important constraints for the evolution of the YT terrane but are from geographically scattered locations; thus, it is hoped that geochemistry and Sm-Nd analyses of Nisutlin assemblage schist presented in this chapter will provide new constraints.

Another outstanding problem is the origin of the mafic bodies, often called the Anvil assemblage or SM terrane, that are intricately associated with the YT terrane. Mafic material is imbricated at various scales within the YT terrane. Some interlayered mafic bodies, assumed to be volcanic interbeds, are considered to belong to the Nisutlin assemblage (e.g. volcanic component of the Middle Unit of Mortensen and Jilson (1985)). Larger, structurally imbricated mafic bodies are usually included with the Anvil assemblage (Tempelman-Kluit 1979, Stevens et al. 1994) or are correlated to the SM terrane (Monger 1984, Wheeler et al. 1991). The SM terrane, originally defined in east central British Columbia (Mortensen 1992b), is composed of oceanic floor and associated pelagic sediments (Monger 1984). However, there is little evidence to suggest that all these mafic bodies are necessarily of the same origin. For instance, Mortensen (1992b) suggests that the larger mafic bodies located along the northeastern leading edge of the YT terrane may be unrelated to smaller mafic bodies imbricated within the Nisutlin assemblage further to the southwest. Furthermore, Mortensen (1992b) suggests that the mafic bodies at the leading edge of the YT terrane may be correlated to the Slide Mountain terrane, but that the mafic bodies further to the southeast may have different origins. Recent work on some of these mafic bodies in the northeast leading edge by Plint and Gordon (1997) in the Campbell Range suggests that they represent mid-ocean ridge basalt (MORB), which is compatible with correlation to the SM terrane. However, recent work on Anvil assemblage rocks from the TTZ reveals calc-alkalic trends, making it unlikely that these mafic rocks are related to the Slide Mountain terrane (Creaser et al. 1997a)). Analyses of other mafic bodies within the YT terrane would help establish whether the SM designation is appropriate in all cases.

The primary goal of the work presented in this chapter is to evaluate the potential sources of material that contributed to the formation of the supracrustal Nisutlin assemblage. This task will be accomplished by examining the major element, trace element, and Sm-Nd composition of the Nisutlin assemblage rock from the Money klippe

(Fig. 4.1). Although cataclasis, alteration, and metamorphism have destroyed sedimentary structures and have altered the primary mineralogy, geochemical and isotopic analysis provide a means to investigate the sedimentary provenance. Well defined sedimentological controls are important for provenance studies involving Nd isotopes (Boghossian et al. 1996), but are not possible for metamorphosed and strongly deformed rocks like those of the Nisutlin assemblage. Even at the broadest level, however, such studies could help differentiate between detritus shed from mature upper crust sources or juvenile, mantle-derived sources (Creaser et al. 1997a). Comparisons of geochemical and isotopic characteristics of the Money klippe area rocks with the previous studies of YT terrane supracrustal rocks (eg. McCulloch and Wasserburg 1978, Samson et al. 1991, and Creaser et al. 1997a) will help establish whether trends discovered elsewhere are terrane-wide phenomena or simply local variations. Additionally, the isotopic signature of the Nisutlin assemblage rocks may be compared with those of the miogeoclinal sequence to test the hypothesis that the YT terrane is a displaced portion of the miogeocline.

The secondary goal of this chapter is to examine the Anvil assemblage in the Money klippe area (Fig. 4.1) and determine the tectonic environment in which it was created. Trace elements resistant to mobility may provide discrimination between the different types of basalt. For instance, bivariate and ternary diagrams (eg. Pearce and Cann 1973) employing Zr, Y, and Sr have shown their utility in discriminating between different types of basalt. Multielement plots such as the one devised by Pearce (1983), in which trace elements are arrayed according to one or more of their geochemical properties, are also useful as a means to examine geochemical trends of the rocks, and interpreting their tectonic environment (Pearce 1983). Using these tools, it may be possible to determine whether the Anvil assemblage rocks have MORB-like properties, allying them to the SM terrane, or whether they have characteristics that indicate different origins. Another problem to be addressed is whether there is any relation between mafic bodies mapped as part of the Anvil assemblage and those considered to be volcanic interbeds within the Nisutlin assemblage (e.g. MS rock type).

Twelve samples were collected from Nisutlin assemblage rocks in the field area for geochemical and Sm-Nd isotopic analyses; representative samples from the MQS, QP, and MS units, defined and lithologically described in Chapter 2, were all included in the sample base (Fig. 4.1). Attention was also paid to spatial distribution, so that samples were chosen from most of the perimeter of the klippe. Handsample and thin-section descriptions are presented in Appendices 2 and 3. Three samples from the Anvil assemblage were also chosen for geochemical analyses (Fig. 4.1), although only one of these was analyzed for Sm-Nd isotopes. Samples were cleaned, crushed, and prepared for analyses following the procedures outlined in Appendix 6.

## 4.2 PROVENANCE OF THE NISUTLIN ASSEMBLAGE

### *Major elements*

Major element geochemistry was performed by XRF at Washington State University (see Hooper et al. (1993) for analytical procedures) and are presented in Table 4.1. Analytical errors for XRF data are given in Appendix 11. The $SiO_2$ content of the samples reflects their lithological groupings (Fig. 4.2a, b, and c); QP samples (quartz-rich phyllites) have high $SiO_2$ (88 % to 98 %), MS samples (mafic schists) have low $SiO_2$ values (51 % to 68 %), and MQS samples have intermediate values (73 % to 78 %). QP samples also have low concentrations of $Al_2O_3$ (1.2 % to 6.6 %), alkalis ($K_2O + Na_2O$ = 0.3 % to 1.7 %), and ferromagnesian elements (FeO* (total iron) + MgO = 0.5 % to 2.7 %) because of low abundances of any mineral except quartz (Fig. 4.2a, b, and c). Corresponding to their high concentrations of mafic minerals such as chlorite and amphibole, MS samples have higher FeO* + MgO concentrations (12 % to 19 %) than the MQS (2.0 % to 5.0 %) and QP samples (0.5 % to 2.7 %) (Fig. 4.2b). MQS samples have high concentrations of alumina and alkalis (12.4 % to 13.5 % and 4.2 % to 9.7 %, respectively), reflecting greater mica concentration in these samples.

Figure 4.2d presents $SiO_2/Al_2O_3$ vs. CIA (chemical index of alteration: CIA = $[Al_2O_3 /(Al_2O_3 + CaO + Na_2O + K_2O)] * 100$ (Nesbitt and Young 1982)). During weathering, feldspars alter to clays. This results in a loss of alkalis, which increases the

CIA value. Shales typically have CIA values ranging from 70 to 75, whereas more highly weathered residual clays have CIA values approaching 100 (Nesbitt and Young 1982; Taylor and McLennan 1985,). QP samples are distinguished by higher CIA values (75 to 79) and higher $SiO_2/Al_2O_3$ (~12 to 80) (Fig. 4.2d). MQS and MS samples (except for MS sample SG94-80) have uniform $SiO_2/Al_2O_3$ values ( ~5.5 to 6.5), which are similar to average values for post-Archean shales (~4.5 to 5.5) (Taylor and McLennan 1985), and more moderate CIA values (45 to 72). QP samples have the highest CIA values, which may indicate that these samples have undergone a higher degree of weathering than the other Nisutlin assemblage samples. Also, the QP samples have high $SiO_2/Al_2O_3$, and the highest quartz contents, indicating that they most likely represent mature sediments.

The three Nisutlin assemblage rock types have distinctive major-element characteristics. It may be possible to use major element data to constrain the tectonic setting of the sedimentary basin (Bhatia 1983). However, the use of major element geochemistry for such a task may be inappropriate because some major elements may be disturbed by the processes of chemical weathering, transport, deposition, diagenesis, and metamorphism. For instance, the smaller alkali and alkaline earth elements (eg. Na, K, Ca) are strongly partitioned into water (Taylor and McLennan 1985), thus sediment deposited subaqueously may be depleted in these elements with respect to their source. Thus, further geochemical discrimination for the Nisutlin assemblage samples will be accomplished using relatively immobile trace elements.

### *Rare-earth elements*

Several features of the REE plots make them useful for determining the origin of igneous rock and the provenance of metasedimentary rock; one is the degree of light rare earth element (LREE) enrichment, which can be measured by the $La_N/Sm_N$ ratio (the 'N' subscript indicates normalized values). Geochemically primitive rocks generally have relatively flat or depleted REE patterns (e.g., MORB: $La_N/Sm_N = 0.71$, $La_N/Yb_N = 0.68$ ), showing that they are depleted in LREE relative to bulk earth, or chondritic values (McLennan 1989). Felsic rock derived by partial melting and fractional crystallization usually have LREE enrichment because the LREE's, with larger ionic radii, are concentrated in the melts (McLennan 1989). Examples of LREE-enriched rock types include andesites, the North American Shale Composite (NASC), and the upper continental crust that have $La_N/Sm_N$ values of 3.23, 3.53, and 4.20, respectively and $La_N/Yb_N$ = 5.84, 6.98, and 9.21, respectively (Taylor and McLennan 1985, Gromet et al. 1984 : as compiled in McLennan 1989).

Another factor for evaluating fractionation trends is the degree of Eu depletion. Eu, like other REE's, normally has a valance state of +3, but also has a valance state of +2 under reducing conditions (McLennan 1989). As a +2 ion, $Eu^{+2}$ will easily substitute for $Ca^{+2}$ and enter into plagioclase or potassium feldspar. If feldspar is removed from a melt through fractional crystallization, the melt will be Eu-depleted (as are many felsic rocks) and the residue will be Eu-enriched (McLennan 1989). Eu depletion is measured by Eu/Eu*, which represents a ratio of normalized measured Eu (Eu) to a hypothetical value of Eu assuming no anomaly (Eu*). The Eu* parameter is calculated by assuming a smooth pattern from Sm to Gd) (see Taylor and McLennan 1985 for calculation of Eu/Eu*). Chondritic, MORB, and andesitic Eu/Eu* values (1.00, 1.02, and 0.92 respectively) show little or no Eu anomaly; typical upper crust and NASC have moderate Eu depletion (Eu/Eu* = 0.65 and 0.70, respectively (Taylor and McLennan 1985, Gromet et al. 1984: as quoted in McLennan 1989)).

Analyses for REE's were performed by ICP-MS at WSU (see Knaak et al. 1993). Analytical errors for ICP-MS data are given in Appendix 11. The REE plots for each of the three Nisutlin assemblage rock types are displayed in Figure 4.3 a,b, and c. MS samples have the most primitive characteristics. For instance, the degree of LREE enrichment for MS samples ($La_N/Sm_N$ = 2.63 to 1.58), is intermediate between that of andesite and MORB (as quoted above). Eu depletion in two of the MS samples (Eu/Eu*= 0.89 to 0.97) (Fig. 4.3a) is similar to that measured for andesites and MORB's but is far less than that measured for typical upper continental crust values. The other MS sample, SG94-82, has the lowest overall REE abundances and also has a large negative Eu anomaly (Eu/Eu* = 0.07) and heavy REE (HREE) enrichment. Note also that the REE pattern for SG94-82, except for the large Eu anomaly, is similar to REE pattern of Anvil sample SG94-74 (discussed in Section 4.3). This abnormally large Eu anomaly may be due in part to ICP-MS analytical artifacts, caused by low overall REE abundances of sample SG94-82 coupled with imprecise mass-interference corrections (Jenner et al. 1990). Alternatively, the low Eu could be the result of weathering of feldspar from the sample.

REE plots show that QP samples (Fig. 4.3b) display more felsic characteristics than MS samples. QP samples possess a degree of LREE enrichment ($La_N/Sm_N$ = 3.62 to 4.53) that is similar to that of the upper continental crust. Also, the Eu/Eu* range of 0.69 to 0.68 for QP samples SG94-89A and SG94-90C is similar to values of the upper continental crust and North American Shale Composite (Gromet et al. 1984). The third QP sample (SG94-35A) has an extreme degree of Eu depletion ( Eu/Eu* = 0.09), although otherwise it has a similarly shaped REE pattern to the other QP samples. The high $SiO_2$ concentration of SG94-35A (~98 %) may explain the low REE abundances, although the reason for the large Eu anomaly is uncertain (as in sample SG94-82, possibly an analytical artifact).

Five MQS samples have a similar range of LREE-enrichment ($La_N/Sm_N$ = 3.16 to 5.21, excluding SG94-5B) to QP samples (Fig, 4.3a). The degree of Eu depletion in five MQS samples (Eu/Eu* = 0.54 to 0.15) is lower than for QP samples (excluding anomalous SG94-35) and also seems extreme compared to the average Eu anomalies of typical upper continental crust and NASC. MQS sample SG94-5B has a highly anomalous nature. SG94-5B has very high LREE enrichment ($La_N/Sm_N$ = 12.26), possibly because of the presence of LREE-enriched trace minerals such as allanite or monazite (see Section 2.4). SG94-5B also has a small positive Eu anomaly (Eu/Eu* = 1.12). This feature is more difficult to explain, but may be due in part to the presence of plagioclase in this sample (although other MQS samples contain plagioclase but do not possess positive europium anomalies).

### *Provenance-sensitive trace elements*

The provenance of sedimentary deposits can be constrained by examining their immobile trace element composition. Immobile trace elements are useful because they have a systematic relationship with fractionation process that created the source rock, and because immobile trace elements are not easily affected by weathering and diagenesis (Bhatia and Crook 1986), which are inherent parts of sedimentary processes. Large-ion lithophile (LIL) elements (eg. Th, Sr, Rb, U) and rare-earth elements (REE), and other high-field strength (HFS) elements (e.g. Zr, Hf, Nb, Ta ) are not easily incorporated into most rock forming minerals, thus they will preferentially enter the first melt during partial melting or the last crystallized liquid during fractional crystallization, which tend to be more felsic. Thus, LIL and HFS elements are enriched in upper felsic crust. Other trace elements are predominantly compatible in character (eg. V, Sc, Ni, Cr), and are easily incorporated into mafic minerals (Bhatia and Crook 1986). Thus, a ratio of incompatible vs. compatible elements provides a good index of the degree of geochemical differentiation undergone by a sedimentary rock's provenance (Taylor and McLennan 1985).

Unfortunately, during the processes of weathering and diagenesis, sediment may loose part of its elemental inheritance, because of mobility. For instance many compatible elements and also many LIL elements (e.g. Sr, Rb, and Pb) can be mobile. Taylor and McLennan (1985) suggest that certain immobile trace elements, such as Th, REE's, Y, Sc and Co, are quantitatively retained by sediment through transport and deposition, making them useful for comparing the sediments to possible sources. Bhatia and Crook (1986) also employed Zr and Ti in discrimination systems with success, although Taylor and McLennan (1985) caution that Zr commonly is a constituent of heavy minerals, and may have a different environment of deposition than the trace elements incorporated in clays. Whereas few compatible elements are immobile, Sc is unlikely to be strongly affected by weathering and metamorphism (McLennan 1989). The existence of both compatible and incompatible immobile trace elements allows the application of several key ratios to sedimentary systems. For instance, sedimentary rock consisting of detritus shed from oceanic and continental island arcs have lower Th/Sc ratios (Th/Sc $\approx$ 0.15 and 0.85 respectively) than rocks formed in active and passive continental margin environments (Th/Sc $\approx$ 2.6 and 3.1, respectively) (values quoted in Bhatia and Crook 1986).

The three Nisutlin assemblage rock types can be distinguished from one another on the basis of Th/Sc ratios (Fig. 4.4a). The MS rock type possesses low Th/Sc (< 0.2), QP samples have intermediate Th/Sc (0.5 to 2), and MQS samples have the highest Th/Sc range (1 to 7). These results roughly conform to the findings of the REE plots that the general degree of geochemical differentiation is the least in MS, intermediate in QP and greatest in MQS. Five of the MQS samples have a restricted range of Sc and Th and Th/Sc values (2.5 to 7) higher than all QP samples. However, the sixth MQS sample, SG94-53, does not fall in the tight cluster defined by the other MQS samples, and has a Th/Sc value (~1) that falls in the range defined for the QP samples. Samples with anomalously low Eu/Eu* values, SG94-35 and SG94-82, have very low concentrations of Th and Sc, as well as many other incompatible elements (see below).

Sc behaves similarly to V, a ferromagnesian element (Fig. 4.4b). MS samples have elevated concentrations of Sc and V, distinguishing them from both QP and MQS samples. It is more difficult to distinguish between QP and MQS samples because of their lower abundances of these elements, although QP samples have higher V/Sc ratios than the MQS samples (Fig. 4.4b).

The rough positive correlation between La and Th for the Nisutlin samples (Fig. 4.4c) indicates that these elements behaved similarly during sedimentary processes (Bhatia and Crook 1986). The MS and QP rock types generally overlap in Th and La abundances, but MS samples have higher La/Th ratios (5.5 to 12.6) (see Fig. 4.4c). Although the ranges of La/Th for QP and MQS overlap, QP rocks generally have a higher range of La/Th than MQS. One of the MQS samples (SG94-5B) has a high La/Th ratio, similar to values for MS samples (Fig. 4.4c), but this is because of the extreme LREE enrichment (see Fig. 4.3c) of this sample, as discussed above. Overall high concentrations of La and Th of SG94-5B establishes its similarity to other MQS samples.

Zr is generally incompatible in most rock forming minerals, but can be a major component of accessory minerals such as zircon and monazite, which have high densities. Thus, Zr can be fractionated by sedimentary processes, which may make its use in sedimentary provenance studies perilous (Taylor and McLennan 1985). However, as in the La vs. Th plot (Fig. 4.4c), Zr and Th display a rough positive correlation (Fig. 4.4d), suggesting that for this suite, Zr acts in a similar fashion to dispersed incompatible elements (with the possible exception of sample SG94-18, as discussed below). The Zr/Th ratio successfully distinguishes between the three assemblages: MS samples have the highest Zr/Th range (40 to 200), QP samples have intermediate values (25 to 35), and MQS (excluding sample SG94-18) has the lowest range (6 to 15). One exception is MQS sample SG94-18, which has a very high Zr concentration (592 ppm), boosting its Zr/Th ratio to values more similar to MS samples. The elevated Zr concentrations are likely a result of small semi-rounded zircons observed in thin-sections of this sample (although zircon was observed in other MQS samples without producing such a notable effect).

Bhatia and Crook (1986) designed several trace element plots for sedimentary rock that discriminate between major tectonic settings of deposition (Fig. 4.5a, b, c). On the Th - La - Sc ternary diagram (Fig. 4.5a), MS samples plot closest to the Sc pole and QP and MQS (in that order) plot further away from the Sc pole. The data plot similarly on the Sc - Th - Zr/10 diagram (Fig. 4.5b) with MS samples plotting nearest to, and QP and MQS samples plotting the farthest from the Sc pole. Additionally, this plot discriminates in terms of Th and Zr. For instance MQS samples generally have the lowest Zr/Th values (5-16), whereas QP samples have higher Zr/Th values (25-35). Bhatia and Crook (1986) also defined tectonic setting fields on a Ti/Zr vs. La/Sc plot (Fig. 4.5c). The y-axis plots a ratio of Ti/Zr, (both Ti and Zr are group IVA elements), where Ti is ferromagnesian in nature, and the larger Zr ion associates with felsic rock. The samples plot along a hyperbolic-shaped trend (Fig. 4.5c), proceeding from mafic MS samples, which have high Ti/Zr and low La/Sc, through QP samples (intermediate Ti/Zr and La/Sc) to felsic MQS samples (low Ti/Zr, high La/Sc). There is a rough correspondence between the Nisutlin assemblage rock types and the tectonic setting fields of Bhatia and Crook (1986) on the three discrimination diagrams. MS samples overlap with the 'oceanic island arc' field. MQS samples predominantly overlap the 'passive margin' and 'active continental margin' fields, but their Zr/Th values are most similar to those of the active continental margin values make them most similar to active continental margin. QP samples overlap the 'continental island arc field' and 'passive margin' fields.

***Sm-Nd isotope sytematics***

$^{147}$Sm, a radioactive element with a very long half-life (~106 Ga) (Faure 1986) decays into $^{143}$Nd; thus a ratio of radiogenic $^{143}$Nd verses stable $^{144}$Nd in a closed system (initially containing both Sm and Nd) increases over time, but the rate of increase depends on the degree of Sm enrichment relative to Nd. Light rare earth element (LREE) enrichment in partial melts causes felsic rocks to have lower Sm/Nd ratios, and thus a slower rate of $^{143}$Nd/$^{144}$Nd increase, than mafic rocks. At the instant a crustal rock is extracted from the depleted mantle, the $^{143}$Nd/$^{144}$Nd ratio of the depleted mantle and the partial melt will be the same, but the Sm/Nd (and thus $^{147}$Sm/$^{144}$Nd) ratio will be lower in the partial melt. Therefore, from that moment on, the $^{143}$Nd/$^{144}$Nd ratio of the mantle will grow faster than that of the crust extracted from it. However, because $^{147}$Sm has such a slow rate of decay and because Sm and Nd behave relatively similarly, the range of $^{143}$Nd/$^{144}$Nd values in terrestrial samples is quite small compared with other radioactive systems (eg. Pb-U, Rb-Sr, K-Ar) (Faure 1986). Thus, the ratios are often expressed in terms of the εNd parameter (see Faure 1986 for calculation), which recasts the $^{143}$Nd/$^{144}$Nd ratio of a measured sample in terms of its deviation in parts of 10000 from the $^{143}$Nd/$^{144}$Nd of the chondritic uniform reservoir (CHUR) (DePaolo and Wasserburg 1976). CHUR represents the undifferentiated material that comprised the early solar system, as recorded by chondritic meteorites (Faure 1986). CHUR is unlikely to have geological significance in terrestrial rocks, but does provide a useful reference point.

Often εNd values are quoted at time T=0, or present day. Present-day values of εNd range from about +10 in juvenile mantle-derived rocks (Goldstein 1984), like MORB, to low negative values (eg. εNd ≈ -36 in Churchill Archean province (Thériault and Ross 1991)) in Archean cratonic rock. It is also useful to determine εNd values at the time of formation of a rock ($\varepsilon Nd_T$) (see Faure 1986), which helps constrain the nature of the formative materials. For instance, a rock with a highly negative initial εNd value would be predominantly composed of preexisting crustal material, whereas positive εNd values indicates that a rock includes much relatively juvenile, mantle-derived material. Many crustal rocks, however, are constructed from a mixture of starting materials; thus, the Nd isotopic composition of such rocks will be a mixture of its sources, which can make interpretation difficult.

Depleted mantle model ages are another useful parameter used in the study of Nd isotope systematics. A depleted mantle model age ($T_{DM}$) uses the radioactive growth equations to calculate the amount of time that has elapsed since the sample in question was produced from the model depleted mantle. To construct a model age, one assumes that the initial εNd of the rock is equal to the εNd of the depleted mantle at the time when that rock was produced (Faure 1986). This is accomplished by combining the equation that calculates the εNd of the rock at time T with the equation that calculates the εNd of the mantle at the time of the rock's formation, and then solving for T. There are different models of mantle evolution, however. DePaolo (1981) developed a model for mantle evolution that assumes that the mantle has become more enriched in Sm/Nd as crust has been extracted from the mantle over the last 4.5 billion years, causing the rate of εNd increase to grow. The equation that describes this model of mantle evolution is quadratic, so the combination of this equation with the equation describing the εNd of the rock through time cannot directly yield a unique solution for T by rearrangement of terms. Thus, T must be derived iteratively.

A simpler model of mantle evolution proposed by Goldstein et al, (1984) suggests linear growth of the mantle εNd from $T \approx 4.55$ Ga (εNd =0) to $T \approx 0$ Ga (εNd = +10). This model implies that the production of crust is insignificant in terms of the large volume of the mantle, so the εNd of the DM at time T is solved in the same manner as for a closed system rock sample. Using this model of mantle evolution to obtain a $T_{DM}$ age makes it possible to derive a unique solution for T. This thesis will adopt the Goldstein et al. (1984) model because of its relative simplicity. Model ages are not true ages (i.e. rarely do they correspond to crystallization ages derived by the U-Pb zircon method) but provides an estimate of the average length of time that has elapsed since the material that has made up the rock has resided in the crust. Note that most crustal rocks are not pure mantle fractionates or derived from melting within the crust, but have components of both. Thus the model age is a composite of all the components that have been incorporated into the rock.

Interpreting the Nd ratios and $T_{DM}$ model ages (sometimes called 'crustal residence' ages ($T_{CR}$) (O'Nions et al. 1983)) of sediments is more complicated than for the simple scenario outlined above because of the possibility of many different sources contributing detritus to a sedimentary basin. However, several characteristics of the Sm-Nd system make them suitable for provenance work. These include the afore-mentioned properties of a long half life of $^{147}$Sm, which make it applicable to track material over a long period of time, and the systematic behavior between Sm and Nd during crustal formation episodes. Especially important for provenance studies, however, is the property that Sm and Nd are immobile elements, allowing sedimentary detritus to retain the Nd characteristics of the rock from which it was eroded (Boghossian et al. 1996). Moreover, Sm and Nd should remain immobile even during low-grade metamorphic events (DePaolo 1981).

Sm-Nd isotope analyses were performed on the same twelve Nisutlin assemblage samples analyzed for geochemistry (Appendix 7). The results of Nd and Sm isotope analyses on Nisutlin assemblage rocks are presented in table 4.2 and plotted on figure 4.6 (a to d). εNd values of Nisutlin assemblage at 350 Ma ago ($\varepsilon Nd_{350}$), the minimum age of deposition for Nisutlin assemblage (Stevens et al. 1996), have been calculated. Model ages ($T_{DM}$) have not been calculated for samples with $^{147}$Sm/$^{144}$Nd > 0.16, because the ratios are too similar to those of the depleted mantle to be meaningful (Samson et al. 1991). There is a considerable range of $\varepsilon Nd_{350}$ values (Fig. 4.6a, b and c), ranging from +4.9 to -16.5. The MS unit (Fig. 4.6c) has the highest range of values of $\varepsilon Nd_{350}$ (+4.9 to -0.9), QP samples (Fig. 4.6b) have the lowest $\varepsilon Nd_{350}$ values (-9.9 to -16.5), and MQS samples (Fig. 4.6a) have intermediate $\varepsilon Nd_{350}$ values (-1.7 to -11.4). For most of the samples, $^{147}$Sm/$^{144}$Nd ranges from 0.1086 to 0.1461, and generally decreases with decreasing εNd (Fig. 4.6d). Two samples show extreme fractionation. SG94-5B (MQS) has a low $^{147}$Sm/$^{144}$Nd value of 0.0650 (Fig. 4.6a), a result of anomalously high LREE enrichment (see figure 4.3c) possibly because of detrital allanite or monazite (McLennan

1989). SG94-82 (MS), which shows HREE (see figure 4.3) has a $^{147}$Sm/$^{144}$Nd value of 0.2531 (Fig. 4.6d), which causes its εNd value to grow faster than that of the depleted mantle curve (Fig. 4.6c). A model age was not calculated for SG94-82.

McLennan et al. (1988) plotted the εNd parameter against the Th/Sc ratio, which is a useful tool because it combines the age discrimination power of Nd isotopes with the mafic-felsic indicator of Th/Sc. MS samples, with εNd and Th/Sc similar to that of arc andesites (Fig. 4.6e), are clearly separated from QP samples, which have εNd and Th/Sc values similar to that of the upper continental crust (Alberta basement). MQS, which overall shows greater felsic fractionation (here represented by Th/Sc), has intermediate $\varepsilon Nd_{350}$ values.

### *Summary*

The geochemistry of the three Nisutlin assemblage rock types is closely linked to their lithology. MS samples have the lowest quartz contents and the highest chlorite and amphibole contents of any of the three Nisutlin assemblage rock types, which explains the low $SiO_2$ and high FeO*, MgO, and Ti contents, as well as the enrichment of compatible trace elements (Sc, V) relative to incompatible trace elements (e.g. Th, La). The MQS samples contain abundant mica, which explains the relatively high concentrations of incompatible elements such as Th, La, and Zr in these rocks. The QP samples, being highly quartz rich, have low abundances of most elements. The lithological descriptions of the rocks hints at their sedimentary precursors. MS samples may represent basaltic material, or first-order sediment shed from mafic rock. The high quartz content of the QP samples suggests that they are derived from mature sedimentary rock. MQS samples may be derived from arkosic sandstone.

Trace element geochemistry indicates that the provenance of the supracrustal Nisutlin assemblage includes input from felsic upper crust and more primitive mafic material. Felsic members of the Nisutlin assemblage include the QP and MQS rocks, which typically have negative Eu anomalies, LREE enrichment, and high Th/Sc values. Relatively flat REE plots, low Th/Sc values and high Ti/Zr values of the MS assemblage indicate its mafic nature. The groupings of this study show good correspondence with suites used by Bhatia and Crook (1986) to define tectonic settings. In several of the discrimination plots, MS sample data overlap the field of 'oceanic island arc'. Most MQS samples overlap the 'passive margin' and 'active continental margin' fields although the range of Zr/Th is more similar to those of active continental margins. Two of the QP samples consistently plot in the 'continental island arc' field; the third QP sample, SG94-89, consistently plots in the 'passive continental margin' field. The comparison between the rock types of this study and the tectonic setting fields of Bhatia and Crook (1986) helps to illustrate that there is both primitive mafic material (MS) and more chemically evolved upper crustal material (MQS and QP) contributing to the Nisutlin assemblage provenance. Moreover, MQS have some characteristics of sediment shed from active continental margins. QP and MQS samples have moderately negative $\varepsilon Nd_{350}$ values, which indicates that they have material derived from crust that was extracted from the mantle and has been evolving separately for a considerable length of time ($T_{DM}$ age range: 1.2 to 2.4 Ga). The MS unit has higher $\varepsilon Nd_{350}$ values that suggests a more juvenile source.

## 4.3 ANVIL ASSEMBLAGE

The Anvil assemblage data have been plotted on figures 4.2 through 4.6 along with the Nisutlin assemblage data. In most respects, Anvil samples are similar to the MS unit of the Nisutlin assemblage in overall mafic character. The $SiO_2$ range of the three Anvil assemblage samples examined (47 to 58%) is lower than, but overlaps, that of the MS assemblage (52 to 68 %). Examining other major elements (Fig. 4.2), it can be noted that SG94-52 and SG94-75A are most similar to the MS unit; the $Al_2O_3$ (14 to 17%) and FeO* + MgO (12 to 17 %) ranges of the Anvil samples SG94-52 and SG94-75A overlaps those of the MS samples. The range of alkalis for SG94-52 and SG94-75A ($K_2O + Na_2O$ = 5 to 6 %) is higher than but similar to the range of alkalis for the MS samples. SG94-74 has strikingly different characteristics. This sample, possessing the lowest $SiO_2$ of any sample in the Nisutlin or Anvil assemblages, has the lowest range of $Al_2O_3$ and alkalis (2

% and 0% respectively) and the highest range of FeO* + MgO (9% FeO* and 39% MgO). These are values characteristic of peridotite (McDonough and Frey 1989) and the textures noted for this samples (Section 2.4) are typical of sepentinite.

Two of the Anvil samples have REE patterns that suggests they were intermediate-mafic rocks (Fig. 4.3d). Sample SG94-75A is the most REE enriched of the Anvil samples ($La_N/Sm_N$ = 2.6 and $La_N/Yb_N$ = 4.86) and has a degree of LREE enrichment intermediate between andesites and MORB's (see Section 4.2). Anvil sample SG94-52 is flatter, but still has a higher degree of LREE enrichment ($La_N/Sm_N$ =1.8 and $La_N/Yb_N$ = 2.0) than MORB's. The third Anvil sample, SG94-74, has a slightly U-shaped REE pattern featuring progressive HREE enrichment ($Gd_N/Yb_N$ = 0.6 to 0.7), and Ce depletion (Fig. 4.3d). U-shaped REE patterns are common features of ultramafic peridotites, and Ce anomalies may suggest interaction with seawater (eg. McDonough and Frey 1989). This interpretation is consistent with the major element composition and textures that suggests that this sample is a serpentinized peridotite. Rare-earth plots of the Anvil samples (Fig. 4.3d) show similarities to those of the MS samples (Fig. 4.3c). Anvil sample SG94-75A has a pattern roughly parallel to those of Nisutlin MS samples SG94-80 and SG94-85 ($La_N/Sm_N$ = 2.2 to 2.6 and $La_N/Yb_N$ = 4.15 to 5.88) (Fig. 4.3 c and d). MS sample SG94-82, except for the abnormal degree of Eu depletion, shares several similarities to the REE pattern of Anvil sample SG94-74; SG94-82 possesses a slight U-shaped pattern, features progressive HREE enrichment may also have a slight Ce anomaly.

Like the MS samples, Anvil assemblage samples are low in incompatible elements such as Th, La, and Zr and high in compatible elements such as Sc and V (Fig. 4.4a-d). The Anvil samples share the same low range of Th/Sc (0.1 to .003) and high ranges of La/Th (3.5 to 12) and Zr/Th (36 to 190) with MS samples. For comparison, the Anvil samples are also plotted on the Bhatia and Crook (1986) discrimination diagrams (Fig. 4.5 a-c), where they typically occupy a similar range as MS samples on the two ternary diagrams (Fig. 4.5 a,b). On the Ti/Zr vs. La/Sc diagram, the Anvil samples share a similar low range of La/Sc as the MS samples, but SG94-52 and SG94-74 have very high and low values, respectively, of Ti/Zr (Fig. 4.5 c). Only one Anvil sample, SG94-52, was analyzed for Nd isotopes (Appendix 7). The present day εNd ($\varepsilon Nd_0$ = +0.21) and $^{147}Sm/^{144}Nd$ ratio ($^{147}Sm/^{144}Nd$ = 0.17) is very similar to that of the MS samples (Fig. 4.6c and d). SG94-52 also overlaps with the MS Nisutlin samples on a plot of εNd vs. Th/Sc (Fig. 4.6e).

As discussed in Chapter 2, the Anvil assemblage is commonly correlated to the Slide Mountain terrane. However, this correlation implies that Anvil assemblage rocks should be ocean floor MORB's, an assertion on which some doubt has been cast by preliminary evidence (Creaser et al. 1997a). In order to better constrain the tectonic environment in which the Anvil assemblage rocks were created, several additional plots will be presented Fig. 4.7(a-e). Because of the overall similarity of the Anvil and MS Nisutlin assemblage samples highlighted above, the MS Nisutlin samples will also be presented on these diagrams.

The Anvil data were plotted on several tectonic discrimination diagrams devised by Pearce and Cann (1973) for basaltic rock. On a Zr - Ti/100 - Y∗3 ternary diagram (Fig. 4.7 a), sample SG94-75A plots in the field for calc-alkalic basalt (CAB) and SG94-52 plots in a poorly constrained field in which low-potassium tholeiite (LKT) and CAB overlap with OFB. The principal result from this diagram is that none of the samples plot in the within-plate basalt (WPB) field. Better discrimination of non-WPB samples can be achieved on a Ti vs. Zr (Fig. 4.7b) plot (Pearce and Cann 1973), on which SG94-75A plots as a CAB and SG94-52 as an OFB. Sample SG94-74 plots outside all fields defined by Pearce and Cann (1973) on these two diagrams.

A multi-element plot devised by Pearce (1983) arranges elements (normalized to MORB) on the basis of decreasing distribution coefficient between garnet lherzolite and melt (in small degree partial melting) from Th to Yb (Fig. 4.7d and e). In effect, this plot shows decreasing incompatibility from Th to Yb (Pearce 1983); Y and Yb, the least incompatible elements on the plot, are not enriched over MORB values, so they can be used to establish a baseline from which the degree of enrichment for the remaining elements may be judged. The enrichment of Nb, Zr, Hf, $TiO_2$, and Y relative to MORB's is very slight in SG94-52 (Fig. 4.7d). However, Ce, $P_2O_5$, and Sm (also LIL's - not shown except Th) show considerable enrichment, manifested as prominent positive anomalies. The presence of positive Ce, $P_2O_5$, and Sm anomalies in otherwise non-enriched basalt is characteristic of basalt produced in a calc-alkalic island arc setting (Pearce 1983). Also, the Zr/Y value of sample SG94-52 (Zr/Y = 2.5) is similar to that of oceanic island arcs (Zr/Y < 3) (Pearce 1983). Sample SG94-75A is similar to SG94-52 in that it also possesses positive Ce, $P_2O_5$, and Sm anomalies, but differs in that the remaining elements show progressive enrichment from Yb (non-enriched) to Ta (enriched) (Fig. 4.7e). This type of pattern is interpreted by Pearce (1983) to be the result of the superposition of a calc-alkalic signature (enriched Ce, $P_2O_5$, and Sm) on a WPB signature (steadily increasing enrichment from Yb and Y to Th) - a pattern typically displayed by basalts produced at active continental margins (eg.: the Andean chain). Additionally, Zr/Y of SG94-75A (Zr/Y = 4.46) shows enrichment comparable to active continental margins (Zr/Y > 3) (Pearce 1983). The remaining Anvil sample, SG94-74, has a jagged pattern that does not lend itself to simple interpretation regarding tectonic settings (Fig. 4.7 d), but may instead be a result of melt-crystal relations or possibly alteration.

The three MS Nisutlin samples were plotted on the tectonic discrimination diagrams as well. Samples SG94-80 and SG94-85, the samples most similar to Anvil samples SG94-75A in terms of REE patterns (Fig. 4.3e), do not consistently plot in the same tectonic field on the ternary and bivariate diagrams (Fig. 4.7a to c). However, they possess strikingly similar multielement patterns as Anvil sample SG94-75A (Fig. 4,7 e). Sample SG94-82 has a jagged pattern (Fig. 4.7d), not unlike sample SG94-74, which bears no resemblance to patterns of normal tectonic settings.

### *Summary*

The three Anvil samples examined in this study are mafic, and share some broad major and trace element characteristics with the Nisutlin assemblage MS's. The three Anvil samples are not uniform, however. Anvil sample SG94-75A shows the highest degree of LREE enrichment of the three and plots as a CAB on bivariate and ternary tectonic discrimination diagrams devised by Pearce and Cann (1973). The multielement pattern and enriched Zr/Y and Th/Yb ratios (Zr/Y = 4.46, Th/Yb = 1.25) of SG94-75A clearly shows that it is a CAB originating from an active continental margin (Pearce 1983). The tectonic setting of Anvil sample SG94-52 is not as clearly delimited as that of SG94-75A. SG94-52 has only slight LREE-enrichment and plots as an OFB on the bivariate and ternary tectonic discrimination plots devised by Pearce and Cann (1973). The multielement plot for SG94-52 also shows that Zr, Ti, and Y (used in the bivariate and ternary diagrams) are not enriched relative to MORB, but Ce, $P_2O_5$, and Sm are enriched, which is indicative of CAB's produced in oceanic island arcs (Pearce 1983). Despite the fact that the data are somewhat conflicting, it is interpreted that SG94-52 likely represents oceanic island arc CAB, because multielement plots show more complete geochemical trends than simpler bivariate or ternary plots. The third Anvil sample, SG94-74, has the texture and major element composition of a serpentinite. The REE pattern is relatively flat but is slightly depleted with respect to middle -REE's, and also has a negative Ce anomaly, which are common features of ultramafic peridotite (McDonough and Frey 1989). Also, SG94-74 has major element characteristics of peridotite (MgO = 39%), and serpentinite textures. Because it is an altered ultramafic rock, the tectonic discrimination diagrams are not applicable to this sample.

REE and multielement plots of Nisutlin MS samples SG94-80 and SG94-85 bear a resemblance to those of Anvil sample SG94-75. They do not plot consistently on the simpler bivariate and ternary diagrams, which may be a function of a higher degree of metamorphism (they are more deformed than the Anvil assemblage), or that they may have had some sediment input or tectonic mixing with more felsic Nisutlin assemblage. The third MS sample, SG94-82, has a similar REE pattern to Anvil sample SG94-74 in terms of Ce anomalies and HREE enrichment, although SG94-82 also has a large Eu anomaly. SG94-82 also has a similar multielement pattern to Anvil sample SG94-74 and these samples together have the lowest concentrations of incompatible elements, lowest Th/Sc and La/Sc, and highest Zr/Th values of any Nisutlin or Anvil assemblage samples. Sample SG94-82 is not as similar to SG94-74 with respect to major elements, (MgO = 11.75), but the trace element similarities are striking. Whether SG94-82 is related to

SG94-74 is not known, but these two samples contrast strongly with the other MS and Anvil rocks of this study.

## 4.4 DISCUSSION

### *Nisutlin assemblage*

The Nisutlin assemblage in the locality around the Money klippe contains much felsic material with a long crustal residence (QP and MQS), but also contains juvenile mafic material (MS) as well. On the basis of the high quartz contents and high degree of weathering, the QP samples likely represent mature sediment. REE patterns and key trace element ratios of the QP samples suggest that they are derived from a continental island arc or a passive margin. The material comprising the QP unit has a long crustal residence history ($T_{DM} \approx 1.97$ to 2.35 Ga). MQS samples are more mica-rich than QP samples, suggesting that they represent less mature sediment, such as arkosic sandstone. On trace element discrimination diagrams, MQS samples plot in fields delineated for passive margin or active continental margin settings; low Zr/Th ratios favour the latter setting. Nd isotopes indicate that the MQS samples are slightly more juvenile ($T_{DM} \approx 1.23$ to 1.98 Ga) than QP samples. MS samples, notably darker and greener in the field than MQS or QP samples, contain abundant chlorite and amphibole. They have low abundances of most incompatible trace elements and the lowest degree of enrichment of incompatible elements relative to compatible elements. The high range of εNd ($\varepsilon Nd_0 \approx -3.2$ to $+6.4$) indicates that they are composed of relatively juvenile material.

Other YT terrane supracrustal rocks have provenance from both ancient crustal material and juvenile material. Samson et al. (1991) identified four small metamorphic terranes in the Coast Belt that consist, in part, of crustally evolved material, which contrasts strongly with juvenile rock in surrounding terranes. Samson et al. (1991) correlated these four Coast Belt terranes to the YT terrane (often called the Nisling terrane in the Coast Belt) based on lithological similarity and the ancient Nd $T_{DM}$ ages of some samples from the Coast Belt terranes. The YT terrane rocks of the Coast Belt contain not only evolved crustal material, however; the data form three distinct groupings in terms of Nd isotopes - 'juvenile': $\varepsilon Nd_0 \approx +3$ to -5; 'intermediate: $\varepsilon Nd_0 \approx -7$ to -14; and 'evolved crustal': $\varepsilon Nd_0 \approx -23$ to -27 (Fig. 4.9). These groupings broadly coincide with groupings defined by Creaser et al. (1997a) for YT terrane rocks from the TTZ (Fig. 4.9a). Nisutlin assemblage rock crops out in the TTZ, where Stevens et al. (1996) have correlated it to the Middle Unit of the Layered Metamorphic Sequence described by Mortensen and Jilson (1985). Samples were grouped according to geochemical parameters into three 'types': type N I, type N II, and type N III. These types also have relatively distinct $\varepsilon Nd_0$ groupings ($\varepsilon Nd_0 \approx +4.3$ to -7.2 for type N I; $\varepsilon Nd_0 \approx -6.9$ to -18.3 for type N II; $\varepsilon Nd_0 \approx -23.9$ to -28.4 for type N III), which overlap in range to those from the Coast Belt (Fig. 4.9). Briefly, the TTZ data form an array from geochemically and isotopically primitive type N I to crustally evolved type N III; type N II possesses intermediate Nd isotopic and geochemical characteristics (Creaser et al. 1997a) (Fig. 4.8b). This may indicate that material comprising the Nisutlin assemblage in the TTZ represents two end-member-mixing between juvenile material and ancient crustal material (Creaser et al. 1997a).

There are broad similarities between the Nd data of supracrustal rock from the Money klippe area and from the TTZ and Coast Belt (Fig. 4.9); however, several important differences exist. Firstly, both the YT terrane rocks examined in the Coast belt and in the TTZ show little correlation between rock type and Nd characteristics, unlike samples from the Money klippe area. Secondly, whereas $\varepsilon Nd$ and $T_{DM}$ data from the MK area Nisutlin assemblage show a wide range of values that broadly overlap those of the Coast Belt and TTZ rock, they do not form the same groupings. For instance MQS and QP $\varepsilon Nd$ and $T_{DM}$ data are largely concentrated between the 'intermediate' (eg. type N II of the TTZ) and the 'crustally evolved' (eg. type N III) groups (Fig. 4.9). One important aspect of this discrepancy is that the oldest $T_{DM}$ ages ($T_{DM} \approx 2.5$ to 2.8 Ga) and lowest $\varepsilon Nd_0$ values ($\varepsilon Nd_0 \approx -23$ to -29) typified by type N III (and Coast Belt equivalents) are not represented in the MK area. It is also possible that the old crustal rocks are under-represented in the MK area because of the small size of the MK database. Trace element geochemistry was performed on the TTZ rocks but not on the Coast Belt rocks, so only the latter can be compared to the MK rocks in this manner.

In terms of trace element geochemistry, the MS and QP samples from the MK area share similarities with the TTZ data, whereas MQS samples may have a distinct derivation. The MS and type N I overlap in geochemical properties; both likely are derived in large part from juvenile mafic material (Fig. 4.8). The QP data have geochemical properties intermediate between type N III and type N II (Fig. 4.8). The MQS unit has a much higher degree of enrichment of incompatible elements relative to compatible elements (eg. La/Sc and Th/Sc), and lower Zr/Th ratios compared to the other Nisutlin samples. The negative Eu anomalies of the MQS samples are also the lowest of any Nisutlin samples and seem extreme compared with Eu/Eu* values of typical passive margin sediment (McLennan et al. 1990, Bhatia 1985, Creaser et al. 1997a). Thus, whereas QP and MS data fall on the same trend shown by the TTZ samples on an εNd vs. Th/Sc plot (Fig. 4.8b), the majority of MQS samples do not. This indicates that MQS samples are not compatible with the two end-member mixing model (between crustally evolved material and mafic-intermediate volcanism) proposed for the TTZ Nisutlin assemblage by Creaser et al. (1997a) The MQS samples may instead represent detritus shed by felsic volcanism in an active continental margin. Also, whereas the MS and QP units from the MK area and all Nisutlin TTZ rocks correlate to the Middle Unit of Mortensen and Jilson (1985), MQS samples are interpreted to belong to the Lower Unit of Mortensen and Jilson (1985). However, the available data are limited and from widely scattered areas in the YT terrane, so further studies would help constrain these preliminary findings greatly.

### *Anvil assemblage*

Two of the three Anvil assemblage samples from the Money klippe area have some characteristics of calc-alkalic basalt, which is difficult to reconcile with the third Anvil sample, which is a serpentinized ultramafic rock. The presence of CAB material in the Anvil assemblage complicates its correlation to the Slide Mountain terrane. The term 'Slide Mountain terrane' originally described sequences of oceanic crust and related pelagic sediments in British Columbia, but has since been applied to many mafic bodies tectonically intermixed with the YT terrane as well (Monger 1984, Wheeler et al. 1991, Mortensen 1992b). Geochemical analyses from mafic bodies within the YT terrane have only recently been performed to test the correlation to the Slide Mountain terrane. Whereas Plint and Gordon (1997) found that mafic bodies near the YT-autochthon interface in the Campbell Range have MORB characteristics and thus are consistent with the 'Slide Mountain' appellation, Creaser et al. (1997a) found that mafic bodies complexly intermixed with the Nisutlin assemblage in the TTZ have calc-alkalic characteristics and thus are inconsistent with correlation to the Slide Mountain terrane. It can be seen that mafic bodies associated with the YT terrane are not uniform; mafic rock from two YT terrane localities have characteristics of CAB's produced at arcs (eg. Anvil assemblage from the TTZ and the Money klippe) whereas the third locality (Campbell Range) yields mafic rock that is more likely MORB. One way around this discrepancy is a suggestion made by Mortensen (1992b) that mafic rock located along the boundary of the YT terrane and North America correlates to the Slide Mountain terrane, but the generally smaller mafic bodies imbricated within the YT terrane southwest of the interface have other origins. The idea is intriguing, but supporting data are sparse and the amount of similar yet unanalyzed mafic bodies throughout the YT terrane is large. Another difficulty with this model is that the third Anvil sample collected at the MK locality has characteristics that indicate that it is a serpentinized ultramafic rock, which does not fit with the CAB setting, unless it represents some type of xenolith or oceanic substrate tectonically entrained with the CAB rock.

Another preliminary finding is that mafic members of the Nisutlin assemblage, here represented by the MS unit, share some geochemical similarities to the Anvil assemblage rocks in the Money Klippe area. Mafic material dispersed throughout the Nisutlin assemblage may represent volcanic interbeds within the more quartzofeldspathic metasedimentary sequences of the Nisutlin assemblage (eg. volcanic component of the Middle Unit - correlated to the MS unit in the MK area). Larger mafic bodies have been mapped as the Anvil assemblage (or Anvil Allochthon) or more recently, the Slide

Mountain terrane. However, these preliminary data show that some similarities exist between the two entities as mapped.

### *Comparison to the miogeocline and Alberta basement*

In order to test assertions that the YT terrane is a metamorphosed and deformed equivalent of the miogeocline, the Nd data of Nisutlin assemblage and the Anvil assemblage from the MK and TTZ, as well as similar supracrustal rocks from the Coast Belt (Nisling/YT terrane) (Samson et al. 1991), will be compared to the Nd data available for the cratonic and miogeoclinal rocks to the east. The data available for the craton and miogeocline are limited to Nd isotopes; little geochemistry was performed. Also, it would have been preferable to compare the Nisutlin data to miogeoclinal rocks directly adjacent to the YT terrane in the Yukon, Northwest Territories and northern British Columbia rather than those from the southern Canadian Cordillera. However, data were only available for the latter. The next few paragraphs will present brief summaries of the data from the main miogeoclinal packages (Fig. 4.9), followed by comparisons to the YT terrane data. The main packages to which the YT terrane data will be compared are the Alberta Basement, the Belt-Purcell Supergroup, the Windermere Supergroup, and the Early Phanerozoic. Note that all $T_{DM}$ ages reported in the text have been recalculated from the published data (where necessary) according to the model and parameters of Goldstein et al. 1984, for ease of comparison.

Thériault and Ross (1991) reported U-Pb and Sm-Nd analyses from five domains of the Early Proterozoic basement underlying almost the entire northern half of Alberta. These Early Proterozoic domains of the Alberta basement, covered by the miogeoclinal sequences, lie to the west of the exposed Archean Churchill province (Thériault and Ross 1991). U - Pb zircon (and some monazite) crystallization ages of the Alberta basement domains range from 1.8 Ga to 2.2 Ga (Thériault and Ross 1991) (Fig. 4.9). The range of εNd values (+1.0 to -9.7) at the time of formation are an average of ~8.3 εNd units less than the depleted mantle (εNd ≈ +5.0 to +6.0) at that time, indicating that older recycled Archean crust constitutes a major component of these rocks; Thériault and Ross (1991) calculate that a minimum of 10% Archean material comprises the Alberta basement domains. That the Early Proterozoic crust of the Alberta basement has incorporated Archean material is also borne out by the 2.3 to 2.6 Ga $T_{DM}$ model ages of the domains, which are in excess of their age of formation (Fig. 4.9).

Much subsequent sedimentation on the edge of the craton was dominated by recycling of the Alberta basement and Archean material. The Late Proterozoic Windermere Supergroup, which is considered to represent the beginning of the true miogeocline, contains predominantly coarse grained clastics (Ghosh and Lambert 1989, Boghossian et al. 1996). The majority of Windermere Supergroup samples have Nd characteristics ($\varepsilon Nd_0$ = -21.5 to -29.5) that overlap with those of the Alberta basement (Burwash et al. 1988, Ghosh and Lambert 1989, Boghossian 1996) (Fig. 4.9). For instance, the Nd model ages of the Windermere Supergroup ($T_{DM} \approx$ 2.4 to 2.7 Ga; average ≈ 2.54 Ga) are very similar to the range of model ages for the Alberta Basement (2.3 to 2.6 Ga) (Fig. 4.9). Cambrian to Ordovician strata of the Foreland Belt, which unconformably lay on the Windermere Supergroup, have a slightly lower, but overlapping, range of model ages ($T_{DM} \approx$ 1.9 to 2.7 Ga; average ≈ 2.35 Ga) and similar range of $\varepsilon Nd_0$ (-21.0 to -27.1) as the Alberta Basement (Boghossian et al. 1996) (Fig. 4.9). Notice, however, that the Cambrian to Ordovician strata of the Omineca Belt are more variable and generally more juvenile than those of the Foreland Belt (Ghosh and Lambert 1989) (Fig. 4.9). Nevertheless, the Windermere to Ordovician stratigraphic record of the miogeocline preserves material that was primarily derived from the Alberta basement (Burwash et al. 1988, Boghossian et al. 1996)

Not all sedimentary units on the western margin of the North American craton have been as heavily influenced by recycling of Archean material. The Middle Proterozoic Belt Purcell Supergroup lies on top of the Alberta Basement and beneath the Late Proterozoic Windermere Supergroup in the Cordillera of southern Canada and northern United States, but unlike either of these heavily Archean-influenced units, typically has $T_{DM}$ ages in the range of 1.9 to 2.1 Ga, and $\varepsilon Nd_0$ values ranging from -11 to -20 (Frost and O'Nions 1984, Frost and Winston 1986, Burwash et al. 1988, and Ghosh and Lambert 1989) (Fig. 4.9). Proposed sediment sources for the Belt-Purcell Supergroup include a mixing of sediment shed from the Trans-Hudson orogen with Archean material (Burwash et al. 1988), 'efficient fluvial mixing' from a continental-scale fluvial drainage system (Frost and O'Nions 1984), derivation from a continent (Siberia, Australia?) adjacent to western North America prior to Middle Proterozoic rifting (Frost and Winston 1987), or sediment from the Wopmay orogen (Ghosh and Lambert 1989). Most of these models have difficulties and no consensus has been reached. The Devonian to Triassic strata of the miogeocline in the Foreland Belt show a distinct break in Nd characteristics from the Cambrian to Ordovician record (Boghossian et al. 1989). These rocks have similar characteristics ($\varepsilon Nd_0 \approx -9.3$ to $-13.3$; $T_{DM} \approx 1.4$ to 1.9 Ga) to the Belt-Purcell rocks (Fig. 4.9). Boghossian et al. (1996) consider three explanations to account for the observations; Mixing of juvenile Cordilleran and Alberta Basement sediments, derivation from the Appalachian or Grenville orogens, and derivation from the Canadian Arctic (Innuitian Foldbelt). Boghossian et al. (1996) disfavour the former two scenarios (the first because of the lack of abundant material with appropriate Sm/Nd ratios formed at the same time; the second because of paleogeographic constraints) and favour the third possibility. While acknowledging the lack of Nd data to positively establish the Innuitian foldbelt rocks as a possible source, Boghossian et al. (1996) indicate that the age of the Ellesmerian orogen (Late Devonian to Early Mississippian) and the paleogeography of the time make it a plausible source.

Results from this thesis as well as from studies by Creaser et al. (1997a) and Samson et al. (1991) show that whereas Nd characteristics of some YT terrane rocks strongly suggest that Archean material is a significant component, other samples are more juvenile than even the Belt Purcell and Devonian-Triassic miogeoclinal samples. This is a significant finding that shows that the YT terrane does not directly represent the North American miogeocline. Broadly, the TTZ and Coast Belt samples with the oldest $T_{DM}$ ages and lowest $\varepsilon Nd$ values (eg. Type N III from the TTZ) overlap the data from the Windermere and Cambrian-Ordovician samples (Fig. 4.9), and are compatible with derivation from the Alberta Basement (Creaser et al. 1997a, Samson et al. 1991). The YT terrâne rocks with juvenile Nd characteristics ($\varepsilon Nd_0$ = +4.3 to -7.2; $^{147}Sm/^{144}Nd$ = 0.13 to 0.17), however, are compatible with derivation from a mafic-intermediate calc-alkalic arc, perhaps represented by the Anvil assemblage (Creaser et al. 1997a). It is important to stress, however, that the juvenile rocks from the TTZ and the Coast Belt have no systematic relationship between lithology and Nd isotopes, which suggests that they may have received juvenile detritus from mafic-intermediate calc-alkalic basalt, but do not directly represent basalt. However, it is not as easy to rule out the possibility that the juvenile MS unit from the Money klippe directly represents metamorphosed calc-alkalic basalt, because it contains abundant mafic minerals. It is also possible that the MS unit represents first-cycle sediment derived from calc-alkalic basalt. Regardless, the TTZ or Coast belt rocks with juvenile Nd characteristics have few counterparts from any of the miogeocline, including the relatively juvenile Belt-Purcell and Devonian-Triassic rocks (Fig. 4.9). 'Intermediate' Nd characteristics of some YT terrane rocks (eg. Type N II) may be explained by mixing of the juvenile and ancient crustal sources (Creaser et al. 1997a), but not all. The MQS samples have intermediate Nd characteristics, but geochemically do not fit on a mixing trend (Fig. 4.9). Instead, these samples likely originate from felsic volcanism from an active continental margin.

Much juvenile mafic material is associated with the YT terrane. In the TTZ and in the MK field areas, sheared greenstones of the Anvil assemblage are commonly entrained within the Nisutlin assemblage. Geochemistry from the TTZ (Creaser et al. 1997a) and from the Money klippe area (this study), however, show that calc-alkalic material is contained within the Anvil assemblage, although some ultramafic rocks are present as well. Additionally, MS rocks from the Nisutlin assemblage surrounding the Money klippe area, are broadly similar to the Anvil assemblage and may represent volcanic interbeds, or immature sediment derived from the Anvil assemblage. Creaser et al. (1997a) suggests sediment shed from the CAB's, represented by the Anvil assemblage, imparted their juvenile characteristics to Nisutlin rocks such as the type N I. None of the miogeocline sequences have material as juvenile as that found in the YT terrane (Fig. 4.9), thus it is difficult to support models that suggest that the YT terrane directly represents a metamorphosed and deformed miogeocline sequence. However, the data do support models that suggest the YT terrane formed as a distal portion of the miogeocline (Mortensen 1992b, Creaser et al. 1997a), receiving some ancient crustal material from the east, but also influenced by juvenile calc-alkalic magmatism.

Table 4.1. Geochemistry of samples from the Nisutlin and Anvil assemblages

| SG94- | 5B | 17B | 18A | 24 | 35A | 53 | 65 | 80 | 82 | 85 | 89A | 90C | 52 | 74 | 75A |
|---|---|---|---|---|---|---|---|---|---|---|---|---|---|---|---|
| unit | MQS | MQS | MQS | MQS | QP | MQS | MQS | MS | MS | MS | QP | QP-g | Anvil | Anvil | Anvil |
| **Major elements (ppm)** | | | | | | | | | | | | | | | |
| $SiO_2$ | 75.42 | 75.15 | 74.24 | 75.92 | 97.93 | 76.88 | 77.70 | 51.37 | 58.72 | 68.11 | 91.79 | 88.62 | 52.80 | 47.18 | 58.24 |
| $Al_2O_3$ | 13.22 | 12.04 | 13.48 | 12.70 | 1.20 | 12.30 | 12.36 | 18.93 | 10.02 | 11.18 | 4.47 | 6.58 | 14.30 | 2.17 | 17.14 |
| $TiO_2$ | 0.202 | 0.173 | 0.339 | 0.292 | 0.045 | 0.191 | 0.171 | 2.047 | 0.166 | 1.225 | 0.198 | 0.318 | 1.685 | 0.028 | 0.637 |
| FeO* | 1.79 | 1.53 | 3.11 | 2.23 | 0.32 | 2.45 | 2.12 | 9.80 | 7.06 | 7.28 | 1.29 | 2.03 | 12.71 | 9.17 | 7.02 |
| MnO | 0.035 | 0.037 | 0.011 | 0.028 | 0.005 | 0.040 | 0.021 | 0.102 | 0.250 | 0.151 | 0.043 | 0.008 | 0.110 | 0.142 | 0.125 |
| MgO | 0.19 | 0.56 | 0.42 | 0.67 | 0.13 | 0.45 | 2.86 | 6.18 | 11.75 | 5.36 | 0.64 | 0.64 | 5.49 | 39.27 | 5.61 |
| CaO | 0.91 | 0.80 | 0.96 | 0.75 | 0.06 | 1.99 | 0.56 | 6.23 | 8.93 | 3.66 | 0.23 | 0.06 | 7.07 | 2.02 | 5.88 |
| $K_2O$ | 5.836 | 875 | 0.89 | 4.32 | 0.30 | 0.84 | 3.05 | 1.21 | 1.29 | 0.45 | 1.20 | 1.60 | 0.26 | 0.00 | 0.81 |
| $Na_2O$ | 2.37 | 0.92 | 6.51 | 3.02 | 0.00 | 4.85 | 1.14 | 3.54 | 1.78 | 2.37 | 0.00 | 0.05 | 5.34 | 0.00 | 4.42 |
| $P_2O_5$ | 0.028 | 0.040 | 0.049 | 0.072 | 0.014 | 0.025 | 0.021 | 0.596 | 0.040 | 0.204 | 0.134 | 0.097 | 0.239 | 0.12 | 0.127 |
| **Trace elements (ppm)** | | | | | | | | | | | | | | | |
| Ba | 2882 | 467 | 684 | 467 | 769 | 1209 | 626 | 492 | 38.53 | 766 | 1569 | 734 | 70 | 6 | 445 |
| Rb | 117.85 | 226.21 | 17.24 | 94.44 | 13.35 | 27.32 | 116.91 | 44.18 | 28.00 | 12.49 | 50.01 | 66.27 | 4.24 | 1.02 | 19.16 |
| $Sr^\dagger$ | 161 | 36 | 69 | 62 | 4 | 424 | 39 | 456 | 196 | 154 | 19 | 12 | 165 | 32 | 294 |
| Cs | 1.84 | 3.65 | 0.60 | 0.87 | 0.20 | 0.77 | 7.13 | 9.33 | 2.04 | 0.35 | 1.74 | 2.36 | 0.24 | 2.11 | 0.86 |
| Pb | 9.49 | 4.20 | 2.69 | 12.47 | 1.71 | 8.51 | 29.68 | 13.07 | 4.25 | 1.98 | 7.69 | 7.56 | 3.92 | 1.39 | 3.12 |
| Th | 24.63 | 21.77 | 16.18 | 17.46 | 0.59 | 11.22 | 26.96 | 3.38 | 0.11 | 2.50 | 3.87 | 5.91 | 0.78 | 0.10 | 1.97 |
| U | 2.73 | 3.64 | 3.87 | 4.52 | 0.34 | 4.62 | 6.06 | 0.86 | 0.13 | 1.12 | 1.35 | 1.85 | 0.49 | 0.14 | 1.25 |
| $Zr^\dagger$ | 257 | 169 | 592 | 224 | 19 | 172 | 172 | 204 | 21 | 109 | 136 | 154 | 88 | 10 | 72 |
| Nb | 11.41 | 18.30 | 47.56 | 23.29 | 1.10 | 11.84 | 20.64 | 25.76 | 0.53 | 10.92 | 5.57 | 6.85 | 3.80 | 0.19 | 5.51 |
| Hf | 6.12 | 5.69 | 16.54 | 6.63 | 0.37 | 4.43 | 5.76 | 4.62 | 0.68 | 2.61 | 3.56 | 4.20 | 2.26 | 0.07 | 1.83 |
| Ta | 0.81 | 1.89 | 3.64 | 2.00 | 0.33 | 0.95 | 1.97 | 1.76 | 0.10 | 0.77 | 0.55 | 0.60 | 0.29 | 0.05 | 0.38 |
| Y | 12.32 | 33.92 | 52.15 | 35.98 | 2.38 | 32.76 | 35.80 | 45.51 | 9.77 | 24.87 | 9.70 | 11.60 | 35.05 | 2.35 | 16.14 |
| La | 132.88 | 33.78 | 39.06 | 49.40 | 2.05 | 38.80 | 46.30 | 32.52 | 1.38 | 13.71 | 9.64 | 14.80 | 9.39 | 0.42 | 11.30 |
| Ce | 213.41 | 74.28 | 82.41 | 114.06 | 4.37 | 68.55 | 60.33 | 60.36 | 2.13 | 27.38 | 18.16 | 29.45 | 21.06 | 0.59 | 22.00 |
| Pr | 19.63 | 7.00 | 8.57 | 9.58 | 0.43 | 7.30 | 9.25 | 7.62 | 0.37 | 3.41 | 2.04 | 3.41 | 2.95 | 0.10 | 2.58 |
| Nd | 60.06 | 24.55 | 32.91 | 29.18 | 1.61 | 27.02 | 32.38 | 32.12 | 1.72 | 14.68 | 7.94 | 12.72 | 14.52 | 0.42 | 10.94 |
| Sm | 6.82 | 5.54 | 7.77 | 5.97 | 0.30 | 5.52 | 6.95 | 7.77 | 0.55 | 3.91 | 1.34 | 2.55 | 4.61 | 0.15 | 2.72 |
| Eu | 1.72 | 0.40 | 0.95 | 0.57 | 0.01 | 0.92 | 0.31 | 2.44 | 0.02 | 1.18 | 0.30 | 0.48 | 1.62 | 0.06 | 0.82 |
| Gd | 3.21 | 4.77 | 7.22 | 4.73 | 0.37 | 4.95 | 5.68 | 7.54 | 1.21 | 4.21 | 1.39 | 1.84 | 5.23 | 0.21 | 2.64 |
| Tb | 0.41 | 0.96 | 1.46 | 0.96 | 0.07 | 0.90 | 1.12 | 1.32 | 0.25 | 0.77 | 0.24 | 0.33 | 0.99 | 0.05 | 0.46 |
| Dy | 2.23 | 5.97 | 9.25 | 6.13 | 0.40 | 5.56 | 6.87 | 7.98 | 1.65 | 4.71 | 1.50 | 2.05 | 6.09 | 0.38 | 2.86 |
| Ho | 0.42 | 1.22 | 2.02 | 1.30 | 0.09 | 1.17 | 1.35 | 1.60 | 0.39 | 0.97 | 0.31 | 0.44 | 1.24 | 0.09 | 0.60 |
| Er | 1.19 | 3.68 | 6.23 | 4.00 | 0.27 | 3.42 | 3.81 | 4.56 | 1.20 | 2.71 | 0.87 | 1.32 | 3.69 | 0.30 | 1.74 |
| Tm | 0.17 | 0.53 | 0.95 | 0.56 | 0.04 | 0.49 | 0.55 | 0.62 | 0.17 | 0.36 | 0.12 | 0.19 | 0.52 | 0.04 | 0.24 |
| Yb | 1.18 | 3.29 | 6.33 | 3.52 | 0.28 | 2.94 | 3.35 | 3.74 | 1.23 | 2.23 | 0.81 | 1.27 | 3.26 | 0.28 | 1.57 |
| Lu | 0.21 | 0.48 | 1.03 | 0.53 | 0.04 | 0.46 | 0.48 | 0.58 | 0.25 | 0.34 | 0.14 | 0.21 | 0.51 | 0.05 | 0.25 |
| $Sc^\dagger$ | 5 | 4 | 5 | 5 | 1 | 11 | 4 | 36 | 39 | 22 | 2 | 6 | 26 | 9 | 29 |
| $V^\dagger$ | 0 | 0 | 14 | 16 | 21 | 4 | 8 | 234 | 195 | 182 | 80 | 62 | 383 | 45 | 154 |
| $Cr^\dagger$ | 0 | 8 | 2 | 3 | 15 | 1 | 1 | 192 | 815 | 170 | 36 | 43 | 22 | 2009 | 51 |
| $Ni^\dagger$ | 6 | 11 | 8 | 10 | 27 | 7 | 9 | 66 | 239 | 92 | 36 | 11 | 0 | 1838 | 15 |
| $Cu^\dagger$ | 0 | 4 | 0 | 105 | 22 | 215 | 2 | 77 | 56 | 47 | 21 | 20 | 0 | 39 | 6 |
| $Zn^\dagger$ | 14 | 2 | 1 | 86 | 5 | 15 | 47 | 94 | 57 | 71 | 74 | 23 | 20 | 61 | 36 |
| $Ga^\dagger$ | 11 | 18 | 24 | 18 | 2 | 10 | 17 | 21 | 7 | 12 | 4 | 8 | 15 | 5 | 16 |
| **Calculated parameters** | | | | | | | | | | | | | | | |
| $La_N$ | 362.07 | 92.04 | 106.43 | 134.60 | 5.59 | 105.72 | 126.16 | 88.61 | 3.76 | 37.36 | 26.27 | 40.33 | 25.59 | 1.14 | 30.79 |
| $Sm_N$ | 29.52 | 23.98 | 33.64 | 25.84 | 1.30 | 23.90 | 30.09 | 33.64 | 2.38 | 16.93 | 5.80 | 11.04 | 19.96 | 0.65 | 8.95 |
| Eu/Eu* | 1.12 | 0.24 | 0.39 | 0.33 | 0.09 | 0.54 | 0.15 | 0.97 | 0.07 | 0.89 | 0.67 | 0.68 | 1.01 | 1.03 | 0.94 |
| $Gd_N$ | 10.49 | 15.59 | 23.59 | 15.46 | 1.21 | 16.18 | 18.56 | 24.64 | 3.95 | 13.76 | 4.54 | 6.01 | 17.09 | 0.69 | 8.63 |
| $Yb_N$ | 4.76 | 13.27 | 25.52 | 14.19 | 1.13 | 11.85 | 13.51 | 15.08 | 4.96 | 8.99 | 3.27 | 5.12 | 13.14 | 1.13 | 6.33 |
| CIA | 59.20 | 53.49 | 61.72 | 61.09 | 76.92 | 61.56 | 72.24 | 63.29 | 45.50 | 63.31 | 75.76 | 79.37 | 53.02 | 51.79 | 60.67 |

Major element analyses performed by XRF and normalized to 100% (volatile free). All Fe reported as FeO*. Trace elements denoted with '†' performed by XRF; all others by ICP-MS; all analyses by Washington State University, details given in Hooper et al. (1993). Calculated parameters utilize raw geochemistry listed above, 'N' denotes normalization to chondritic values given in Taylor and McLennan (1985). Analytical errors given in Appendix 11.

Table 4.2. Sm-Nd isotope systematics for the Nisutlin and Anvil assemblages

| sample name | rock type | $\frac{^{143}Nd}{^{144}Nd}$ | | error (2σ) | Nd (ppm) | Sm (ppm) | $\frac{^{147}Sm}{^{144}Nd}$ | $\varepsilon Nd_0$ | $\varepsilon Nd_{350}$ | $T_{DM}$ (Ga) |
|---|---|---|---|---|---|---|---|---|---|---|
| SG94-5B | MQS | 0.511958 | ± | 0.000013 | 65.90 | 7.08 | 0.0650 | -13.3 | -7.4 | 1.23 |
| SG94-17A | MQS | 0.512074 | ± | 0.000009 | 27.87 | 5.66 | 0.1227 | -11.0 | -7.7 | 1.82 |
| SG94-18A | MQS | 0.512399 | ± | 0.000012 | 36.85 | 7.88 | 0.1293 | -4.7 | -1.7 | 1.38 |
| SG94-24 | MQS | 0.512041 | ± | 0.000010 | 31.83 | 5.71 | 0.1086 | -11.7 | -7.7 | 1.62 |
| SG94-35A | QP | 0.511960 | ± | 0.000011 | 1.58 | 0.32 | 0.1209 | -13.2 | -9.9 | 1.97 |
| SG94-53 | MQS | 0.511866 | ± | 0.000019 | 28.98 | 5.47 | 0.1141 | -15.1 | -11.4 | 1.98 |
| SG94-65 | MQS | 0.512042 | ± | 0.000013 | 35.16 | 6.84 | 0.1176 | -11.6 | -8.1 | 1.77 |
| SG94-80 | MS | 0.512734 | ± | 0.000008 | 35.49 | 7.61 | 0.1297 | 1.9 | 4.9 | 0.78 |
| SG94-82 | MS | 0.512964 | ± | 0.000023 | 1.73 | 0.73 | 0.2531 | 6.4 | 3.8 | - |
| SG94-85 | MS | 0.512474 | ± | 0.000008 | 15.63 | 3.78 | 0.1461 | -3.2 | -0.9 | 1.55 |
| SG94-89A | QP | 0.511653 | ± | 0.000026 | 8.60 | 1.60 | 0.1128 | -19.2 | -15.5 | 2.27 |
| SG94-89Ar | QP | 0.511595 | ± | 0.000011 | 8.60 | 1.60 | 0.1128 | -20.4 | -16.6 | 2.36 |
| SG94-90C | QP-g | 0.511767 | ± | 0.000009 | 13.43 | 2.44 | 0.1099 | -17.0 | -13.1 | 2.04 |
| SG94-52 | Anvil | 0.512649 | ± | 0.000010 | 16.41 | 4.57 | 0.1685 | 0.21 | 1.48 | - |

'r' denotes repeat analysis as a nitrate; all other samples run as chlorides. The $^{143}Nd/^{144}Nd$ uncertainties are quoted as 2σ mean. Model ages were not calculated for samples with $^{147}Sm/^{144}Nd > 0.16$.

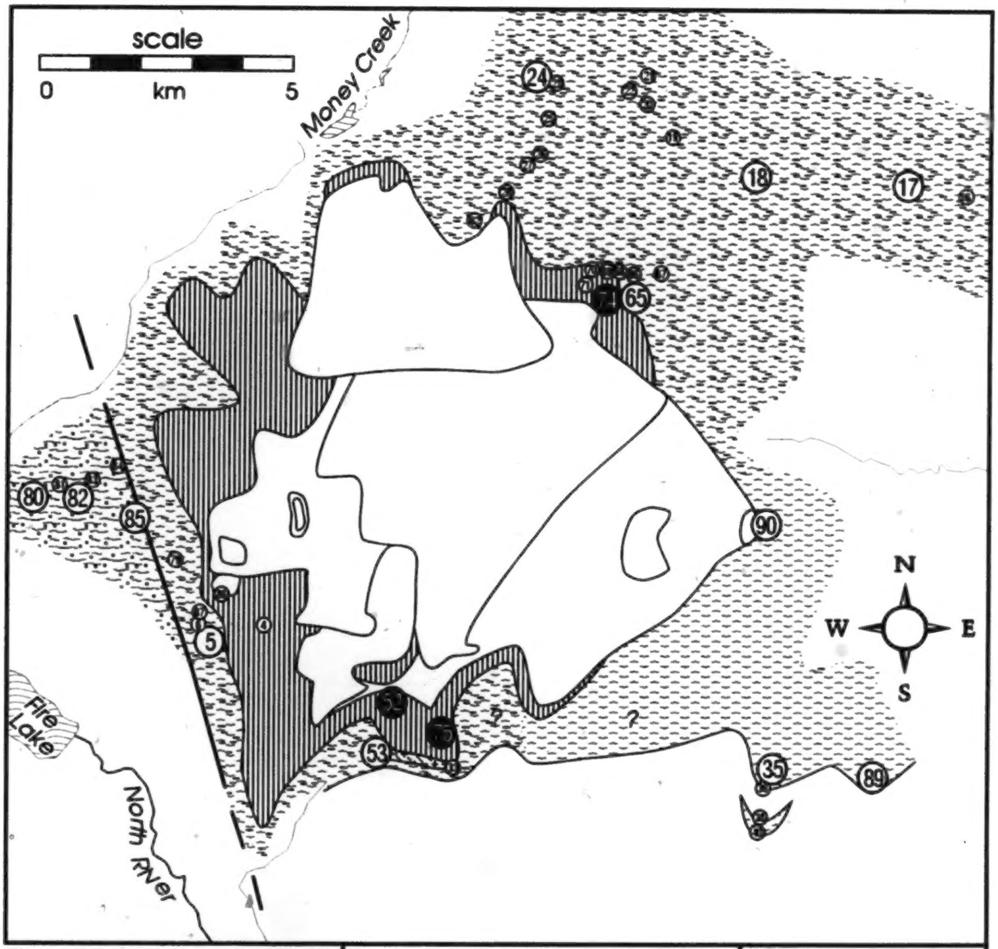

Figure 4.1. Locations of analyzed Nisutlin and Anvil assemblage samples. Nisutlin assemblage samples analyzed for geochemistry and Nd isotopes (large white circles). Anvil assemblage samples analyzed for geochemistry (large black circles); only sample SG94-52 analyzed for Nd isotopes. Contacts between the Nisutlin assemblage subunits are uncertain. Largely undeformed SRPS units (white) are in the center of the Money klippe.

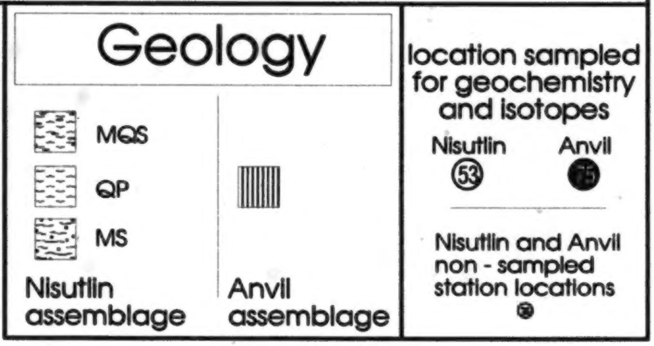

Geology
MQS
QP
MS
Nisutlin assemblage
Anvil assemblage
location sampled for geochemistry and isotopes
Nisutlin
53
Anvil
75
Nisutlin and Anvil non - sampled station locations

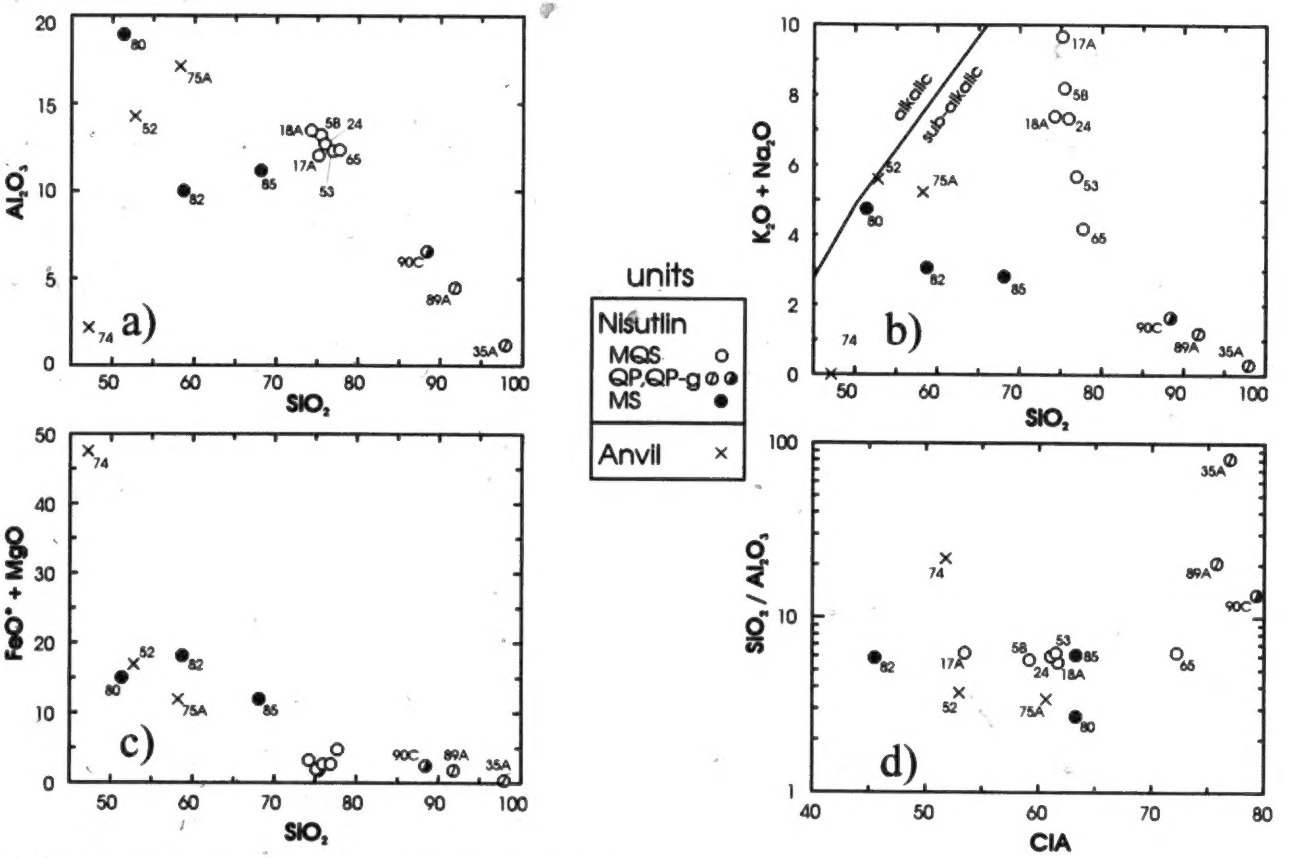

Figure 4.2. Major element data for the Nisutlin assemblage and Anvil assemblage schists.

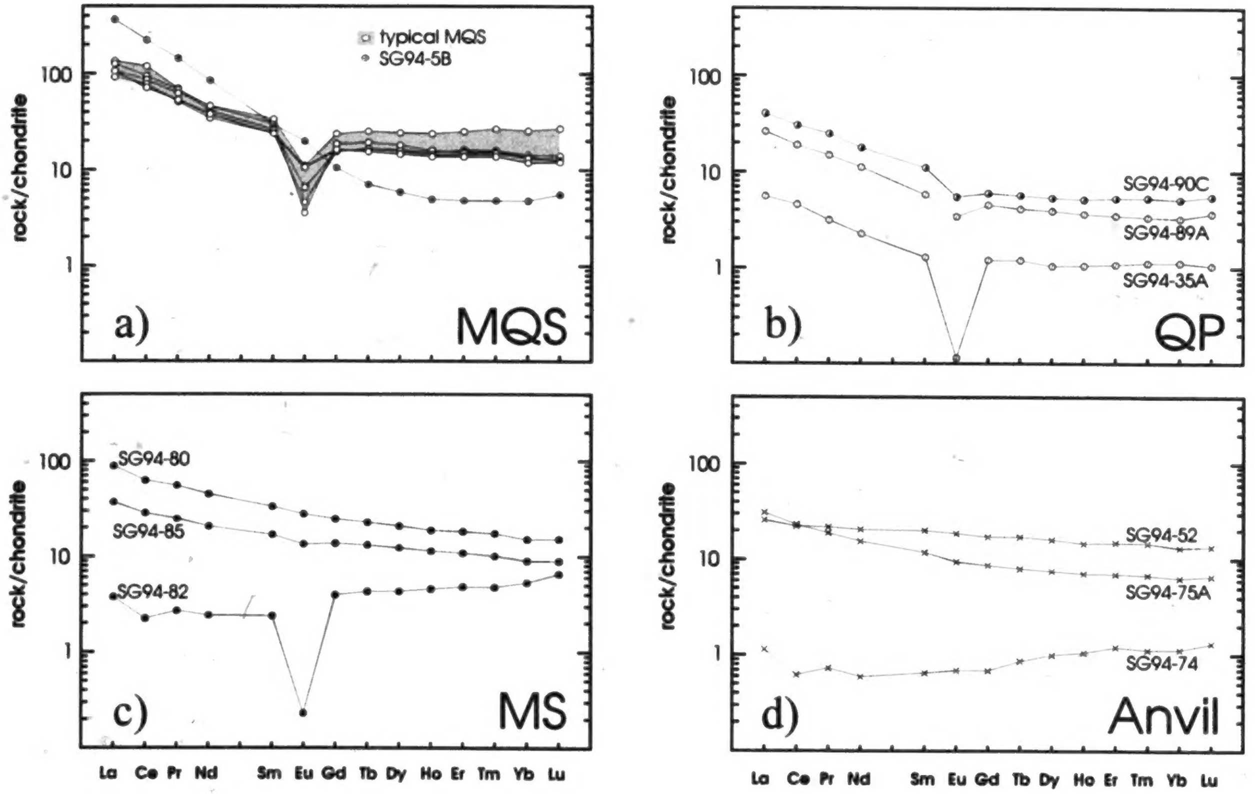

Figure 4.3 Rare-earth element plots of the three subunits of Nisutlin assemblage schists (a-c) and the Anvil assemblage schists (d). Chondritic normalization values from Taylor and McLennan (1985).

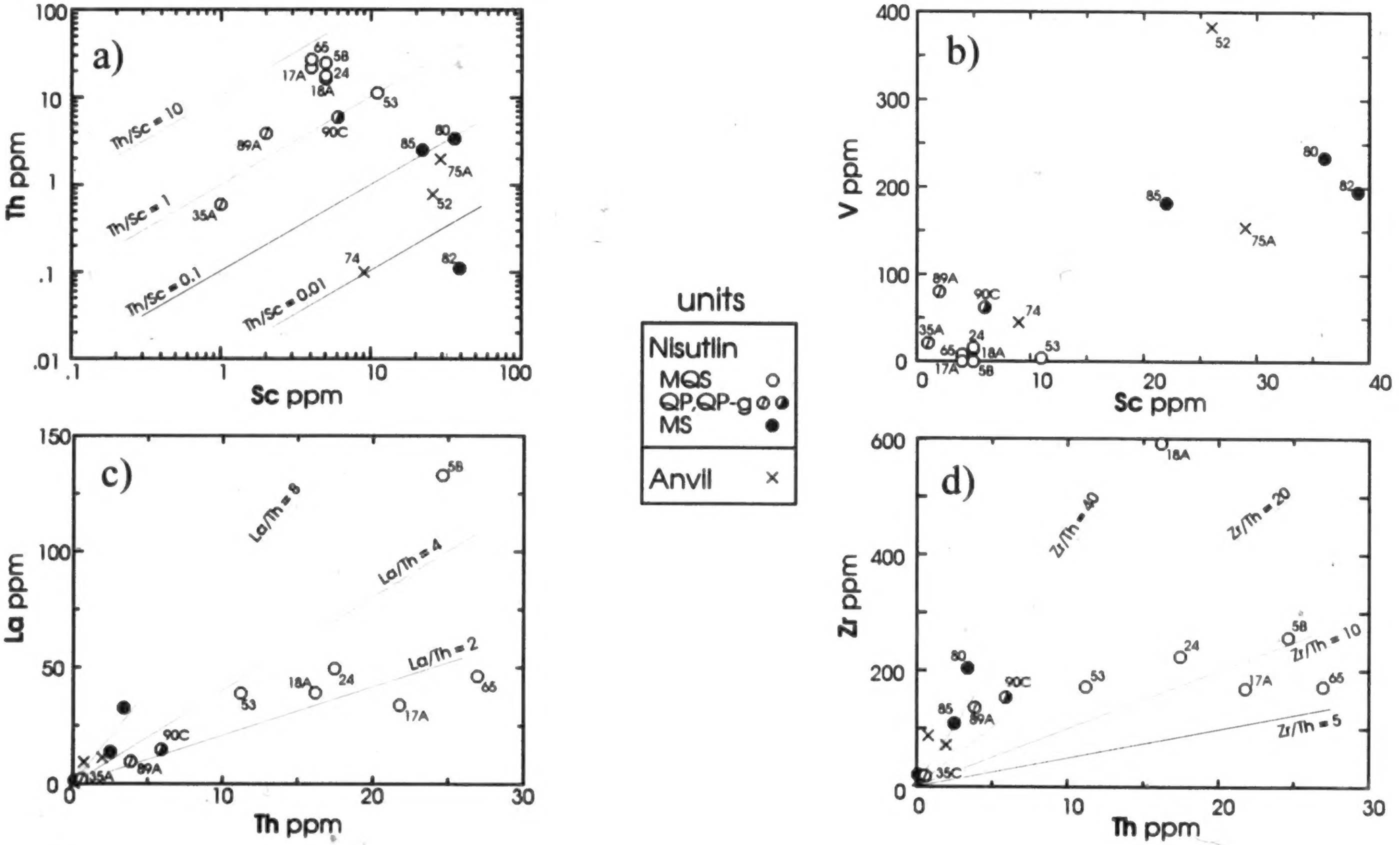

Figure 4.4. Nisutlin assemblage and Anvil assemblage data on trace element discrimination diagrams. Reference ratios are shown as lines on a, c, and d.

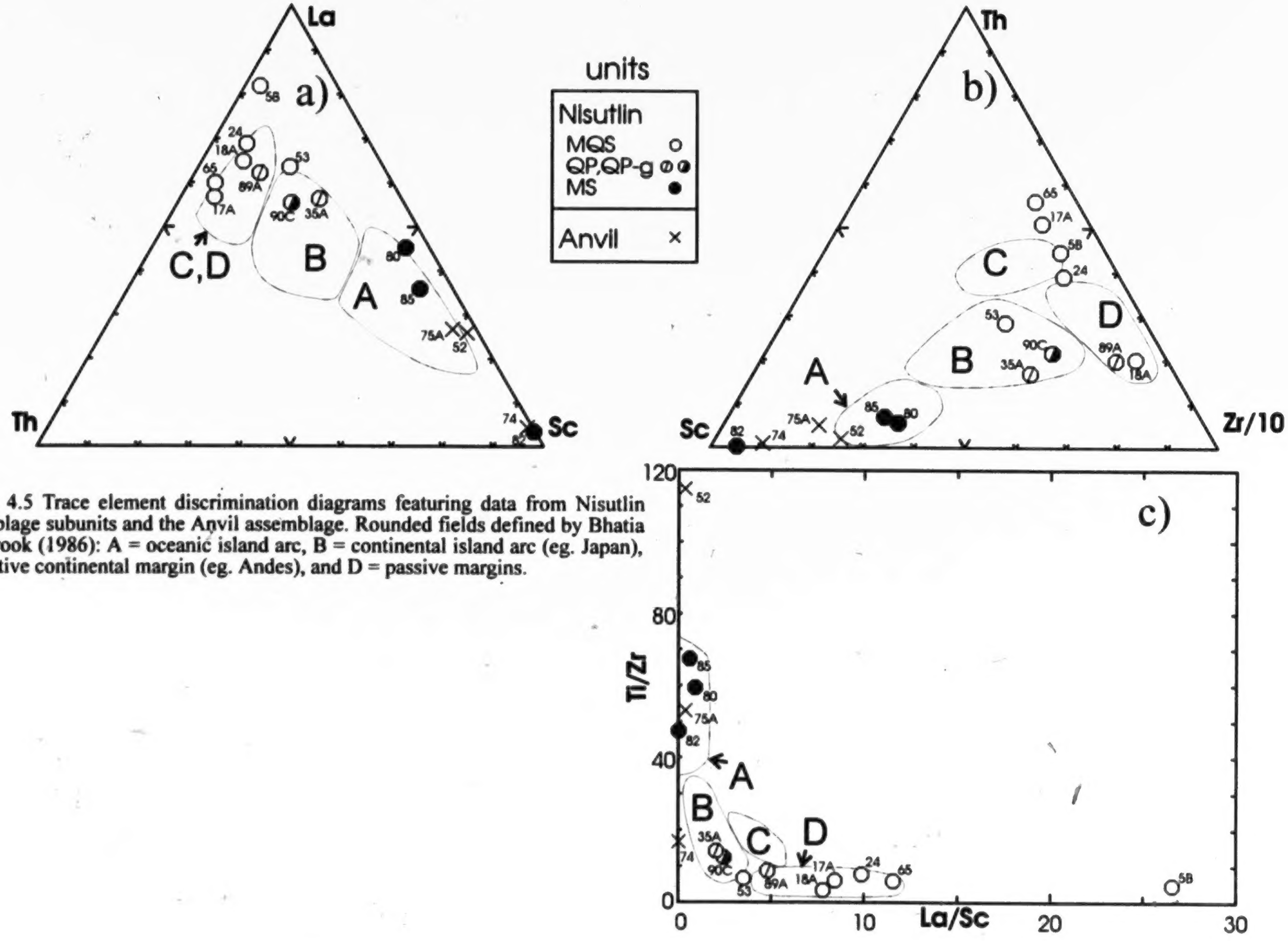

Figure 4.5 Trace element discrimination diagrams featuring data from Nisutlin assemblage subunits and the Anvil assemblage. Rounded fields defined by Bhatia and Crook (1986): A = oceanic island arc, B = continental island arc (eg. Japan), C = active continental margin (eg. Andes), and D = passive margins.

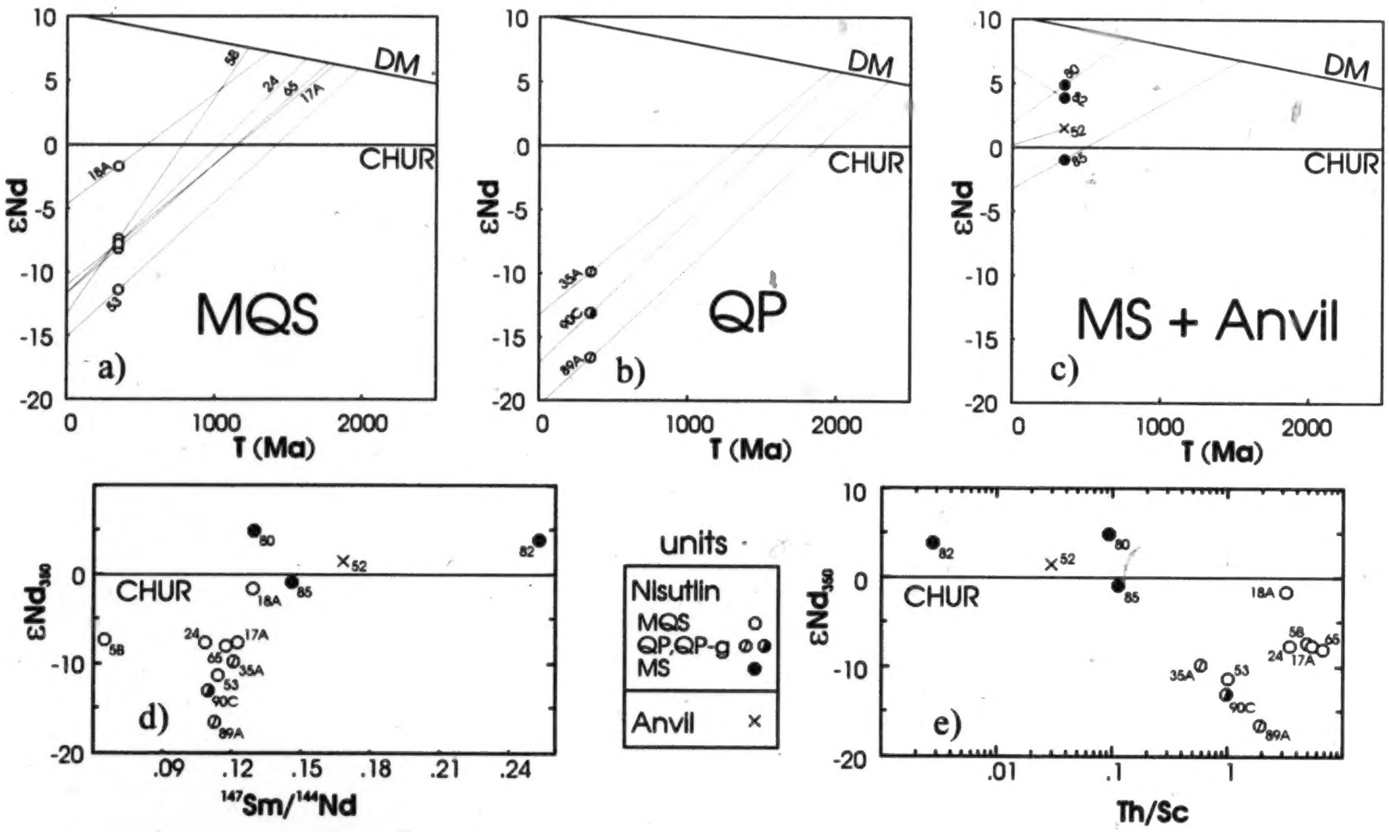

Figure 4.6. Nd isotopic data. The εNd data at time T in the past is represented by the lines in Figures 4.6 a, b, and c; symbols are placed at εNd at 350 Ma because this is the minimum age. $T_{DM}$ model ages are represented by the intersection of the sample lines with the depleted mantle evolution curve (DM) as calculated using the model of Goldschmidt et al. (1984). Model ages were not calculated for samples possessing $^{147}$Sm/$^{144}$Nd > 0.16. Most samples show increasing $^{147}$Sm/$^{144}$Nd with increasing εNd$_{350}$, but samples SG94-5B and SG94-82 have very low and very high $^{147}$Sm/$^{144}$Nd ratios, respectively (d). Samples with evolved crustal εNd sigature typically have a higher degree of incompatible:compatible enrichment, as shown by the εNd$_{350}$ vs. Th/Sc plot (e), whereas samples with juvenile Nd characteristics have lower Th/Sc (e).

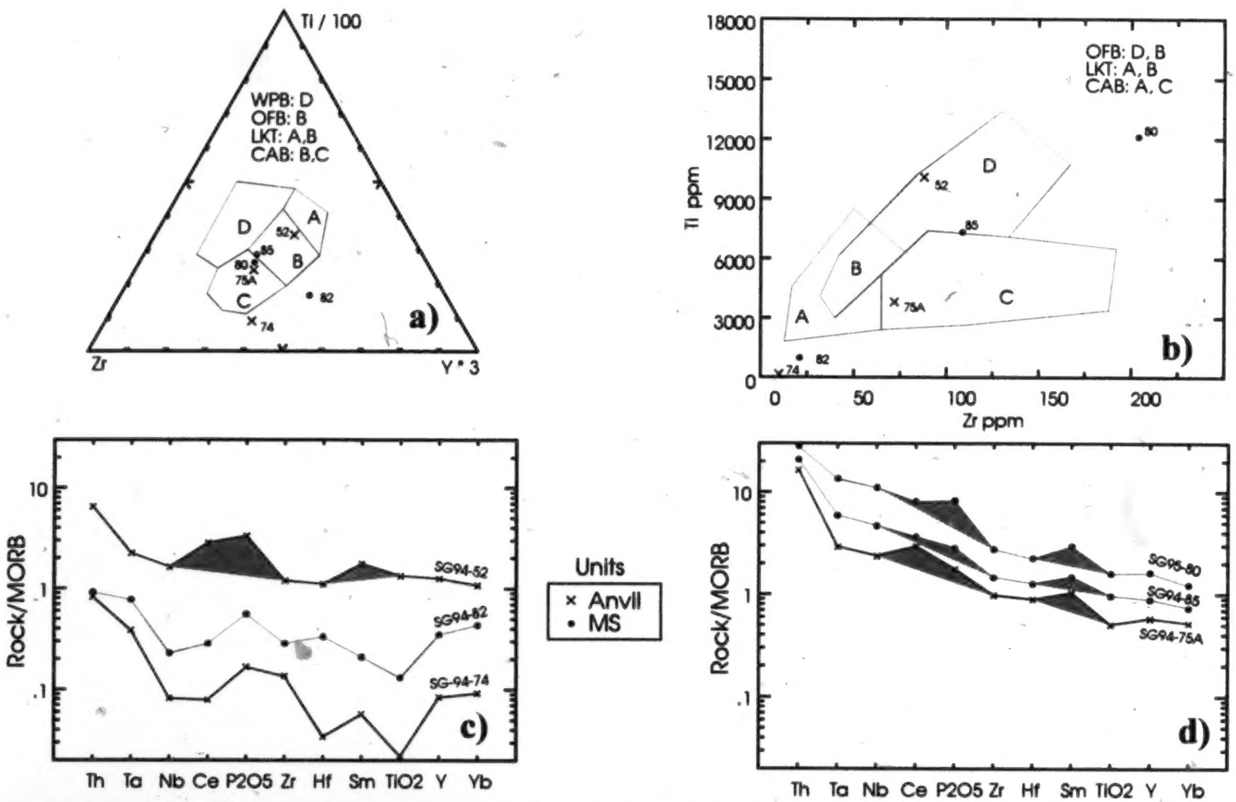

Figure 4.7. Tectonic discrimination diagrams for basaltic rock. Both the Anvil and the MS unit of the Nisutlin assemblage are plotted. Plots a and b are from Pearce and Cann (1974) and use trace elements to define the tectonic environment of the basalt. Abbreviations for basalt types include: WPB: within-plate basalt, OFB: ocean floor basalt, LKT: low-potassium tholeiite, CAB: calc-alkalic basalt, and IAB: island arc basalt. The Anvil and MS data are plotted on two separate multielement plots (c and d) for ease of viewing. Ce, $P_2O_5$, and Sm enrichments, represented by shaded areas underneath the curves, are indicative of CAB material. Samples SG94-75A, SG94-80, and SG94-85 also feature gently sloping curves from Ta to Yb (neglecting the Ce, $P_2O_5$ and Sm enrichments); an indication that these samples are CAB's produced in an active continental margin. Data from sample SG94-52, on the other hand, are not significantly enriched relative to MORB, except for Ce, $P_2O_5$, and Sm, which may indicate that the sample is a CAB produced in a island arc. Multielement plots (c and d) modified from Pearce (1983); MORB normalizing values from Pearce and Parkinson (1993).

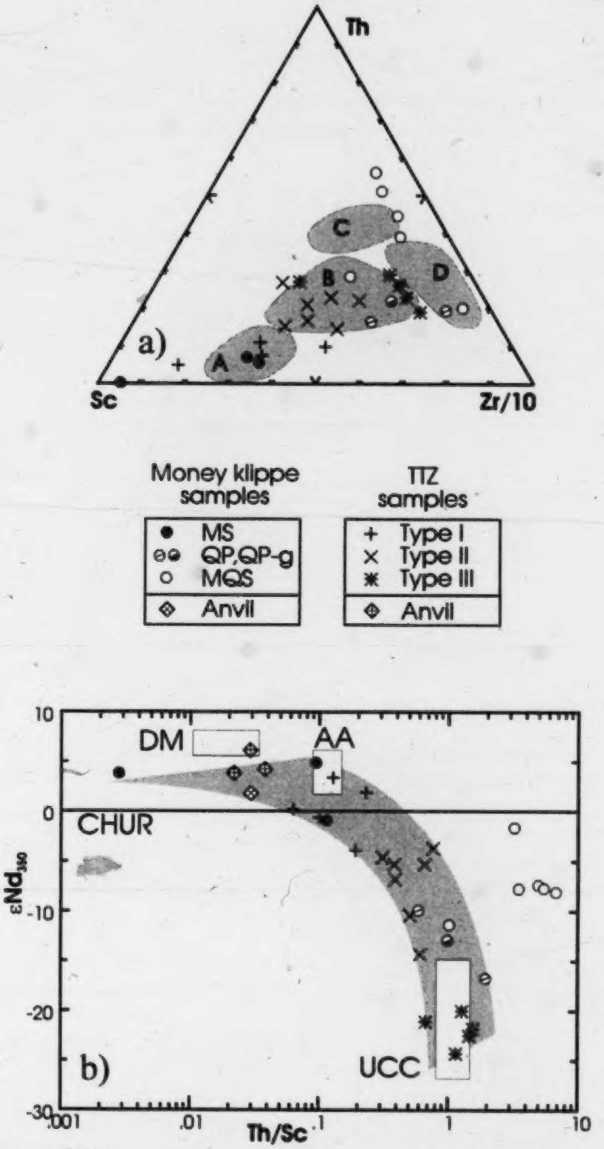

Figure 4.8. Comparison of Nisutlin samples from the Money klippe area and the TTZ. The fields of Bhatia and Crook (1986) are shown in the Sc - Th - Zr/10 ternary diagram (a); field abbreviations as per Fig. 4.5. On a Th/Sc diagram (b) QP and MS samples fall on the trend defined by Creaser et al. (1997a) for TTZ samples, as shown in light grey. All MQS samples except for SG94-53 form a distinct field with a more felsic signiture. AA= arc andesites, DM = depleted mantle, and UCC = upper continental crust. TTZ data and data for fields plotted on (b) from Creaser et al. (1997a).

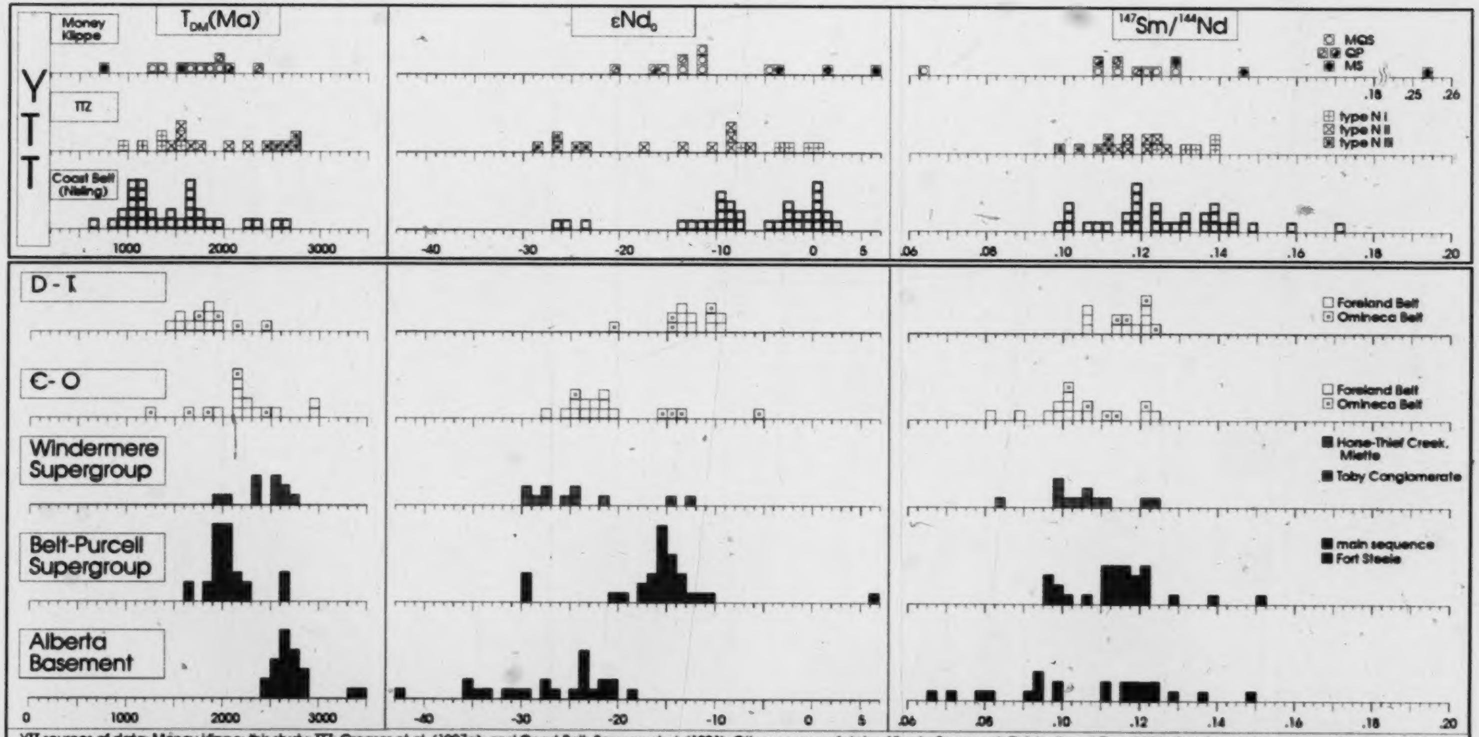

YTT sources of data: Money klippe: this study; TTZ: Creaser et al. (1997a); and Coast Belt: Samson et al. (1991). Other sources of data: Alberta Basement: Thériault and Ross (1990); Belt Purcell Supergroup: Frost and O'Nions (1984), Frost and Winston (1987), Burwash et al. (1988), and Ghosh and Lambert (1989); Windermere Supergroup: Burwash et al. (1988), Ghosh and Lambert (1989), and Boghossian et al. (1996); and Phanerozoic (C-O & D-T): Ghosh and Lambert (1989) and Boghossian et al. (1996).

Figure 4.9. Histograms showing the concentration of Nd data for the YT terrane, various members of the miogeocline succession, and the Alberta basement. Each box represents one analysis. Symbols for subdivisions within the datasets, where necesary, are shown on the right of the respective panel.Three parameters are represented: depleted mantle model ages ($T_{DM}$)(left), εNd (middle), and $^{147}Sm/^{144}Nd$ (right). All model ages have been recalculated according to the model of Goldstein et al. 1984. The three areas in the YT terrane for which Nd data are available are shown in the top three panels. Alberta Basement data have the oldest range of $T_{DM}$ ages and lowest range of εNd values. Notice that the Fort Steele formation, the basal unit of the Belt Purcell Supergroup, is compatible with derivation from the underlying Alberta basement, but that the bulk of the Belt Purcell Supergroup is significantly more juvenile (Burwash et al. 1986). Similarly, the basal unit of the Windermere Supergroup, the Toby conglomerate, records the juvenile charcteristics of the underlying Belt Purcell, but the Horsethief Creek Group is derived largely from the Alberta basement (Burwash et al. 1986). While Cambrian to Ordovicain strata also are largely derived from the Alberta basement, Devonian to Triassic strata are more juvenile (Boghossian et al.1996). Literature sources for the miogeocline are listed at the bottom of the figurebox.

# CHAPTER 5. GEOCHEMISTRY AND ISOTOPE SYSTEMATICS OF THE SIMPSON RANGE PLUTONIC SUITE

## 5.1 INTRODUCTION

Magmatic episodes in Late Devonian - Early Mississippian, Mid-Permian, and Late Triassic-Early Jurassic are responsible for many of the igneous rocks of the YT terrane (Mortensen 1992b). Devonian-Mississippian magmatism has resulted in the largest volume of igneous rocks in the YT terrane, which occur as two distinct suites (Fig. 2.2). The most widespread of the two suites, consisting of peraluminous granitoids, shows strong zircon inheritance, has very radiogenic Pb and Sr isotopic ratios, and unradiogenic Nd isotopic ratios (Mortensen 1992b), which indicates that old continental crust provided a large component to their petrogenesis. The less widespread of the two Devonian-Mississippian suites, represented by the Simpson Range plutonic suite (SRPS) in southeastern Yukon and correlated rocks such as the Fiftymile Batholith and other smaller bodies in western Yukon and eastern Alaska (Mortensen 1992b, 1986, Wheeler and McFreely 1991), and by quartz diorite to tonalitic plutons in the TTZ (Stevens et al. 1996), has more moderate zircon inheritance, moderately radiogenic Sr isotopic signatures, and slightly negative initial εNd values (Mortensen 1983, 1992b; Stevens et al. 1996). Compared to the peraluminous suite, geochemical and isotopic data are scarce for the SRPS. Also, most studies of igneous rocks from the YT terrane only examine one or two isotopic systems and often do not present geochemistry (Aleinikoff et al. 1981, 1986, 1987; Mortensen 1983, 1992a; Bennett and Hansen 1988). Thus, one of the aims of this study is to provide a comprehensive database containing major and trace element geochemistry, as well as Rb-Sr, Sm-Nd, Pb-Pb, and U-Pb isotope data. Geochemistry was used to further classify these rocks and helps constrain their tectonic affinity. The duration of crustal residence of material contributing to the rocks is examined using tracer isotopes and U-Pb zircon systematics. Precise U-Pb dates for most of the igneous units are also presented. Also, these results are compared to other Devonian-Mississippian igneous rocks throughout the YT terrane in order to determine the relation of these diverse igneous rocks to one another.

This study examines the SRPS contained within the Money klippe in southeastern Yukon (Fig. 5.1). One of the reasons that the Money klippe was chosen for field work is that a wide variety of SRPS rocks could be sampled from a small area. Sections 2.3 and 2.4 contain descriptions of the field area and rock types, respectively. SRPS units cropping out within the Money klippe include: hornblende-granodiorite (HbGd), biotite-monzogranite (BtMg), gabbro, and a composite volcanic plug, which has been subdivided into a mafic subunit (MVP) and a felsic subunit (FVP). A sheared granodiorite (Sh-Gd) crops out ~1km south of the klippe. Whereas some previous studies have not included the gabbro (Tempelman-Kluit 1977a, Erdmer 1985) or the composite plug (Tempelman-Kluit 1977a) in the SRPS, field relationships presented in Section 2.3 indicate that these units belong to the SRPS.

## 5.2 GEOCHEMISTRY

### *Major elements*

Four samples were chosen from each of the SRPS units of the Money Klippe (Fig, 5.1) on which to perform XRF and ICP-MS analyses (see Appendix 6 for rock preparation; Hooper et al. (1993) for XRF analytical methods, and Knaack et al (1994) for ICP-MS methods). XRF yielded major and some trace element data, presented in Table 5.1. Analytical errors for XRF data are given in Appendix 11. Two broad groupings of SRPS rocks are apparent from $SiO_2$ data: a mafic group consisting of the MVP and gabbro samples (49.2 to 54.6 % $SiO_2$) and a felsic group consisting of the BtMg, HbGd, Sh-Gd, and FVP samples (63.1 to 77.1 % $SiO_2$). The alkalis increase systematically with $SiO_2$ content and form a subalkalic trend (Fig. 5.2g); $Al_2O_3$, $TiO_2$, FeO* (total iron), MnO, MgO, CaO, and $P_2O_5$ decrease with increasing $SiO_2$ (Fig. 5.2 a-f,h). In the felsic group of SRPS rocks, the silica content generally increases in the following order: granodiorite (both HbGd and Sh-Gd), BtMg, and FVP. The BtMg and the FVP rocks each have restricted ranges of major-element composition, whereas the HbGd and especially the Sh-Gd show greater compositional ranges. Note that SG94-88, more felsic than the other Sh-Gd samples, has a similar compositional range to the FVP and BtMg units in most of the major elements. SG94-88 has large k-spar phenocrysts (0.5 x 1 cm), which are not present in any other plutonic unit except for a pegmatitic phase of the biotite-monzogranite (SG94-30). Thus, it is possible that SG94-88 represents sheared monzogranite pegmatite, although this is speculative. Regardless, the contrast between SG94-88 and the other Sh-Gd samples indicates that the sheared 'granodiorite' unit is more heterogeneous than its name implies. Whereas for the felsic rocks the major elements vary systematically with $SiO_2$ (ie. they form a linear trend), they behave somewhat differently for each of the two mafic units. The MVP samples have higher concentrations of $TiO_2$, FeO*, MnO, MgO, and $P_2O_5$; overlapping concentrations of CaO and alkalis; and lower concentrations of $Al_2O_3$ than the gabbro samples.

After determining that a suite of rocks is subalkalic, as has been done for the SRPS, the next step is to assign the suite to one of either the tholeiitic (Fe-enriched) or calc-alkalic (Fe-depleted) series (Miyashiro 1974). The SRPS rocks fall within the calc-alkalic field on an alkali - FeO* - MgO (AFM) plot (Irvine and Baragar 1971), except that the gabbros straddle the tholeiite - calc-alkalic boundary (Fig. 5.3a). However, the MVP and the gabbro plot as calc-alkalic on the $SiO_2$ vs. FeO*/MgO and FeO* vs. FeO*/MgO plots (Fig. 5.3 b and c) by Miyashiro (1974). The SRPS samples (especially the felsic ones) also form a linear trend on most of the Harker-type diagrams (Fig. 5.2), which is typical of calc-alkalic suites (McBirney 1984). Finally, whereas the total amount of $Al_2O_3$ decreases with increasing $SiO_2$, the molar ratio of $Al_2O_3$ / ($K_2O$ + $Na_2O$ + CaO) generally increases with increasing $SiO_2$ for the SRPS suite. Rocks that have values of molar $Al_2O_3$ / ($K_2O$ + $Na_2O$ + CaO) greater than 1 (ie. excess $Al_2O_3$) are termed 'peraluminous'; those with values less than 1 are termed 'metaluminous' (Shand 1947). SRPS rocks straddle the metaluminous / peraluminous boundary, with some of the more felsic rocks (eg. BtMg and FVP), representing about a third of the SRPS suite, plotting in the 'peraluminous' field (Fig. 5.3d).

Major elements can be used as a means to classify igneous rocks (Fig. 5.4 a-b). Normative compositions (calculated from the major element geochemistry using Newpet software) plotted on an alkali feldspar (A) - quartz (Q) - plagioclase (P) diagram (Fig. 5.4a) show that the felsic SRPS rocks classify as monzogranite to granodiorite, and the mafic SRPS rocks classify as monzodiorite/gabbro/anorthosite to diorite/gabbro/anorthosite according to the IUGS modal classification scheme (Streckeisen 1976). Despite the fact that the biotite-monzogranite unit rocks straddle the 'granite - granodiorite' boundary and the 'sheared granodiorite' SG94-88 plots as monzogranite' on Fig. 5.4a, the field names previously assigned to the rocks will be retained for convenience. The volcanic rocks of the Money klippe can be classified according to the IUGS chemical classification scheme developed by Le Bas et al. (1992), based on a plot of alkalis vs. silica (Fig. 5.4b). By this scheme, the FVP samples plot as 'rhyolite' and the MVP plot as 'basalt' to 'basaltic andesite'.

### *Rare-earth elements*

REE element patterns (Fig. 5.5 a-e) are useful for displaying the overall fractionation trends of plutonic rocks (see Section 4.2; *Rare-earth elements)*. Rare-earth elements were obtained by ICP-MS analysis at Washington State University (Analytical details given in Knack et al. (1994); analytical errors listed in Appendix 11). The felsic igneous rocks of the Money Klippe (Fig.5.5 a-c, e) have similar degrees of LREE enrichment ($La_N/Sm_N$ = 3.5 to 8). Broadly, the BtMg (Fig. 5.5 a) has the highest degree of LREE enrichment and the HbGd (Fig. 5.5 b) has the lowest range, but there is a considerable degree of overlap. Almost all felsic plutonic SRPS rocks have moderate negative europium anomalies (average Eu/Eu* = 0.76) (Fig. 5.5 a-c), whereas the FVP and Sh-Gd sample SG94-88 have more extreme Eu/Eu* values of 0.5 to 0.3 (Fig. 5.5 c,e), which may indicate feldspar removal or retention as a residual mineral in the source region. Figure 5.5 d-e shows that the mafic Money klippe rocks have more primitive, flatter REE patterns ($La_N/Sm_N$ = 0.9 to 2.4). Notice that gabbro sample SG94-3A and MVP sample SG94-60 are especially flat ($La_N/Sm_N \approx 0.9$ to 1.1) even compared to the other four mafic samples ($La_N/Sm_N \approx 1.5$ to 2.4); the primitive nature of SG94-3A and

SG94-60 will be demonstrated again in subsequent diagrams. The gabbros and MVP samples have Eu/Eu* value ranges of 1 to 1.25 and 0.95 to 0.8, respectively. The positive europium anomalies of some gabbro samples may indicate magmatic accumulation of feldspar.

### *Trace-element discrimination diagrams*

Most trace elements reported were obtained by ICP-MS analysis at Washington State University (see Knack et al. 1994) except for Sr, Zr, Sc, V, Cr, Ni, Cu, Zn, and Ga, which were obtained by XRF at Washington State University (see Hooper et al. 1993). Analytical errors for XRF and ICP-MS data are given in Appendix 11. Most trace elements vary in a regular fashion with $SiO_2$ (see Figs. 5.6a-h). Incompatible elements like Rb, Th, Nb, Ta, Zr, and Hf increase with increasing $SiO_2$ (Figs. 5.6 a-h) whereas compatible elements like V and Sc decrease with increasing $SiO_2$ (Figs. 5.6 i-j). Yb, a HREE, and Y, are less regular, and have broadly similar values for mafic and felsic SRPS rocks. The aim of using trace element discrimination diagrams is to interpret the tectonic setting in which the SRPS were formed. Because discrimination diagrams are often designed for a restricted range of silica content, the felsic SRPS rocks will be plotted on diagrams designed for 'granitoids'. The gabbro and MVP rocks will be plotted on diagrams designed for rocks of basaltic composition.

Felsic SRPS rocks are shown to be most similar to volcanic arc granite (VAG) using a multielement pattern devised by Pearce et al. (1984) (Fig, 5.7a-d). This multielement plot designed for granites is similar to the plot of Pearce (1983) used in Fig. 4.7d-e for basalts, except that instead of normalizing to MORB values, they are normalized to the hypothetical composition of ocean ridge granite (ORG), which was calculated by assuming they are the product of fractional crystallization of average N-type MORB (Pearce et al. 1984). Broadly, the elements used in this diagram increase in incompatibility from Yb to Rb, with $K_2O$ added to the left side of the plot (Pearce et al. 1984). The patterns of the SRPS show considerable enrichment of $K_2O$ and LIL's (Rb to Th), and depletion of Y and Yb, with respect to the ORG normalizing values, as well as prominent Ce and slight Sm enrichment with respect to the rest of the Ta to Yb portion of the pattern (Fig. 5.7a-d). Enriched LIL and Ce + Sm enrichments are common features of many of the calc-alkalic VAG, within-plate granite (WPG), syn-collisional granite (syn-COLG), and post-collisional granite patterns (Pearce et al. 1984). However, the Hf to Yb portion of WPG patterns are not significantly different from the ORG normalizing values and many patterns have large negative Ba anomalies, which contrasts with the SRPS patterns. Distinguishing between calc-alkalic and syn- / post-collisional granites is more difficult, but the SRPS are broadly more similar to VAG's because of the lower degree of Rb enrichment and lack of Ba anomalies, which are common feature of collisional granites. The relations shown in the multielement patterns are emphasized in several bivariate plots (Fig. 5.7 e - h) designed by Pearce et al. (1984). The lower Y and Yb content of VAG and syn-COLG distinguishes them from ORG (Fig. 5.7 e - f), whereas WPG typically has higher values of Nb and Ta than VAG, syn-COLG, and ORG (Fig. 5.7 e -f ). Syn-COLG can be distinguished from VAG generally on the basis of higher Rb contents (Fig. 5.7 h - i). In a couple of the plots one sample (SG94-88) plots near or in the syn-COLG field, but as a whole, the felsic SRPS rocks plot in the VAG field (Fig. 5.7 e - h).

Several systems are available for determining the tectonic setting of rocks with a basaltic composition, which the gabbro and MVP units have. One of the most widely used schemes is that of Pearce and Cann (1973). The chief utility of the Zr - Ti/100 - Y*3 diagram (Fig. 5.8a) is distinguishing between WPB and non-WPB compositions; all 6 mafic SRPS samples fall in the latter category. The samples plot primarily in field 'B', which corresponds to CAB, ocean floor basalt (OFB), and low potassium tholeiites (LKT) settings, but also in or near field 'C', which includes rocks of CAB composition. Because the majority of SRPS samples plot in indeterminate field B, the samples are also plotted on a Ti vs. Zr diagram (Fig. 5.8 b), which is able to better differentiate between non-WPB settings (Pearce and Cann 1973). A unique setting is not achieved using the Ti vs. Zr plot either, but samples largely fall in the fields of LKT and CAB. Note that one gabbro (SG94-3A) and one MVP (SG94-60) sample have higher Ti/Zr ratios than the others, and have more affinity with OFB (they plot in field 'B' on Fig. 5.8 b), although their Ti and Zr values are too low to be definite OFB (Fig. 5.8b). The more primitive nature of these two samples, also shown by their flatter REE patterns (Fig. 5.5d - e), is apparent in the following tectonic discrimination diagrams as well.

Wood et al. (1989) and Wood (1980) discussed the use a Th - Hf / 3 - Ta ternary plot (Fig. 5.8 c) for distinguishing between different types of MORB, WPB and destructive plate margins. Note that four of the mafic SRPS rocks plot decisively in the 'destructive plate margin' field, but that SG94-60 and SG94-3A plot in the field of E-type MORB (MORB that has been enriched with respect to incompatible elements) and tholeiitic WPB. One problem with the use of this diagram, however, is that a tungsten carbide mill was used (albeit briefly) during the crushing procedures (see Appendix 6), which can contribute, besides W, some Ta to the sample. Ta contamination would cause the samples to plot closer to the Ta pole of the diagram than if not contaminated. When fields were originally delineated for this diagram using samples of known tectonic setting, Wood et al. (1979) used the equation Ta ≈ Nb / 16 in order to use databases that contained Nb, but not Ta data, because the relationship between the Ta and Nb varies by less than 5% in nature (Wood et al. 1979). Thus, a second plot is presented in which Ta is replaced by Nb/16 (Fig. 5.8 d), which may help to alleviate the potential Ta contamination problem. On this diagram, note that all samples plot in the destructive plate margin field, but that SG94-60 and SG94-3A have more tholeiitic affinity than the other samples, primarily because of lower Th contents. Th is a LIL that is especially enriched in continental lithosphere.

The mafic SRPS samples have also been plotted on a Th/Yb vs. Ta/Yb diagram (Fig. 5.8 e) designed by Pearce (1983). In MORB's and WPB's the degree of Th and Ta enrichment relative to Yb is roughly the same, thus samples from these setting will plot along a Th/Yb : Ta/Yb ≈ 1:1 line. However, in arc settings, Th is enriched relative to Yb to a greater degree than Ta, thus samples from an arc setting will plot above and to the left of the 1:1 line in Fig, 5.8 e (Pearce 1983). The latter situation is the case for the majority of the SRPS samples, which plot close to fields delineated for basalts from the Andes and Japan. Note however, that SG94-60 and SG94-3A plot as tholeiitic arc or

MORB and WPB, respectively. On the whole, however, the mafic SRPS rocks have characteristics of rock produced in a volcanic arc setting that is dominantly of calc-alkalic affinity. Figure 5.8 f shows that the majority of the rocks are compatible with derivation from a continental arc, but that the more primitive members (SG94-60 and SG94-3A) may have been produced in an oceanic arc.

### *Summary of geochemical evidence*

Despite the wide range of composition displayed by the SRPS ($SiO_2$ ranges from 49% to 78%), the majority of major element trends and trace element discrimination diagrams indicate that the SRPS belongs to the calc-alkalic series and was produced in a volcanic arc setting. Evidence from trace elements suggest that the calc-alkalic arc was at least in-part built on continental lithosphere. For instance, some of the mafic gabbro and MVP units have enriched Th/Yb and Zr/Y ratios that are similar to those of basalt produced in continental arcs. Also, whereas the majority of SRPS rocks are metaluminous, many of the felsic SRPS 'granitoids' and rhyolites are peraluminous, which is a common feature of rocks that have incorporated supracrustal material into their make-up. However, primitive components to the arc are also represented: two of the mafic SRPS rocks are not significantly enriched in incompatible elements with respect to MORB, and may represent a segment of the arc built on oceanic crust, or the earliest stages of arc activity. This evidence helps illustrate the diversity of magmatism associated with the SRPS, but on the whole, the geochemical evidence suggests that the SRPS represents a calc-alkalic arc built dominantly at a continent - ocean interface. Section 5.4 introduces tracer isotope data to support this interpretation. At this point it is also worthwhile pointing out that the calc-alkalic nature of the gabbro unit is further evidence that it does not belong to the Slide Mountain terrane, as previously suggested (Mortensen 1992a, Erdmer 1985) (see Section 2.3).

## 5.3 PRECISE U-Pb GEOCHRONOLOGY

Zircon fractions were obtained from five of the SRPS rocks. The analytical procedures are listed in Appendix 8. Table 5.2 and Fig. 5.9 presents U-Pb data for the zircon fractions. Multiple fractions were obtained for each of the felsic igneous rocks in or near the Money klippe. Significantly, one fraction from a gabbro was obtained. Below are brief discussions of the results from each of the felsic rock types, followed by one result from a gabbro.

### *Biotite-monzogranite (SG94-2)*

Two multigrained zircon populations were selected from a very slightly magnetic zircon fraction (see Appendix 8). Both fractions were euhedral, clear colourless grains (except for a few grains with fluid inclusions) and had low masses (40 to 50 μg). Fraction 2-Z-2, composed of ~175 small prismatic grains was nearly concordant (-0.67% discordant) with a $^{207}$Pb/$^{206}$Pb age of 344.1 ± 4.0 Ma. The 4.77% discordant analyses of fraction 2-Z-1 (containing ~108 equidimensional crystalline grains) yields a $^{207}$Pb/$^{206}$Pb age of 362.6 ± 10 Ma, but overlaps in error with the nearly concordant 2-2-Z analyses (Fig. 5.9, Table 5.2). Weighted averages of the $^{206}$Pb/$^{238}$U and $^{207}$Pb/$^{235}$U ages of fractions 2-Z-1 and 2-Z-2 yield ages of 345.9 ± 1.2 Ma and 346.8 ± 1.7 Ma, respectively (Table 5.2). A discordia was not calculated for these analyses because of the geologically improbable trajectory that such a discordia would have, thus the weighted average of the $^{206}$Pb/$^{238}$U ages, 345.9 ± 1.2 is interpreted as the age of crystallization. The overlap of error among the of the $^{206}$Pb/$^{238}$U weighted average age, the nearly concordant $^{207}$Pb/$^{206}$Pb age of fraction 2-Z-1, and the $^{207}$Pb/$^{235}$U weighted average age lends support to the adoption of this age as the crystallization age of the BtMg, although further analyses would help to constrain this result.

### *Hornblende-granodiorite (SG94-14)*

Three multi-grained fractions were analyzed for sample SG94-14. All three fractions were picked from zircons that were non-magnetic or very weakly magnetic. $^{207}$Pb/$^{206}$Pb ages range from 377.4 ± 6.3 Ma for the least discordant fraction 14-Z-3 (8.35% discordant) to 392.8 ± 2.6 Ma for the 10.75% discordant 14-Z-1 to 606.6 ± 2.7 Ma for the 38.26% discordant 14-Z-2 (Table 5.2). The three analyses form a nearly linear array on a standard discordia diagram, yielding a discordia with a lower intercept of 345.2 ± 1.9 Ma and a poorly constrained upper intercept of 1809 +90/-82 Ma (Fig. 5.9). The lower intercept is interpreted to be the time of crystallization of the HbGd. The Proterozoic - aged upper intercept indicates that inherited zircon constitutes, perhaps as (non-apparent) cores, a portion of the zircons. Discordant fraction 14-Z-2 contains large grains that, although generally crystalline and clear, are more likely to have inherited cores than fraction 14-Z-3, which is composed of smaller zircons. Also the zircons of fraction 14-Z-3 are more uniform in size and shape than either 14-Z-1 and 14-Z-2.

### *Sheared-granodiorite (SG94-55)*

Three analyses of zircons from Sh-Gd sample SG94-55 were performed. Fraction 55-Z-1 was slightly magnetic, and the 17 grains were largely colourless and clear, with large stubby shapes. Some grains had what appeared to be some type of internal zoning. In order to test if these faint features represented cores of inherited zircon, one single zircon with an apparent core (55-Z-1C), and one single zircon with no hint of a core (55-Z-1N) were selected to determine if there was any appreciable difference between the two most widely different zircons (this is a qualitative judgment based on appearance only). The two single grains were not abraded because it was desirable to retain as much material as possible, and it was thought that if there were differences, they would be large. The two single grain analyses were discordant and of relatively high error as a result of the low intensity of the Pb and U emission. The -3.2% discordant 55-Z-1N fraction has a 332.2 ± 15.9 Ma $^{207}$Pb/$^{206}$Pb age (Table 5.2). The single grain 55-Z-1C has a 366.5 ± 10.3 Ma $^{207}$Pb/$^{206}$Pb age with 9.33% discordancy (Table 5.2). The similarity in ages and the fact that the $^{207}$Pb/$^{235}$U and $^{206}$Pb/$^{238}$U values of 55-Z-1C are less than the 'non-cored' 55-Z-1N, suggest that 55-Z-1C does not contain a core of old inherited zircon. Thus, the remaining 15 grains of 55-Z-1 were analyzed (after abrasion) with the hopes of obtaining good, low analytical error analyses, with their higher mass. The analytical error was indeed better than the single grain analyses, but the sample was 32.39 % discordant and had $^{207}$Pb/$^{235}$U and $^{206}$Pb/$^{238}$U ages of about ~250 Ma (Table 5.2). A discordia fit through the three analyses has an upper intercept of 357 +21.2/-17.2 Ma and a lower intercept of 22.6 +39.8/-45.6 Ma (Fig. 5.9). The upper intercept is interpreted as the age of crystallization. The poorly constrained lower intercept indicates that lead loss affected the rock subsequent to formation.

### *Quartz-porphyry volcanic (SG94-11)*

Zircons from this porphyritic phase of the FVP unit are characteristically iron stained externally and brown or yellow in colour internally. There were virtually no zircons that were nonmagnetic at a side tilt less than 10°. Two fractions 11-Z-1 and 11-Z-2 analyzed from the 10° magnetic fraction. Both fractions are clear, pale yellow, with fluid inclusions, and have long prismatic shapes. The two discordant fractions (5.6% and 18.8%) define a discordia with a lower intercept of 356.5 +3.4/-4.0 Ma and a very poorly constrained upper intercept of 1682 +486/-361 Ma (Fig. 5.9, Table 5.2). The lower intercept is interpreted as the age of crystallization, and the upper intercept reflects Proterozoic inheritance.

### *Gabbro (SG94-1)*

One fraction of small, slightly magnetic zircons was extracted from a quartz-normative, pegmatitic phase of a gabbro (SG94-1). This fraction, 1-Z-1, has $^{206}$Pb/$^{238}$U and $^{207}$Pb/$^{235}$U ages of 346.5 ± 0.9 Ma and 348.7 ± 1.1 Ma respectively, and has a $^{207}$Pb/$^{206}$Pb age of 363.3 ± 6.1 Ma with 4.76% discordance (Table 5.2, Fig. 5.9). Without further analyses, it is impossible to determine whether this sample could have suffered from lead loss, or inheritance; comparison with the other SRPS zircon analyses may provide an approximate maximum and minimum to the age of the gabbro. If a discordia with a lead-loss trend (similar in fashion to SG94-55) plotted through 1-Z-1, an upper intercept would yield an age similar to the $^{207}Pb/^{206}Pb$ age of ~363 Ma (Fig. 5.9). An inheritance trend (similar to SG94-14 or SG94-11) passing through the 1-Z-1 analyses would form a discordia with a lower intercept similar to the lower intercept of the Hb-granodiorite discordia of ~345Ma (1-Z-1 plots very close to the SG94-14 discordia) (Fig. 5.9). As well, 1-Z-1 overlaps in error with 2-Z-1, 2-Z-2, 14-Z-3, and 55-Z-1N, all of which belong to samples with crystallization ages of ~345 - 357 Ma (Fig. 5.9). The above evidence lends weight to the interpretation that the gabbro is contemporaneous with the other SRPS igneous rocks. However, it should also be noted that 1-Z-1 could fall on a discordia that is near parallel to the concordia and has either an upper or lower intercept yielding a crystallization age considerably different than any of the other four SRPS rocks. Given the available U-Pb evidence for contemporaneity with the other SRPS rocks, however, and the intrusive and geochemical relationships noted above, the interpretation that the gabbro formed at or near the same time as the other ~350 Ma SRPS rocks is well substantiated.

### ***Summary of U-Pb data***

All the SRPS units analyzed in this study were formed between 345 to 360 Ma, including the gabbro, based on U-Pb zircon data (Fig. 5.9, table 5.2). Two of the SRPS rocks, the HbGd (SG94-14) and the FVP (SG94-11) have upper intercepts that are interpreted to be from inheritance of broadly Proterozoic material. Pb-loss is also apparent in the sheared granodiorite (SG94-55). The fact that the gabbro has the same age as the rest of the SRPS samples is further evidence that that it belongs to the SRPS and not to the Slide Mountain terrane.

Mortensen (1983, 1992a) also performed Rb-Sr and U-Pb analyses of several SRPS rocks in or near the Money klippe (as well as the 'peraluminous orthogneisses', discussed below). Mortensen (1983) obtained an upper intercept of 349 +3/-2 Ma from five zircon fractions of the BtMg (referred to as 'quartz monzonite' in Mortensen 1983) and interpreted it as the age of crystallization, which overlaps in error with ages obtained in this study for the BtMg (345.9 ± 1.2 Ma). The lower intercept of the zircon array, not observed in the present study, is interpreted to be the result of Pb loss (Mortensen 1983). The HbGd (referred to as the quartz diorite / granodiorite in Mortensen 1983) was also analyzed, and an array of five zircons was found to have an upper intercept of 359 +4/-3 Ma, interpreted as the crystallization age, and a lower intercept of 26 +47/-48 Ma, which is attributed to Pb loss (Mortensen 1983). This result is similar to that of Sh-Gd sample SG94-55, which also shows Pb-loss trends, but HbGd sample SG94-14 shows inheritance of broadly Proterozoic age. Proterozoic inheritance trends were also observed in analyses of the FVP (referred to as the quartz-feldspar porphyry in Mortensen 1992a) in the present study and in the analyses made by Mortensen (1992a); both also yielded similar lower intercept ages (356.5 +3.4/-4.0 and 360.5 ± 0.9, respectively) interpreted as the age of crystallization. Mortensen (1992a), however, assigned this unit to the Slide Mountain terrane, whereas in the present study, it is assigned to the SRPS. Mortensen (1983) also analyzed a single slightly discordant zircon fraction from the gabbro unit and obtained a similar age estimate to the gabbro analysis from the present study. The high U content of the gabbro zircon prompted Mortensen (1983) to suggest that the gabbro may be comagmatic with the SRPS rather than belong to an ophiolite complex (later called Slide Mountain terrane).

## 5.4 RADIOGENIC TRACER ISOTOPES

### *Rb-Sr*

Rb and Sr data were obtained for 10 SRPS igneous rocks (a pair from each of the major SRPS units). The preparation and analytical procedures are outlined in Appendices 6 and 9, respectively. The results are presented in Table 5.3 and Fig. 5.10a. The present day $^{87}Sr/^{86}Sr$ ratios from the SRPS rocks range from 0.7088 to 0.7311. $^{87}Rb/^{86}Sr$ values range from 0.021 for the gabbro to 4.507 for the Sh-Gd sample SG94-88. If the $^{87}Sr/^{86}Sr$ ratios are back-corrected to 350 Ma (approximate U-Pb age of crystallization), they cluster between 0.7074 to 0.7099 (Fig. 5.10a). These high initial $^{87}Sr/^{86}Sr$ ratios suggest that continental crust has contributed significantly to all the magmas. The fact that the initial ratios are similar could argue for homogenization of Sr ratios by resetting the Sr radiogenic system. The data form an array on a plot of $^{87}Sr/^{86}Sr$ vs. $^{87}Rb/^{86}Sr$ (Fig. 5.10b), to which a poorly constrained isochron can be fitted. The isochron has an initial $^{87}Sr/^{86}Sr$ = 0.7090, which is similar to those calculated individually (Fig. 5.10a), and an age of 345 ± 30 Ma (Model 3 of York 1967). This age cannot be considered reliable because of the large amount of scatter of data (M.S.W.D = 3920), but does overlap the range given by U-Pb analyses (see Section 5.3).

***Sm-Nd***

Nd isotopic analyses were performed on the same 10 SRPS samples as those analyzed for Sr; the results are presented in Table 5.4 and figure 5.11. The preparation and analytical procedures are outlined in Appendices 6 and 7, respectively. Depleted mantle model ages were not calculated for samples possessing $^{147}Sm/^{144}Nd > 0.16$, because these ratios are too similar to those of the depleted mantle (Samson et al. 1991) Figure 5.11 shows that there is a significant gap between the Nd isotopic signatures of the mafic rocks and those of the felsic rocks; the felsic SRPS samples range from $\varepsilon Nd_0$ = -11.8 to -17.07, the mafic samples range from $\varepsilon Nd_0$ = -3.30 to - 5.33. The initial εNd values, calculated to 350 Ma ago (U-Pb zircon crystallization ages) range from -7.97 to -12.77 for the felsic SRPS members to -3.16 to -1.71 for the mafic SRPS members (Table 5.4). $T_{DM}$ model ages fall in the range of 1.66 to 2.10 Ga for the felsic SRPS members. The mafic SRPS rocks have higher $^{147}Sm/^{144}Nd$ ratios (0.147 to 0.161) compared to the felsic rocks (0.095 to 0.115). The $T_{DM}$ ages in excess of the ~350 Ma crystallization ages suggests that old continental crust provides a significant contribution to the petrogenesis of all the rocks. Even the gabbros and MPV rocks, which are geochemically quite primitive, have negative $\varepsilon Nd_{350}$ values (-1.7 to -3.2), which suggests that these rocks are not likely pure mantle derivatives but have crustal input.

### *Pb-Pb*

Potassium feldspars were extracted from three felsic SRPS rocks (Bt-Mg sample SG94-2A, Hb-Gd sample SG94-14, and Sh-Gd sample SG94-55) by heavy-liquid and magnetic separation procedures, and finally by hand picking techniques (see Appendix 10). The feldspars were leached (leaching technique modified from Lugmair and Galer 1992) in order to remove Pb that has been incorporated subsequently to the time of feldspar genesis; this "excess" Pb may be radiogenic Pb released from nearby U-rich minerals such as zircon (Faure 1986). The more recently acquired Pb dissolves more easily than the common Pb incorporated at the time of crystallization (Ludwig and Silver 1977) thus it may be removed by successive stages of leaching with increasingly stronger acids (see Appendix 10), leaving the original common Pb behind in the residue.

The isotopic compositions of the first leach (L1), last leach (L4), and the residue (R) analyzed from the three SRPS samples are plotted in figure 5.12 and listed in table 5.5. As mentioned above, Pb removed by successive leaching is usually more radiogenic than the Pb remaining in the residue. This is the case in SG94-55, where L1 has higher $^{206}Pb/^{204}Pb$, $^{207}Pb/^{204}Pb$, and $^{208}Pb/^{204}Pb$ ratios than L4, and L4 in turn has higher ratios than the residue (Fig. 5.12 a - b). However, in SRPS samples SG94-2 and SG94-14, this was not the case. Their residue Pb is more radiogenic than either L1 or L4 for these samples, which is somewhat puzzling, but may suggest that 'excess' Pb subsequently incorporated into the feldspars had a less radiogenic source. However, the residues are of primary concern, because they are interpreted to contain the Pb incorporated into the feldspars at the time of formation. The three SRPS samples plot above and to the right of the terminus of the Pb-Pb growth curves defined by Stacey and Kramers (1975) on the $^{207}Pb/^{204}Pb$ vs. $^{206}Pb/^{204}Pb$ (Fig. 5.12a) and $^{208}Pb/^{204}Pb$ vs. $^{206}Pb/^{204}Pb$ (Fig. 5.12b); that is, the $^{206}Pb/^{204}Pb$, $^{207}Pb/^{204}Pb$, and $^{208}Pb/^{204}Pb$ ratios of the three SRPS rocks are greater than those of the uniform reservoir at present. This indicates that these SRPS rocks must have included a major contribution from preexisting crust at the time of their formation (~ 350 Ma crystallization from U-Pb zircon see Section 5.3). This preexisting crust that contributed to the petrogenesis of the SRPS rocks must have had enriched U/Pb and

Th/Pb ratios for a significant amount of time in order to have generated Pb with such high $^{206}Pb/^{204}Pb$, $^{207}Pb/^{204}Pb$, and $^{208}Pb/^{204}Pb$ ratios. As shown in Section 5.3, zircon from several of the SRPS samples, including SG94-14, have inheritance of broadly Proterozoic age. This evidence for previously existing sialic crust is compatible with the model that the SRPS magmatism has taken place in a continental arc or active continental margin. The Pb-Pb isotope findings of the SRPS in this study are similar to those of Aleinikoff et al. (1987), who performed Pb-Pb isotopic studies of Devonian-Mississippian granitoids from the YT terrane in Alaska. Two of the SRPS samples from the present study, SG94-2 and SG94-55, plot in the fields defined by Aleinikoff et al. (1987) for the YT terrane augen gneisses (Fig. 5.12); SG94-14 is slightly less radiogenic than samples that plot in these fields. Aleinikoff et al. (1987) suggest that the radiogenic Pb in the Alaskan YT terrane augen gneisses results from contribution by Archean material, as evidenced by zircon dating.

## 5.5 DISCUSSION

A wide range of rock types is encountered in the SRPS, including mafic gabbros and volcanic rock with basaltic composition, intermediate-felsic granodiorite to monzogranite, and felsic rhyolite. From geochemistry, it has been shown that the SRPS is subalkalic, and forms a calc-alkalic suite. The slightly peraluminous nature of many of the felsic granitoids and high Th/Yb and Ta/Yb values of the gabbros and MVP samples indicates that the volcanic arc in which they formed was built at least in part on continental crust. This interpretation that ancient crust has been involved in the genesis of the SRPS is borne out by Rb-Sr, Sm-Nd, Pb-Pb, and U-Pb studies. Initial Sr ratios for all the units are relatively consistent and range from 0.7074 to 0.7097. Just as the $Al_2O_3/(K_2O + Na_2O + CaO)$ parameter for the SRPS indicates that they straddle the boundary between 'peraluminous' and metaluminous', so too the narrow range of initial Sr ratios falls at the boundary between 'S-type' and 'I-type' granites (Chappell and White 1974). Regardless of into which group the SRPS should be classified, these Sr ratios indicate that the SRPS rocks are enriched relative to mantle values because of the contribution of material from continental crust. Also, $^{206}$Pb/$^{204}$Pb, $^{207}$Pb/$^{204}$Pb, and $^{208}$Pb/$^{204}$Pb ratios of feldspars from three SRPS samples are greater than the uniform reservoir at present, indicating that radiogenic Pb was incorporated from preexisting crust at the time of feldspar crystallization (~350 Ma). This preexisting crust, with higher U/Pb and Th/Pb ratios than the uniform reservoir, had been evolving separately from the uniform reservoir of U -Th-Pb for a significant amount of time in order to have produced the high $^{206}$Pb/$^{204}$Pb, $^{207}$Pb/$^{204}$Pb, and $^{208}$Pb/$^{204}$Pb ratios observed. Nd model ages of 1.66 to 2.06 Ga are in excess of the ~350 Ma U-Pb zircon crystallization ages for the SRPS, demonstrating that preexisting crust contributed to the petrogenesis of the SRPS. Unlike the relatively uniform initial Sr ratios, however, the initial εNd values of the felsic SRPS rocks ($\varepsilon Nd_{350}$ = -12.8 to -8.0) are significantly lower than those of the mafic SRPS rocks ($\varepsilon Nd_{350}$ = -1.7 to -3.2), which shows that the continental crust, on which the volcanic arc was at least in part formed, affected rocks to different degrees. Regardless, that the mafic gabbros have negative $\varepsilon Nd_{350}$ values shows that they received crustal input. Finally, zircon from two of the felsic SRPS samples have inherited material of approximately Middle to Early Proterozoic age, which broadly overlaps with the Nd model ages for the SRPS.

Igneous rocks in other locations in the YT terrane have also been correlated to the SRPS, based on similarity of lithology and especially U-Pb and Rb-Sr. These include the Fiftymile batholith (or a least part of it, Mortensen 1986) that straddles the Yukon-Alaska border, the Selwyn Gneiss in western Yukon (Mortensen 1986), quartz diorite and tonalite of the Teslin Tectonic zone (Stevens et al. 1996), the Lake George and Macomb subterranes in eastern Alaska, and other bodies throughout the YT terrane (Mortensen 1992b), which have U-Pb zircon analyses broadly grouping in the 341 to 375 Ma range. Some of these locations, such as portions of the Fiftymile batholith and Selwyn Gneiss, have yielded zircons that have no inherited zircon component (Mortensen 1986, Mortensen 1992b). However, inheritance of broadly Middle to Early Proterozoic age were demonstrated in zircons extracted from quartz diorite and tonalite from the TTZ

(Stevens et al. 1993) and from granitoids of the Macomb and Lake George subterranes of Alaska (Aleinikoff and Nokleberg 1985, as quoted in Mortensen 1992b).

Available Rb-Sr and Sm-Nd analyses of the SRPS and correlated rocks are sparse, but are similar to those reported in this study. Mortensen (1983) performed Rb-Sr analyses of SRPS rocks from near or within the Money Klippe, and determined initial ratios of $^{87}Sr/^{86}Sr \approx 0.710$, which is similar to those determined in the present study. The only previous Nd isotopic studies of rocks correlated to the SRPS are reported from quartz diorites and tonalites of the TTZ (Stevens et al. 1996). Here, the initial εNd values of -2.5 to -6.2 at 350 Ma for the broadly intermediate rocks (56.8 to 69.4 % $SiO_2$) indicate that the magmas were influenced by continental material (Stevens et al. 1996). These results are similar to those found in the present study, although the intermediate to felsic SRPS rocks have lower εNd values than those found in the TTZ (Fig. 5.13).

More isotopic data is available for the second, more voluminous, suite of Devonian-Mississippian rocks, which are referred to in this thesis as the peraluminous orthogneisses. Compared to the SRPS and related rocks discussed above, the peraluminous rocks have a much greater degree of input from continental material. As their name implies, geochemical analyses (Dusel-Bacon and Aleinikoff 1985) show that they are strongly peraluminous and, as a group, are more felsic that the SRPS rocks. Most zircon analyses, which show that the peraluminous granitoids have an age range of 343 to 364 Ma (Mortensen 1992b) have strong inheritance patterns. Also, initial εNd range of -14 to -16 (Bennett and Hansen, 1988; Aleinikoff et al. 1981) for the peraluminous orthogneisses are lower than the SRPS. Initial Sr ratios of the peraluminous orthogneiss in particular are much more radiogenic than those of the SRPS; they range from 0.716 to 0.738 (Mortensen 1983, 1992b, Aleinikoff et al. 1986, Hansen et al. 1989). The data can be interpreted to suggest that the peraluminous orthogneisses were derived from Precambrian crust in the continental arc (Hansen et al. 1989).

Taken together, the two contemporaneous Devonian-Mississippian magmatic suites can be thought of as a continuum between predominantly mantle-derived mafic rock with minor continental influence (eg. SRPS gabbro from the Money klippe), and highly felsic and peraluminous granitoids produced with a large degree of crustal input. This can be seen in plot of initial εNd verses $SiO_2$ (Fig. 5.13a), which shows that broadly, as the $SiO_2$ content increases, the initial εNd decreases. Similarly, as FeO*/MgO (another mafic-felsic indicator) increases, εNd decreases (Fig. 5.13b). Notice, however, that the TTZ samples seem to have a relatively consistent range of εNd regardless of how felsic the samples are. Scatter of this sort would be expected with widely scattered igneous bodies intruding the large, and likely heterogeneous, YT terrane. Also, comprehensive sets of data (ie. several sets of isotope systems and geochemistry performed on the same suite of rocks) are lacking, so such attempts to generalize (eg. Fig. 5.13) are somewhat sketchy. However, the data do suggest that mafic rocks like the gabbro from the Money klippe are mantle-derived but with some crustal contribution, whereas the peraluminous orthogneisses are crustally derived.

The relationships shown above are compatible with the model that Devonian - Mississippian magmatism was produced in a dominantly continental-type arc. The extent of the peraluminous orthogneiss, with evidence of inheritance from older sialic crust, suggests that the continental crust on which the arc was in part built was substantial. Other igneous rocks such as the SRPS exhibit less crustal enrichment, which could indicate that they were evolved in portions of the arc with thinner continental crust. The implications of these relationships will be examined, along with results obtained from the study of the Nisutlin and Anvil assemblage supracrustal rocks (Chapter 4), in the following discussion (Chapter 6)

Table 5.1. Geochemistry of Simpson Range Plutonic Suite samples.

| SG94-<br>unit | 36<br>ShGd | 54<br>Sh-Gd | 57<br>Sh-Gd | 88A<br>ShGd | 8<br>HbGd | 14<br>HbGd | 73<br>HbGd | 90B<br>HbGd | 2A<br>BtMg | 50<br>BtMg | 76A<br>BtMg | 78<br>BtMg | 11A<br>FVP | 63<br>FVP | 10B<br>MVP | 60<br>MVP | 1A<br>Gb | 3A<br>Gb | 44<br>Gb | 77A<br>Gb |
|---|---|---|---|---|---|---|---|---|---|---|---|---|---|---|---|---|---|---|---|---|
| | **Major elements (wt. %)** | | | | | | | | | | | | | | | | | | | |
| $SiO_2$ | 70.70 | 67.92 | 66.80 | 76.08 | 67.18 | 67.72 | 70.58 | 63.08 | 74.32 | 74.34 | 72.58 | 72.72 | 77.07 | 76.67 | 53.58 | 51.09 | 53.05 | 49.23 | 54.55 | 50.09 |
| $Al_2O_3$ | 14.26 | 15.25 | 15.37 | 12.93 | 15.25 | 15.11 | 14.82 | 14.74 | 14.08 | 13.22 | 14.65 | 14.43 | 12.69 | 12.50 | 13.11 | 16.42 | 20.57 | 20.85 | 17.03 | 17.41 |
| $TiO_2$ | 0.292 | 0.375 | 0.428 | 0.172 | 0.427 | 0.395 | 0.330 | 0.535 | 0.164 | 0.284 | 0.196 | 0.221 | 0.139 | 0.163 | 0.747 | 0.893 | 0.495 | 0.536 | 0.326 | 0.623 |
| FeO* | 3.43 | 4.42 | 5.23 | 1.38 | 4.80 | 4.58 | 4.43 | 6.31 | 2.12 | 2.68 | 2.43 | 2.68 | 1.05 | 1.87 | 8.66 | 7.51 | 5.19 | 4.73 | 5.90 | 7.76 |
| MnO | 0.080 | 0.113 | 0.128 | 0.031 | 0.092 | 0.091 | 0.217 | 0.139 | 0.047 | 0.045 | 0.059 | 0.058 | 0.025 | 0.023 | 0.199 | 0.211 | 0.102 | 0.097 | 0.118 | 0.142 |
| MgO | 2.18 | 1.69 | 1.96 | 0.43 | 2.06 | 1.77 | 1.53 | 4.20 | 0.43 | 0.58 | 0.52 | 0.77 | 0.55 | 0.62 | 9.22 | 9.22 | 4.87 | 7.44 | 7.24 | 9.08 |
| CaO | 2.61 | 4.88 | 4.26 | 0.63 | 4.72 | 4.07 | 1.72 | 5.97 | 2.14 | 2.72 | 2.93 | 2.85 | 0.52 | 0.48 | 10.51 | 11.07 | 12.38 | 14.95 | 10.89 | 12.06 |
| $K_2O$ | 3.32 | 2.76 | 3.63 | 5.59 | 2.77 | 3.19 | 1.87 | 2.63 | 3.29 | 3.04 | 3.63 | 3.26 | 5.04 | 4.26 | 0.91 | 1.39 | 0.10 | 0.07 | 1.23 | 0.61 |
| $Na_2O$ | 3.06 | 2.50 | 2.08 | 2.71 | 2.61 | 2.97 | 4.42 | 2.30 | 3.37 | 3.03 | 2.94 | 2.94 | 2.89 | 3.37 | 2.86 | 2.06 | 3.15 | 2.04 | 2.68 | 2.17 |
| $P_2O_5$ | 0.062 | 0.093 | 0.108 | 0.037 | 0.104 | 0.101 | 0.083 | 0.114 | 0.039 | 0.057 | 0.054 | 0.058 | 0.25 | 0.33 | 0.202 | 0.123 | 0.080 | 0.048 | 0.046 | 0.054 |
| | **Trace elements (ppm)** | | | | | | | | | | | | | | | | | | | |
| Ba | 1084 | 877 | 920 | 505 | 1068 | 1033 | 538 | 881 | 809 | 912 | 1006 | 951 | 2536 | 2721 | 361 | 228 | 40 | 27 | 481 | 182 |
| Rb | 113.74 | 85.31 | 119.48 | 203.82 | 79.39 | 79.39 | 66.56 | 79.95 | 94.40 | 66.60 | 98.22 | 87.00 | 111.00 | 105.00 | 28.12 | 31.42 | 2.71 | 2.00 | 35.61 | 18.57 |
| Sr$^{\dagger}$ | 419 | 369 | 452 | 153 | 309 | 305 | 217 | 226 | 221 | 241 | 297 | 256 | 103 | 114 | 306 | 338 | 390 | 221 | 278 | 292 |
| Cs | 1.62 | 1.16 | 0.79 | 2.18 | 0.58 | 0.42 | 2.16 | 0.68 | 0.66 | 0.46 | 0.64 | 0.94 | 0.67 | 0.78 | 1.78 | 0.38 | 0.07 | 0.05 | 0.29 | 0.72 |
| Pb | 5.77 | 18.60 | 28.05 | 17.66 | 10.29 | 10.64 | 25.94 | 6.81 | 13.99 | 7.73 | 15.75 | 7.58 | 27.70 | 4.66 | 2.51 | 8.76 | 2.03 | 2.99 | 2.08 | 1.99 |
| Th | 5.51 | 7.91 | 9.49 | 22.13 | 5.60 | 8.14 | 15.63 | 6.11 | 12.72 | 13.77 | 15.39 | 5.31 | 11.91 | 8.82 | 1.59 | 0.40 | 1.24 | 0.18 | 2.78 | 0.97 |
| U | 1.61 | 1.75 | 1.29 | 3.43 | 1.20 | 1.53 | 1.39 | 1.37 | 2.03 | 2.36 | 2.26 | 1.84 | 2.84 | 2.18 | 0.63 | 0.16 | 0.33 | 0.07 | 0.81 | 0.29 |
| Zr$^{*\dagger}$ | 105 | 104 | 115 | 111 | 128 | 127 | 119 | 107 | 107 | 126 | 123 | 108 | 111 | 109 | 70 | 48 | 65 | 40 | 74 | 56 |
| Nb | 7.89 | 7.85 | 8.67 | 13.39 | 9.83 | 9.72 | 9.21 | 8.79 | 8.29 | 10.44 | 8.94 | 7.13 | 8.70 | 7.59 | 5.36 | 221 | 2.65 | 0.79 | 3.40 | 1.89 |
| Hf | 2.52 | 2.49 | 2.68 | 3.24 | 3.17 | 2.94 | 3.00 | 2.76 | 2.85 | 3.39 | 3.12 | 2.61 | 3.45 | 3.02 | 1.57 | 1.13 | 1.44 | 0.83 | 1.83 | 1.23 |
| Ta | 0.67 | 0.78 | 0.86 | 1.60 | 0.85 | 0.85 | 0.97 | 0.67 | 0.80 | 1.28 | 0.86 | 0.66 | 1.04 | 0.80 | 0.39 | 0.22 | 0.24 | 0.15 | 0.35 | 0.19 |
| Y | 12.40 | 12.48 | 13.50 | 17.60 | 17.36 | 16.01 | 12.70 | 17.76 | 12.05 | 23.64 | 13.37 | 10.98 | 27.01 | 22.40 | 19.72 | 17.42 | 17.17 | 13.60 | 20.97 | 16.30 |
| La | 15.08 | 18.29 | 25.84 | 21.53 | 20.26 | 22.42 | 35.65 | 21.62 | 29.65 | 32.63 | 37.59 | 13.34 | 29.64 | 28.89 | 9.75 | 3.40 | 6.57 | 2.17 | 10.54 | 4.69 |
| Ce | 27.53 | 32.47 | 42.18 | 51.99 | 38.13 | 41.75 | 57.05 | 42.44 | 48.81 | 60.31 | 63.69 | 21.96 | 52.57 | 50.11 | 21.74 | 7.55 | 12.94 | 4.75 | 20.41 | 9.61 |
| Pr | 3.10 | 3.25 | 4.13 | 3.97 | 4.50 | 4.47 | 5.12 | 4.71 | 4.66 | 5.80 | 5.72 | 2.36 | 5.51 | 5.34 | 2.90 | 1.13 | 1.66 | 0.83 | 2.43 | 1.29 |
| Nd | 11.39 | 11.47 | 14.24 | 13.58 | 17.77 | 16.46 | 16.92 | 17.52 | 15.23 | 20.01 | 18.13 | 8.66 | 20.32 | 19.16 | 13.05 | 5.51 | 7.26 | 3.95 | 9.88 | 5.92 |
| Sm | 2.20 | 2.25 | 2.86 | 2.79 | 3.44 | 3.10 | 3.00 | 3.62 | 2.36 | 3.87 | 2.82 | 1.63 | 3.71 | 3.46 | 3.58 | 1.97 | 2.16 | 1.48 | 2.76 | 1.96 |
| Eu | 0.55 | 0.66 | 0.71 | 0.36 | 0.80 | 0.76 | 0.63 | 0.77 | 0.53 | 0.68 | 0.60 | 0.53 | 0.39 | 0.54 | 1.07 | 0.59 | 0.93 | 0.68 | 0.94 | 0.85 |
| Gd | 1.99 | 2.07 | 2.28 | 2.29 | 2.96 | 2.71 | 2.25 | 3.07 | 1.78 | 3.26 | 2.07 | 1.62 | 3.79 | 3.51 | 3.47 | 2.57 | 2.44 | 1.86 | 2.94 | 2.42 |
| Tb | 0.33 | 0.34 | 0.39 | 0.43 | 0.49 | 0.46 | 0.38 | 0.52 | 0.29 | 0.62 | 0.36 | 0.28 | 0.67 | 0.59 | 0.60 | 0.51 | 0.48 | 0.37 | 0.57 | 0.48 |
| Dy | 2.01 | 2.10 | 2.41 | 2.72 | 3.06 | 2.67 | 2.24 | 3.08 | 1.83 | 3.77 | 2.019 | 1.72 | 4.32 | 3.71 | 3.53 | 3.19 | 3.02 | 2.40 | 3.59 | 2.87 |
| Ho | 0.41 | 0.43 | 0.50 | 0.59 | 0.61 | 0.54 | 0.45 | 0.65 | 0.40 | 0.81 | 0.46 | 0.37 | 0.91 | 0.79 | 0.72 | 0.67 | 0.64 | 0.51 | 0.77 | 0.60 |
| Er | 1.24 | 1.28 | 1.48 | 1.87 | 1.78 | 1.64 | 1.32 | 1.88 | 1.29 | 2.52 | 1.46 | 1.15 | 2.87 | 2.35 | 2.08 | 1.95 | 1.85 | 1.46 | 2.31 | 1.72 |
| Tm | 0.18 | 0.19 | 0.21 | 0.30 | 0.26 | 0.24 | 0.19 | 0.27 | 0.20 | 0.39 | 0.22 | 0.18 | 0.42 | 0.34 | 0.28 | 0.26 | 0.25 | 0.20 | 0.32 | 0.23 |
| Yb | 1.22 | 1.28 | 1.37 | 1.97 | 1.63 | 1.56 | 1.33 | 1.71 | 1.45 | 2.51 | 1.45 | 1.17 | 2.74 | 2.25 | 1.82 | 1.63 | 1.63 | 1.23 | 2.02 | 1.47 |
| Lu | 0.19 | 0.21 | 0.22 | 0.31 | 0.27 | 0.26 | 0.23 | 0.28 | 0.25 | 0.40 | 0.24 | 0.20 | 0.47 | 0.37 | 0.28 | 0.26 | 0.24 | 0.19 | 0.32 | 0.23 |
| Sc$^{\dagger}$ | 11 | 13 | 14 | 3 | 17 | 12 | 8 | 27 | 8 | 10 | 11 | 3 | 1 | 8 | 36 | 40 | 32 | 44 | 32 | 33 |
| V$^{\dagger}$ | 71 | 94 | 94 | 0 | 92 | 91 | 72 | 152 | 24 | 33 | 38 | 47 | 0 | 15 | 9 | 8 | 134 | 147 | 142 | 168 |
| Cr$^{\dagger}$ | 32 | 10 | 7 | 0 | 35 | 23 | 13 | 102 | 0 | 1 | 1 | 0 | 0 | 0 | 333 | 188 | 53 | 429 | 574 | 351 |
| Ni$^{\dagger}$ | 12 | 7 | 2 | 8 | 10 | 8 | 8 | 23 | 14 | 10 | 8 | 7 | 10 | 9 | 63 | 50 | 27 | 93 | 50 | 124 |
| Cu$^{\dagger}$ | 0 | 2 | 0 | 2 | 6 | 12 | 14 | 16 | 18 | 6 | 0 | 3 | 6 | 24 | 98 | 0 | 6 | 66 | 0 | 69 |
| Zn$^{\dagger}$ | 39 | 49 | 606 | 22 | 49 | 53 | 116 | 64 | 26 | 27 | 30 | 28 | 34 | 15 | 83 | 101 | 34 | 29 | 40 | 45 |
| Ga$^{\dagger}$ | 13 | 15 | 16 | 15 | 18 | 16 | 14 | 15 | 13 | 17 | 15 | 13 | 12 | 14 | 14 | 14 | 20 | 16 | 15 | 13 |

Major element analyses performed by XRF and normalized to 100% (volatile free). All Fe reported as FeO*. Trace elements denoted with '†' performed by XRF; all others by ICP-MS; all analyses by Washington State University, details given in Hooper et al. (1993). Analytical errors given in Appendix 11.

## Table 5.2. U-Pb analyses of zircon from SRPS rocks

| Rock/ Fraction | Magnetic fraction | Desrciption | Grains (#) | Mass (mg) | U (ppm) | Pb rad (ppm) | Pb C tot (pg) | $\frac{^{206}Pb}{^{238}U}$ | $\frac{^{207}Pb}{^{235}U}$ | $\frac{^{207}Pb}{^{206}Pb}$ | | apparent ages (Ma) $\frac{^{206}Pb}{^{238}U}$ | apparent ages (Ma) $\frac{^{207}Pb}{^{206}U}$ | apparent ages (Ma) $\frac{^{207}Pb}{^{206}Pb}$ | Disc (%) |
|---|---|---|---|---|---|---|---|---|---|---|---|---|---|---|---|
| gabbro/ | | | | | | | | | | | | | | | |
| 1-Z-1 | M@1° | sm prism | 46 | 0.027 | 301 | 17 | 16 | 0.05522 ± 14 | 0.4097 ± 15 | 0.05382 | 15 | 346.5 | 348.7 | 363.3 | 4.76 |
| Bt-Mg/ | | | | | | | | | | | | | | | |
| 2-Z-1 | M@0.5° | eqt cryst abr | 108 | 0.038 | 120 | 7 | 9 | 0.05510 ± 12 | 0.4087 ± 20 | 0.05380 | 23 | 345.8 | 347.9 | 362.6 | 4.77 |
| 2-Z-2 | M@0.5° | sm prism abr | 175 | 0.048 | 286 | 16 | 9 | 0.05520 ± 20 | 0.4061 ± 16 | 0.05336 | 09 | 346.3 | 346.1 | 344.1 | -0.67 |
| FVP/ | | | | | | | | | | | | | | | |
| 11-Z-1 | M@10° | lg prism abr | 25 | 0.076 | 529 | 31 | 27 | 0.05740 ± 19 | 0.4291 ± 15 | 0.05422 | 05 | 359.8 | 362.6 | 380.4 | 5.57 |
| 11-Z-2 | M@10° | sm prism abr | 100 | 0.028 | 139 | 8 | 7 | 0.05917 ± 15 | 0.4571 ± 21 | 0.05603 | 21 | 370.6 | 382.3 | 453.5 | 18.82 |
| HbGd/ | | | | | | | | | | | | | | | |
| 14-Z-1 | M@0° | lg stb abr | 16 | 0.060 | 396 | 23 | 30 | 0.05608 ± 12 | 0.4216 ± 11 | 0.05433 | 06 | 351.7 | 357.2 | 392.8 | 10.75 |
| 14-Z-2 | NM@0° | lg prism abr | 50 | 0.062 | 535 | 34 | 71 | 0.06092 ± 18 | 0.5047 ± 16 | 0.06008 | 08 | 381.2 | 414.9 | 606.6 | 38.26 |
| 14-Z-3 | NM@0° | sm stb avr | 70 | 0.025 | 359 | 21 | 25 | 0.05526 ± 13 | 0.4126 ± 16 | 0.05415 | 15 | 346.7 | 350.8 | 377.4 | 8.35 |
| Sh-Gd/ | | | | | | | | | | | | | | | |
| 55-Z-C | M@1° | lg stb cor n-ab | 1 | 0.012 | 380 | 21 | 21 | 0.05304 ± 11 | 0.3941 ± 21 | 0.05389 | 25 | 333.2 | 337.4 | 366.5 | 9.33 |
| 55-Z-NC | M@1° | lg stb n-cor n-ab | 1 | 0.008 | 381 | 21 | 20 | 0.05475 ± 13 | 0.4009 ± 31 | 0.05310 | 37 | 343.6 | 342.3 | 333.2 | -3.20 |
| 55-Z-1 | M@1° | lg rounded abr | 15 | 0.059 | 244 | 9 | 14 | 0.03736 ± 10 | 0.2752 ± 10 | 0.05342 | 11 | 236.5 | 246.8 | 346.7 | 32.39 |

$^{206}Pb/^{238}U$, $^{207}Pb/^{235}U$, and $^{207}Pb/^{206}Pb$ ratios corrected for fractionation, blank (8.0pg Pb, 2.0 pg U), spike, and common Pb; and $^{206}Pb/^{238}U$, $^{207}Pb/^{235}U$, and $^{207}Pb/^{206}Pb$ ages calculated using the ROMAGE software package. All errors in isotopic ratios shown as 1σ. PbC = common Pb measured in the analysis, Disc. = discordance. Description abbreviations: abr = abraded, cor = cored., eqt = equant, lg = large, n-ab = non-abraded, n-cor = non-cored, prism = prismatic, sm = small, stb = stubby. Magnetic fractions: NM = nonmagnetic, m = magnetic; degree shown is side tilt of chute in Frantz magnetic separator.

Table 5.3. Rb-Sr isotope systematics for the Simpson Range Plutonic Suite

| sample name | rock type | $^{87}Sr/^{86}Sr$ | | error ($2\sigma$) | Sr (ppm) | Rb (ppm) | $^{87}Rb/^{86}Sr$ | $^{87}Sr/^{86}Sr$ @350 Ma |
|---|---|---|---|---|---|---|---|---|
| SG94-54 | Sh-Gd | 0.712897 | ± | 0.000022 | 261.0 | 67.1 | 0.7442 | 0.7092 |
| SG94-88A | Sh-Gd | 0.731085 | ± | 0.000024 | 138.3 | 214.9 | 4.5075 | 0.7086 |
| SG94-73 | HbGd | 0.713860 | ± | 0.000025 | 202.7 | 65.6 | 0.9368 | 0.7092 |
| SG94-90B | HbGd | 0.715147 | ± | 0.000028 | 214.1 | 80.7 | 1.0916 | 0.7097 |
| SG94-2A | BtMg | 0.716271 | ± | 0.000034 | 204.9 | 94.9 | 1.3416 | 0.7096 |
| SG94-50 | BtMg | 0.713076 | ± | 0.000025 | 229.0 | 67.6 | 0.8542 | 0.7088 |
| SG94-10B | MVP | 0.708789 | ± | 0.000022 | 357.5 | 34.6 | 0.2800 | 0.7074 |
| SG94-63 | FVP | 0.723328 | ± | 0.000019 | 104.6 | 107.5 | 2.9785 | 0.7085 |
| SG94-1 | Gab | 0.709962 | ± | 0.000025 | 364.4 | 2.6 | 0.0206 | 0.7099 |
| SG94-44 | Gab | 0.710522 | ± | 0.000022 | 237.8 | 35.0 | 0.4255 | 0.7084 |

All measurements performed on the VG 354 at the University of Alberta. See Appendices 6 and 9 for details of rock preparation and sample analysis, respectively. $^{87}Sr/^{86}Sr$ uncertainties are quoted as $2\sigma$. Rock types: BtMg = biotite monzogranite, FVP = felsic volcanic plug member, Gab = gabbro, HbGd = hornblende granodiorite, MVP = mafic volcanic plug member, Sh-Gd = sheared granodiorite

Table 5.4. Sm-Nd isotope systematics for the Simpson Range Plutonic Suite

| sample name | rock type | $\frac{^{143}Nd}{^{144}Nd}$ | | error (2σ) | Nd (ppm) | Sm (ppm) | $\frac{^{147}Sm}{^{144}Nd}$ | $\varepsilon Nd_0$ | $\varepsilon Nd_{350}$ | $T_{DM}$ (Ga) |
|---|---|---|---|---|---|---|---|---|---|---|
| SG94-54 | Sh-Gd | 0.511964 | ± | 0.000027 | 12.19 | 2.27 | 0.1128 | -13.2 | -9.4 | 1.81 |
| SG94-54r | Sh-Gd | 0.511922 | ± | 0.000008 | 12.24 | | | -14.0 | | |
| SG94-54r2 | Sh-Gd | 0.511926 | ± | 0.000009 | 12.25 | 2.27 | 0.1123 | -13.9 | -10.1 | 1.85 |
| SG94-88A | Sh-Gd | 0.511869 | ± | 0.000008 | 14.75 | 2.78 | 0.1141 | -15.0 | -11.3 | 1.97 |
| SG94-73 | HbGd | 0.511763 | ± | 0.000015 | 18.63 | 2.94 | 0.0954 | -17.1 | -12.6 | 1.80 |
| SG94-90B | HbGd | 0.511801 | ± | 0.000017 | 18.53 | 3.53 | 0.1151 | -16.3 | -12.7 | 2.10 |
| SG94-90Br | HbGd | 0.511858 | ± | 0.000014 | 18.58 | 3.53 | 0.1150 | -15.2 | -11.6 | 2.01 |
| SG94-2A | BtMg | 0.511800 | ± | 0.000023 | 15.96 | 2.45 | 0.0929 | -16.4 | -11.7 | 1.71 |
| SG94-2Ar | BtMg | 0.511801 | ± | 0.000008 | 16.52 | 2.48 | 0.0907 | -16.3 | -11.6 | 1.68 |
| SG94-50 | BtMg | 0.512032 | ± | 0.000008 | 21.93 | 4.00 | 0.1104 | -11.8 | -8.0 | 1.67 |
| SG94-10B | MVP | 0.512383 | ± | 0.000008 | 13.86 | 3.37 | 0.1469 | -5.0 | -2.8 | 1.77 |
| SG94-63 | FVP | 0.511791 | ± | 0.000009 | 20.32 | 3.78 | 0.1125 | -16.5 | -12.8 | 2.06 |
| SG94-1 | Gab | 0.512469 | ± | 0.000012 | 8.22 | 2.19 | 0.1612 | -3.3 | -1.7 | 2.00 |
| SG94-44 | Gab | 0.512365 | ± | 0.000012 | 11.06 | 2.71 | 0.1482 | -5.3 | -3.2 | 1.85 |

All measurements performed on the VG-354 mass-spectrometer at the university of Alberta. See appendices 6 and 7 for details of rock preparation and sample analysis, respectively. The $^{143}Nd/^{144}Nd$ uncertainties are quoted as 2σ. Repeat analysis denoted by 'r'. Rock types: BtMg = biotite monzogranite, FVP = felsic volcanic plug member, Gab = gabbro, HbGd = hornblende granodiorite, MVP = mafic volcanic plug member, Sh-Gd = sheared granodiorite.

Table 5.5. Pb-Pb composition of K-feldspar from SRPS samples.

| Sample | $^{206}$Pb/$^{204}$Pb | $^{207}$Pb/$^{204}$Pb | $^{208}$Pb/$^{204}$Pb |
|---|---|---|---|
| 2 L1 | 19.196 | 15.691 | 39.335 |
| 2 L4 | 19.069 | 15.711 | 38.920 |
| **2 R** | **19.606** | **15.727** | **39.631** |
| 14 L1 | 18.869 | 15.695 | 38.874 |
| 14 L4 | 18.857 | 15.694 | 38.844 |
| **14 R** | **19.025** | **15.723** | **38.885** |
| 55 L1* | 21.160 | 15.817 | 40.892 |
| 55 L4* | 20.046 | 15.739 | 39.483 |
| 55 L4 | 20.161 | 15.856 | 39.954 |
| **55 R** | **19.508** | **15.740** | **39.511** |

All measuresments made at 1250°C on the VG Micromass-30 mass-spectrometer at the University of Alberta, except for those marked with '*', which were analyzed on the VG-354 mass-spectrometer at the University of Alberta. See Appendix 10 for analytical methods. Samples run on VG Micromass-30 have a reproducabilty of 0.24, 0.32, and 0.36 per mil (1σ) for $^{206}$Pb/$^{204}$Pb, $^{207}$Pb/$^{204}$Pb, and $^{208}$Pb/$^{204}$Pb, respectively, and a mass-fractionation level of 1.3 per mil per mass unit difference as determined by repeated measurements of NBS standards SRM 981 and SRM 982 lead standards (Sundblad et al. 1991).

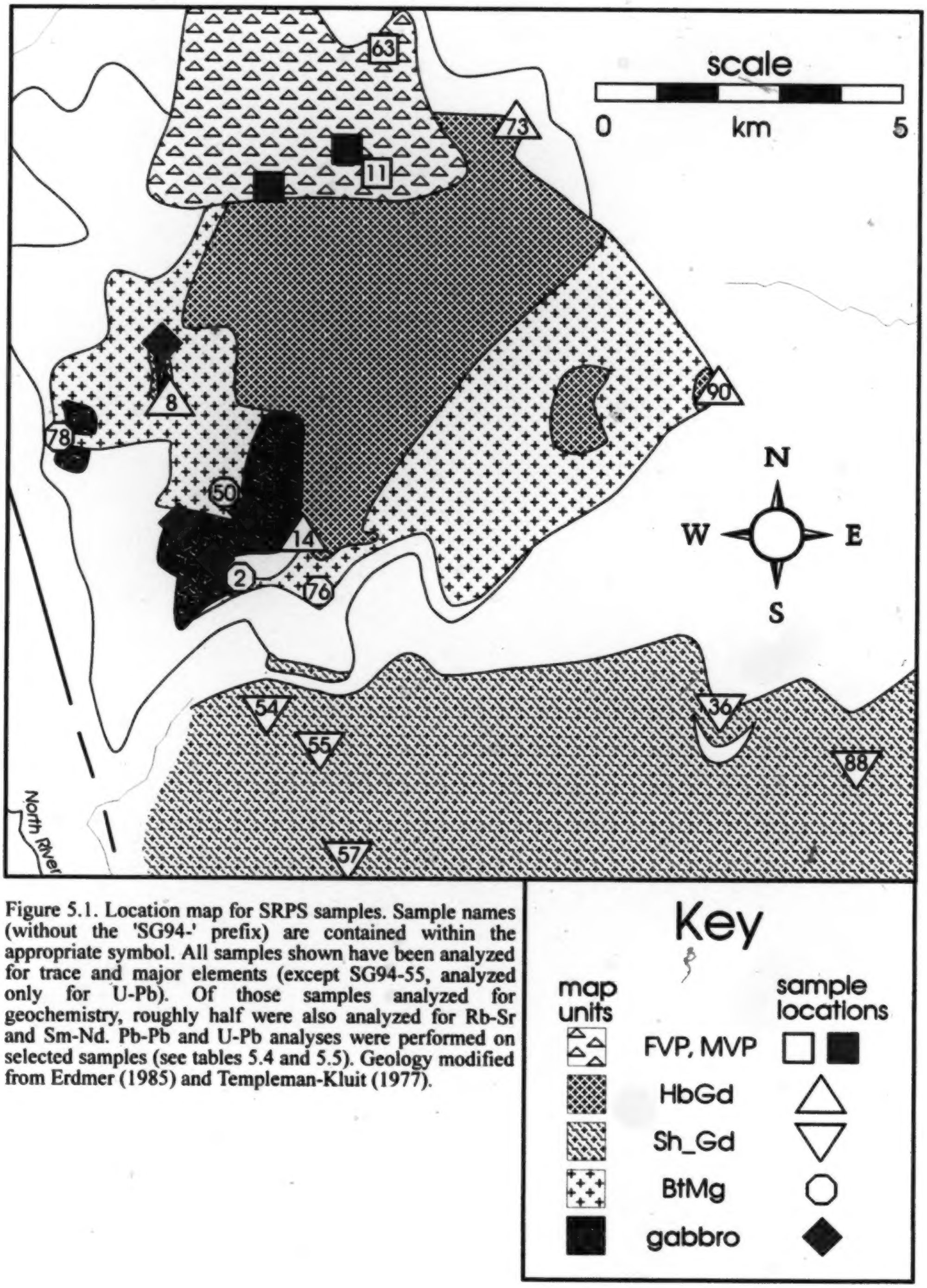

Figure 5.1. Location map for SRPS samples. Sample names (without the 'SG94-' prefix) are contained within the appropriate symbol. All samples shown have been analyzed for trace and major elements (except SG94-55, analyzed only for U-Pb). Of those samples analyzed for geochemistry, roughly half were also analyzed for Rb-Sr and Sm-Nd. Pb-Pb and U-Pb analyses were performed on selected samples (see tables 5.4 and 5.5). Geology modified from Erdmer (1985) and Templeman-Kluit (1977).

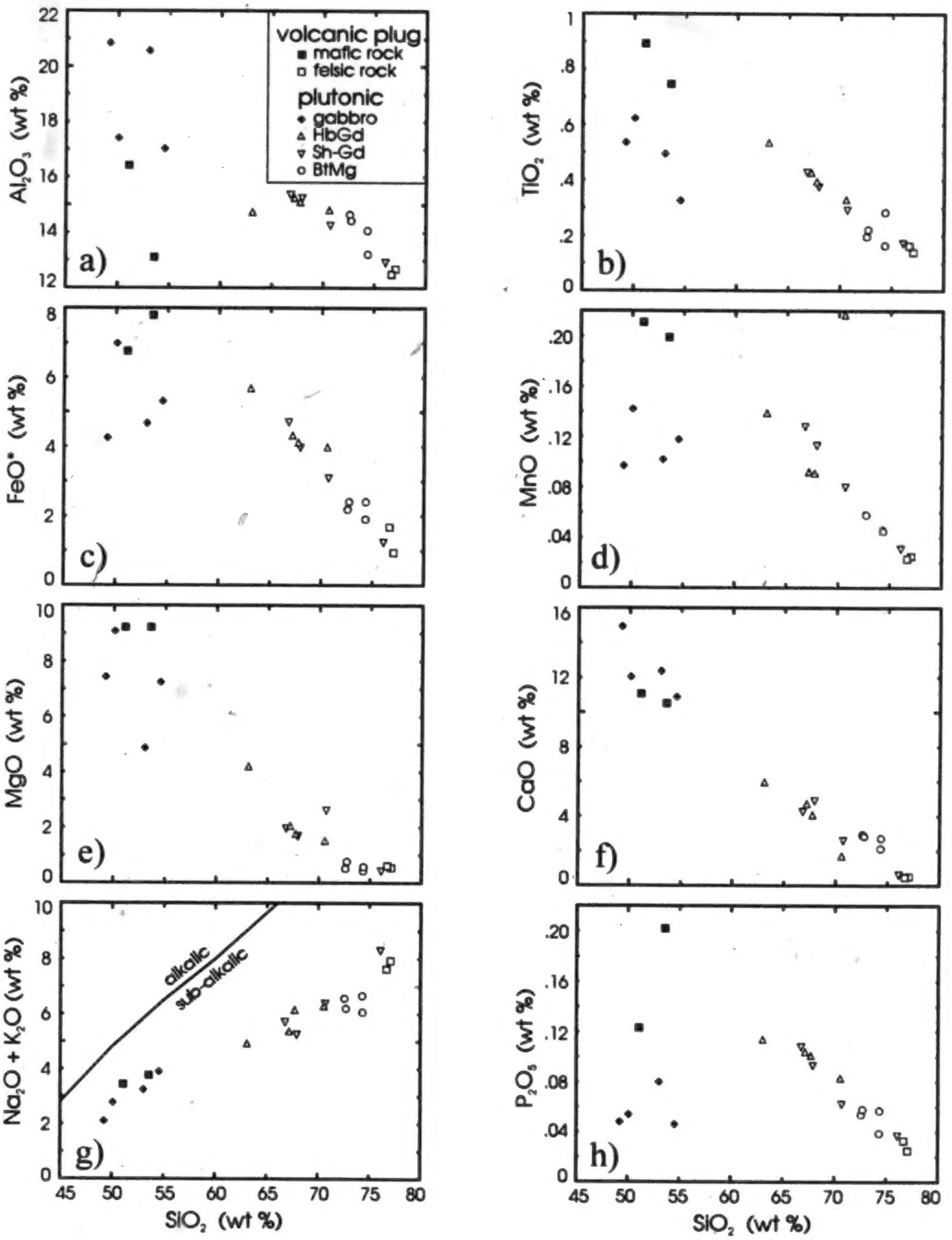

Figure. 5.2 Major element Harker-type diagrams. The $Na_2O + K_2O$ vs. $SiO_2$ plot (g) shows that the SRPS are subalkalic (from Irvine and Baragar 1971).

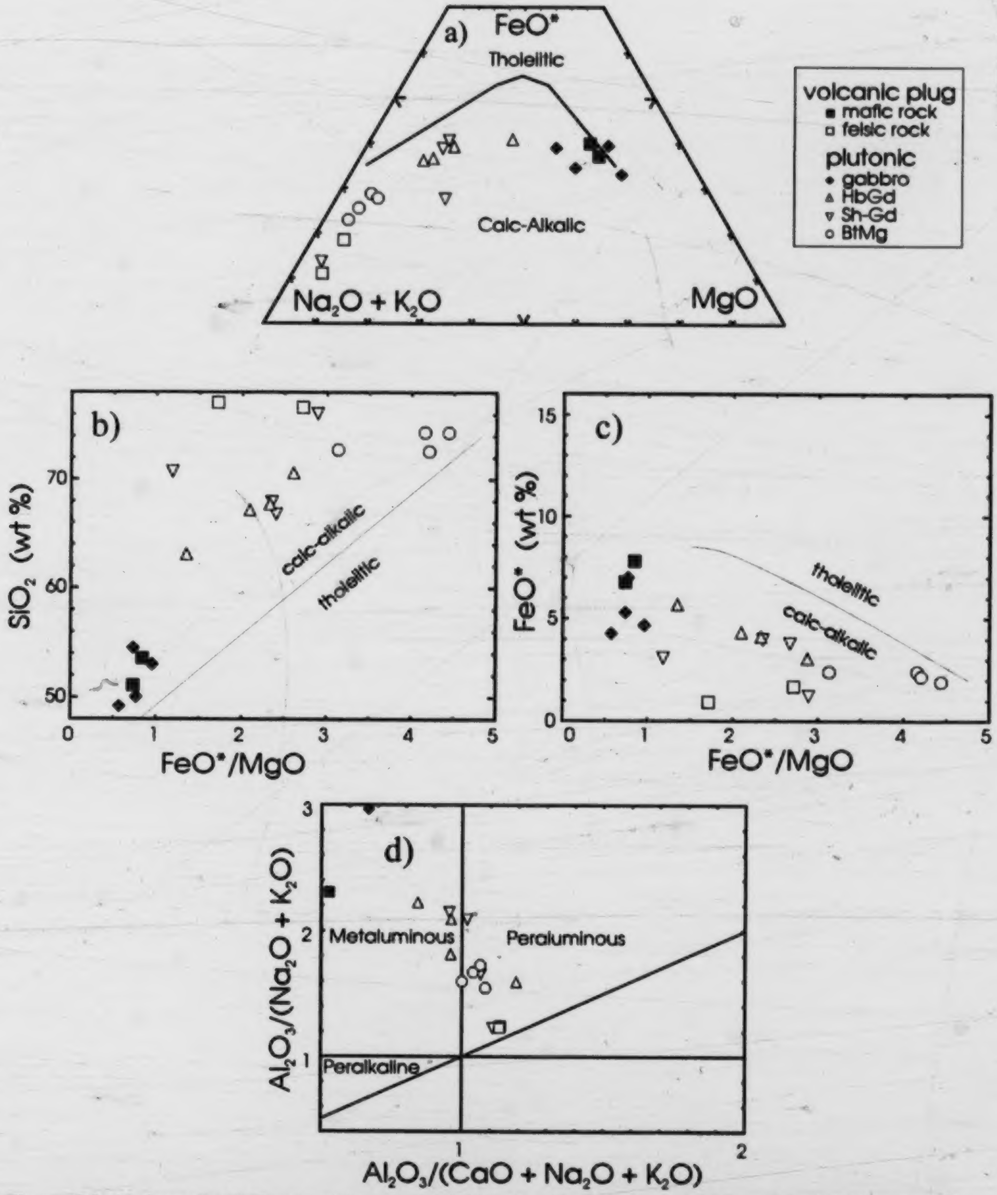

Figure 5.3. Various discrimination diagrams. SRPS rocks dominantly plot in the calc-alkalic fields in the ternary $K_2O + Na_2O$ - FeO* - MgO diagram (a). $SiO_2$ and FeO* vs. FeO*/(FeO* + MgO) diagrams (b and c) also show that the SRPS rocks are dominantly calc-alkalic. Finally, characterizing the SRPS rocks with respect to alumina saturation, it can be seen that they straddle the boundary between 'peraluminous' and 'metaluminous' fields, with the more felsic members (FVP and BtMg) falling in the former field and the more mafic members (some granodiorites and the gabbros and MVP) falling in the latter. $K_2O + Na_2O$ - FeO* - MgO diagram (a) modified from Irvine and Baragar (1971); $SiO_2$ and FeO* vs. FeO*/MgO diagrams (b and c) modified from Miyashiro (1974); and alumina saturation diagram (d) modified from Shand (1947).

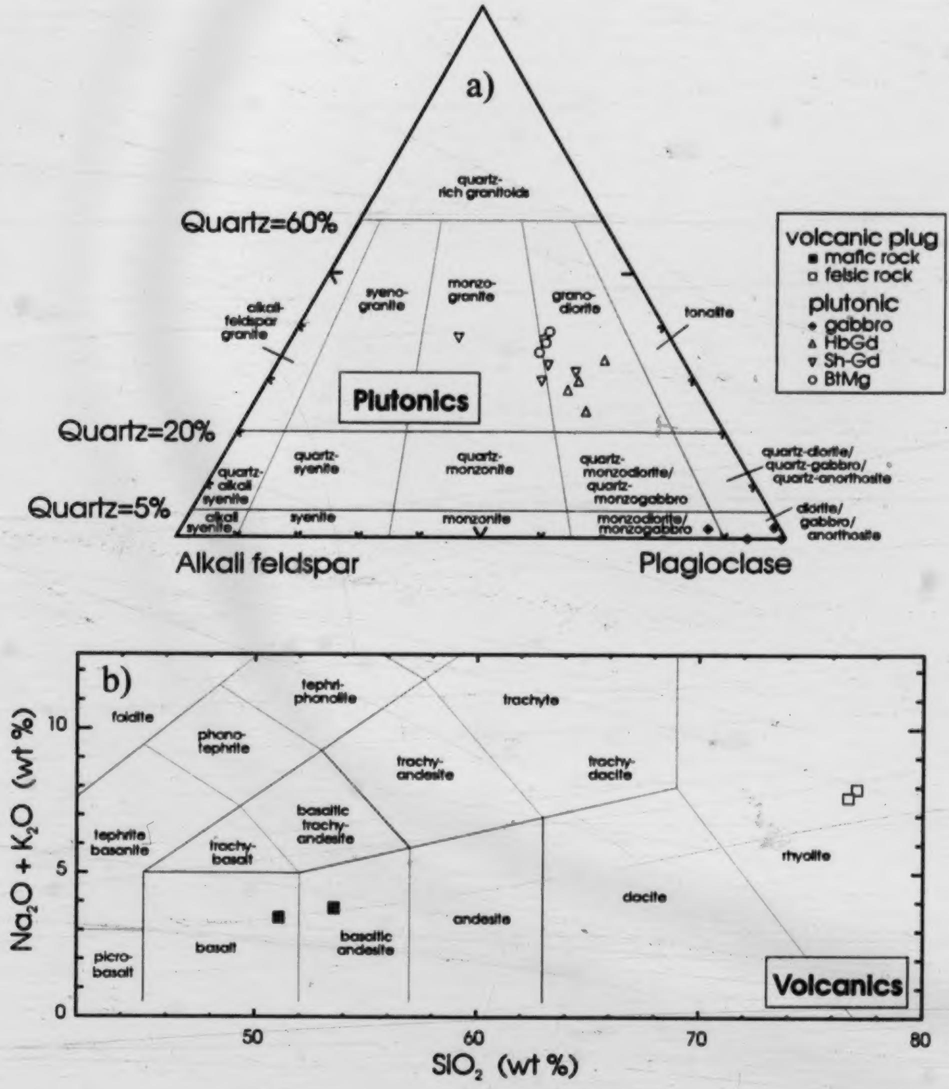

Figure 5.4. Classification of the SRPS rocks. Normative mineral compositions have been calculated from the major-element geochemistry and plotted on a QAP (quartz - alkali feldspar - plagioclase) ternary diagram (a). Plots of $Na_2O + K_2O$ vs. $SiO_2$ can also be used to classify volcanic rock (b) using fields defined by Le Bas et al. (1992).

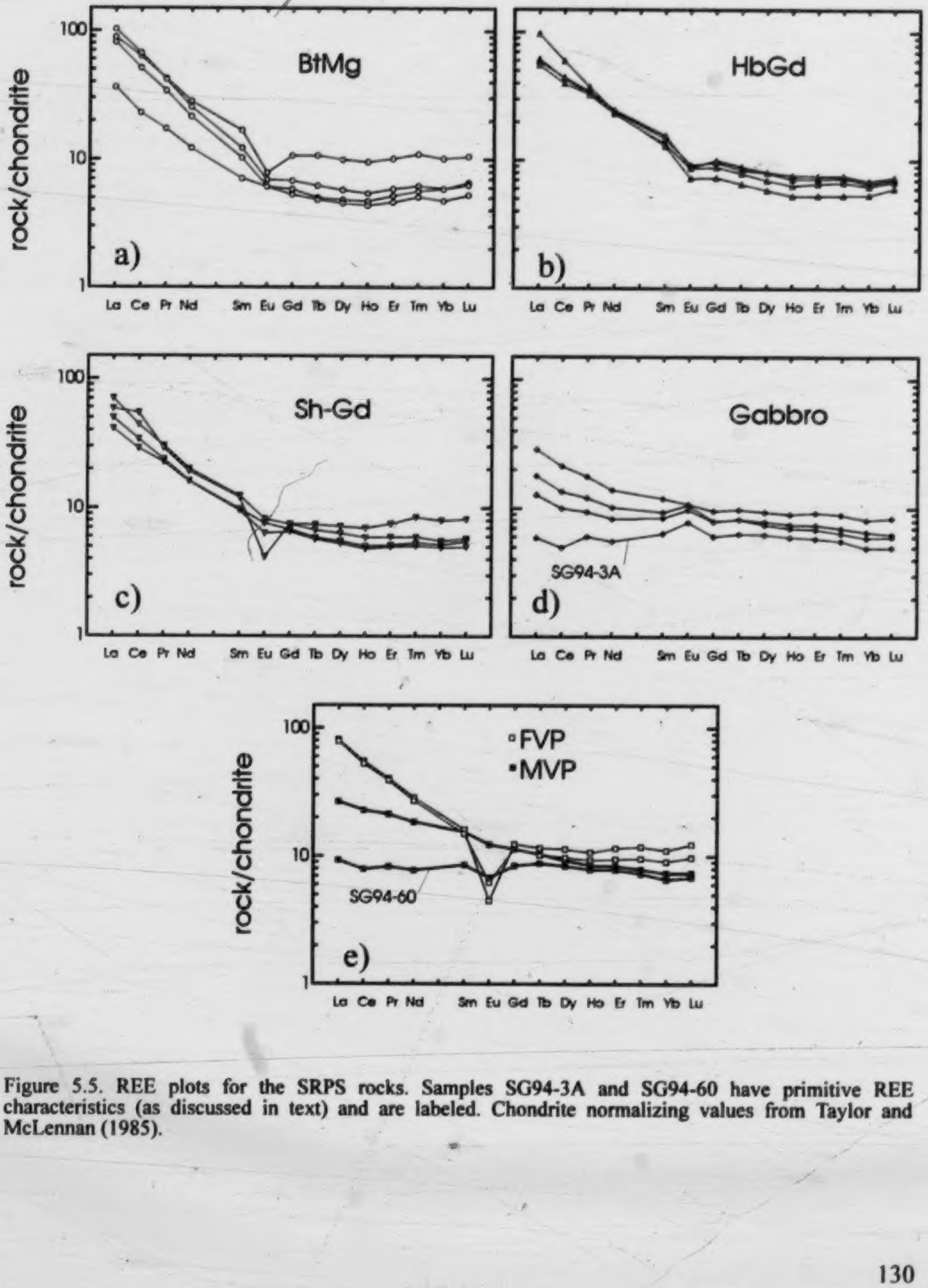

Figure 5.5. REE plots for the SRPS rocks. Samples SG94-3A and SG94-60 have primitive REE characteristics (as discussed in text) and are labeled. Chondrite normalizing values from Taylor and McLennan (1985).

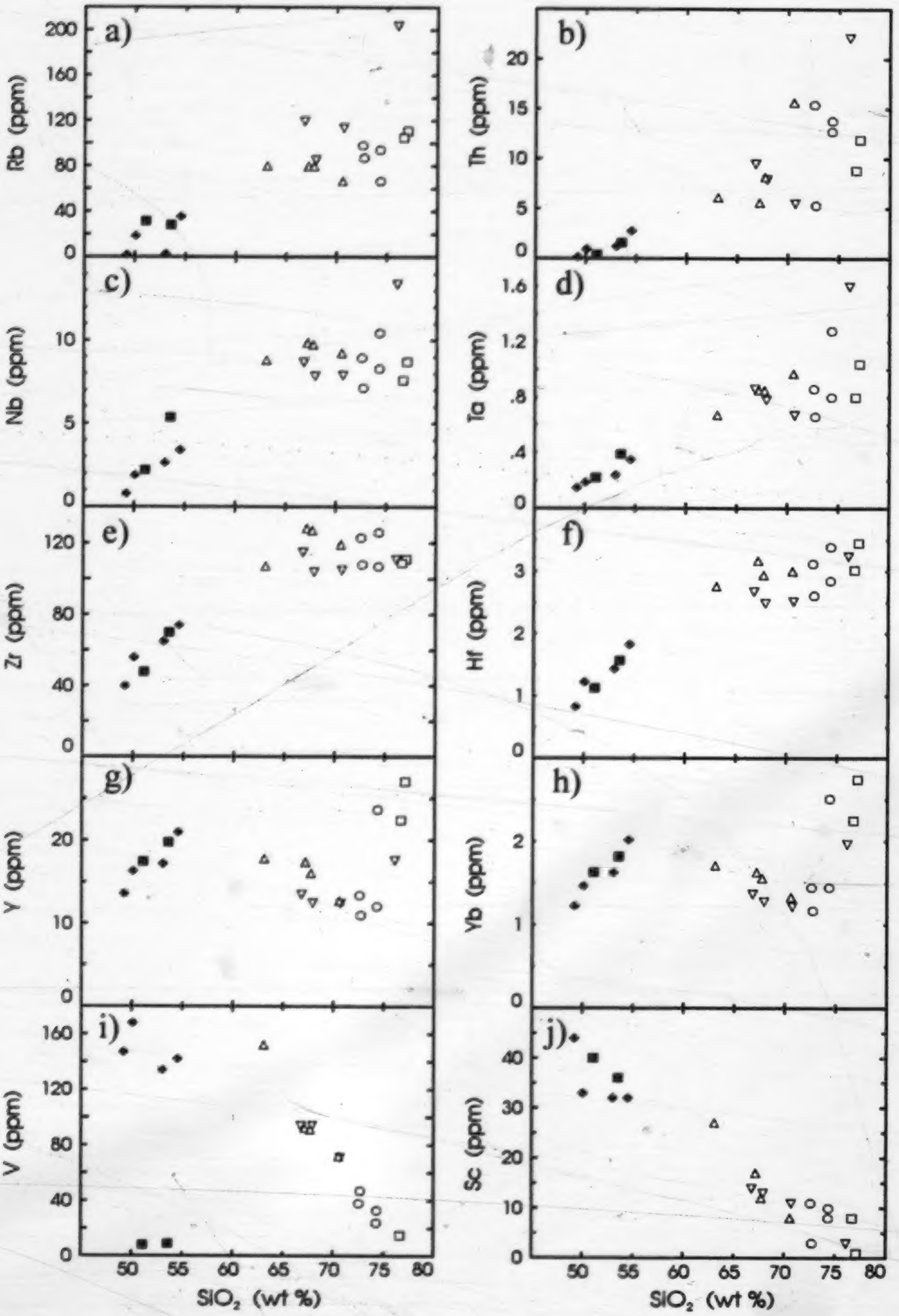

Figure 5.6. Trace elements verses $SiO_2$

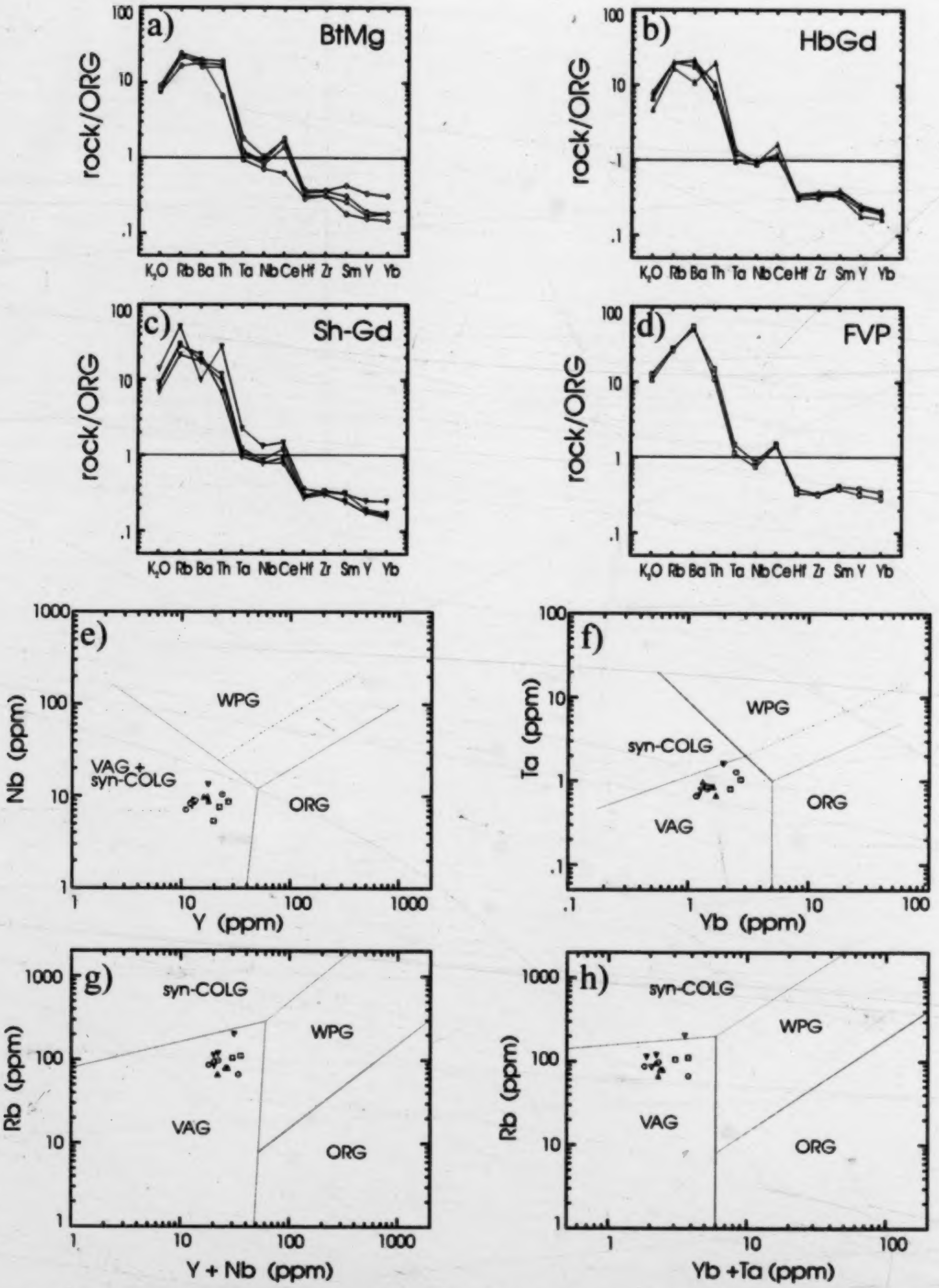

Figure 5.7. Trace element discrimination diagrams used to determine the tectonic setting of the felsic SRPS rocks. The multielement patterns (a-d) are normalized to hypothetical ocean ridge granite (ORG) as given in Pearce et al. (1984). Fields for tectonic settings on the tectonic discrimination diagrams (e-h) are from Pearce et al. (1984). Settings include: volcanic arc granite (VAG), syn-collisional granite (syn-COLG), within-plate granite (WPG), and ocean ridge granite (ORG).

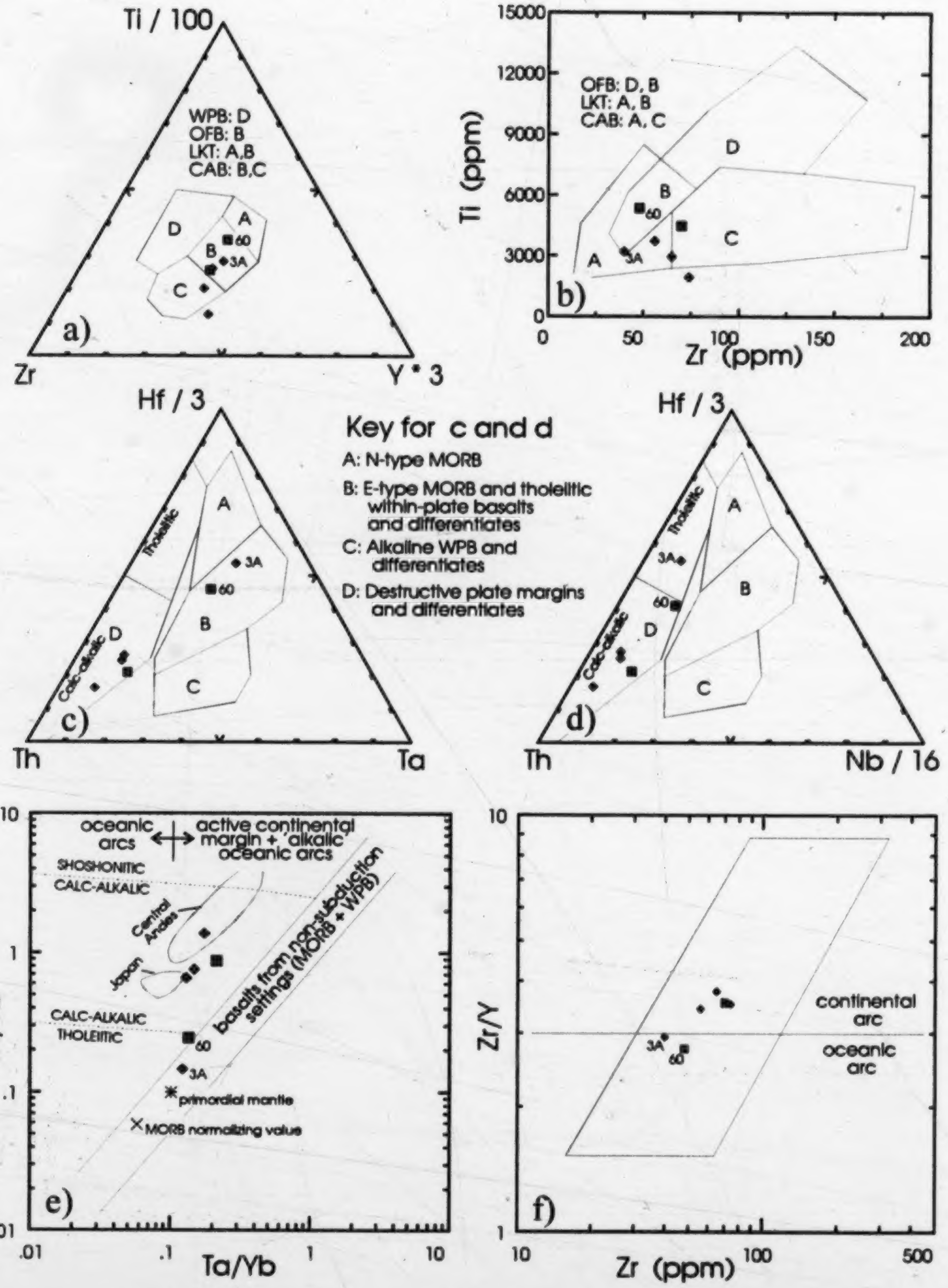

Figure 5.8. SRPS gabbro and MVP units plotted on discrimination diagrams designed for rocks of basaltic composition. SG94-3A and SG94-60, which are more primitive than the other mafic SRPS (see text) are identified. Abbreviations for rocks and tectonic settinds include: calc-alkalic basalt (CAB), Low-potassium tholeiite (LKT), mid-ocean ridge basalt (MORB), ocean floor basalt (OFB), and within-plate basalt (WPB). Plots (a) and (b) from Pierce and Cann (1973); (c) and (d) from Wood (1980); and (e) and (f) from Pearce (1983).

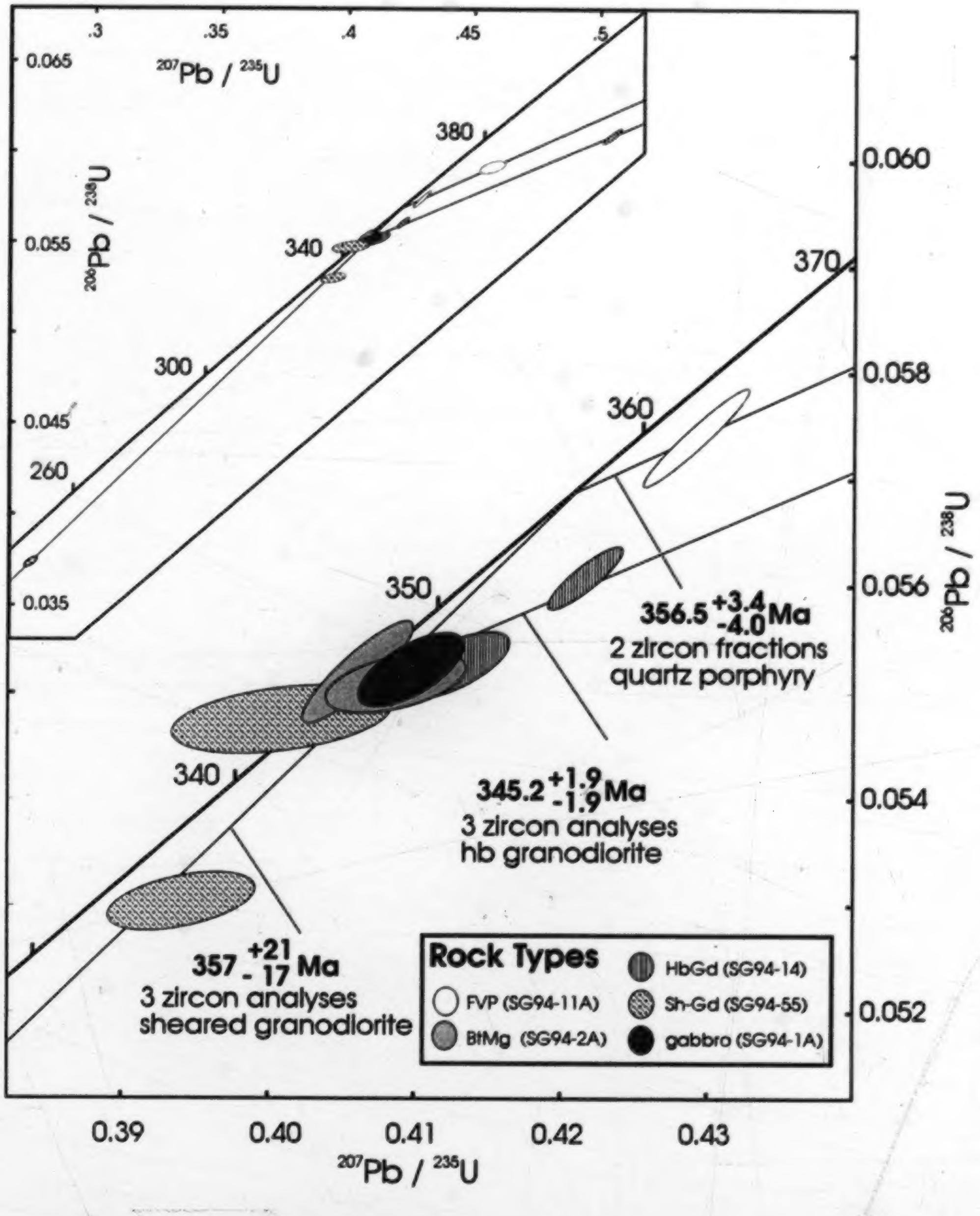

Figure 5.9. U-Pb zircon analyses of SRPS samples. Error ellipses are shown at 2σ. The insert diagram (top left) contains a portion of the concordia from 240 Ma to 400 Ma, showing all zircon analyses. The main portion of the diagram shows an enlargement of the concordia from about 330 to 370 Ma. The chords joining discordant data arrays from three SRPS rocks are shown in the main diagram; two of these, SG94-11A and SG94-14, have upper intercepts of 1682 +486/-361 Ma and 1809 +90/-82 Ma, respectively. These upper intercepts are interpreted to reflect Proterozoic zircon inheritance. SG94-55 has a lower intercept of 22.6 +39.8/-45.6, reflecting late-stage Pb-loss. Notice the clustering of analyses from different SRPS samples, including the gabbro, at around 345 Ma.

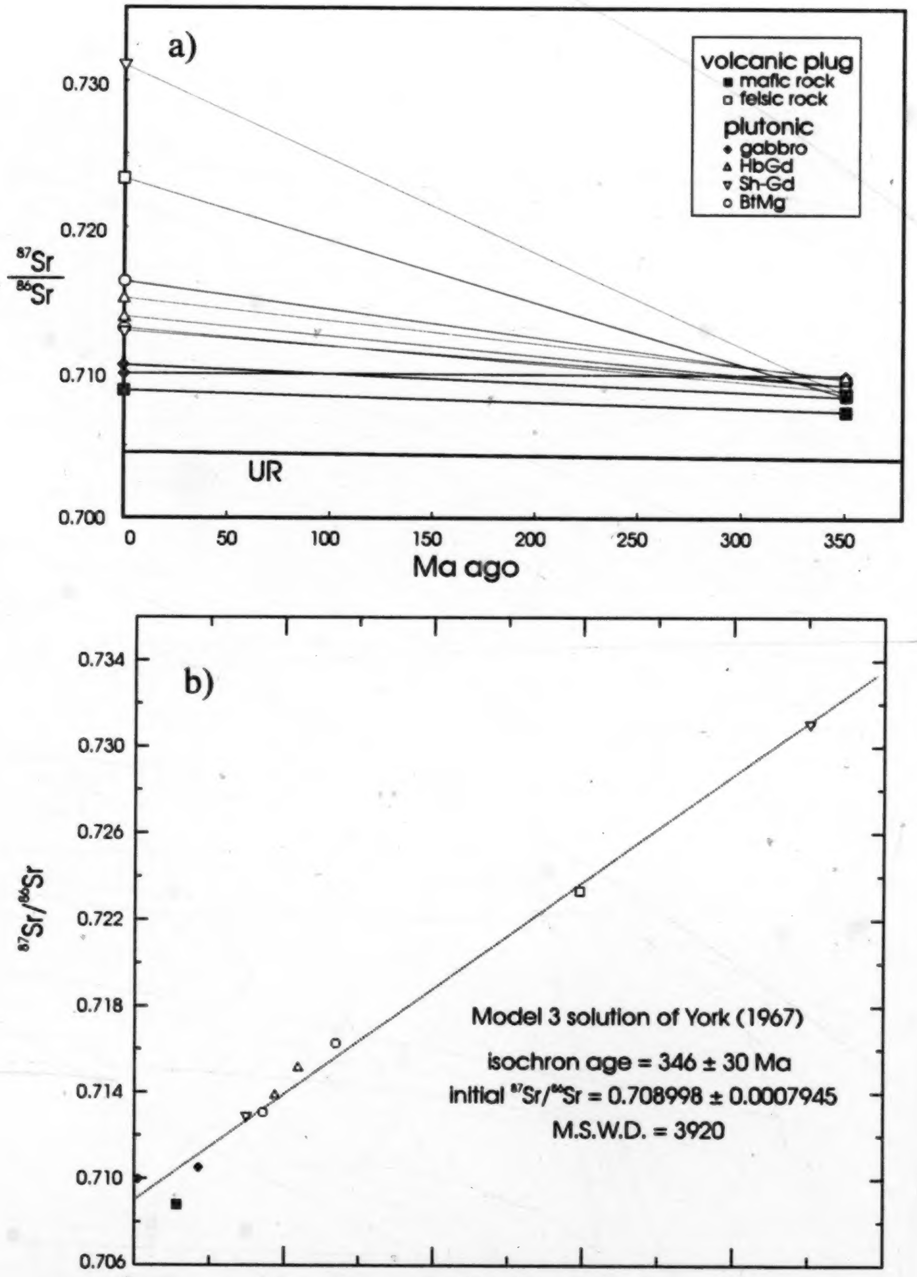

Figure 5.10. Growth curves for the SRPS rocks (a) show that at 350 Ma (age of crystallization of the SRPS rocks), the $^{87}$Sr/$^{86}$Sr ratios of the SRPS rocks cluster between 0.7074 and 0.7097. Due to low Rb/Sr ratios, the $^{87}$Sr/$^{86}$Sr of the mafic SRPS have grown very little, compared to the felsic SRPS. The initial $^{87}$Sr/$^{86}$Sr as calculated from a poorly constrained isochron (b) is similar to those calculated individually. The calculated isochron age of 346 ± 30 Ma is similar to the age derived by individual U-Pb zircon analyses, but is poorly constrained (MSDW = 3920). Error ranges for the analyses are smaller than the symbols plotted. UR = uniform reservoir.

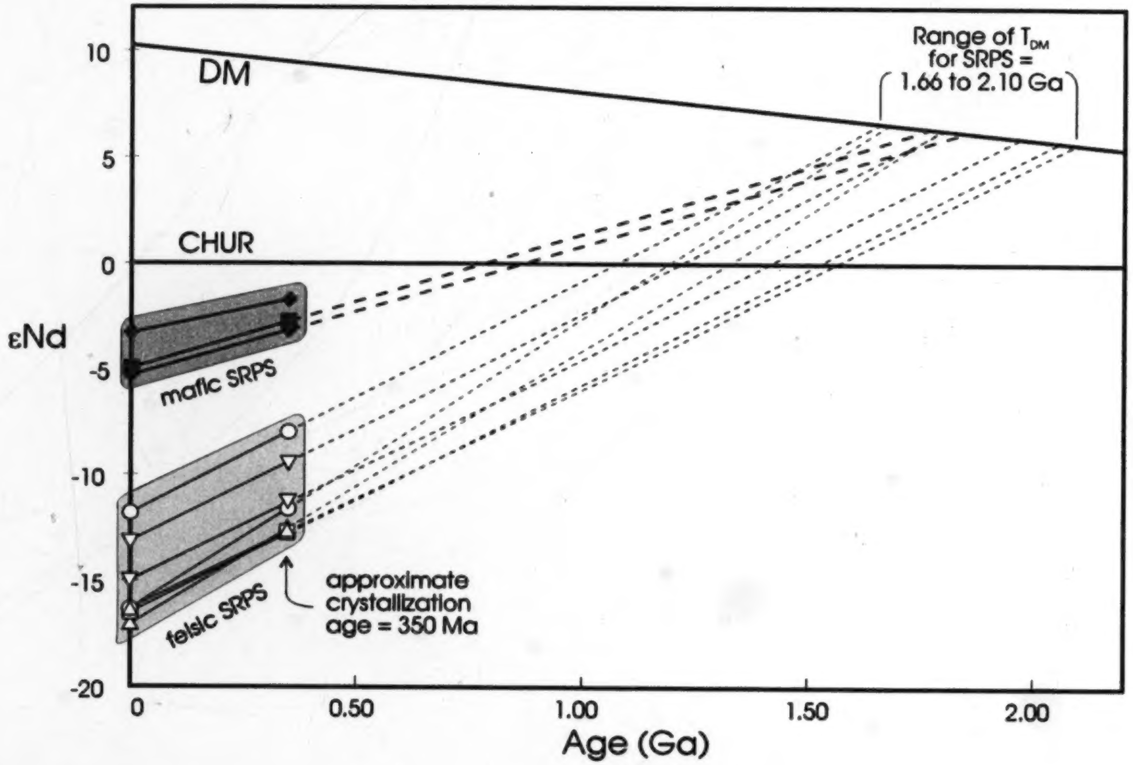

Figure 5.11. εNd vs. time. Symbols represent the εNd values at present day and for the time of crystallization at 350 Ma (determined from U-Pb zircon ages). The range of depleted mantle model ages ($T_{DM}$) is labeled above the position where the sample growth curves intersect the depleted mantle growth curve (DM) as defined by Goldstein et al. (1984). Model ages were not calculated for samples which had $^{147}Sm/^{144}Nd > 0.16$. The mafic SRPS have higher εNd values than those of the felsic SRPS. CHUR = chondritic uniform reservoir.

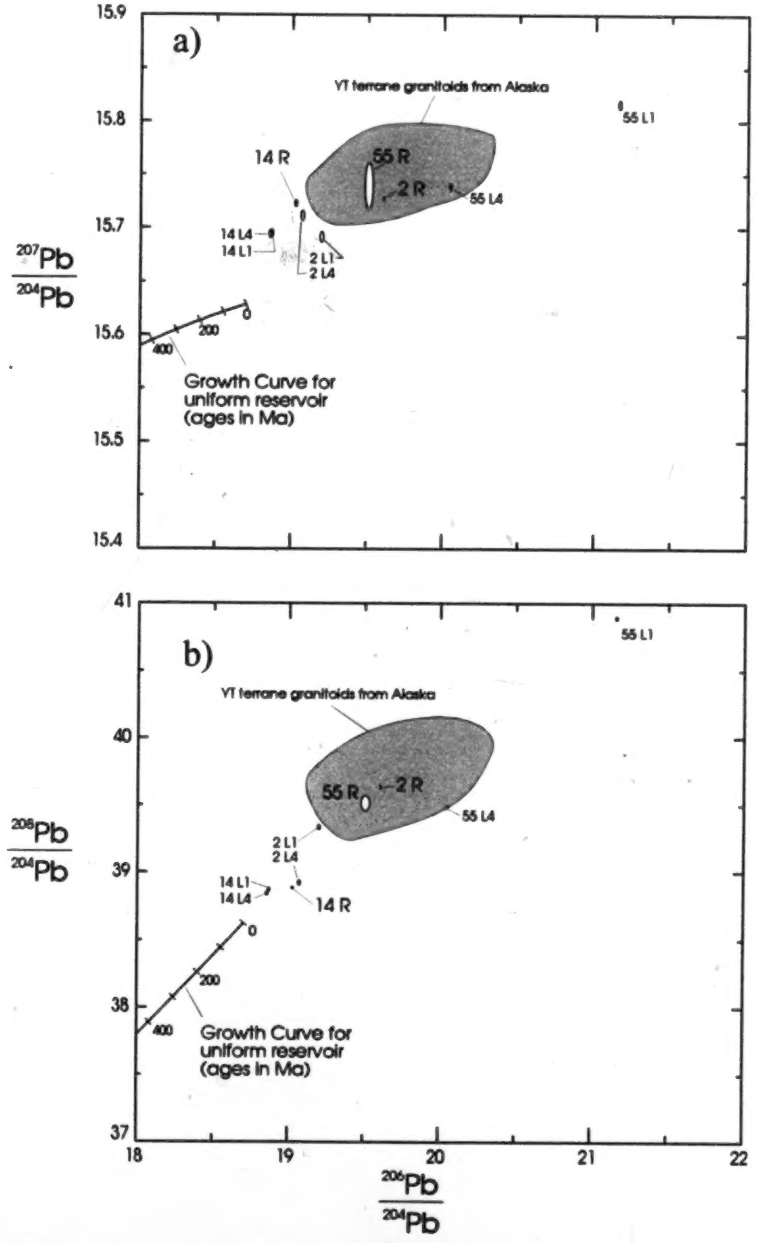

Figure 5.12. $^{207}\mathrm{Pb}/^{204}\mathrm{Pb}$ vs. $^{206}\mathrm{Pb}/^{204}\mathrm{Pb}$ (a) and $^{208}\mathrm{Pb}/^{204}\mathrm{Pb}$ vs. $^{206}\mathrm{Pb}/^{204}\mathrm{Pb}$ (b) plots. The feldspar residues (denoted 'R', larger script) as well as leaches ( denoted 'L1' or 'L4'; smaller script) are plotted. Data points are shown as error ellipses $(2\sigma)$. Plotted on both diagrams are the fields of Pb-Pb compositions from Alaskan YT terrane granitoids (Aleinikoff et al. 1987) for comparison. These fields include peraluminous orthogneisses as well as rocks correlated to the SRPS (Macomb and Lake George subterranes). Feldspar residues from SG94-2 and SG95-55, which should represent the Pb incorporated into the feldspar at the time of crystallization, plot within the field for the Alaskan granitoids. SG94-14 is somewhat less radiogenic, but still has higher Pb ratios than the uniform reservoir, shown here by the growth curve of Stacey and Kramers (1975).

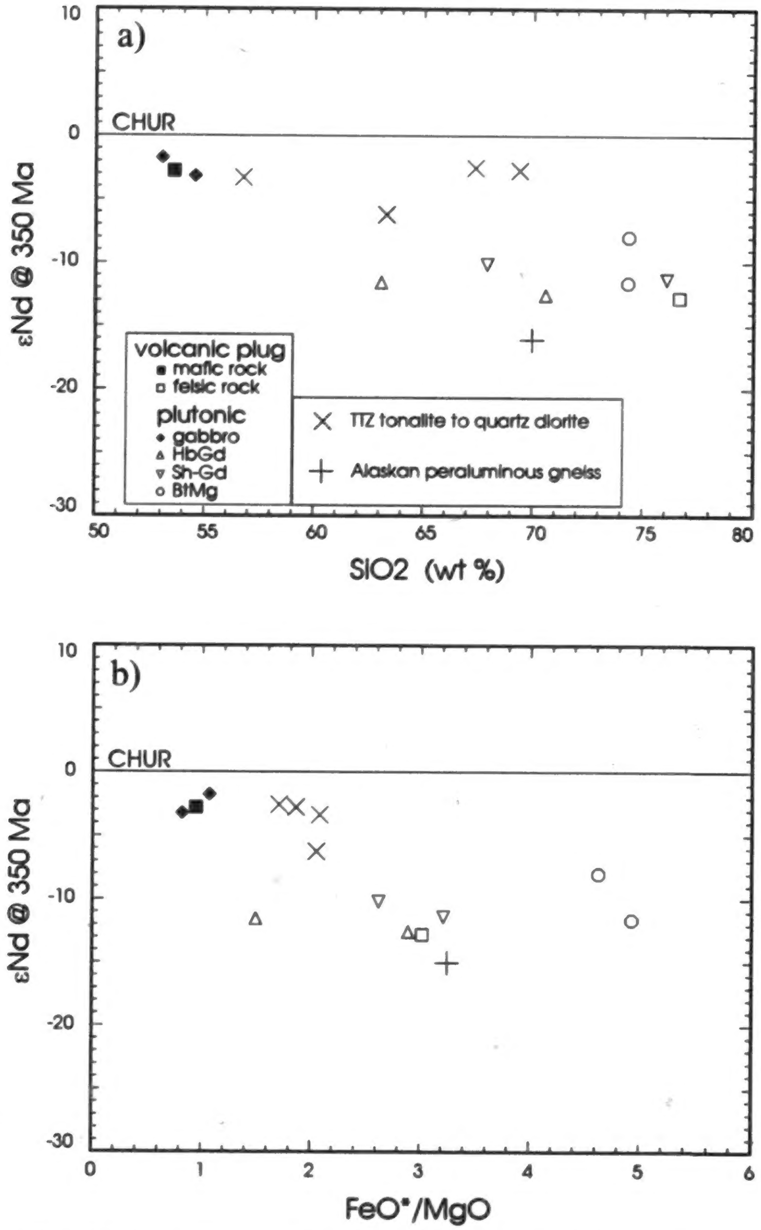

Figure 5.13. εNd vs. SiO$_2$ (a) and FeO*/MgO (b) for the Money klippe SRPS samples, TTZ samples (data from Stevens et al. 1996), and one peraluminous orthogneisses sample (data from Aleinikoff et al. 1981, and Dusel-Bacon and Aleinikoff (1985); symbol key is shown in plot (a). Notice that the peraluminous sample (AG5) plotted has one of the lower values of SiO$_2$ reported for the peraluminous orthogneisses by Dusel-Bacon and Aleinikoff (1985). Generally, felsic upper crustal rocks have higher SiO$_2$ and FeO*/Mg than primitive mafic rock. These plots broadly show that as SiO$_2$ and FeO*/MgO of the Devonian Mississippian igneous rocks increase, εNd values become more negative, indicating a longer crustal residence time. More data would help to show this trend, but most available studies of Devonian- Mississippian igneous rocks do not present both geochemistry and isotope data for the same sample suite. CHUR = chondritic uniform reservoir.

# CHAPTER 6. DISCUSSION AND CONCLUSIONS

### *Relations from the Money klippe field area*

Nisutlin assemblage rock located around the perimeter of the Money klippe was subdivided into three distinct rock types based on field and petrographic evidence: the mica-quartz-schist (MQS), the quartz-rich phyllite (QP), and the mafic schist (MS). The QP unit, composed predominantly of quartz and sometimes containing carbonaceous material, is interpreted to be metasedimentary in origin. The MS unit, which contains mafic minerals such as hornblende and chlorite, may represent metamorphosed basalt, or first-cycle sediment derived from basalt. Together, the QP and MS units are interpreted to correlate to the metasedimentary and metavolcanic components (respectively) of the Middle Unit of the Layered Metamorphic Sequence described by Mortensen and Jilson (1985). The MQS unit, if originally a sedimentary rock, represents less mature arkosic sandstone. The MQS unit may represent the Lower Unit of Mortensen and Jilson (1985), although this correlation is tentative. The only contact between the MQS and the combined QP + MS (Middle Unit) in the field area was a large normal fault. The QP unit appears to be cut by a dyke of SRPS granodiorite (Sh-Gd), although the contacts have been sheared. This field relationship, though ambiguous, supports the finding by Stevens et al. (1996) that SRPS magmatism intrudes the Nisutlin assemblage at ~350 Ma.

SRPS units within the Money Klippe are broadly contemporaneous. Despite the mapping of thrust faults between the SRPS units by Tempelman-Kluit (1977a) and Erdmer (1981, 1985), intrusive relationships between them show that they probably did not move far relative to one another. Significantly, a gabbro is intruded by a thin dyke of SRPS monzogranite. This relationship, along with a U-Pb zircon analysis of the gabbro that establishes that it was formed at approximately 350 Ma along with the rest of the SRPS, and similar geochemical trends, supports the correlation of this unit to the SRPS. This gabbro unit was previously grouped with the Anvil assemblage (Tempelman-Kluit 1977a, 1979; Erdmer 1981, 1985)

Kinematic analyses of the Nisutlin assemblage failed to give reliable shear-sense results. Nisutlin assemblage rocks to the north of the Money klippe ('north group') contained consistently north-south oriented lineations, and shear-sense indicators predominantly record top-to-the-south shear-sense. A second area ('west and south groups') had more variable lineation and shear-sense indicators loosely recorded top-to the west movement. However, only one type of shear-sense indicator, asymmetrical extensional shear bands (AESB), could be employed over the vast majority of the field area. Reliance on a single type of shear-sense indicator casts doubt over the validity of the recorded shear-sense. Finally, the lack of boundary conditions on the presumed shear zone, the contrasting lineation orientations within the field area and the variability of lineation directions throughout the Nisutlin assemblage in southeastern Yukon (Mortensen 1983), precludes the establishment of useful shear-sense direction. The variability of lineation directions may be the result of thrust faults within the Nisutlin assemblage throughout the southeastern Yukon that rotated panels of Nisutlin rock, off-setting lineation. Alternatively, the domains of differing lineation and shear-sense may indicate that small-scale local effects governed the development of kinematic structures in an area during ductile D1 deformation, so application of observed shear-sense from a small area to a large deformed terrane in order to obtain an overall transport direction may not be valid.

### *Nisutlin and Anvil assemblage provenance*

The geochemistry and Nd isotope systematics of the Nisutlin assemblage MS and QP samples from the Money klippe area are compatible with a model proposed by Creaser et al. (1997a), which suggests that the Nisutlin assemblage has sediment contribution from the Alberta basement-influenced miogeocline and from a juvenile mafic arc source. In the TTZ, samples fall on a trend from the felsic, crustally derived samples to relatively juvenile mafic-intermediate rock, which implies that the Nisutlin samples are derived from either of these two sources, or represent a mixture of the two. The QP ($\varepsilon Nd_{350}$ = -9.85 to -16.61; Th/Sc ≈ 0.6 to 2.0) and MS samples ($\varepsilon Nd_{350}$ = +4.87 to

-0.94; Th/Sc ≈ 0.11 to 0.003) are compatible with this model (Fig. 4.8), but MQS samples ($\varepsilon Nd_{350}$ = -4.66 to -15.06; Th/Sc ≈ 1 to 7) from the Money klippe area have a much higher degree of enrichment of incompatible elements relative to compatible elements than any other unit from the TTZ or Money klippe area. The MQS are thus not compatible with the two-endmember mixing model suggested by Creaser et al. (1997a) but may be mainly derived from felsic volcanism from an active continental margin (Zr/Th = 5 to 16). If this is the case, then εNd and Nd model ages ($T_{DM}$ = 1.23 to 1.98 Ga) suggests that older crust was involved in this volcanism.

Two of the Anvil assemblage samples from the field area appear to be the product of calc-alkalic magmatism (Ce, $P_2O_5$, and Sm enrichments); the third sample has geochemical characteristics of serpentinized ultramafic rock. These results are not as consistent as those of three Anvil rocks from the TTZ, which all have calc-alkalic signatures (Creaser et al. 1997a), but do help to show that correlating all mafic bodies within the YT terrane to the Slide Mountain terrane (Wheeler et al. 1991, Mortensen et al. 1992b) may be premature. However, Plint and Gordon (1997) found that a large mafic body associated with the YT terrane - North American boundary in the Campbell Range has characteristics of MORB, and thus may correlate to the Slide Mountain terrane. Mortensen (1992b) suggests that the generally larger mafic bodies near the boundary fault between the YT terrane and North America may be similar to the Slide Mountain terrane, but that the smaller bodies further to the southeast may have different origins. This hypothesis gains some support from the preliminary data outlined above, but much more work is needed to fully categorize and classify the many mafic bodies within the YT terrane.

The MS subunit of the Nisutlin assemblage described in the present study shares similarities with the Anvil assemblage. The MS unit in the field area is dark green and contains abundant chlorite and amphibole, and is closely associated with graphitic phyllite. The MS unit in the field area has been tentatively correlated to the Middle Unit of Mortensen and Jilson (1985) (see Section 2.4), but bears several similarities to the three analyzed Anvil assemblage rocks from the field area with respect to REE patterns, trace elements characteristics (Th/Sc < 0.5, Zr/Th > 35), and Nd isotopes ($\varepsilon Nd_{350}$ = -0.94 to +4.87). This lends weight to the suggestion by Stevens et al. (1996) that the Anvil assemblage, which interfingers with the Nisutlin assemblage in the TTZ, may correlate to the Middle Unit of Mortensen (1992b). Notice that the MS unit also shares trace element and Nd isotopic similarities with the juvenile end-members from the TTZ and Coast belts (Creaser et al. 1997a, Samson et al. 1991). It is important to realize, however, that in these two latter studies, the lithology has no systematic relationship with the Nd isotopic systematics, and some of the isotopically juvenile rocks may resemble in hand-sample rocks with highly negative εNd. This suggests that the isotopically juvenile rocks in the TTZ and the Coast belt are compatible with sedimentary derivation from Anvil rocks (Creaser et al. 1997a), but do not directly represent Anvil rocks. With the MS unit, however, it is not as easy to exclude the possibility that they directly represent metamorphosed and deformed basaltic rock, like the Anvil, instead of detritus shed from them, because they contain abundant mafic minerals. If they are metasediments, then they have undergone little weathering from their source.

Overall, the Nisutlin assemblage must have developed within the sedimentary influence of both ancient cratonic material and juvenile mafic to intermediate arc material prior to Mississippian time. The Anvil assemblage, representing a calc-alkalic continental arc, is a possible source of the juvenile detritus (Creaser et al. 1997a) and may be depositionally interfingered with the Nisutlin assemblage (Stevens et al. 1996), implying the arc was proximal to the basin in which Nisutlin assemblage sediments were depositing. It is not known how the continental arc that produced the Anvil assemblage relates to the widespread Devonian-Mississippian continental arc magmatism that intrudes the Nisutlin assemblage, but generally would have had to have been earlier if the Anvil assemblage is depositionally linked to the Nisutlin assemblage.

### ***Devonian-Mississippian magmatism***

Widespread Devonian-Mississippian magmatism in the YT terrane is very diverse, ranging from gabbroic rock to highly fractionated felsic volcanic rock and peraluminous granitoids. Peraluminous gneisses throughout much of the YT terrane have

2.0 to 2.3 Ga $T_{DM}$ model ages, strong inherited zircon components, and high initial Sr ratios ($^{87}Sr/^{86}Sr$ = 0.716 to 0.738 suggesting that ancient continental crust is a major constituent of these rocks (Aleinikoff et al. 1981, 1986, 1987, Mortensen 1983, 1992b, Bennett and Hansen 1988, and Hansen et al. 1989). The SRPS and correlated rocks are more diverse than the peraluminous orthogneisses in terms of rock type, because they range from mafic gabbro and andesitic basalt (50 to 55% $SiO_2$) to monzogranite and rhyolite (70 to 78 % $SiO_2$). The SRPS rocks have less crustal input than the peraluminous suite, as emphasized by Mortensen (1992b), but Proterozoic zircon inheritance and Nd model ages ($T_{DM}$ = 1.66 to 2.10 Ga) show that these rocks contain some crustal contribution. Even the gabbroic rocks have negative initial εNd ($\varepsilon Nd_{350}$ = -1.7 to -3.2), which suggests that they too interacted with the crust into which they were intruded. There is a broad pattern of increasing crustal contribution with increasing degree of felsic fractionation (Section 5.5), so that the mafic SRPS record predominantly mantle derivation with a small crustal component, whereas the peraluminous orthogneisses are dominated by the crustal component. It is possible that the peraluminous orthogneisses are derived completely from anatexis of upper continental crust (Hansen et al. 1989). The majority of peraluminous orthogneisses and SRPS record calc-alkalic magmatism produced in a continental arc. Two of the gabbro samples analyzed in this study, however, may represent more primitive oceanic island arc magmatism (lower Th/Yb, flatter REE).

Devonian-Mississippian arc magmatism may have intruded continental crust of variable thickness. The widespread peraluminous orthogneiss has high initial Sr ratios, strong inheritance of Proterozoic zircon and Proterozoic Nd model ages, which suggests it developed in a region of substantial continental crust. The contemporaneous Devonian-Mississippian SRPS (and correlated rocks) also interacted with continental crust (Proterozoic zircon inheritance moderately negative initial εNd), but generally to a lesser degree than the peraluminous orthogneiss. Some of the mafic SRPS have more primitive geochemical trends. Thus, the SRPS may have intruded continental crust that ranged in thickness from intermediate to very thin.

### *Tectonic setting*

There is abundant evidence that the ancient continental crust influenced the YT terrane. The supracrustal sequence represented by the Nisutlin assemblage of the YT terrane shares similarities with the miogeocline with respect to stratigraphic sequences (Mortensen and Jilson 1985) and geochemical and isotopic characteristics (Creaser et al. 1997a, Samson et al. 1991, this study). As well, the most abundant Devonian-Mississippian igneous rocks in the YT terrane, the peraluminous orthogneisses, have a strong continental affinity. These relations, along with the position of the YT terrane directly adjacent to autochthonous North America, have led to the suggestion that the YT terrane represents a displaced, deformed and metamorphosed portion of the North American miogeocline (Nokleberg et al. 1994). However, it is important to note that the YT terrane is not directly equivalent to the miogeocline. The miogeocline is not strongly deformed or metamorphosed, and lacks Devonian-Mississippian magmatism (Mortensen and Jilson 1985). Also, juvenile mafic material makes up a large part of the Nisutlin assemblage supracrustal sequence, unlike the miogeocline. The Nisutlin assemblage contains schist with juvenile isotopic systematics in close association with lithologically indistinguishable schist with strong crustal component (Creaser et al. 1997a, Samson et al. 1991). The miogeocline, for which a much greater Nd isotope database exists (Frost and O'Nions 1984, Frost and Winston 1987, Burwash et al. 1988, Ghosh and Lambert 1989, Boghossian et al. 1996), lacks such abundant juvenile material (Fig. 4.9). Also, some igneous rocks of the SRPS show only a small crustal influence, and two of the mafic SRPS samples are compatible with derivation from an oceanic arc.

In order to accommodate both the obvious strong continental nature of many of the YT terrane rocks as well as the abundance of juvenile material, the YT terrane has been envisioned as a distal portion of the North American miogeocline (Mortensen and Jilson 1985, Mortensen 1983, Coney 1989, Rubin et al. 1991, Creaser et al. 1997a). In the model of Creaser et al. (1997a) the distal position of the YT terrane relative to North America during pre-Mississippian Paleozoic time places it within the influence of continentally derived sedimentation from the east, but also under the influence of material shed from a juvenile arc to the west. The model of Stevens et al. (1996) suggests that much of the Nisutlin assemblage supracrustal package was a passive margin sequence developed on the eastern edge of a continental fragment separated from North America by the Slide Mountain ocean during Mississippian time. The continental fragment, consisting of the Lower Unit - peraluminous orthogneiss assemblage (Hansen 1990, Mortensen 1992b), may have been an oceanic plateau or bank, or a previously rifted portion of the North American continent. The model of Stevens et al. (1996) model also bears some resemblance to the model proposed by Nelson and Mihalynuk (1993), which features an arc located offshore of North America, in part built on continental crust (YT and Nisling) and in part on oceanic crust (Stikinia and Quesnellia) described in greater detail in Section 2.1. After collision of the central YT/Nisling portion of the arc with a north-moving oceanic plateau embedded within the subducting Cache Creek ocean, the oceanic limbs of the arc rotated around and enclosed a portion of the Cache Creek ocean (Nelson and Mihalynuk 1993). The whole assemblage then collided with the edge of North America by Middle Jurassic (Nelson and Mihalynuk 1993).

The data available, including new results reported here, are compatible with the YT terrane evolving as a distal portion of the western North American continent with periodic igneous input from a fringing arc complex, which culminated with widespread Devonian-Mississippian magmatism. Prior to the main phase of Devonian-Mississippian arc activity, sediment from cratonal North America was shed westward to distal portions of the miogeocline, where it was mixed to varying degrees with detritus from a relatively juvenile mafic - intermediate arc (Creaser et al. 1997a), forming the Nisutlin assemblage. This arc, perhaps represented by the Anvil assemblage, was at least in part built on continental crust. Highly fractionated felsic rock, derived from a continental arc, contributed to the Nisutlin assemblage as well, represented by the MQS unit of the Nisutlin assemblage. However, this may be a localized or short lived event, because evidence exists in the Money klippe area, but not in the TTZ. Also, if the MQS does correlate to the Lower Unit of Mortensen (1992b), it would have been earlier than the rest of the Nisutlin rocks, and thus not sampled in the TTZ. In Devonian-Mississippian time, a large continental arc developed at the edge of the continental crust, producing widespread magmatism that intruded the Nisutlin and Anvil assemblages. The thickness of continental margin must have been variable, based on the contrasting degree of crustal contribution evident in the Devonian-Mississippian granitoids. The peraluminous orthogneiss has strong continental affinity, suggesting it was built on crust of substantial thickness, whereas SRPS and related igneous bodies show that they received less crustal input, suggesting they intruded thinner crust. This scenario fits with the growing evidence for a fringing late Paleozoic arc that lay on the western margin of North America, sometimes referred to as the McCloud Belt (Miller 1987, Rubin et al. 1991, Mortensen 1992b). An oceanic basin with Devonian to Permian fossil and isotopic ages (Coney 1989, Mortensen 1992b), represented by the SM terrane near the YT terrane - North America boundary (but probably not the Anvil assemblage of the Money klippe or TTZ), may have opened up between the arc and the miogeocline, but would have been consumed during Permian to Triassic subduction before the arc recollided with the craton during Late Triassic to Early Jurassic times (Mortensen 1992b, Stevens et al. 1996). The strong deformation features seen in the Nisutlin assemblage may be the result of the collision of the arc with North America (Stevens et al. 1996).

## CONCLUSIONS

1) The gabbro and composite plug units found within the YT terrane are considered to be part of the SRPS, based on field evidence, geochemical trends and U-Pb zircon dating, which shows that all SRPS rocks were formed between 345 to 360 Ma, including the gabbro unit. Although Mortensen (1983, 1992a) previously dated several of these units previously, zircon inheritance was documented only for the quartz-feldspar porphyry in the Money klippe, which Mortensen (1992a) assigned to the Slide Mountain terrane. The present study also reports zircon inheritance in a granodioritic phase of the SRPS from Money klippe.

2) Structural and kinematic studies of the deformational fabrics contained within the Nisutlin and Anvil assemblages proved inconclusive. Despite the fact that shear-sense was determined with some degree of consistency within two domains (subhorizontal 'north group' schists record dominantly top-to-the-south shear; 'south and west group' schists record a poorly defined top-to-the- west shear), the value of the shear-sense indicators is called into question because of poor boundary constraints, and contrasting lineation orientations. Thus, the shear-senses observed in the Nisutlin assemblage near the Money klippe may be the result of local effects, and have no systematic relation to the overall tectonic transport direction.

3) The Nisutlin assemblage in the Money klippe areas includes both juvenile mafic rock, represented by the MS unit ($\varepsilon Nd_{350}$ = +4.87 to -0.94), and rock with more evolved crustal signatures, represented by the MQS unit ($\varepsilon Nd_{350}$ = -1.65 to -11.38; $T_{DM}$ = 1.23 to 1.98 Ga) and the QP unit ($\varepsilon Nd_{350}$ = -9.85 to -16.61; $T_{DM}$ = 1.66 to 2.36 Ga). The QP and MS units are compatible with two-endmember mixing between material shed from a relatively juvenile mafic-intermediate source and evolved upper crust as proposed by Creaser et al. (1997) for Nisutlin assemblage rocks in the TTZ. The MQS samples, however, with lower Zr/Th, Eu/Eu* and higher Th/Sc ratios than other Nisutlin assemblage rocks, are not compatible with two-endmember mixing, but may instead be the result of felsic volcanism in a continental margin.

4) All Anvil assemblage rocks from the TTZ and 2 out of 3 from the Money klippe area have trace element characteristics of calc-alkalic basalt (enriched Ce, $P_2O_5$, and Sm). Three Anvil rocks from the TTZ (Creaser et al. 1997a) and one from the Money klippe area (SG94-75A) are compatible with derivation from a continental arc (Th/Yb = 0.6 to 1.2), a second Anvil sample from the Money klippe area (SG94-52) may represent calc-alkalic basalt from an oceanic arc (Th/Yb = 0.2). The presence of calc-alkalic trends in some of the Anvil samples makes it difficult to correlate these Anvil samples to the MORB-dominated Slide Mountain terrane. Mafic rock from the boundary zone between

the YT terrane and North America in the Campbell range do have MORB characteristics and could correlate to the Slide Mountain terrane (Plint and Gordon 1997). This may indicate that the Slide Mountain terrane is present near the YT terrane - North America contact, but not throughout the YT terrane. A third Anvil sample from the Money klippe area resembles serpentinite. The significance of this single ultramafic sample is not known. It could suggest that the Anvil assemblage is composite, containing both CAB arc material as well as slivers of ultramafic oceanic crust material, or the serpentinite may be an ultramafic xenolith.

5) The MS unit of the Nisutlin assemblage is similar to the Anvil assemblage not only in terms of geochemistry and isotopes, but also with respect to lithology. These may be equivalent to the Anvil assemblage. This would lend weight to the suggestion made by Stevens et al. (1996) that the Anvil assemblage may correlate to the volcanic component of the Middle Unit of Mortensen and Jilson (1985).

6) Simpson Range plutonic suite (SRPS) rocks from the Money klippe were produced in a calc-alkalic, continental arc. Trace element diagrams using Nb, Ta, Rb, Y, and Tb show that the SRPS felsic rocks are volcanic arc granites. The majority of mafic SRPS rocks show that they were produced in a continental arc (Th/Yb = 0.6 to 1.3; Zr/Y = 3.4 to 3.8), although two of the mafic SRPS probably were derived in an oceanic arc (Th/Yb = 0.1 to 0.2; Zr/Y = 2.8 to 2.9). Although the moderately high Sr ratios ($^{87}Sr/^{86}Sr$ = 0.7074 to 0.7099), which suggest the influence of old sialic crust, are similar for all the SRPS rocks, initial εNd are considerably lower for the felsic SRPS ($\varepsilon Nd_{350}$ = -9.4 to -12.8) than for the mafic SRPS ($\varepsilon Nd_{350}$ = -1.7 to -3.2). This suggests that old, felsic upper crust contributed more to the petrogenesis of the felsic SRPS than the mafic SRPS. However, the negative initial εNd for the mafic SRPS shows that they must have been influenced by continental crust to some degree.

7) Devonian-Mississippian magmatism in the YT terrane was diverse. Peraluminous orthogneisses, which are the most abundant igneous rocks in the YT terrane, have high initial Sr ratios ($^{87}Sr/^{86}Sr = 0.716$ to 0.738), low initial εNd (εNd = -14 to -16) and strong Proterozoic inheritance in zircons (Aleinikoff et al. 1981, 1986, 1987, Mortensen 1983, 1992b, Bennett and Hansen 1988, and Hansen et al. 1989), which suggests that the crustal component to these granitoids is dominant. The SRPS and correlated rocks, as shown by results in this study and in those of Mortensen (1983, 1992b) and Stevens et al. (1996), have more variable but generally less crustal contribution than the peraluminous orthogneiss suite.

8) The available data suggest that the YT terrane developed as a distal portion of the miogeocline in the Paleozoic, with a fringing arc producing abundant magmatic rocks in Devonian-Mississippian time. The Nisutlin assemblage developed within the influence of sediment derived from the Archean-influenced miogeocline of North America, but also received juvenile mafic-intermediate arc material as well, which may be represented by the Anvil assemblage. Widespread Devonian-Mississippian magmatism was produced in a fringing arc proximal to North America at this time. The basement to this arc must contain ancient continental material in order to account for the U-Pb, Sr, and Nd isotope evidence for the contribution of older sialic crust to the granitoids. The thickness of this crust was varied, causing the degree of crustal contamination to be greatest where thickest, and be the least where thinnest. This model fits in with a growing body of evidence for a late Paleozoic fringing arc developing along much of the length of the western North American margin.

# LITERATURE CITED

Aleinikoff, J.N., Dusel-Bacon, C., Foster, H.L., and Futa, K. 1981. Proterozoic zircon from augen gneiss, Yukon-Tanana Upland, east-central Alaska. *Geology*, **9**: 469-473.

Aleinikoff, J.N., Dusel-Bacon, C., and Foster, H.L. 1986. Geochronology of augen gneiss and related rocks, Yukon-Tanana terrane, east-central Alaska. *Geological Society of America Bulletin*, **97**: 626-637.

Aleinikoff, J.N., Dusel-Bacon, C., Foster, H.L., Nokleberg, W.J. 1987. Lead isotopic fingerprinting of tectono-stratigraphic terranes, east-central Alaska. *Canadian Journal of Earth Sciences*, **24**: 2089-2098.

Aleinikoff, J.N. and Nokleberg, W.J. 1985. Age of Devonian igneous-arc terranes in the northern Mt. Hayes quadrangle, eastern Alaska Range. *U.S. Geological Survey Circular*, **967**: 44-49.

Behrmann, J.H. 1987. A precautionary note on shear bands as kinematic indicators. *Journal of Structural Geology*, **9**: 659-666.

Bennett, V.C. and Hansen, V.L. 1988. Neodymium isotope similarities between the Yukon-Tanana terrane, Yukon territory and Continental North America. *Geological Society of America Abstracts with Programs*, **20**: A111.

Berthé, P., Choukoune, P., and Gapais, D. 1979a. Orientations préférentielles du quartz et orthogneissification progressive en régime cisaillant: l'example du cisaillement sud-amoricain. *Bulletin de Minérologie*, **102**: 265-272.

Berthé, P., Choukoune, P., and Jegouzo, P. 1979b, Orthogneiss, mylonite, and non-coaxial deformation of granites: the example of the South Armoricain shear zone. *Journal of Structural Geology*, **1**: 31-42.

Bevier, M.L. and Anderson, R.G. 1991. Jurassic geochronometry in NW Stikinia (56-57°N), British Columbia. *Geological Society of America Abstracts with Programs*, **23**: A191.

Bhatia, M.R. 1983. Plate tectonics and geochemical compositions of sandstones. *The Journal of Geology*, **91**: 611-627.

Bhatia, M.R. 1985. Rare earth element geochemistry of Australian Paleozoic graywackes and mudrocks: provenance and tectonic control. *Sedimentary Geology*, **45**: 97-113.

Bhatia, M.R. and Crook, K.A.W. 1986. Trace element characteristics of graywackes and tectonic setting discrimination of sedimentary basins. *Contributions to Mineralogy and Petrology*, **92**: 181-193.

Boghossian, N.D., Patchett, P.J., Ross, G.M., and Gehrels, G.E. 1996. Nd isotopes and the source of sediments in the miogeocline of the Canadian Cordillera. *Journal of Geology*, **104**: 259-277.

Burwash, R.A., Cavell, P.A., and Burwash, E.J. 1988. Source terranes for sedimentary Proterozoic sedimentary rocks in southern British Columbia: Nd isotopic and petrographic evidence. *Canadian Journal of Earth Sciences*. **25**: 824-832.

Chappell, B.W. and White, A.J.R. 1974. Two contrasting granite types. *Pacific Geology*, **8**: 173-174.

Clarke, D. 1993. *Newpet*. Memorial University of Newfoundland, Department of Earth Sciences

Coney, P.J. 1989. Structural aspects of suspect terranes and accretionary tectonics in western North America. *Journal of Structural Geology*, **11**: 107-125.

Coney, P.J., Jones, D.L., and Monger, W.H. 1980. Cordilleran suspect terranes. *Nature*, **288**: 329-333.

Creaser, R.A., Erdmer, P.E., Stevens, R.A., and Grant, S.G. 1997a. Tectonic affinity of Nisutlin and Anvil assemblage strata from the Teslin tectonic zone, northern Canadian Cordillera: constraints from neodymium isotope and geochemical evidence. *Tectonics*, **16**: 107-121.

Creaser, R.A., Heaman, L.H., and Erdmer, P.E. 1997b. Timing of high pressure metamorphism in the Yukon-Tanana terrane, Canadian Cordillera: constraints from U-Pb zircon dating of eclogite from the Teslin tectonic zone. *Canadian Journal of Earth Sciences*, **34**: 709-715.

DePaolo. D.J. 1981. Neodymium isotopes in the Colorado Front Ranges and crust-mantle evolution in the Proterozoic. *Nature*, **291**: 193-196.

DePaolo. D.J., and Wasserburg, G.J. 1976. Nd isotopic variations and petrogenetic models. *Geophysical Research Letters*, **3**: 249-252.

Dusel-Bacon, C. and Aleinikoff, J.N. 1985. Petrology and tectonic significance of augen gneiss from a belt of Mississippian granitoids in the Yukon-Tanana terrane, east-central Alaska. *Geological Society of America Bulletin*, **96**: 411-425.

Erdmer, P.E. 1981. Comparative studies of cataclastic allochthonous rocks in the White Mountains, Last Peak, and Fire Lake areas. in: *Yukon Geology and Exploration 1979-1980, Department of Indian and Northern Affairs, Whitehorse, Y.T.*, 60-64.

Erdmer, P.E. 1985. An examination of the cataclastic fabrics and structures of parts of the Nisutlin, Anvil and Simpson allochthons, central Yukon: test of the arc-continent collision model. *Journal of Structural Geology*, **7**: 57-72.

Erdmer, P.E. 1987. Blueschist and eclogite in mylonitic allochthons, Ross River and Watson Lake areas, southeastern Yukon. *Canadian Journal of Earth Sciences*, **24**: 1439-1449.

Erdmer, P.E. 1992. Eclogitic rocks in the St.Cyr klippe, Yukon, and their tectonic significance. *Canadian Journal of Earth Sciences*, **29**: 1296-1304.

Erdmer, P.E., Helmstaedt, H. 1983. Eclogite from central Yukon: a record of subduction at the western margin of ancient North America. *Canadian Journal of Earth Sciences*, **20**: 1389-1408.

Faure, G. 1986. *Principles of Isotope Geology (Second Edition)*. John Wiley & Sons, New York. pp. 589.

Frost, C.D. and O'Nions, R.K. 1984. Nd evidence for Proterozoic crustal development in the Belt-Purcell Supergroup. *Nature*, **312**: 53-56.

Frost, C.D., and Winston, D. 1986. Nd isotope systematics of coarse- and fine-grained sediments: examples from the middle Proterozoic Belt-Purcell Supergroup. *The Journal of Geology*, **95**: 309-327.

Ghosh, D.K. and Lambert, R. St J. 1989. Nd-Sr isotopic study of Proterozoic to Triassic sediments from southeastern British Columbia. *Earth and Planetary Science Letters*, **94**: 29-44.

Goldstein, S.L., O'Nions, R.K., and Hamilton, P.J. 1984. A Sm-Nd isotopic study of atmospheric dusts and particulates from major river systems, *Earth and Planetary Science Letters*, **70**: 221-236.

Gromet, L.P., Dymek, R.F., Haskin, L.A., and Korotev, R.L. 1984. The "North American shale composite": Its compilation, major and trace element characteristics. *Geochimica et Cosmochimica Acta*, **48**: 2469-2482.

Hanmer, S., and Passchier, C. 1991. Shear-sense indicators: a review. *Geological Survey of Canada, Paper*: **90-17**: pp. 72.

Hansen, V.L. 1988. A model for terrane accretion: Yukon-Tanana and Slide Mountain Terranes, northwest North America. *Tectonics*, **7**: 1167-1177.

Hansen, V.L. 1989. Structural and kinematic evolution of the Teslin suture zone, Yukon: record of an ancient transpressional margin. *Journal of Structural Geology*, **11**: 717-733.

Hansen, V.L. 1990. Yukon-Tanana terrane: a partial acquittal. *Geology*, **18**: 365-369.

Hansen, V.L. 1992. Backflow and margin-parallel shear within an ancient subduction complex. *Geology*, **20**: 71-74.

Hansen, V.L. 1992. P-T evolution of the Teslin suture zone and Cassiar tectonites, Yukon, Canada: evidence for A- and B-type subduction. *Journal of Metamorphic Geology*, **10**: 239-263.

Hansen, V.L., Heizler, M.T., and Harrison, T.M. 1991. Mesozoic Thermal evolution of the Yukon-Tanana composite terrane: new evidence from 40Ar/39Ar data. *Tectonics*, **10**: 51-76.

Hansen, V.L., Mortensen, J.K., and Armstrong, R.L. 1989. U-Pb, Rb-Sr, K-Ar, isotopic constraints for ductile deformation and related metamorphism in the Teslin suture zone, Yukon-Tanana terrane, south-central Yukon. *Canadian Journal of Earth Sciences*, **26**: 2224-2235.

Holmden, C. 1995. Hydrology, salinity, and environment of ancient water masses determined by C, O, Sr and Nd isotopes in carbonates, phosphates, and silicates. Unpublished PhD thesis, University of Alberta, Edmonton, Alberta.

Hooper, P.R., Johnson, D.M., and Conrey, R.M. 1993. Major and trace element analyses of rocks and minerals by automated X-ray spectrometry, open file report, Washington State University, Pullman, Washington.

Irvine, T.N. and Baragar, W.R.A. 1971. A guide to the chemical classification of the common volcanic rocks. *Canadian Journal of Earth Sciences*, **8**: 523-546.

Jackson. J.L., Gehrels, G.E., Patchett, P.J., and Mihalynuk, M.G. 1991. Stratigraphic and isotopic link between the northern Stikine terrane and an ancient continental margin assemblage, Canadian Cordillera. *Geology*, **19**: 1177-1180.

Jenner, G.A., Longrich, H.P., Jackson, S.E., and Fryer, B.J. 1990. ICP-MS - a powerful tool for high-precision trace-element analysis in Earth Sciences: Evidence from analysis of selected U.S.G.S. reference samples. *Chemical Geology*, **83**: 133-148.

Johnston, S.T. and Erdmer, P.E. 1995. Hot-side up aureole in southwest Yukon and limits on terrane assembly of the northern Canadian Cordillera. *Geology*, **23**, 419-422.

Knaack, C., Cornelius, S. and Hooper, P. 1994. *Trace element analysis of rocks and minerals by ICP-MS.* Department of Geology, Washington State University.

Le Bas, M.J., Le Maitre, R.W, and Woolley, A.R. 1992. The construction of the total alkali-silica chemical classification of volcanic rocks. *Mineralogy and Petrology*, **46**:1-22.

Ludwig, K.R. and Silver, L.T. 1977. Lead-isotope inhomogeneity in Precambrian igneous K-feldspars. *Geochimica et Cosmochimica Acta*, **41**: 1457-1471.

Lugmair, G.W. and Galer, S.J.G. Age and isotope relationships among the angrites Lewis Cliff 86010 and Angra dos Reis*. *Geochimica et Cosmochimica Acta*, **56**: 1673-1694.

McBirney, A.R. 1984. *Igneous Petrology*. W.H. Freeman and Company, San Francisco, pp 504.

McConnell, R.G.1905. Report on the Klondike Goldfields: *Canada Geological Survey Annual Report* **14**, n.s., B pp. 71. reprinted in: Bostock, H.S., 1957, pp. 64-113.

McCulloch, M.T. and Wasserburg, G.J. 1978. Sm-Nd and Rb-Sr chronology of continental crust formation. *Nature*, **200**: 1004-1011.

McDonough, W.F. and Frey, F.A. 1989. Rare earth elements in upper mantle rocks. in: Lipin, B.R. and McKay, G.A. [eds], *Review of Mineralogy* **21**: 99-145.

McLennan, S.M. (1989). Rare earth elements in sedimentary rocks: influence of provenance and sedimentary processes. in: Lipin, B.R. and McKay, G.A. [eds], *Review of Mineralogy* **21**: 169-200.

Middlemost, E.A.K. 1985. *Magmas and Magmatic Rocks*. Longman Group Limited, Essex, pp. 266.

Miller, M.M. 1987. Dispersed remnants of a northeast Pacific fringing arc: Upper Paleozoic terranes of Permian McCloud faunal affinity, western U.S. *Tectonics*, **6**: 807-830.

Miyashiro, A. 1974. Volcanic rock series in island arcs and active continental margins. *American Journal of Science*, **274**: 321-355.

Monger, J.W.H. 1977. Upper Paleozoic rocks of the western Canadian Cordillera and their bearing on Cordilleran evolution. *Canadian Journal of Earth Sciences*, **14**: 1832-1859.

Monger, J.W.H. 1984. Cordilleran tectonics: a Canadian perspective. *Bulletin de la Societe Geologique de France*, **26**: 255-278.

Monger, J.W.H. 1992. Canadian Cordilleran tectonics: from geosynclines to crustal collage. *Canadian Journal of Earth Sciences*, **30**: 209-231.

Monger, J.W.H., Price, R.A., and Tempelman-Kluit, D.J. 1982. Tectonic accretion and the origin of the two major metamorphic and plutonic welts in the Canadian Cordillera. *Geology*, **10**: 70-75.

Monger, J.W.H., Ross, C.A. 1971. Distribution of fusilinaceans in the western Canadian Cordillera. *Canadian Journal of Earth Sciences*. **8**: 259-278.

Morin, J.A. 1981. Volcanogenic iron and base metal occurrences in Klondike Schist. in: *Yukon Geology and Exploration 1979-1980, Department of Indian and Northern Affairs, Whitehorse, Y.T.*, 60-64.

Mortensen, J.K. 1983. *Age and evolution of the of the Yukon-Tanana terrane, southeastern Yukon Territory*. Unpublished Ph.D. Thesis, University of California, Santa Barbara.

Mortensen, J.K. 1986. U-Pb ages for granitic orthogneiss from western Yukon Territory: Selwyn Gneiss and Fiftymile Batholith revisited. in: *Current Research, Part B, Geological Survey of Canada, Paper* **86-1B**: 141-146.

Mortensen, J.K. 1992a. New U-Pb ages for the Slide Mountain Terrane in southeastern Yukon Territory; in: *Radiogenic and Isotope Studies, Report 5; Geological Survey of Canada, Paper* **91-2**: 167-173.

Mortensen, J.K. 1992b. Pre-mid-Mesozoic tectonic evolution of the Yukon-Tanana terrane, Yukon and Alaska. *Tectonics*, **11**: 836-853.

Mortensen, J.K., and Jilson, G.A. 1985. Evolution of the Yukon-Tanana terrane: evidence from the southeastern Yukon Territory. *Geology*, **13**: 806-810.

Mortimer, N. 1986. Late-Triassic, arc-related, potassic igneous rocks in the North American Cordillera. *Geology*, **14**: 1035-1038.

Mortimer, N. 1987. The Nicola Group: Late Triassic and early Jurassic subduction-related volcanism in British Columbia. *Canadian Journal of Earth Sciences*. **24**: 2521-2536.

Nelson, J, and Mihalynuk, M. 1993. Cache Creek ocean: closure or enclosure? *Geology*, **21**: 173-176.

Nesbitt, H.W., and Young, G.M. 1982. early Proterozoic climates and plate motions inferred from major element chemistry of lutites. *Nature*, **299**: 230-249.

Nokleberg, W.J., Parfenov, L.M., Monger, J.W.H., and 21 others. 1994. Circum-North Pacific tectonostratigraphic terrane map. *United States Geological Survey, Open File Report* **94-714**: pp. 221.

Norrell, G.T., Teixell, A., and Harper, G.D. 1989. Microstructure of sepentinite mylonites from the Josephine ophiolite and serpentinization in retrogressive shear zones, California. *Geological Society of America Bulletin*, **101**: 673-682.

O'Nions, R.K., Hamilton, P.J., and Hooker, P.J. 1983. A Nd isotopic investigation of sediments related to crustal developments in the British Isles. *Earth and Planetary Science Letters*, **63**: 229-240.

Pangaea Scientific (1995). Spheristat 2.0 for Windows 3.1; manual pp. 198.

Pearce, J.A. 1983. Role of sub-continental lithosphere in magma genesis at active continental margin. in: Hawkesworth, C.J. and Norry, M.J. [eds.] *Continental Basalts and Mantle Xenoliths,* Shiva Publishing Limited, Nantwich, U.K., pp. 230-249.

Pearce, J.A. and Cann, J.R. 1973. Tectonic setting of basic rocks determined using trace element analyses. *Earth and Planetary Science Letters*, **19**: 290-300.

Pearce, J.A., Harris, N.B.W., and Tindle, A.G. 1984. Trace element discrimination diagrams for the tectonic interpretation of granitic rocks. *Journal of Petrology*, **25**: 956-983.

Pearce, J.A., and Parkinson, I.J. 1993. Trace element models for mantle melting: application to volcanic arc petrogenesis; in: Pritchard, H.M., Alabaster, T., Harris, N.B.W., and Neary, C.R. [eds.] *Magmatic Processes and Plate Tectonics: Geological Society Special Publication No.* **76**, 373-403.

Platt, J.P. and Vissers, R.L.M. 1980. Extensional structures in anisotropic rocks. *Journal of Structural Geology*, **2**: 397-410.

Plint, H.E. and Gordon, T.M. 1995. The Slide Mountain terrane and Finlayson fault zone: marginal basin rocks in a transpressive setting? Evidence from the Campbell Range, southeastern Yukon; in *Lithoprobe Slave-Northern Cordillera Lithospheric Evolution: Lithobrobe Report No.* **44**: 33-50.

Plint, H.E. and Gordon, T.M. 1996. Structural evolution and rock types of the Slide Mountain and Yukon-Tanana terranes in the Campbell Range, southeastern Yukon; in *Lithoprobe Slave-Northern Cordillera Lithospheric Evolution / Cordilleran Tectonics Workshop: Lithoprobe Report No.* **50**: 73-90.

Plint, H.E., and Gordon, T.M. 1997. The Slide Mountain terrane and the structural evolution of the Finlayson Lake fault zone, southeastern Yukon. *Canadian Journal of Earth Sciences*, **34**: 105-126.

Preto, V.A., Osatenko, M.J., McMillan, W.J., and Armstrong, R.L. 1979. Isotopic dates and strontium isotopic ratios for plutonic and volcanic rocks in the Quesnel Trough and Nicola Belt, south-central British Columbia. *Canadian Journal of Earth Sciences*, **16**: 1658-1672.

Roback, R.C., Sevigny, J.H., and Walker, N.W. 1994. Tectonic setting of the Slide Mountain terrane, southern British Columbia, *Tectonics*, **13**, 1242-1258.

Rubin, C.M., Miller, M.M., and Smith, G.M. 1990. Tectonic development of Cordilleran mid-Paleozoic volcano-plutonic complexes; evidence for convergent margin tectonism. *Geological Society of America Special Paper*, **255**: 1-16.

Samson, S.D., McClellend, W.C., Patchett, P.J., Gehrels, G.E., and Anderson, R.G. 1989. Evidence from neodymium isotopes for mantle contributions to Phanerozoic crustal genesis in the Canadian Cordillera. *Nature*, **337**: 705-709.

Samson, S.D., Patchett, J.P., McClelland, W.C., and Gehrels, G.E. 1991. Nd isotopic characterization of metamorphic rocks in the Coast Mountains, Alaskan and Canadian Cordillera: ancient crust bounded by juvenile terranes. *Tectonics*, **10**: 770-780.

Shand. S.J. 1947. *Eruptive Rocks. Their Genesis, Composition, Classification, and their relation to Ore-deposits, 3rd edition.* J. Wiley and Sons, New York, pp 488.

Stacey, J.S. and Kramers, J.D. 1975. Approximation of terrestrial lead isotope evolution by a two-stage model. *Earth and Planetary Science Letters*, **26**: 207-221.

Stevens, C.H., and Rycerski, B.A. 1983. Permian colonial rugose corals in the western Americas - aids in positioning of suspect terranes, in: Stevens, C.H. [ed.]. *Pre-Jurassic Rocks in Western North American Suspect Terranes.* Pacific Section, Society of Economic Paleontologists and Mineralogists, Los Angeles. pp. 23-36.

Stevens, R.A. 1994. *Structural and tectonic evolution of the Teslin tectonic zone, Yukon: a doudly-vergent transpressive shear zone.* Ph.D. Thesis, University of Alberta, Edmonton, pp. 252.

Stevens, R.A., Erdmer, P.E., Creaser, R.A., and Grant, S.G. 1996. Mississippian assembly of the Nisutlin assemblage: evidence from primary contact relationships and

Mississippian magmatism in the Teslin tectonic zone, part of the Yukon-Tanana terrane of the south-central Yukon. *Canadian Journal of Earth Sciences*, **33**: 103-116.

Stevens, R.A., Mortensen, J.K., Hunt, P.A. 1993. U-Pb and $^{40}$Ar-$^{39}$Ar geochronology of plutonic rocks from the Teslin suture zone, Yukon Territory. In: *Radiogenic age and Isotopic Studies, Report 7; Geological Survey of Canada, Paper* **93-2**, 83-90.

Streckeisen, A. 1976. To each plutonic rock its proper name. *Earth Science Reviews*. **12**: 1-33.

Sundblad, K., Cumming, G.L., and Krstic, D. 1991. Lead isotopic evidence for the formation of epithermal gold quartz veins in the Chortis Block, Nicaragua. *Economic Geology*, **86**: 944-959.

Taylor, S.R. and McLennan, S.M. 1985. *The continental crust: its composition and Evolution.* Blackwell Scientific Publications, Oxford, 312 pp.

Tempelman-Kluit, D.J. 1976. The Yukon Crystalline Terrane: enigma in the Canadian Cordillera. *Geological Society of America Bulletin*. **87**: 1343-1357.

Tempelman-Kluit, D.J. 1977a. Quiet Lake (105F) and Finlayson Lake (105G) map areas, Yukon. *Geological Survey of Canada, Open File* **486**.

Tempelman-Kluit, D.J. 1977b. Stratigraphic and structural relations between the Selwyn Basin, Pelly-Cassiar Platform, and Yukon Crystalline Terrane in the Pelly Mountains, Yukon. in: *Report of Activities, Part A, Geological Survey of Canada, Paper* **77-1A**: 223-227.

Tempelman-Kluit, D.J. 1979. Transported cataclasite, ophiolite, and granodiorite in Yukon: Evidence of arc-continent collision. *Geological Survey of Canada, Paper*, **79-14**: pp. 27.

Tempelman-Kluit, D.J., Abbott, G., Gordey, S., and Read, B.1975. Stratigraphic and structural studies in the Pelly Mountains, Yukon Territory. in: *Report of Activities, Part A, Geological Survey of Canada, Paper* **75-1AB**: 45-49.

Tempelman-Kluit, D.J., Gordey, S.P., and Read, B.C. 1976. Stratigraphic and structural studies in the Pelly Mountains, Yukon Territory. in: *Report of Activities, Part A, Geological Survey of Canada Paper*, **76-1A**: 97-106.

Tempelman-Kluit, D.J. and Wanless, R.K. 1980. Zircon ages for the Pelly Gneiss and Klotassin granodiorite in western Yukon. *Canadian Journal of Earth Sciences*, **17**: 297-306.

Thériault, R.J. and Ross, G.M. 1991. Nd isotopic evidence for crustal recycling in the ca. 2.0 Ga subsurface of Western Canada. *Canadian Journal of Earth Sciences*, **28**: 1140-1147.

Thorkelson, D.J., Mortensen, J.K., Marsden, H., and Taylor, R.P. 1995. Age and tectonic setting of Early Jurassic episodic volcanism along the northeastern margin of the Hazelton Trough, northern British Columbia, in Miller, D. and Busby, C. [eds.] *Jurassic magmatism and tectonics of the North American Cordillera, Geological Society of America Special Paper*, **299**: 83-94.

Wasserburg, G.J., Jacobsen, S.B., DePaolo, D.J., McCulloch, M.T., and Wen, T. 1981. Precise determination of Sm/Nd ratios, Sm and Nd isotopic abundances in standard solutions. *Geochimica et Cosmochimica Acta*, **45**: 2311-2323.

Wernicke, B. and Klepacki, D.W. 1988. Escape hypothesis for the Stikine block. *Geology*, **16**: 461-464.

Wheeler, J.O., Green, L.H., and Roddick, J.A. 1960. Quiet Lake, Yukon Territory. *Geological Survey of Canada, Map* **7-1960**.

Wheeler, J.O., Brookfield, A.J., Gabrielse, H., Monger, J.W.H. Tipper, H.W., and Woodsworth, G.J. 1991. Terrane map of the Canadian Cordillera. *Geological Survey of Canada*, Map **1713A.**

Wheeler, J.O. and McFreely, P. [comp.]. 1991. Tectonic assemblage map of the Canadian Cordillera and adjacent parts of the United States of America. *Geological Survey of Canada*, Map **1712A**.

White, S.H., Burrows, S.E., Carreras, J., Shaw, N.D., and Humphreys, F.J. 1980. On mylonites in ductile shear zones. *Journal of Structural Geology*, **2**: 175-187.

Wood, D.A.1980. The application of a Th-Hf-Ta diagram to problems of tectonomagmatic classification and to establishing the nature of crustal contamination of basaltic lavas of the British Tertiary Volcanic province. *Earth and Planetary Science Letters*, **50**: 11-30.

Wood, D.A., Joron, J., and Treuil, M. 1979. A reappraisal of the use of trace elements to classify and discriminate between magma series erupted in different tectonic settings. *Earth and Planetary Science Letters*, **45**: 326-336.

York, D. 1967. The best isochron. *Earth and Planetary Science Letters*, **2**: 479-482

# APPENDIX 1. LATITUDE AND LONGITUDE OF FIELD STATIONS

| SG94- | latitude | longitude |
|---|---|---|
| 1 | 61° 12' 16" | 130 25' 38" |
| 2 | 61° 12' 10" | 130 25' 08" |
| 3 | 61° 12' 39" | 130 26' 00" |
| 4 | 61° 12' 45" | 130 27' 12" |
| 5 | 61° 12' 23" | 130 28' 20" |
| 6 | 61° 12' 37" | 130 28' 50" |
| 7 | 61° 13' 39" | 130 26' 43" |
| 8 | 61° 13' 48" | 130 26' 31" |
| 8.5 | 61° 14' 06" | 130 26' 20" |
| 9 | 61° 15' 34" | 130 25' 18" |
| 10 | 61° 15' 52" | 130 24' 47" |
| 11 | 61° 15' 57" | 130 22' 45" |
| 12 | 61° 13' 02" | 130 23' 00" |
| 13 | 61° 12' 37" | 130 24' 12" |
| 14 | 61° 12' 22" | 130 24' 05" |
| 15 | 61° 12' 11" | 130 23' 37" |
| 16 | 61° 17' 54" | 130 12' 19" |
| 16.5 | 61° 17' 53" | 130 13' 13" |
| 17 | 61° 17' 54" | 130 13' 36" |
| 18 | 61° 17' 53" | 130 16' 05" |
| 19 | 61° 18' 21" | 130 18' 34" |
| 20 | 61° 18' 42" | 130 18' 59" |
| 21 | 61° 19' 07" | 130 19' 06" |
| 22 | 61° 18' 52" | 130 19' 42" |
| 23 | 61° 18' 58" | 130 20' 47" |
| 23.5 | 61° 19' 04" | 130 20' 55" |
| 24 | 61° 19' 05" | 130 21' 25" |
| 25 | 61° 18' 27" | 130 21' 16" |
| 26 | 61° 18' 09" | 130 21' 16" |
| 27 | 61° 18' 04" | 130 21' 31" |
| 28 | 61° 17' 42" | 130 22' 08" |
| 29 | 61° 12' 06" | 130 25' 00" |
| 30 | 61° 11' 47" | 130 25' 49" |
| 31 | 61° 11' 49" | 130 25' 07" |
| 32 | 61° 11' 14" | 130 23' 40" |
| 33 | 61° 11' 12" | 130 23' 31" |
| 34 | 61° 11' 09" | 130 16' 32" |
| 35 | 61° 11' 14" | 130 16' 10" |
| 36 | 61° 10' 56" | 130 16' 28" |
| 37 | 61° 10' 44" | 130 16' 30" |
| 38 | 61° 10' 39" | 130 16' 30" |
| 39 | 61° 10' 19" | 130 16' 32" |
| 40 | 61° 10' 16" | 130 16' 32" |
| 41 | 61° 10' 08" | 130 16' 30" |
| 42 | 61° 10' 00" | 130 15' 55" |
| 43 | 61° 11' 17" | 130 23' 51" |
| 44 | 61° 12' 42" | 130 25' 08" |
| 45 | 61° 12' 47" | 130 25' 09" |
| 46 | 61° 13' 00" | 130 25' 18" |
| 47 | 61° 13' 43" | 130 24' 54" |
| 48 | 61° 13' 12" | 130 25' 28" |
| 49 | 61° 13' 02" | 130 25' 30" |
| 50 | 61° 12' 55" | 130 25' 11" |
| 51 | 61° 12' 38" | 130 25' 07" |
| 52 | 61° 11' 56" | 130 24' 30" |
| 53 | 61° 11' 33" | 130 24' 52" |
| 54 | 61° 11' 01" | 130 24' 23" |
| 55 | 61° 10' 38" | 130 23' 44" |
| 56 | 61° 9' 38" | 130 22' 25" |
| 57 | 61° 9' 28" | 130 23' 08" |
| 58 | 61° 9' 20" | 130 23' 17" |
| 59 | 61° 9' 20" | 130 24' 34" |
| 60 | 61° 16' 08" | 130 23' 21" |
| 61 | 61° 16' 31" | 130 22' 33" |
| 62 | 61° 17' 30" | 130 22' 41" |
| 63 | 61° 17' 16" | 130 22' 37" |
| 64 | 61° 16' 44" | 130 22' 31" |
| 65 | 61° 16' 36" | 130 19' 19" |
| 66 | 61° 16' 51" | 130 19' 20" |
| 67 | 61° 16' 53" | 130 18' 21" |
| 68 | 61° 17' 00" | 130 19' 32" |
| 69 | 61° 16' 59" | 130 19' 58" |
| 70 | 61° 16' 58" | 130 20' 09" |
| 71 | 61° 16' 50" | 130 20' 27" |
| 72 | 61° 16' 42" | 130 20' 41" |
| 73 | 61° 16' 28" | 130 20' 32" |
| 74 | 61° 16' 41" | 130 19' 49" |
| 75 | 61° 11' 33" | 130 23' 15" |
| 76 | 61° 12' 05" | 130 23' 52" |
| 77 | 61° 14' 05" | 130 26' 19" |
| 78 | 61° 13' 28" | 130 28' 20" |
| 79 | 61° 13' 23" | 130 29' 03" |
| 80 | 61° 14' 13" | 130 32' 15" |
| 81 | 61° 14' 18" | 130 31' 29" |
| 82 | 61° 14' 17" | 130 31' 15" |
| 83 | 61° 14' 17" | 130 30' 58" |
| 84 | 61° 14' 36" | 130 30' 24" |
| 85 | 61° 14' 00" | 130 29' 30" |
| 86 | 61° 13' 04" | 130 28' 09" |
| 87 | 61° 12' 37" | 130 28' 51" |
| 88 | 61° 11' 03" | 130 14' 14" |
| 89 | 61° 11' 36" | 130 14' 22" |
| 90 | 61° 14' 00" | 130 16' 42" |

# APPENDIX 2. HANDSAMPLE DESCRIPTION OF NISUTLIN SAMPLES.

| Sample | colour | weathering | foliation | grain size | compositional notes | subunit |
|---|---|---|---|---|---|---|
| SG94-5A | grey-yellow | | porphyroclastic mylonite, CB 2mm | F [2-3] | quartzofeldspathic with dark wisps, Fs porphyroclasts, mica sheen | MQS |
| SG94-5B | grey-orange | | porphyroclastic schist, no CB, flattening slight | F [1-2] | quatzofeldspathic with a few dark wisps, Fs porphyroclasts, micas | MQS |
| SG94-5C | grey-green | slight red | porphyroclastic phyllonite, wispy CB 2mm | A[1-2] | dark green with some quartzy wisps, Fs porphyroclasts, mica flecks | MQS |
| SG94-6 | grey-green | | phyllonite, slight CB | F | mottled green , some Qt | MQS |
| SG94-17A | light grey | brown-red | schist | 1 | quartzofeldspathic with some dark blebs, mica (Bt?) | MQS |
| SG94-17B | grey | orange | schist,CB 1-2mm | F [2] | quartzofeldspathic with dark wisps throughout, Bt | MQS |
| SG94-18A | pale yellow | orange | schist, CB 1mm | 1 | quartzofeldspathic with a few dark layers, Bt | MQS |
| SG94-20 | pale green | yellow-orange | schist, CB 1 | F | quartzofelfspathic with dark layers, Bt | MQS |
| SG94-23 | grey green | | phyllonite, squished porphyroclasts, CB 1mm | A [2] | quartzofeldspathic with dark layers, porphyroclasts, mica flecks (Bt?) | MQS |
| SG94-24 | pale yellow | yellow-orange | phyllonite, CB 1 mm | F | quartzofeldspathic with grey layers, mica flecks | MQS |
| SG94-26 | pale yellow | yellow-orange | phyllonite, CB 2 mm | F | quartzofeldspathic with grey layers, mica flecks | MQS |
| SG94-33C | white | yellow | mylonite | A | quartzose with a few dark wisps | MQS |
| SG94-35A | silver-white | yellow | phyllite, stylolitic | A | quartzose with mica sheen, anastomozing orange weathered cracks | QP |
| SG94-35B | dark grey | orange | phyllite, CB 5-10mm, stylolitic | A | graphitic with anastomozing Qt blebs, mica sheen | QP-g |
| SG94-35C | grey | orange | phyllite, undulous, CB 5-10mm, stylolitic | A | graphitic with anastamozing Qt blebs, mica sheen | QP-g |
| SG94-53 | pale grey-green | orange | phyllonite, CB 2mm | A | pale green with some quartzofeldspathic wisps, mica sheen | MQS |
| SG94-62 | green | brown | phyllonite, CB 1mm | A | green with quartzose blebs, mica sheen | MQS |
| SG94-65 | grey | yellow orange | schist, CB 1mm | F | quartzofeldspathic, with many dark specks, micas | MQS |
| SG94-67 | white | orange | phyllonite | F | quartzose with thin orange wispy layers, mica sheen (Ms?) | MQS |
| SG94-68A | pale yellow | orange | phyllonite, CB 1mm | F | quartzofeldspathic with some dark layers,mica sheen (Ms?) | MQS |
| SG94-68B | green | orange | schist | 1-2 | green Am-bearing, some Qt and Fs, mica | MQS |
| SG94-69 | dark-green | | phyllonite, CB1mm | A | dark green with some white wisps, mica sheen | MQS? |
| SG94-80 | dark grey | orange-brown | schist, blebby | 1 | green Am bearing, quartzose blebs, mica (Ms) | MS |
| SG94-81 | dark-green | | schist, CB 2mm | 1 | dark green Am bearing, quartofeldspathic layers, Bt | MS |
| SG94-82 | green | orange | mylonite, slight CB | A | dark green with a few thin quatzose layers | MS |
| SG94-84 | dark-grey | orange | phyllite, slight CB .05mm | A | graphitic with a few thin Qt wisps. mica sheen | MS |
| SG94-85 | dark green | | mylonite, CB 1 mm | A | dark geen with some quartzofeldspathic layers, mica sheen | MS |
| SG94-89A | light grey | orange brown | mylonite, stylolitic | A | quartzose with mica (Ms?) sheen, anastomozing orange weathered cracks | QP |
| SG94-90C | dark grey | orange | mylonite, CB 2mm | A | graphitic-quartofeldspathic with anastomozing orange cracks | QP-g |
| SG94-90D | dark grey | orange | phyllite, stylolites | A | graphitic with some quartoze layers, mica sheen | QP-g |

CB = compositional banding. Grain size: F = fine, A = aphanitic, number indicates average grain size in mm, number in parantheses gives size of porphyroclasts in mm. Mineral abbreviations: Am = amphibole, Bt = biotite, Fs = Feldspar, Ms = muscovite, Qt = quartz. Subunit abbreviations: MQS = mica quartz schist, MS = mafic schist, QP = quartz-rich phyllite.

# APPENDIX 3. THIN SECTION DESCRIPTIONS OF NISUTLIN ASSEMBLAGE SAMPLES

| Samp/ unit | minerals | | Md % | size mm | comments: |
|---|---|---|---|---|---|
| 5A<br>MQS | Gm: | quartz | 70 | 0.1 | -compositionally banded<br>-opaque minerals concentrated in bands.<br>-fractured k-spar phenocrysts<br>-trace mineral is clear, surrounded by pleiochroic halos - monazite |
| | | K-feldspar | 5 | 0.1 | |
| | | calcite | 5 | i | |
| | | muscovite | 5 | 0.1 | |
| | Pc: | microcline | 10 | 1-3 | |
| | | plagioclase | 1 | 0.5-1 | |
| | | muscovite | <5 | 0.2-0.5 | |
| | Tr: | yellow? | 1 | | |
| 5B<br>MQS | Gm: | quartz | 70 | <0.3 | -no compositional banding<br>-interstitial calcite |
| | | K-feldspar | 10 | <0.3 | |
| | | plagioclase | 1 | <0.1 | |
| | Pc: | muscovite | 10 | <0.3 | |
| | | K-feldspar | 5 | 1-2 | |
| | Tr: | monazite | | | |
| | | zircon | | | |
| 6A<br>MQS | Gm: | quartz | 75 | 0.1-0.5 | -quartzofeldspathic welts surrounded by phyllosilicates<br>-chlorite as nebulous masses<br>-very disaggregated amphibole present |
| | | K-feldspar | 10 | 0.1-0.5 | |
| | | plagioclase | <5 | 0.1 | |
| | | chlorite | <5 | - | |
| | Pc: | K-feldspar | 5-10 | 1 | |
| | | muscovite | 5-10 | 2-3 | |
| | Tr: | | | | |
| 17A<br>MQS | Gm: | quartz | 70 | 0.1 | -mostly small subgrained quartz and K-feldspar.<br>-biotite and amphibole (hornblende?) define the foliation.<br>-plag almost completely sericitized<br>-trace (?): clear, low biref, high relief, biax+, fractured, 1 cleavage(?), possibly spatially related to amphibole. |
| | | K-feldspar | 10 | 0.1 | |
| | | plagioclase | <1 | <0.1 | |
| | Pc: | biotite | 5 | 0.5-1 | |
| | | amphibole | 5 | 0.5-1 | |
| | Tr: | ? | | | |
| 17B<br>MQS | Gm: | quartz | 80 | 0.2 | -quartzofeldspathic<br>-foliation defined by biotite<br>-trace: (?): clear colourless, med relief, low biref, biax+ |
| | | K-feldspar | 10 | 0.2 | |
| | Pc: | biotite | 10 | 0.5-1 | |
| | Tr: | ? | | | |

| sample | minerals | | Md % | size mm | comments: |
|---|---|---|---|---|---|
| **18A**<br>**MQS** | Gm: | quartz | 50 | 0.2 | -biotite rich layers define foliation<br>-trace (epidote?): yellow aggregated masses, undulatory blue extinction. |
| | | K-feldspar | 20 | 0.2 | |
| | | plagioclase | 15 | 0.2 | |
| | Pc: | biotite | 10 | 0.5 | |
| | Tr: | zircon | | | |
| | | epidote? | | | |
| **18B**<br>**MQS** | Gm: | quartz | 40 | 0.5 | -weakly foliated<br>-cracked and partially disaggregated garnet |
| | | K-feldspar | 20 | 0.2 | |
| | | plagioclase | 10 | 0.2 | |
| | Pc: | plagioclase | 10 | 1-2 | |
| | | garnet | 5 | 0.5-2 | |
| | | muscovite | 15 | 1 | |
| | Tr: | zircon | | | |
| **20**<br>**MQS** | Gm: | quartz | 70 | 0.2 | -quartzofeldspathic with anastomozing micaceous layers |
| | | K-feldspar | 10 | 0.2 | |
| | Pc: | K-feldspar | <2 | 1 | |
| | | plagioclase | <2 | 1 | |
| | | biotite | 10 | 0.5 | |
| | | muscovite | 10 | 0.5 | |
| | Tr: | zircon | <1 | | |
| **24**<br>**MQS** | Gm: | quartz | 60 | 0.1 | -quartzofeldspathic with layers of mica<br>-square holes (formerly pyrite?) filled with red opaque material |
| | | K-feldspar | <10 | 0.1 | |
| | | plagioclase | <5 | 0.1 | |
| | | biotite | 10 | 0.1 | |
| | Pc: | muscovite | 10 | 0.5 | |
| | Tr: | red opaque? | | | |
| **26**<br>**MQS** | Gm: | quartz | 80 | 0.1 | -small-grained quartzofeldspathic layers alternate with mica-rich layers.<br>-red hematitic(?) material in cracks |
| | | K-feldspar | 5 | 0.1 | |
| | Pc: | muscovite | 10 | 0.5-1 | |
| | | biotite | 5 | 0.5-1 | |
| | Tr: | red opaque | | | |
| **35A**<br>**QP** | Gm: | quartz | >95 | 0.1-0.5 | -strained, subgrained quartz<br>-anastomozing cracks filled with red opaque material |
| | | biotite? | <5 | 0.1 | |
| | Pc: | | | | |
| | Tr: | red opaque | | | |
| **35C**<br>**QP** | Gm: | quartz | >90 | 0.1-2 | -variable grain sizes<br>-graphite in anastomozing fractures<br>-trace (hydrogrossular?): medium relief, almost isotropic, yellow, hexagons |
| | Pc: | muscovite | <5 | 1 | |
| | Tr: | graphite | <5 | | |
| | | red opaque | | | |
| | | hydrogross. | | | |

| **sample** | **minerals** | | **Md** % | **size** mm | **comments:** |
|---|---|---|---|---|---|
| **53**<br>**MQS** | Gm: | quartz | 70 | 0.1-1 | -fine grained quartofeldspathic layers<br>-small chlorite grains mostly aligned, but some in random orientation<br>-chlorite grains overgrow quartz grains<br>-trace(?): high relief, high biref, possible cleavage, fractured, aggregated |
| | | K-feldspar | 10 | 0.1-1 | |
| | | chlorite | 20 | 0.1-0.2 | |
| | Pc: | | | | |
| | Tr: | ? | | | |
| **62**<br>**MQS** | Gm: | quartz | 60 | 0.1 | -alternating thin quartzofeldspathic bands and chloritic bands<br>-many rootless recumbant folds, now passively transported.<br>-amphibole likely actinolite |
| | | K-feldspar | 10 | 0.1 | |
| | | chlorite | 10 | 0.1 | |
| | Pc: | K-feldspar | <5 | 1 | |
| | | plagioclase | <5 | 1 | |
| | | actinolite? | 10 | 0.1x2 | |
| | Tr: | | | | |
| **65**<br>**MQS** | Gm: | quartz | 80 | 0.1-0.5 | -quartzofeldspathic layers with mica fish |
| | | K-feldspar | 10 | 0.1-0.5 | |
| | | biotite | <5 | 0.1 | |
| | Pc: | muscovite | 10 | 1 | |
| | Tr: | | | | |
| **67**<br>**MQS** | Gm: | quartz | 80 | 0.1 | -quartzofeldspathic layers with mica |
| | | K-feldspar | 10 | 0.1 | |
| | | muscovite | <5 | 0.2 | |
| | | biotite | <5 | 0.2 | |
| | Pc: | muscovite | <5 | 0.5-1 | |
| | Tr: | | | | |
| **68A**<br>**MQS** | Gm: | quartz | 70 | 0.1-0.3 | -quartzofeldspathic layers with mica fish<br>-red opaque material (hematite?) in the AESB and cracks. |
| | | K-feldspar | 10 | 0.1-0.3 | |
| | Pc: | muscovite | 10 | 0.5-1 | |
| | | biotite | 10 | 0.5 | |
| | Tr: | red opaque | | | |
| **68B**<br>**MQS?** | Gm: | quartz | 50 | 0.2 | -quartzofeldspathic groundmass with large amphibole crystals and biotite<br>-layering not well developed; foliation defined by amphiboles and biotites |
| | | K-feldspar | 10 | 0.2 | |
| | Pc: | amphibole | 30 | 1-2 | |
| | | biotite | >5 | 0.5-1 | |
| | | chlorite | <5 | 0.5 | |
| | Tr: | | | | |
| **80**<br>**MS** | Gm: | quartz | 50 | 0.1-0.2 | -fairly quartzofeldspathic, with biotites and amphiboles defining wobbly foiation. |
| | | K-feldspar | 10 | 0.1-0.2 | |
| | | chlorite | 10 | 0.1-0.2 | |
| | Pc: | amphibole | 20 | 1-2 | |
| | | biotite | 10 | 2-5 | |

| **sample** | **minerals** | | **Md %** | **size mm** | **comments:** |
|---|---|---|---|---|---|
| **82 MS** | Gm: | chlorite | 5 | 0.1-0.2 | -dominantly chlorite and amphibole with small discontinuous layers of quartz |
| | | amphibole | 50 | 0.1-0.5 | |
| | | quartz | 10 | 0.1 | |
| | Pc: | amphibole | 30 | 1-2 | |
| | | biotite | 5 | 0.5-1 | |
| | Tr: | | | | |
| **85 MS** | Gm: | quartz | 40 | 0.1-0.2 | -subgrained quartz and K-feldspar interlayered with chloritic layers.<br>-interstitial calcite |
| | | K-feldspar | 10 | 0.1-0.2 | |
| | | chlorite | 40 | 0.1-0.2 | |
| | | calcite | 10 | I | |
| | Pc: | K-feldspar | <1 | 0.5-1 | |
| | Tr: | dark opaque | | | |
| **89A QP** | Gm: | quartz | 95 | 0.1-0.5 | -mostly subgarined quartz.<br>- red opaque material concentrated in anastomozing fractures. |
| | | K-feldspar | <5 | 0.1-0.5 | |
| | | muscovite | <5 | 0.1-0.2 | |
| | Pc: | | | | |
| | Tr: | red opaque | | | |
| **90C QP** | Gm: | quartz | 85 | 0.1-0.2 | -mostly subgrained quartz<br>-graphite concentrated in anastomozing fractures<br>-older foliations can seen to be transposed by the anstomozing fractures |
| | | K-feldspar | <5 | 0.1-0.2 | |
| | | muscovite | 2.5 | 0.1 | |
| | | biotite | 2.5 | 0.1 | |
| | | graphite | <10 | | |
| | Pc: | | | | |
| | Tr: | | | | |
| **90D QP** | Gm: | quartz | 85 | 0.1-0.2 | -mostly subgrained quartz<br>-graphite concentrated in anastomozing fractures |
| | | K-feldspar | <1 | 0.1-0.2 | |
| | | muscovite | <2 | 0.1 | |
| | | biotite | <2 | 0.1 | |
| | Pc: | | | | |
| | Tr: | graphite | <15 | | |

abbreviations: Gm = groundmass, Pc = porphyroclasts, Tr = trace minerals, I = interstitial

# APPENDIX 4. STRUCTURAL MEASUREMENTS

North Group

| LOC | foliation | | lineation | | UNIT |
|---|---|---|---|---|---|
| (SG94-) | dd | dip | trend | plunge | |
| 16.5 | 180 | 12 | | | N |
| | 185 | 6 | 185 | 6 | N |
| ave | 183 | 9 | 185 | 6 | N |
| 17 | 265 | 5 | 180 | 0 | N |
| | 90 | 10 | 175 | 1 | N |
| ave | 178 | 8 | 178 | 1 | N |
| 19 | 310 | 17 | 10 | 14 | N |
| | 292 | 12 | 10 | 1 | N |
| | 313 | 12 | 15 | 5 | N |
| | 290 | 11 | | | N |
| ave | 301 | 13 | 12 | 7 | N |
| 20 | 305 | 10 | 354 | 6 | N |
| | 262 | 10 | 325 | 10 | N |
| | 297 | 13 | 5 | 8 | N |
| | 275 | 16 | 10 | 4 | N |
| ave | 285 | 12 | 354 | 7 | N |
| 21 | 235 | 22 | 200 | 20 | N |
| | 260 | 18 | 185 | 11 | N |
| | 260 | 12 | 350 | 1 | N |
| ave | 252 | 17 | 185 | 10 | N |
| 22 | 195 | 7 | 175 | 5 | N |
| 22.5 | 260 | 9 | 175 | 6 | N |
| 23 | 267 | 7 | 167 | 1 | N |
| 23.5 | 204 | 4 | | | N |
| 24 | 120 | 4 | 165 | 2 | N |
| 25 | 348 | 30 | 358 | 28 | N |
| | 8 | 26 | 358 | 26 | N |
| | 5 | 24 | 4 | 24 | N |
| | 2 | 28 | 350 | 28 | N |
| ave | 1 | 27 | 358 | 27 | N |
| 26 | 55 | 16 | 360 | 8 | N |
| | 18 | 14 | 348 | 9 | N |
| | 20 | 26 | | | N |
| ave | 31 | 19 | 354 | 9 | N |
| 27 | 255 | 8 | 350 | 1 | N |
| 28 | 100 | 21 | 10 | 4 | A/N |
| 62 | 300 | 21 | 360 | 11 | N |
| | 310 | 26 | | | N |
| | 310 | 16 | 358 | 10 | N |
| ave | 307 | 21 | 359 | 11 | N |
| 65 | 240 | 41 | 170 | 21 | N |
| | 245 | 31 | 180 | 20 | N |
| | 225 | 30 | 177 | 19 | N |
| | 230 | 34 | | | N |
| ave | 235 | 34 | 176 | 20 | N |
| 66 | 250 | 15 | 360 | 3 | N |
| | 260 | 10 | 350 | 3 | N |
| ave | 255 | 13 | 355 | 3 | N |
| 67 | 70 | 7 | 180 | 6 | N |
| | 250 | 11 | 180 | 6 | N |
| ave | 250 | 2 | 180 | 6 | N |
| 68 | 270 | 30 | 355 | 4 | N |
| | 230 | 17 | 170 | 10 | N |
| ave | 250 | 24 | 178 | 3 | N |
| 69 | 216 | 22 | | | A/N |
| 70 | 260 | 90 | | | A |
| 71 | 40 | 20 | 345 | 20 | A |
| 90 | 250 | 50 | 210 | 40 | N |

South group

| LOC | foliation | | lineation | | UNIT |
|---|---|---|---|---|---|
| (SG94-) | dd | dip | trend | plunge | |
| 33 | 350 | 35 | | | A/SG |
| | 350 | 45 | 340 | 40 | A/SG |
| ave | 350 | 40 | 340 | 40 | A/SG |
| 34 | 350 | 30 | 290 | 15 | SG/N |
| | 335 | 32 | | | SG/N |
| ave | 343 | 31 | 290 | 15 | SG/N |
| 35 | 320 | 30 | 240 | 10 | A |
| | 320 | 50 | | | A |
| | 330 | 33 | 310 | 29 | A |
| | 340 | 33 | | | A |
| ave | 328 | 37 | | | A |
| 36 | 350 | 5 | | | A/SG |
| 37 | 335 | 17 | | | SG |
| 37.5 | 290 | 19 | | | SG |
| 38 | 292 | 34 | | | SG/N |
| 39 | 285 | 19 | | | SG |
| | 330 | 20 | | | SG |
| | 330 | 30 | | | SG |
| ave | 315 | 23 | | | SG |
| 40 | 330 | 21 | | | N/SG |
| 41 | 325 | 42 | | | SG |
| 42 | 335 | 22 | | | SG |
| 47 | 50 | 34 | 90 | 25 | BM/HG |
| | 20 | 39 | | | BM/HG |
| | 60 | 45 | | | BM/HG |
| | 10 | 32 | | | BM/HG |
| | 355 | 45 | | | BM/HG |
| | 80 | 52 | 175 | 15 | BM/HG |
| ave | 36 | 41 | | | BM/HG |
| 52 | 335 | 45 | | | A |
| | 355 | 22 | | | A |
| | 345 | 32 | | | A |
| ave | 345 | 33 | | | A |
| 53 | 350 | 50 | | | A/N |
| | 350 | 55 | | | A |
| | 350 | 51 | 60 | 26 | A |
| ave | 350 | 52 | 60 | 26 | A |
| 53.5 | 360 | 28 | 60 | 15 | A |
| 56 | 5 | 6 | | | SG |
| 57 | 11 | 9 | | | SG |
| 59 | 330 | 25 | | | SG |

West group

| LOC | foliation | | lineation | | UNIT |
|---|---|---|---|---|---|
| (SG94-) | dd | dip | trend | plunge | |
| 5 | 105 | 52 | 105 | 45 | N |
| 6 | 105 | 20 | 110 | 15 | N |
| 79 | 74 | 50 | 125 | 35 | N |
| 80 | 57 | 39 | | | N |
| 81 | 140 | 18 | | | N |
| | 170 | 23 | 100 | 4 | N |
| | 165 | 21 | 85 | 6 | N |
| | 167 | 17 | | | N |
| ave | 161 | 20 | 93 | 5 | N |
| 83 | 105 | 32 | | | N |
| 84 | 100 | 23 | | | N |
| 86 | 110 | 60 | | | N |
| | 90 | 67 | | | N |
| ave | 100 | 64 | | | N |
| 87 | 100 | 25 | 130 | 15 | N |
| 88 | 255 | 25 | | | SG |

Foliations given in dip-direction (dd) - dip in degrees. Rock units: A = Anvil, BM = biotite monzogranite, HG = hornblende granodiorite, N = Nisutlin, SG = sheared granodiorite. Averages (ave) are given for sites with multiple measurements.

## APPENDIX 5. SHEAR-SENSE INDICATOR DATA

| | sample | unit | rock-type | foliation | lineation | indicator | shear-sense of 'top' | |
|---|---|---|---|---|---|---|---|---|
| 'west group' | SG94-5A | N | Ms-Qt schist | 015/15 | 105-52 | ROTP | ? | ? |
| | SG94-6A | N | Bt-Cl-Qt schist | 015/20 | 110-15 | d-AESB | DL | 110-15 |
| 'south group' | SG94-33B | A | | 350/45 | ? | - | - | - |
| | SG94-35C | N | graphitic-Qt phyllite | 330/32 | 310-29 | - | - | - |
| | SG94-52 | A | | 335/30 | ? | ROTP | ? | ? |
| | SG94-53 | N | Cl-Qt phyllonite | 350/51 | 060-20 | ROTP/d-AESB | DL | 060-20 |
| | SG94-88C | SG | Bt-Kf-Qt schist | 255/25 | ? | ROTP? | ? | ? |
| 'north group' | SG94-17B | N | Bt-Qt schist | 090/10 | 175-01 | f-AESB | DL | 175-01 |
| | SG94-20 | N | Bt-Qt schist | 275/16 | 010-04 | d-AESB | UL | 190-04 |
| | SG94-24 | N | Ms-Bt-Qt schist | 120/04 | 165-02 | d-AESB | DL | 165-02 |
| | SG94-26 | N | Ms-Qt phyllonite | 020/18 | 348-09 | AESB | UL | 168-09 |
| | SG94-62 | N | Cl-Qt phyllonite | 300/21 | 000-11 | AESB | DL | 000-11 |
| | SG94-65 | N | Bt-Ms-Qt schist | 240/41 | 350-21 | d-AESB | UL | 170-21 |
| | SG94-67 | N | Ms-Qt phyllonite | 240/11 | 180-06 | f-AESB | DL | 180-06 |
| | SG94-68A | N | Ms-Qt phyllonite | 270/30 | 335-04 | d-AESB | UL | 155-04 |
| | SG94-68B | N | Ab-Qt schist | 230/10 | 170-10 | ROTP? | ? | ? |
| | SG94-71 | A | | 040/30 | 345-20 | AESB | DL | 345-20 |
| | SG94-90C | N | graphitic-Ms-Qt phyllonite | 256/50 | 210-40 | AESB | UL | 030-40 |
| | SG94-90D | N | graphitic-Ms-Qt phyllonite | 250/50 | 210-40 | AESB | UL | 030-40 |

Units: A = Anvil, N = Nisutlin, SG = sheared granodiorite. Mineral abbreviations: Ab = amphibole, Bt = biotite, Cl = chlorite, Kf = K-feldspar, Ms = muscovite,and Qt = quartz. Shear-sense indicators: AESB = asymetrical extensional shear bands ( f =fracture type, d=ductile type), ROTP = rotated porphyroclasts. DL = down-lineation.UL = up-lineation.

## APPENDIX 6. SAMPLE CLEANING, CRUSHING, AND POWDERING

1) Representative samples, usually fist-sized or slightly larger, were chosen from the units.

2) Weathered edges were removed with a diamond-bladed lapidary saw or drop-saw. Any metallic saw marks were removed with a diamond-abrasive grinder

3) Samples were crushed to maximum grape-sized fragments by wrapping the sample in multiple plastic bags, and striking with a 16-pound sledge hammer. Care was taken to rewrap the sample in plastic as soon as the hammer wore through, in order to avoid contact of the metal hammer head with the sample. Samples used only for isotope dilution were further processed using step (4). Samples analyzed for XRF and ICP-MS were further processed using step (5).

4) A tungsten carbide swing mill was employed to powder the samples used only for Sm-Nd analyses, since contamination was not an issue. Crushed samples were loaded into the cleaned mill and run (checking every minute) until crushed to a fine talc-like powder (~35 microns). A typical rock took about 3-5 minutes total to powder. Pure silica sand was ground in the mill and the mill was carefully washed with clean water between samples to prevent cross-contamination. The powdered samples were then stored in 7 dram plastic vials, ready for weighing out in preparation for whole rock Sm-Nd or Rb-Sr analysis.

5) Samples collected for XRF and ICP-MS analysis were not exposed to tungsten carbide for a long period of time, since tungsten carbide can contaminate a sample with respect to Ta. Thus, the tungsten carbide mill was only used on these samples for about 30 seconds to 1 minute, just enough time to reduce the grape-sized fragments to less-than pea-sized fragments (tungsten carbide mill cleaned as per step (4)). Following this preliminary crush, the samples were then crushed to powder (~35 micron) using an automated agate mortar and pestle (typical crushing time: 15 to 20 minutes). Pure silica sand was ground in the agate mortar and pestle for 5 minutes, and the mortar and pestle was washed carefully between samples to prevent cross-contamination. Powdered samples were stored in 7 dram plastic vials, ready for shipment to Washington State University for XRF and ICP analyses.

# APPENDIX 7. Sm - Nd CHEMICAL SEPARATION AND ISOTOPE ANALYSES TECHNIQUES.

1) Powdered samples were weighed (typically 50 to 200 mg) into 25 ml Teflon vials and totally spiked with weighed aliquots of $^{150}$Nd and $^{149}$Sm tracer solution. Samples were then dissolved in a 3:1 mixture of vapour-distilled 24N HF: 16N $HNO_3$ in sealed containers at ~160°C for ~96 hours.

2) After the samples were uncapped and dried down, vapour distilled 6N HCl was added, the samples resealed, and heated at ~160°C for ~24 hours to dissolve fluorides.

3) Samples were uncapped and dried down, then dissolved in 3ml 0.75 N HCl, centrifuged for 10 minutes at 5000 RPM, and loaded into 10 cm columns containing 200-400 mesh AG50W-X8 cation exchange resin for separation by chromatography. The REE cut was collected and dried down.

4) The dried REE cut was dissolved in 0.25ml of 0.025N HCl, centrifuged for 10 minutes at 10000 RPM, and then loaded into columns containing Di(2-ethylhexyl phosphate) (HDEHP) for separation by chromatography. The Nd and Sm cuts were collected individually and dried down. Nd was analyzed for isotopes according to step (5); Sm was analyzed for isotopes using step (6).

5) The dried purified Nd was dissolved in 3.0 µl de-ionized water and half was loaded (the other half saved for repeat analysis, if necessary) onto the side Re filament of a double filament bead. The Nd samples were analyzed on a VG-354 mass-spectrometer at the University of Alberta using dynamic multi-collector routines, and raw ratios were corrected for variable mass-discrimination to $^{146}\mathrm{Nd}/^{144}\mathrm{Nd} = 0.7219$ using an exponential law (Wasserburg et al. 1981), and for the effects of low-abundance (non-$^{150}$Nd) tracer Nd isotopes. Spiked aliquots of La Jolla Nd standard gave spike-unmixed $^{143}\mathrm{Nd}/^{144}\mathrm{Nd} = 0.511848 \pm 0.000008$. External reproducibility is $\pm 0.000016$ ($2\sigma$), determined by repeat analyses of an in-house, unspiked $Nd_2O_3$ standard (as reported in Creaser et al. 1997).

6) The dried purified Sm was dissolved in 1.0 µl de-ionized water and loaded onto the side Re filament of a double filament bead. The Sm samples were analyzed on a VG-Micromass-30 mass-spectrometer at the University of Alberta using a single-collector in peak hopping mode. Raw ratios were corrected for mass-discrimination to $^{152}\mathrm{Sm}/^{154}\mathrm{Sm} = 1.17537$ using an exponential law (Wasserburg et al. 1981), and for the effects of low-abundance (non-$^{149}$Sm) tracer Sm isotopes (as reported in Creaser et al. 1997)

Note: Total procedural blanks for Nd and Sm are 0.5ng (as reported in Creaser et al. 1997).

# APPENDIX 8. ZIRCON EXTRACTION, CLEANING, AND DISSOLUTION; AND U-Pb SEPARATION CHEMISTRY AND ISOTOPIC ANALYSIS.

1) Large (~10 kg) samples were collected in the field. These were then broken into fist sized chunks using a sledge hammer and passed through a jaw-crusher until fragments were pea-sized. Samples were reduced to sand-sized particles using a disc-grinder.

2) Samples were then subjected to various separation techniques in order to concentrate zircons. First, the crush was passed through a Wilfley table. The heavy fraction was passed through the Wilfley table again and collected for further processing. After dried, the heavy fraction from the Wilfley table was tumbled vertically past a Frantz isodynamic magnetic separator to remove excess steel particles from the crushing equipment, and then the remainder was passed through the Frantz (forward tilt of 15° and side tilt of 25°) at a setting of 0.6A in order to remove ferromagnesian minerals (garnet, chlorite hornblende). The non-magnetic fraction was then given a second pass through the Frantz magnetic separator at 1.1 A to further remove minerals with magnetic properties. The non-magnetic fraction from the second pass, which would contain any zircons, was then put in a separatory funnel filled with Tetrabromoethane (TBE) (specific gravity = 2.96); the heavy fraction was collected, washed of TBE, dried, and passed through a separatory funnel filled with Methylene iodide (MI) (specific gravity = 3.32). Zircon (specific gravity = 4.5 to 4.7) is concentrated in the heavy fraction. The concentrate was washed of MI, and dried using acetone.
(Note: most intermediate fractions were saved as well)

3) The concentrate containing zircons was then divided into increasingly non-magnetic fractions by decreasing the side tilt of the Frantz magnetic separator while keeping the forward tilt (15°) and amperage (1.8A) constant. (ie. the concentrate would be separated into a magnetic and non-magnetic fraction at 15° side tilt, then the non-magnetic fraction from this pass would be separated into a magnetic and non-magnetic fraction at a 10° side tilt, etc, until the side tilt was reduced to about 0°). Zircons from less magnetic fractions were desired, since they typically contain the least amount of inclusions.

4) Zircon fractions were hand-picked under ethanol using small tweezers. In this manner, zircons were separated into populations according to crystal shape, colour, size, and quality (lack of inclusions). Usually, several population fractions were obtained from a single magnetic fraction, but for some samples, only one good fraction could be obtained (e.g the SRPS gabbro).

5) Most multi-grained analyses were abraded with pyrite in a small air chamber, in order to remove surface contamination and late overgrowths. Typically, samples would be abraded for ~4 hours, or until the crystals were reduced to smooth football-like shapes. Two single-grained fractions (SG94-55C and SG94-55NC) were not abraded, since it was desired to retain as much material as possible. The samples were then cleaned in

warm 4N $HNO_3$ for about 0.5 hours in order to dissolve away any pyrite detritus. After the acid was replaced with ethanol, and the zircons were removed from the pyrite debris and transferred to a small glass beaker, and cleaned in warm 4N $HNO_3$ again. After careful rinsing of the acid with de-ionized water, the beaker containing the zircons was briefly emersed in an ultrasonic bath, and then the zircons rinsed several more times with water, and finally with acetone (to promote rapid drying).

6) After dried, the samples were weighed. This was accomplished by carefully tipping the zircons out of the glass beaker onto a small boat of clean (pre-weighed) aluminum foil. The boat and zircons were then weighed on a microbalance. The zircons were transferred directly to small ultraclean Teflon bombs (previously cleaned by repeated cycles of alternating $HF+HNO_3$ / HCl acid treatments at high temperature). 20 to 30 small drops of HF and 2 to 3 small drops of $HNO_3$ were added to the bomb, and then the sample was spiked with a $^{205}Pb$-$^{235}U$ mixed tracer solution. The bomb was then encapsulated within a Teflon jacket, and finally sealed in tight-fitting metal jacket. Bombs were heated at 200°C for 96 hours for dissolution, following which they were removed from the oven, cooled, opened, and dried down. Once dried, 8 drops of 3.1N HCl were added, the bombs resealed and jacketed, and heated for an additional 24 hours (200°C) to convert the samples to a chloride form.

7) Bombs were removed from the oven and cooled. After adding a small amount of 3.1N HCl (3 drops) to the bombs to ensure acid strength, samples were loaded directly from the bomb onto the mini-columns columns containing a small amount (~8 drops) of pre-cleaned resin, which consists of sulfonated styrene-divinyl benzene copolymer particles (resin cleaned with at least 4 cycles of ultraclean 6N HCl - $H_2O$ treatments). The columns employ small acid volumes to ensure low blanks. After impurities (Zr and Hf) are washed through in 3.1N HCl, a clean beaker was placed under the column and Pb was eluted using 6N HCl and U was eluted with de-ionized water (both were collected in the same pre-cleaned beaker). 2 drops of $H_3PO_4$ were added to the samples, which were subsequently dried. The above procedures from Creaser et al. (1997b).

8) The dried sample was mixed with 3.5μl of $H_3PO_4$ and 2.2μl of silica gel and loaded onto clean Re filament of a single-filament bead. Samples were analyzed on a VG-354 mass-spectrometer at the University of Alberta using single collector, peak-hopping mode. Details of running conditions and reproducibility in Creaser et al. 1997b).

# APPENDIX 9. Rb - Sr CHEMICAL SEPARATION AND ISOTOPE ANALYSES TECHNIQUES.

1) Powdered samples were weighed (typically 50 to 200 mg) into 25 ml Teflon vials and totally spiked with weighed aliquots of $^{84}$Sr and $^{87}$Rb tracer solution. Samples were then dissolved in a 3:1 mixture of vapour-distilled 24N HF: 16N $HNO_3$ in sealed containers at ~160°C for ~96 hours.

2) After the samples were uncapped and dried down, vapour distilled 6N HCl was added, the samples resealed, and heated at ~160°C for ~24 hours to dissolve fluorides.

3) Samples were uncapped and dried down, then dissolved in 3ml of loading solution (oxalic + HCl acids), centrifuged for 10 minutes at 5000 RPM, and loaded into 10 cm columns containing 200-400 mesh AG50W-X8 cation exchange resin for separation by chromatography. The Sr and Rb cuts were collected and separately passed through the cation exchange resin again to purify the samples. They were subsequently collected and dried down. Sr was isotopically analyzed following step (4); Rb was analyzed according to step (5).

4) The dried Sr was dissolved in 6.0 to 8.0 µl deionized water and one-sixth to one-eighth was loaded (the remainder saved for repeat analysis, if necessary) onto the side Re filament of a double filament bead. The Sr samples were analyzed on a VG-354 mass-spectrometer at the University of Alberta using dynamic multi-collector routines, and raw ratios were corrected for variable mass-discrimination to $^{86}$Sr/$^{88}$Sr = 0.1194 using an exponential law, and for the effects of low-abundance (non-$^{84}$Sr) tracer Sr isotopes. Multiple runs of SRM 987 standard gave spike-unmixed $^{87}$Sr/$^{86}$Sr = 0.710232 ± 000012 (2σ). A minimum estimation of the external reproducibility of $^{87}$Sr/$^{86}$Sr is ±0.00002 (2σ), determined by repeat analyses of SRM 987 standard (as reported in Holmden 1995).

5) The dried purified Rb was dissolved in 2.0-8.0 µl deionized water and one-half to one eighth was loaded onto the side Re filament of a double filament bead. The Rb samples were analyzed on a VG-Micromass-30 mass-spectrometer at the University of Alberta using a single-collector in peak hopping mode.

# APPENDIX 10: K-FELDSPAR SEPARATION TECHNIQUES AND Pb-Pb ANALYSIS.

1) Samples were broken into fist-sized chunks using a sledge hammer and passed through a jaw-crusher until fragments were pea-sized. Samples were reduced to sand-sized particles using a disc-grinder.

2) The crushed sample was then passed through a Wilfley table, and the lighter fractions retained.

3) The samples were lightly ground in a ceramic mortar and pestle until enough sample (~500 ml) would pass through a 70 mesh sieve. Samples were washed by shaking the sample in water until all particles were suspended, letting the sand-sized grains resettle for about ~10 seconds after shaking, and then pouring off the water along with any particles still suspended. This process was repeated several times. The sample was then rinsed with alcohol, and let dry.

4) The sample was then loaded into a separatory funnel filled with TBE. Heavy minerals were removed. Then the TBE was slowly diluted with acetone until the density of the mixture was less than quartz and plagioclase, but greater than K-feldspar. Since the density difference between these minerals is quite small, some K-feldspar were allowed to sink in TBE as well, to ensure a pure K-Feldspar float fraction. After removing the denser plagioclase and quartz, the light K-feldspar float was collected, then washed of all TBE and dried.

5) The concentrated K-feldspar was then passed through a Frantz magnetic separator (1.2 A, 5-10° side tilt) in order to remove magnetic minerals and feldspar with inclusions. A second pass through the Frantz, this time with a small reverse side tilt at 1.8A, was able to remove quartz from the K-feldspar, since quartz is diamagnetic and is repulsed by the magnetic field.

6) The feldspar was then picked under ethanol to remove contaminant grains. Samples ranged in mass from ~275 to 390 mg. Samples were then quickly cleaned in acetone in an ultrasonic bath for 5 minutes. After the acetone was decanted, the samples were dried.

7) Samples were then leached. First, 2.5 to 4 ml of 2N $HNO_3$ were added to the K-feldspar in a 7ml Teflon vial, which was then sealed and put in steel jackets and heated at ~80°C for 24 hours. The resulting solution, leach 1 (L1) was decanted from the K-feldspar and collected in a 15 ml centrifuge tube. The residue was rinsed (rinse collected with L1). For the second leach step, 6 ml of 6N HCl was added to the feldspar residue, the sample sealed and heated for 24 hours at ~80°C, and the resulting solution (L2) was collected and the residue rinsed. For the third leach step, 3 ml of

concentrated $HNO_3$ was added to the feldspar residue, the sample sealed and heated for 24 hours at ~80°C, and the resulting solution (L3) was collected and the residue rinsed twice. For the fourth leach step, 3 ml of concentrated $HNO_3$ and one drop of concentrated HF were added to the feldspar residue, the sample sealed and heated for 24 hours at ~80°C, and the resulting solution (L4), was collected and the residue rinsed. L1 and L4 were dried down in a clean hood, then 1ml of 3N HBr was added, and the leaches dried again. 4 ml of concentrated HF and 1 ml of concentrated $HNO_3$ were added to the residue, which was then sealed and dissolved at ~100°C for ~24 hours.

8) The residues (now dissolved) were dried, then 3.0 ml of 6N HCl were added, samples capped and heated overnight. Half of this sample was taken and stored in a 15 ml centrifuge tube as a back-up; the remaining sample was dried down. 2 ml of 3N HBr were added to the sample, which was then sealed and heated overnight. This sample was then dried down.

9) The samples were dissolved in 2 ml of 0.5N HBr and then centrifuged for 10 minutes at 5000 RPM. The solute was added to small columns containing 125µl of pre-cleaned AG1X8 200-400 mesh resin (resin was pre-cleaned with 1ml 6N HCl, 1 ml Millipore water, and conditioned with 1ml 0.5N Hbr) and rinsed with a small volume of the 0.5N HBr loading solution. Elution used HBr - HNO3 chemistry. The Pb cut was collected and dried down.

10) Pb samples were loaded onto clean, single Re filament beads in 2 µl of deionized water and dried. 3 µl of silica gel - phosphoric acid matrix was loaded on top of the dried sample and heated until solidified as a white residue. Pb analyses of the L1 and L4 leaches and the residues were performed on a VG Micromass 30 mass spectrometer at the University of Alberta, run at 1250°C and measured by a single Faraday collector. Reproducibility of $^{206}Pb/^{204}Pb$, $^{207}Pb/^{204}Pb$, and $^{208}Pb/^{204}Pb$ ratios are 0.24, 0.32, and 0.36 per mil ($1\sigma$) (as reported in Sundblad et al. 1991). Mass fractionation is 1.3 per mil per mass unit difference, determined from repeated measurement of the NBS SRM 981 and SRM 982 standards (as reported in Sundblad et al. 1991).

# APPENDIX 11. ANALYTICAL ERROR FOR XRF AND ICP-MS GEOCHEMICAL DATA

## XRF

| | Average conc. | StDev n=104 | SE (1 sigma) | SE (2 sigma) | %SE/conc (2 sigma) |
|---|---|---|---|---|---|
| | (%) | | | | |
| SiO2 | 68.224 | 0.041 | 0.0040 | 0.0080 | 0.01 |
| Al2O3 | 15.344 | 0.047 | 0.0046 | 0.0092 | 0.06 |
| TiO2 | 0.67 | 0.005 | 0.0005 | 0.0010 | 0.15 |
| FeO* | 3.881 | 0.029 | 0.0028 | 0.0057 | 0.15 |
| MnO | 0.04 | 0.001 | 0.0001 | 0.0002 | 0.49 |
| CaO | 2.071 | 0.012 | 0.0012 | 0.0024 | 0.11 |
| MgO | 0.971 | 0.015 | 0.0015 | 0.0029 | 0.30 |
| K2O | 5.606 | 0.024 | 0.0024 | 0.0047 | 0.08 |
| Na2O | 2.912 | 0.053 | 0.0052 | 0.0104 | 0.36 |
| P2O5 | 0.282 | 0.006 | 0.0006 | 0.0012 | 0.42 |
| | (ppm) | | | | |
| Ni | 18.19 | 1.68 | 0.1647 | 0.3295 | 1.81 |
| Cr | 17.61 | 5.18 | 0.5079 | 1.0159 | 5.77 |
| Sc | 5.93 | 2.62 | 0.2569 | 0.5138 | 8.66 |
| V | 46.44 | 5.93 | 0.5815 | 1.1630 | 2.50 |
| Ba | 1302.42 | 11.06 | 1.0845 | 2.1690 | 0.17 |
| Rb | 253.51 | 1.18 | 0.1157 | 0.2314 | 0.09 |
| Sr | 235.02 | 1.15 | 0.1128 | 0.2255 | 0.10 |
| Zr | 525.97 | 1.74 | 0.1706 | 0.3412 | 0.06 |
| Y | 29.43 | 1.24 | 0.1216 | 0.2432 | 0.83 |
| Nb | 28.52 | 0.602 | 0.0590 | 0.1181 | 0.41 |
| Ga | 22.58 | 1.39 | 0.1363 | 0.2726 | 1.21 |
| Cu | 35.8 | 2.01 | 0.1971 | 0.3942 | 1.10 |
| Zn | 104.47 | 1.92 | 0.1883 | 0.3765 | 0.36 |
| Pb | 53.23 | 1.62 | 0.1589 | 0.3177 | 0.60 |
| La | 182.6 | 7.8 | 0.7649 | 1.5297 | 0.84 |
| Ce | 405.28 | 9.33 | 0.9149 | 1.8298 | 0.45 |
| Th | 105.14 | 1.38 | 0.1353 | 0.2706 | 0.26 |

## ICP-MS

| | Average conc. | StDev n=24 | SE (1 sigma) | SE (2 sigma) | %SE/conc (2 sigma) |
|---|---|---|---|---|---|
| | (ppm) | | | | |
| Ba | 670 | 13 | 2.6536 | 5.3072 | 0.79 |
| La | 26.26 | 0.49 | 0.1000 | 0.2000 | 0.76 |
| Ce | 51.67 | 0.62 | 0.1266 | 0.2531 | 0.49 |
| Pr | 6.32 | 0.06 | 0.0122 | 0.0245 | 0.39 |
| Nd | 27.36 | 0.48 | 0.0980 | 0.1960 | 0.72 |
| Sm | 7.03 | 0.15 | 0.0306 | 0.0612 | 0.87 |
| Eu | 2.13 | 0.05 | 0.0102 | 0.0204 | 0.96 |
| Gd | 6.75 | 0.08 | 0.0163 | 0.0327 | 0.48 |
| Tb | 1.17 | 0.01 | 0.0020 | 0.0041 | 0.35 |
| Dy | 7.14 | 0.1 | 0.0204 | 0.0408 | 0.57 |
| Ho | 1.44 | 0.02 | 0.0041 | 0.0082 | 0.57 |
| Er | 4.05 | 0.06 | 0.0122 | 0.0245 | 0.60 |
| Tm | 0.55 | 0.01 | 0.0020 | 0.0041 | 0.74 |
| Yb | 3.36 | 0.03 | 0.0061 | 0.0122 | 0.36 |
| Lu | 0.52 | 0.01 | 0.0020 | 0.0041 | 0.79 |
| Rb | 48.1 | 0.7 | 0.1429 | 0.2858 | 0.59 |
| Y | 38.11 | 0.29 | 0.0592 | 0.1184 | 0.31 |
| Nb | 13.31 | 0.29 | 0.0592 | 0.1184 | 0.89 |
| Cs | 0.96 | 0.03 | 0.0061 | 0.0122 | 1.28 |
| Hf | 4.67 | 0.07 | 0.0143 | 0.0286 | 0.61 |
| Ta | 0.82 | 0.02 | 0.0041 | 0.0082 | 1.00 |
| Pb | 9.11 | 0.29 | 0.0592 | 0.1184 | 1.30 |
| Th | 5.13 | 0.49 | 0.1000 | 0.2000 | 3.90 |
| U | 1.15 | 0.11 | 0.0225 | 0.0449 | 3.90 |

The table on the left shows the instrumental precision for XRF analyses at Washinton State University, based on 104 repeat analyses of standard bead GSP-1 during many runs performed over a nine-month period (Hooper et al 1993). The table on the right shows the instrumental precision for ICP-MS analyses of a single sample (BCR-P) at Washington State University, based on 24 preparations on 12 runs, performed over a four month period Knaack et al. 1994). The column on the far right of each table shows the percentage $2\sigma$ error relative to the concentration of the element or oxide. Conc. = concentration, StDev = standard deviation, SE = standard error.